General Disclaimer

One or more of the Following Statements may affect this Document

- This document has been reproduced from the best copy furnished by the organizational source. It is being released in the interest of making available as much information as possible.

- This document may contain data, which exceeds the sheet parameters. It was furnished in this condition by the organizational source and is the best copy available.

- This document may contain tone-on-tone or color graphs, charts and/or pictures, which have been reproduced in black and white.

- This document is paginated as submitted by the original source.

- Portions of this document are not fully legible due to the historical nature of some of the material. However, it is the best reproduction available from the original submission.

September, 1982

LIDS-TH-1242

CONIC SECTOR ANALYSIS OF HYBRID CONTROL SYSTEMS

Peter Murray Thompson

Laboratory for Information and Decision Systems

MASSACHUSETTS INSTITUTE OF TECHNOLOGY, CAMBRIDGE, MASSACHUSETTS 02139

September, 1982

CONIC SECTOR ANALYSIS OF HYBRID CONTROL SYSTEMS

by

Peter Murray Thompson

Laboratory for Information and Decision Systems
Massachusetts Institute of Technology
Cambridge, MA 02139

CONIC SECTOR ANALYSIS OF HYBRID CONTROL SYSTEMS

by

Peter Murray Thompson

B.S.E.E., University of Virginia
(1977)

B.S. Applied Math, University of Virginia
(1977)

S.M., Massachusetts Institute of Technology
(1979)

E.E., Massachusetts Institute of Technology
(1980)

SUBMITTED IN PARTIAL FULFILLMENT
OF THE REQUIREMENTS FOR THE
DEGREE OF

DOCTOR OF PHILOSOPHY

at the

MASSACHUSETTS INSTITUTE OF TECHNOLOGY

August 1982

Signature of Author..
Department of Electrical Engineering
and Computer Science, August 13, 1982

Certified by..
Gunter Stein
Thesis Co-Supervisor

Certified by..
Michael Athans
Thesis Co-Supervisor

Accepted by...
Arthur C. Smith
Chairman, Departmental Graduate Committee

CONIC SECTOR ANALYSIS OF HYBRID CONTROL SYSTEMS

by

Peter Murray Thompson

Submitted to the Department of Electrical Engineering and
Computer Science on August 13, 1982 in partial fulfillment
of the requirements for the degree of Doctor of Philosophy

ABSTRACT

A hybrid control system contains an analog plant and a hybrid (or
sampled-data) compensator. In this thesis a new conic sector is determined
which is constructive and can be used to (1) determine closed loop stability,
(2) analyze robustness with respect to modelling uncertainties, (3) analyze
steady state response to commands, and (4) select the sample rate. The use
of conic sectors allows the designer to treat hybrid control systems as
though they were analog control systems. The center of the conic sector
can be used as a rigorous linear time invariant approximation of the hybrid
control system, and the radius places a bound on the errors of this
approximation. The hybrid feedback system can be multivariable, and the
sampler is assumed to be synchronous.

Algorithms to compute the conic sector are presented. Several ex-
amples demonstrate how the conic sector analysis techniques are applied.
Extensions to single loop multirate hybrid feedback systems are presented.
Further extensions are proposed for multiloop multirate hybrid feedback
system and for single rate systems with asynchronous sampling.

Thesis Co-Supervisor: Dr. Gunter Stein
Title: Adjunct Professor of Electrical Engineering

Thesis Co-Supervisor: Dr. Michael Athans
Title: Professor of Systems Science and Engineering

ACKNOWLEDGEMENTS

I would like to thank the people who provided technical and administrative support to this thesis. Helene George and Janet Mahoney typed the manuscript. Arthur J. Giordani drew the figures. Robert C. Burke set up the computer accounts, and Barbara Peacock-Coady and Marian S. Salvo kept track of all of the money that was spent.

These acknowledgements would not be complete without thanking my lovely and talented wife, Michelle Viau Thompson, for her help during my years at MIT.

TABLE OF CONTFNTS

LIST OF FIGURES

CHPATER 6:   MULTIRATE SAMPLING

LIST OF TABLES

1. INTRODUCTION

1.1 Motivation

Digital computers are commonly used to control analog systems. Examples can be found across the spectrum of engineering disciplines - chemical process control, automobile engine control, aerospace systems, mass transit systems, electromechanical servomechanisms, and radar tracking systems. Much of the technology has been pushed by the aerospace industry for use in aircraft, helicopters, missiles, and satellites. Digital computers have gained wide acceptance because they are reliable, easily reprogrammed, and not subject to drifts in parameter values. Control algorithms can be implemented (such as gain scheduling) that are difficult or impossible to implement using analog techniques. Of primary concern to this thesis is the ability of digital computers to mimic (over a certain frequency range) the behavior of analog compensators, in spite of their "sampled-data" nature.

The digital computer is embedded in a compensator that also contains a prefilter, sampler, and hold. This collection of analog and digital devices will be called a "hybrid compensator." A feedback system that has an analog plant controlled by a hybrid compensator is called a "hybrid feedback system." A block diagram of a hybrid feedback system is shown in Figure 1.1. The multivariable analog components are modelled as Laplace transform matrices, and the multivariable digital computer is modelled as a z-transform matrix.

Depending on where the feedback loop of Figure 1.1 is broken the signal is either an analog signal (points 1 and 2) or a discrete sequence (points 3 and 4). At the input and output of the plant the
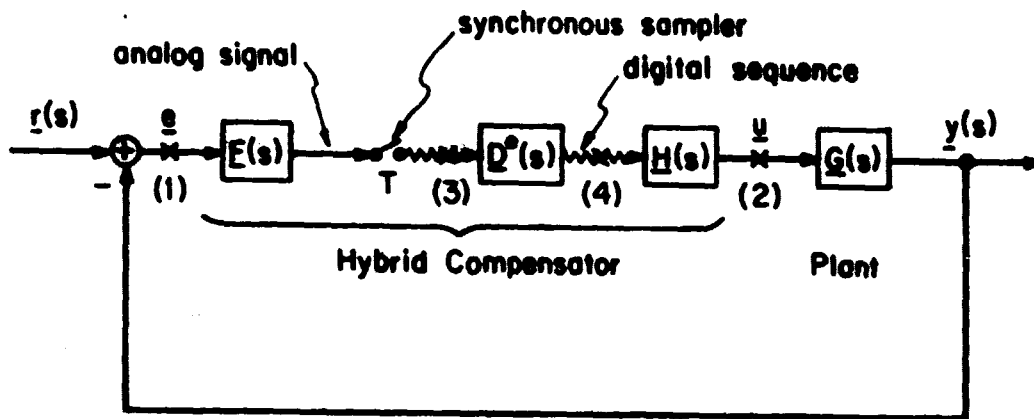
Figure 1.1: The hybrid feedback system.

physical signals are analog. It is only internal to the hybrid com-
pensator that the physical signals are discrete sequences.

If the feedback loop is broken at points 1 or 2 then the transfor-
mation from these points to the output can be modelled by a continuous time
linear time varying (CTLTV) operator. This operator is difficult to
use for analysis techniques because it cannot be represented as a
transfer function.

A major simplification occurs if the feedback loop is broken at
points 3 or 4. Here the hybrid feedback system can be modelled by a
discrete time linear shift invariant (DTLSI) operator, which in turn
can be represented by a z-transform.

The use of z-transforms has led to the development of most of the
analysis and design techniques in use today for hybrid feedback systems.
It must be recognized, however, that these techniques can only be
applied to points 3 and 4 in Figure 1.1. Whenever z-transform techniques
are used the inherent (often unstated) assumption is that good feedback
properties at points 3 and 4 (internal to the compensator) imply good
feedback properties at points 1 and 2 (where the compensator interfaces
with the real world). Whether or not this implication is valid depends
on the choice of prefilter, sample rate, and the nature of the hold
device. Numerous ad-hoc ways to make these choices have been developed
concurrently with the z-transform techniques in the sampled-data control
literature.

The difficult and important problem of analyzing a hybrid feedback
system at points 1 and 2 of Figure 1.1 is the primary motivation of this
thesis:

- Develop analysis techniques for hybrid feedback systems that can be applied, and used constructively, where the signals are analog.

The analysis techniques are divided into three categories:

- closed loop stability
- robustness with respect to plant uncertainties[1]
- steady state response to commands

They should apply to multivariable as well as single input single

output (SISO) hybrid feedback systems.

The major difficulty with the analysis at points 1 and 2 of

Figure 1.1 is that the differential equations that describe the hybrid

feedback system at these points are time varying. One way to lessen

this difficulty is to approximate the CTLTV system with a continuous

time linear time invariant (CTLTI) system. Hence the second motivation:

- Develop rigorous CTLTI approximations of the hybrid feedback system.

The key word here is "rigorous". An approximation is rigorous if it

applies to all possible inputs and disturbances. It is well known that

for low frequency inputs a hybrid feedback system can be approximated by

a CTLTI system. This approximation is not rigorous, however, unless

it can be shown to be valid (in some sense) for all possible inputs.

The research motivated by the above requires a branch of system

theory that is general enough to be used for CTLTV systems and is able

to make use of CTLTI approximations. Such a branch of system theory

does exist ([5] to [9]). It was developed to analyze stability and

robustness properties of nonlinear time varying feedback systems.

One of the techniques is to represent a nonlinear time varying

device by a conic sector. A conic sector has a center and a radius.

[1] A feedback system is robust with respect to plant uncertainties if it remains stable for all perturbations in a defined set of the plant.

The center is an approximation of the device, and the radius is a

rigorous bound on the errors of this approximation (i.e. a bound that

is valid for all possible input-output pairs).

These very general conic sector techniques were known to exist.

The conjecture was made (by Gunter Stein) that they are useful for the

analysis of hybrid feedback systems. Hence the third motivation:

- Determine whether or not conic sector techniques are useful
  for the analysis of hybrid feedback systems, and if so,
  develop these techniques and demonstrate their usefulness.

The full generality of these nonlinear conic sector techniques is not

needed because the hybrid feedback system is linear. The center of the

conic sector can be used as the CTLTI approximation of the CTLTV parts

of the hybrid feedback system.

1.2 Literature Survey

The background material for this thesis can be grouped into three categories: 1)conventional analysis of digital or sampled-data control systems, 2) conic sector analysis of nonlinear time varying feedback systems, and 3) conic sector analysis of hybrid feedback systems. There are many references in the first category, few in the second, and fewer in the third. The third category is the subject of this thesis.

The conventional analysis of digital control systems uses z-transform theory. The hybrid feedback system of Figure 1.1 is broken at points 3 and 4, and z-transforms are used to analyze stability, robustness, and performance. No attempt is made here to survey the extensive literature on digital control. Much of this literature has descended from journals into textbooks and is taught at the undergraduate level. A representative member of this set of textbooks (the one used the most for this research) is the text by Franklin and Powell [4]. The frequency domain (z-transform) techniques presented in [4] can be generalized to the multivariable case by the use of singular value techniques, just as has been done for analog systems [1, 2, 3].

The stability of nonlinear time varying systems is a classic problem in system theory. Our interest in this problem dates back to the landmark papers of Zames [5, 6]. He showed how conic sectors can be used to give sufficient conditions for closed loop stability of nonlinear time varying systems.[1]

---

[1] The landmark papers by Zames are very readable, but for further reference see the textbook by Desoer and Vidyasagar [8].

The starting point for Zames' work is the <u>Small Gain Theorem</u>, which states that a system is closed loop stable if the loop gain (appropriately defined) is less than one. Systems that satisfy this condition are of limited practical use because good command following, disturbance rejection, and insensitivity to modelling errors requires a loop gain much greater than one (most often at low frequencies). A generalization which makes the Small Gain Theorem more useful is made possible by the <u>Loop Transformation Theorem</u>, which states that a system (call it System 1) can be transformed to another system (call it System 2) in such a way that the stability of System 2 implies the stability of System 1. Zames [5] was able to show that if System 1 satisfies conic sector conditions then it can be transformed to another system (System 2) which is stable by the Small Gain Theorem, thereby implying stability of the original system (System 1).

Some important generalizations of Zames' work are due to Safonov [7]. He generalized conic sectors so that the centers and radii can be operators (instead of constant multipliers). In this thesis conic sectors with centers and radii that are CTLTI operators are extensively used.

Safonov [7] goes much further in his generalizations. He defines the feedback system of Figure 1.2 that has two "relations" K and G.[1] The closed loop system is stable if K and $-G^I$ (the inverse relation) are "topologically separated." Conic sectors are one way to show this topological separation. The closed loop system is stable if a conic

---

[1] A "relation" is any subset of a cross product space $X \times Y$, where X and Y are extended normed linear spaces.

$$(\underline{y},\underline{x}) \in G(\underline{u})$$

$$(\underline{x},\underline{y}) \in K(\underline{v})$$
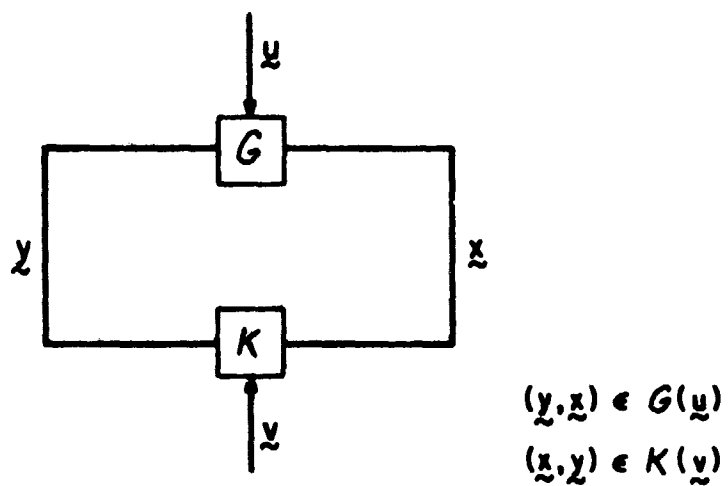
Figure 1.2: The feedback system defined by Safonov [7]

sector can be found that K is strictly inside of and $-G^I$ is outside of.

Conic sector stability theory and Liapunov stability theory are similar in that they are very general results which cannot easily be applied to specific problems[1]. The usefulness of Liapunov stability theory depends on the determination of a specific Liapunov function. Similarly, the usefulness of conic sector techniques depends on the determination of a specific conic sector that is valid for the feedback system of interest. No general guidelines exist that help the engineer in his search for the "right" Liapunov function or conic sector.

The conjecture (or hope) of Stein was that a useful conic sector could be found for hybrid feedback systems. The first conic sector was found by Kostovetsky [17, 18], who was one of Stein's S.M. students at MIT. Kostovetsky concentrated on a particular type of hybrid compensator, which he discovered and named the "optimal hybrid approximation."[2] The center of the conic sector is the CTLTI compensator that the hybrid compensator is closest to, and the radius is a nondynamic operator (i.e. a constant multiplier). Both the analog and hybrid compensator must be open loop stable. Kostovetsky demonstrated by an example that this conic sector gives conservative sufficient conditions for closed loop stability. Because this conic sector applies to only a very particular type of hybrid compensator it is not a "useful" conic sector.

A second conic sector was found by Stein [18], which is a

---

[1] The similarity is no accident. Both conic sector and Liapunov stability theory are special cases of the general results of Safonov [7]. For a description of Liapunov stability theory see Willems [29].

---

[2] The "optimal hybrid approximation" is the hybrid compensator that is optimally closest to a CTLTI compensator. "Optimal" is defined as minimizing the mean square difference of the outputs of the CTLTI and hybrid compensators when the input is white noise. The optimal hybrid approximation turns out not to be practical because the prefilter, computer, and hold all contain copies of the CTLTI compensator.

generalization of the first conic sector and exists for any stable
hybrid compensator. Any stable center can be used (poor choices result
in large radii), and the radius is again a nondynamic operator.

This second conic sector also proved not to be useful. The problem is
that the radius is a nondynamic operator, and any such radius results
in conservative sufficient conditions for closed loop stability. Hybrid
compensators behave like CTLTI compensators for low frequency inputs but
not for high frequency inputs. A nondynamic radius cannot distinguish
between low and high frequency inputs. Because it must be valid for all
inputs it will too large for low frequency inputs, which in turn results
in conservative sufficient conditions for closed loop stability.

Thus began the author's search for a conic sector with a dynamic
radius (i.e. a radius that is an CTLTI operator). The search lasted
for the better part of a year, and ended with the results presented in
this thesis. Preliminary versions of these result have been presented
in [18] and [30].

1.3 Contribu'ions of Thesis

Thi: thesis brings together two disjoint areas of control theory - conventional analysis of digital or sampled-data feedback systems, and conic sector analysis of nonlinear time varying feedback systems. The objective is to determine if conic sectors are useful for the analysis of hybrid feedback systems.[1] The conclusion is yes, with some restrictions, they are useful.

The major results are:

- Proof of the existence of a new conic sector which contains a stable hybrid operator.

- A modification of this new conic sector to create a conic sector that the inverse of a hybrid operator (stable or unstable) is outside of.

- Development of analysis techniques based on these new conic sectors. Those pertaining to robustness form a unified approach to the analysis of robustness properties of hybrid feedback systems.

- Development of algorithms to compute the center and radius of the new conic sectors.

- Demonstration that the new conic sector analysis techniques are useful for the analysis of practical hybrid feedback systems, including the selection of the sampling rate.

- Extension of the conic sector results to single loop multirate hybrid (SLMRH) feedback systems.[2]

The new conic sectors are more useful than previous versions [17, 18] because the radii of the new conic sectors are CTLTI operators and therefore can be represented by Fourier transforms, thus avoiding the inherent

---

[1] The hybrid feedback system may be SISO or multivariable and has a single hybrid compensator with a synchronous sampler.

---

[2] The SLMRH feedback system considered in this thesis (Chapter 6) is SISO and has two hybrid compensators in the same loop. The samplers are synchronized and have sampled rates that form an integer ratio.

conservativeness of conic sectors with radii that are constant multipliers.

The results of this thesis are of interest to both control theoreticians and practitioners. The theoreticians will probably be interested in the abstract properties of conic sectors (reviewed here), the existence of specific conic sectors for hybrid operators, the method of proving their validity, the gain of the hybrid operator, the signals that achieve the gain, the restrictions on the use of conic sectors, and so on. Care has been taken to rigorously develop the mathematical background. The new results are stated as theorems and proved.

Control practitioners are probably more interested in the new analysis techniques - what they do, when they can be used, how they are implemented, whether or not they are conservative, and whether or not they offer anything that can't already be done some other way. This thesis addresses each of these issues. The following results are highlighted as being of particular interest to practitioners: (1) the ability to rigorously approximate a hybrid feedback system by an analog feedback system, (2) robustness analysis techniques for single and multirate hybrid feedback systems that make direct use of the analog perturbation of the nominal plant (Theorem 3.7), and (3) the use of the conic sector radius to help select the sample rate. Both theoreticians and practitioners should be interested in the numerical examples, which complement and help to explain the theoretical results.

1.4 Summary of Thesis

The material in this thesis is organized as follows:

Chapter 2: Preliminary mathematics

Chapter 3: New conic sectors for hybrid compensators

Chapter 4: Algorithms to compute the radius of the new conic sectors

Chapter 5: Examples of the use of conic sector analysis techniques

Chapter 6: Multirate sampling issues

Chapter 7: Summary and extensions

Each of these chapters is now summarized.

Chapter 2 The mathematical review begins in Section 2.2 with analysis techniques for multivariable CTLTI feedback systems. The use of the loop transfer function and singular values is stressed. Plant uncertainties are modelled as additive or multiplicative perturbations that are bounded in magnitude. The relationship between multiplicative perturbations, phase margins, and gain margins is discussed. The goal (not fully realized) of conic sectors analysis techniques is to emulate these powerful multivariable techniques recently developed for CTLTI feedback systems.

The emphasis of Section 2.3 is on the conventional analysis of hybrid feedback systems. The structure of the hybrid compensator is described, and it is shown that the CTLTV input-output transformation can be modelled by time and frequency domain methods. The z-transform analysis techniques are presented for multivariable systems using singular values. Discretizing analog perturbations of the nominal plant is discussed.

The difficult transition is then made to conic sector analysis techniques for general (i.e. nonlinear time varying) feedback systems.

The level of presentation in Section 2.4 is more mathematically precise. Definitions are given for relations, operators, gain, stability, and conic sectors. The sufficient conditions for closed loop stability are fully developed. Preliminary work by Stein [18] on using conic sectors to analyze command response is presented.

As a breather before moving on to the new results, in Section 2.5 it is shown how conic sectors are applied to multivariable CTLTI feedback systems. Results due to Safonov [9] are presented that prove the existence of conic sectors for analog plants which have bounded additive or multiplicative perturbations.

Chapter 3 The major theoretical result of this thesis is the proof of existence of a new conic sector which contains a stable hybrid operator.[1] The most difficult step of this proof is a frequency domain inequality (Lemma 3.A) which makes use of Lebesque Dominated Convergence[2] and the Cauchy-Schwartz inequality. Theorem 3.2 is modified to show (1) the existence of a conic sector that contains the loop transfer operator and (2) the existence of a conic sector that the inverse hybrid operator is outside of (Theorem 3.6).

Chapter 3 contains 8 theorems, which form the basis for the following conic sector analysis techniques:

- An upperbound on the gain of a hybrid operator. For SISO hybrid operators the upperbound equals the gain (Theorem 3.1)

- Sufficient conditions for closed loop stability (Theorem 3.3)

---

[1] The hybrid compensator is modelled mathematically as a hybrid operator.

---

[2] Shankar Sastry and Marcel F. Coderch pointed out the need to check the conditions of Lebesque Dominated Convergence and helped to do so.

- Sufficient conditions for robust closed loop stability, i.e.
  closed loop stability for all perturbations in a defined
  set of the nominal plant (Theorems 3.4, 3.5, and 3.7)

- An upperbound for the steady state error of a hybrid feedback
  system (Theorem 3.8)

A distinction is made as to whether the hybrid operator is inside
of or outside of a conic sector. The inside conic sector techniques
(Theorems 3.1 to 3.5) have the major restriction that the hybrid
operator must be open loop stable. The outside conic sector techniques
(Theorem 3.6 and 3.7) are less restrictive because they only require
that the hybrid feedback system is closed loop stable (which can be
determined by z-transform techniques).

When the hybrid operator is placed inside of a conic sector then
Theorems 3.4 and 3.5 form a unified approach to the analysis of robustness.
Both the hybrid compensator and the actual plant are approximated by
CTLTI operators (centers of conic sectors), and the respective errors
of these approximations are modelled by bounded perturbations (radii
of conic sectors). The point of view taken is that a hybrid compensator
is supposed to mimic a CTLTI compensator. The extent to which it does
not is a sour: of error. By comparing the sizes of the radii as a
function of frequency the errors due to the use of a hybrid compensator
can be compared to the errors due to uncertainties of the plant (unmodelled
higher order dynamics, time delays, and so on).

Chapter 4 Conic sectors would not be useful if it was not possible
to compute the radius.[1] The most difficult parts of computing the radius

---

[1]Computing the center is no problem because any center can be used,
although some centers are better than others.

are the summing of infinite and double infinite series of Fourier.
transforms (each term shifted in frequency). Three ways to compute
the radius are

* Sum a finite number of terms of single infinite series (the
double infinite series can be broken down into several single
infinite series).

* Sum a finite number of terms of the double infinite series.

* Find an exact analytical solution to the single infinite series.

These approaches are discussed and compared. Bounds are placed on the
remainders of the truncated infinite series. Several cases where exact
analytical solutions can be found are presented. In the examples the
second approach is used.

Chapter 5 The conic sector analysis techniques are demonstrated
in the examples of Chapter 5. They are shown to work well for SISO
hybrid feedback systems but to be conservative for multivariable hybrid
feedback systems. More work is needed to remove this conservativeness.

Section 5.2 contains an extensive example of a SISO hybrid feedback
system. A lead-lag compensator is designed for a stable 2nd order plant
using classical control techniques, and then the analog compensator is
discretized to form the digital computer part of the hybrid compensator.
Each of the 8 theorems of Chapter 3 are used to analyze the hybrid feedback
system. In addition, the size of the radius (as a function of frequency)
is used as a measure to

* select sample rates

* compare discretization techniques

* compare different types of errors (due to the use of a hybrid
compensator and due to time delays in the plant)

A control problem with an integral compensator is presented in Section 5.3. The hybrid operator cannot be placed inside of a conic sector, but the inverse hybrid operator can be placed outside of a conic sector, which is then used to analyze robustness.

Section 5.4 contains a SISO and multivariable version of a hybrid feedback system for controlling motion in the pitch axis of a high performance aircraft. The analog compensators are designed using linear quadratic Guassian (LQG) techniques, and then the analog compensators are discretized to form hybrid compensators. The conic sector analysis techniques must be slightly modified when the loop transfer operator is placed inside of a conic sector to account for the fact that the plant is open loop unstable. The multivariable hybrid operator is placed outside of a cone, which is shown to result in a conservative robustness margin.

Chapter 6 extends the conic sector results of Chapter 3 to the single loop multirate hybrid (SLMRH) feedback system of Figure 6.1. These extensions are useful for a limited class of feedback systems, and should be considered preliminary results for the more general and more important problem of analyzing multiloop multirate hybrid feedback systems.

The new conic sectors are based on a frequency domain description of the input-output transformation of the cascaded hybrid compensators. The key observation is that the frequency domain description (6.3) has a similar structure to the description (2.51) of a single rate hybrid compensator operating at the slower of the sample rates. The details are presented in Section 6.2. An example is presented in Section 6.3.

Chapter 7 contains a summary and suggestions for future research.

In the summary the entire thesis is described as revolving around the major result of Theorem 3.2. The suggested topics for future research are:

- Removal of open loop stability restriction

- Generalization of conic sector techniques to sector techniques

- Less conservative multivariable robustness margins

- Synthesis techniques

- Multirate sampling issues

- Asynchronous sampling issues

- Finite wordlength issues

2. MATHEMATICAL PRELIMINARIES

2.1 Introduction

The background material for this thesis is reviewed in this chapter. The starting point is in Section 2.2, where a set of results are presented about multivariable analog linear time invariant (LTI) feedback systems. The emphasis is on analysis techniques to determine closed loop stability, command response, and robustness with respect to modelling uncertainties.

The results presented in Section 2.3 are from the conventional analysis of multivariable hybrid feedback systems. The components of the hybrid compensator are described, and then it is shown how to use z-tranforms to determine closed loop stability, command response, and robustness.

A much more general feedback theory is presented in Section 2.4. The components of the feedback system are modelled as "operators" and "relations." Closed loop stability, command response, and robustness are analyzed with "conic sectors." These analysis techniques are general enough to apply to both analog and hybrid feedback systems.

Section 2.5 reviews how conic sectors are used to analyze analog feedback systems. The contribution of this thesis is to use conic sectors to analyze hybrid feedback systems, which is done in Chapter 3.

The general feedback theory is presented in a rigorous fashion. Starting from a set of definitions, the major results are presented in a series of lemmas. When it is felt to be necessary the proofs are included in the appendix to Chapter 2. An attempt is made to keep the presentation at the minimum required level of generality. This is consistent with the main thrust of this thesis, which is to apply a

general feedback theory to a specific problem.

The reader is assumed to be familiar with Laplace and z-transform theory, state space techniques, and single-input single-output (SISO) analog and digital control. The use of the loop transfer function and the return difference equation for the analysis of feedback systems is stressed. Students of control theory will probably have had exposure to these subjects by the end of their undergraduate curriculum.

The reader is assumed to be less familiar with the use of singular values for the analysis of multivariable control systems, and even less familiar with general feedback theory. Some exposure to the theory of Hilbert Spaces will be helpful for an understanding of the general feedback theory.

There are numerous well-written journal articles and textbooks that can be used for further reference. The use of singular values for the analysis and design of multivariable analog feedback systems is explained in [1, 2, 3]. The analysis and design of SISO digital feedback systems is explained in [4]. Conic sector analysis of general feedback systems is explained in [5] to [9].

2.1.1 Notation

R^n, C^n, $R^{n \times m}$, $C^{n \times m}$ = finite dimensional real and complex Euclidean spaces

L_2^n = n-dimensional space of square integrable functions

L_{2e}^n = extended L_2^n space

ℓ_2 = space of infinite dimensional vectors

R_+ = real numbers ≥ 0

$\underline{A} \in C^{n \times m}$ = matrix (underlined capital Roman letters)

$\underline{a}, \underline{\alpha} \in C^n$ = vector (underlined small Roman and Greek letters)

$a, \alpha \in C^n$ = scalar (small Roman and Greek letters)

$A \in L_{2e}^n \times L_{2e}^m$ = relation or operator (capital script letters)

$\underset{\sim}{a} \in L_{2e}^n$ = function (small Roman letters underlined by a tilda)

$\underline{A}^{-1}$ = matrix inverse

$\underline{A}^T, \underline{a}^T$ = matrix and vector transpose

$\underline{A}^H, \underline{a}^H$ = matrix and vector Hermitian (complex conjugate transpose)

A^I = inverse of relation or operator

$\| \underline{a} \|_E$ = Euclidean vector norm

$\| \underline{A} \|$ = matrix norm, induced by Euclidean vector norms

$\| \underset{\sim}{a} \|_{L_2}$ = L_2 function norm

$\| \underset{\sim}{a} \|_T$ = truncated function norm

$\| A \|_{L_2}$ = operator norm, induced by functions norms

$\sigma_{min} [\underline{A}]$ = minimum singular value of $\underline{A}$

$\sigma_{max} [\underline{A}]$ = maximum singular value of $\underline{A}$

Associated with each LTI operator A (or with each $\underset{\sim}{a} \in L_{2e}^n$):

$\underline{A}(s)$ = Laplace transform

$\underline{A}(j\omega)$ = Laplace transform evaluated at $s = j\omega$

$\underline{A}(t)$ = inverse Laplace transform, impulse response

$\underline{A}(nT)$ = sampled version of $\underline{A}(t)$

$\underline{A}(z)$ = z-transform of $\underline{A}(nT)$

$\underline{A}^*(s) = \dfrac{1}{T} \sum_k \underline{A}(s-j\dfrac{2\pi}{T}k) = \underline{A}(z)\Big|_{z=e^{sT}}$

The following notational abbreviations are used:

$$F_k = F(j\omega - j\omega_s k)$$ (subscript k sometimes replaced by n)

$$\sum_k (\cdot) = \sum_{k=-\infty}^{\infty} (\cdot)$$

$$\sum_{n\neq k} (\cdot) = \sum_{\substack{n=-\infty \\ n\neq k}}^{\infty} (\cdot)$$

2.2 Analysis of Analog Feedback Systems

2.2.1 The Analog Feedback System

The analog feedback system is shown in Figure 2.1. The plant and compensator are multivariable LTI systems with Laplace transform matrices $\underline{G}(s)$ and $\underline{K}(s)$. The output $\underline{y}(s)$ and the error $\underline{e}(s)$ are related to the command input $\underline{r}(s)$ by

$$\underline{y}(s) = \underline{GK} \, (\underline{I} + \underline{GK})^{-1} \, \underline{r}(s) \tag{2.1}$$

$$\underline{e}(s) = (\underline{I} + \underline{GK})^{-1} \, \underline{r}(s) \tag{2.2}$$

Analysis techniques repeatedly use the loop transfer function and the return difference equation, this due to the fact that closed loop properties can be determined by how signals propagate around the loop. For multivariable systems the loop transfer function differs depending on where the loop is broken. Natural places are where signals enter the loop, such as points (1) and (2) of Figure 2.1. Most of the attention in this thesis is focussed on point (1), where the loop transfer function is

$$\underline{T}_1(s) = \underline{G}(s) \, \underline{K}(s) \tag{2.3}$$

and the return difference equation is $\underline{I} + \underline{T}_1(s)$.

2.2.2 Plant Uncertainty

The Laplace transform matrix $\underline{G}(s)$ is a mathematical model of a real system. The model will always be inexact, for many reasons including:

- inaccurately measured or slowly time-varying parameters

- unknown or purposely neglected high frequency dynamics (such as bending modes of mechanical systems)
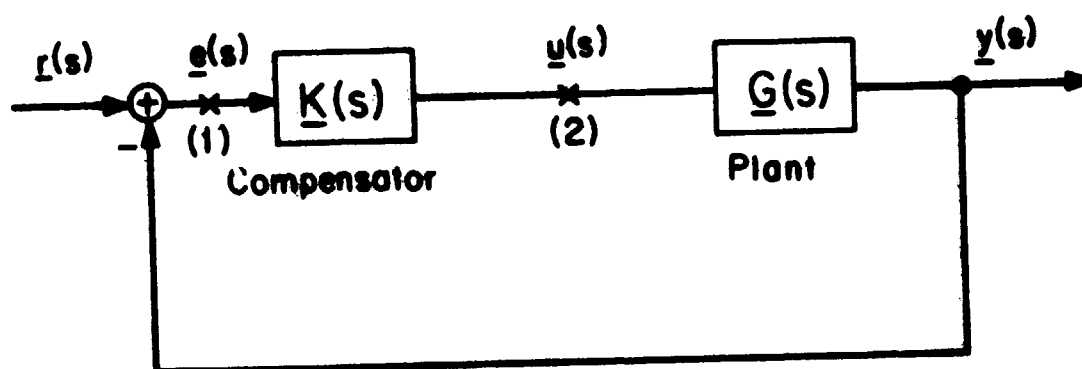
Figure 2.1: The analog feedback system

- neglected time delays (far away right half plane zeros)

- changes in the operating point about which a nonlinear model is linearized

The actual plant is assumed to be $\tilde{\underline{G}}(s)$, which is related to $\underline{G}(s)$ by the additive perturbation

$$\tilde{\underline{G}}(s) = \underline{G}(s) + \underline{E}_a(s) \tag{2.4}$$

It is assumed that $\tilde{\underline{G}}(s)$ and $\underline{G}(s)$ have the same number of unstable poles, which will definitely occur if $\underline{E}_a(s)$ is stable and may occur if $\underline{E}_a(s)$ is unstable.

The only other information known about $\underline{E}_a(s)$ is the following constraint on its magnitude:

$$\sigma_{max} \ [\underline{E}_a(j\omega)] < \ell_a(\omega) \quad \text{for all } \omega \tag{2.5}$$

The symbol "$\sigma_{max} [\underline{E}_a(j\omega)]$" indicates the maximum singular value of $\underline{E}_a(j\omega)$, as defined and discussed in the next subsection. Uncertainties that are bounded in magnitude, such as $\underline{E}_a(j\omega)$, are called "unstructured" uncertainties.

It is also possible to characterize plant uncertainty by the multiplicative perturbation:

$$\tilde{\underline{G}}(s) = \underline{G}(s) \ [\underline{I} + \underline{E}_m(s)] \tag{2.6}$$

It is assumed that $\tilde{\underline{G}}(s)$ and $\underline{G}(s)$ have the same number of open loop unstable poles. The only other information known about $\underline{E}_m(s)$ is

$$\sigma_{max} \ [\underline{E}_m(j\omega)] < \ell_m(\omega) \quad \text{for all } \omega \tag{2.7}$$

The two types of perturbations are related by

$$\underline{E}_a(s) = \underline{G}(s) \ \underline{E}_m(s) \tag{2.8}$$

and their bounds are related by

$$\ell_a(\omega) < \sigma_{max}[\underline{G}(j\omega)]\,\ell_m(\omega) \tag{2.9}$$

Whether the additive or multiplicative perturbation is used is often a matter f convenience, and results using one type of perturbation can usually be expressed using the other. The additive perturbation is more suited to conic sector analysis, whereas the multiplicative perturbation is more natural to use for an analysis of phase and gain margins.

Analysis techniques usually assume that the compensator Laplace transform matrix $\underline{K}(s)$ is exactly known- the reason being that it would be foolish to build an uncertain compensator. Nevertheless, if any perturbations exist they can be combined with the plant perturbations to create a perturbation of the loop transfer function. For example, if the actual plant and compensator are

$$\underline{\tilde{G}}(s) = \underline{G}(s) + \underline{E}_a(s) \tag{2.10}$$

$$\underline{\tilde{K}}(s) = \underline{K}(s) + \underline{E}_{ka}(s) \tag{2.11}$$

then the actual loop transfer function is

$$\underline{\tilde{T}}_1(s) = \underline{\tilde{G}}(s)\,\underline{\tilde{K}}(s) = \underline{G}(s)\,\underline{K}(s) + \underline{E}_{ta}(s) \tag{2.12}$$

where

$$\underline{E}_{ta}(s) = \underline{G}(s)\,\underline{E}_{ka}(s) + \underline{E}_a(s)\,\underline{K}(s) + \underline{E}_a(s)\,\underline{E}_{ka}(s) \tag{2.13}$$

$$\sigma_{max}[\underline{E}_{ta}(j\omega)] < \sigma_{max}[\underline{G}(j\omega)]\,\ell_{ka}(\omega) + \ell_a(\omega)\cdot\sigma_{max}[\underline{K}(j\omega)]$$

$$+ \ell_a(\omega)\cdot\ell_{ka}(\omega) \tag{2.14}$$

More sophisticated (less conservative) techniques for combining perturbations are given by Safonov [10] and Doyle [11].

2.2.3 Singular Values

The singular values of a matrix $\underline{A} \in C^{n \times m}$ are defined as:

$$\sigma_i(\underline{A}) \triangleq [\lambda_i (\underline{A}^H \underline{A})]^{1/2} \quad \text{for } i = 1,\ldots,m \tag{2.15}$$

The notation $\lambda_i(\cdot)$ indicates eigenvalue. Of the many properties of singular values, the ones that used in this thesis are listed in Table 2.1. For further reference see [12].

Singular values are used to determine the gain of a matrix. Suppose the matrix $\underline{A}$ is multiplied by the vector $\underline{x}$. The gain of $\underline{A}$ in the direction $\underline{x}$ is the ratio of the Euclidean vector norms[1] $\| \underline{Ax} \|_E / \| \underline{x} \|_E$. The maximum gain is $\sigma_{max}(\underline{A})$, which by property 2 of Table 1 is equal to the induced vector norm $\| \underline{A} \|$. The minimum gain is $\sigma_{min}(\underline{A})$. If a square matrix A has $\sigma_{min}(\underline{A}) = 0$ then the matrix is singular and cannot be inverted.

Singular values can be used to give a quantitative measure of the "size" of a matrix[2]. The matrix A is "large" if $\sigma_{min}(A) \gg 1$, and

---

[1] The Euclidean vector norm is defined

$$\| \underline{x} \|_E \triangleq \left[\sum_{i=1}^{n} |x_i|^2 \right]^{1/2}$$

where x_i for $i = 1,\ldots,n$ are the elements of the vector $\underline{x}$.

---

[2] The number "1" is used for comparison because the return difference equation has the form $\underline{I} + \underline{A}$. Important properties (used for performance analysis) are that $\sigma_{min}(\underline{I} + \underline{A}) \approx \sigma_{min}(\underline{A})$ if $\sigma_{min}(\underline{A}) \gg 1$ and that $\sigma_{max}(\underline{I} + \underline{A}) \approx 1$ if $\sigma_{max}(\underline{A}) \ll 1$.

(1) σ_i is real and nonnegative, for $i = 1,\ldots,n$ (the σ_i's are ordered from maximum to minimum, with $\sigma_1 = \sigma_{max}$ and $\sigma_n = \sigma_{min}$)

(2) $\sigma_{max}(\underline{A}) = \|\underline{A}\| = \max_{\|\underline{x}\|_E < \infty} \frac{\|\underline{Ax}\|_E}{\|\underline{x}\|_E} = \max_{\|\underline{x}\|_E = 1} \|\underline{Ax}\|_E$

(3) $\sigma_{min}(\underline{A}) = \min_{\|\underline{x}\|_E < \infty} \frac{\|\underline{Ax}\|_E}{\|\underline{x}\|_E} = \max_{\|\underline{x}\|_E = 1} \|\underline{Ax}\|_E$

(4) $\sigma_{min}(\underline{A}) \; \|\underline{x}\|_E \leq \|\underline{Ax}\|_E \leq \sigma_{max}(A) \; \|\underline{x}\|_E$ for all $\|\underline{x}\|_E \leq \infty$

(5) $\sigma_{max}(\underline{A}) = \dfrac{1}{\sigma_{min}(\underline{A}^{-1})}$ if $\underline{A}^{-1}$ exists

(6) $(\underline{A} + \underline{E})^{-1}$ exists if $\underline{A}^{-1}$ exists and $\sigma_{max}(\underline{E}) < \sigma_{min}(\underline{A})$

(7) (Triangle inequality): $\sigma_{max}(\underline{A} + \underline{E}) \leq \sigma_{max}(\underline{A}) + \sigma_{max}(\underline{E})$

(8) (Fan's Theorem [40]): $\sigma_i(\underline{A} + \underline{E}) < \sigma_i(\underline{A}) + \sigma_{max}(\underline{E})$ for $i = 1,\ldots,n$

(Properties 9 and 10 are consequences of Fan's Theorem)

(9) $\sigma_i(\underline{A}) - 1 \leq \sigma_i(\underline{A} + \underline{I}) \leq \sigma_i(\underline{A}) + 1$ for $i=1,\ldots,n$

(10) $\sigma_{min}(\underline{A} + \underline{E}) \geq \sigma_{min}(\underline{A}) - \sigma_{max}(\underline{E})$

Table 2.1: Properties of singular values

"small" if $\sigma_{max}(A) \ll 1$.

Singular values can be computed by stable and reliable algorithms that are easily available well tested, and well documented [13].

Many of the analysis techniques for multivariable systems use singular values. Readers unfamiliar with singular values should note that for complex scalars:

$$\| a \| = \sigma_{max}(a) = \sigma_{min}(a) = |a| \qquad (2.16)$$

When working with SISO systems most of the singular value results can be replace' with absolute values.

2.2.4 Command Response

Specifications for control systems often include a constraint on how well the output $y(t)$ follows certain types of inputs $r(t)$. Such specifications can be stated as constraints on the singular values of the loop transfer function. Specifications for disturbance rejection and sensor noise attenuation can also be stated as constraints on singular values. In this thesis, however, only the command response will be analyzed.[1]

Consider the set of commands that have energy only in the frequency range $\omega_o \leq \omega \leq \omega_1$. The response to these commands will be

---

[1] Specifications for command response (which usually take the form of high gain at low frequency) are the same as specifications for the attenuation of disturbances that are added to the output. Therefore, results for command response can be restated as results for disturbance rejection by replacing $r(t)$ by $r(t) - d(t)$. Specifications for sensor noise attenuation must be treated differently (low gain at high frequency). For a good treatment of the various performance specifications see [1].

good if over this frequency range:

$$\underline{y}(j\omega) \approx \underline{r}(j\omega)$$

$$\Longleftarrow \quad \underline{e}(j\omega) \approx \underline{o}$$

$$\Longleftarrow \quad [\underline{I} + \underline{GK}(j\omega)]^{-1} \approx o \quad [\text{by } (2.2)]$$

$$\Longleftarrow \quad \sigma_{max} \, [\underline{I} + \underline{GK}(j\omega)]^{-1} << 1$$

$$\Longleftarrow \quad \sigma_{min} \, [\underline{I} + \underline{GK}(j\omega)] >> 1 \qquad (\text{property 5, Table 2.1})$$

$$\Longleftarrow \quad \sigma_{min} \, [\underline{GK}(j\omega)] >> 1 \qquad (\text{property 9, Table 2.1}) \qquad (2.17)$$

Hence, a specification for command response can be stated

$$\sigma_{min} \, [\underline{GK}(j\omega)] \geq p(\omega) \qquad \text{for } \omega_o < \omega < \omega_1 \qquad (2.18)$$

For example, if the command is the step function $\underline{r}(t) = \underline{a}$ for $t \geq o$ then the steady state error is

$$\underline{e}(t) = [\underline{I} + \underline{GK}(jo)]^{-1} \, \underline{a} = \underline{b} \qquad (2.19)$$

The relative error, expressed as a ratio of vector norms, has the upper bound

$$\frac{\| \underline{b} \|_E}{\| \underline{a} \|_E} < \sigma_{max} \, [(\underline{I} + \underline{GK})^{-1}] = \frac{1}{\sigma_{min} [\underline{I} + \underline{GK}]} \approx \frac{1}{p(o)} \qquad (2.20)$$

where it is assumed that $p(o) >> 1$.

The command response specification must be satisfied not just for the nominal plant, but also for every possible perturbation of the nominal plant. This is guaranteed by increasing the lower bound of

equation (2.18)[1]:

$$\sigma_{min}[\underline{GK}(j\omega)] > \frac{p(\omega)}{1 - \ell_a(\omega)/\sigma_{max}[\underline{G}(j\omega)]} \tag{2.21}$$

Therefore, if the additive perturbation $\ell_a(\omega)$ is 10% the size of $\sigma_{max}[\underline{G}(j\omega)]$ then command response specification must be increased by about 10%.

2.2.5 Stability

It is important to know whether or not the closed loop system is stable. This is relatively easy to check for analog feedback systems. In fact some design methods, such as the linear quadratic Gaussian method [Athans, 14], guarantee closed loop stability (under mild assumptions).

The closed loop system is stable if all of the closed loop poles are in the left half plane (i.e. $Re(s_i) < o$ for all closed loop poles s_i). It is easiest to check this condition if a state space description is known for $\underline{G}(s) \underline{K}(s)$. In this case the closed loop poles are the eigenvalues of the closed loop system matrix.

It is not always feasible to compute the closed loop poles. This is the case when $\underline{G}(s) \underline{K}(s)$ contains polynominals of very high order or when they contain infinite dimensional terms such as the pure time delay e^{-sT}. For these cases a better way to check closed loop stability is to use the multivariable Nyquist theorem. This is due to Rosenbrock [15]. A nice statement of the theorem is given by Lehtomaki [3]. Basically, this is applied by plotting the imaginary versus the real

---

[1] It is assumed that $\ell_a(\ ) < \sigma_{max}[\underline{G}(j\omega)]$ and that $\sigma_{min}[\underline{GK}(j\omega)] \gg 1$. See [1].

part of $-1 + \det[\underline{I} + \underline{GK}(j\omega)]$ (as ω varies) and counting the number of encirclements of the -1 point.

2.2.6 Robustness

It is not enough just to know whether or not the closed loop system is stable. If it is stable it must also be known how close it is to becoming unstable. This is the subject of stability-robustness (often referred to just as robustness). The closed loop system must be stable for all possible perturbations of the nominal plant $\underline{G}(s)$, in other words for all possible $\underline{\tilde{G}}(s)$ of equation (2.6). Sufficient conditions for this to be true have been derived by Doyle, Stein, Lehtomaki, and others [1, 2, 3].

The sufficient conditions for robust stability have two parts. The first is that the nominal plant $\underline{G}(s)$ must result in closed loop stability. This condition is called "nominal closed loop stability." The second condition can be expressed as a constraint on the maximum singular value of the multiplicative perturbation:

$$\sigma_{max} [\underline{E}_m \underline{GK} (\underline{I} + \underline{GK})^{-1} (j\omega)] < 1 \quad \text{for all } \omega$$

$$<= \sigma_{max} [\underline{E}_m (j\omega)] < \sigma_{min} [\underline{I} + (\underline{GK})^{-1} (j\omega)] \quad \text{for all } \omega \qquad (2.22)$$

Most people find the nominal closed loop stability condition to be entirely reasonable and the singular value inequality to be somewhat less that intuitive. The basic idea of the second condition is that it guarantees that the return difference equation $\underline{I} + \underline{\tilde{G}K}(j\omega)$ remains invertible for all possible $\underline{\tilde{G}}$'s in the set defined by $\underline{E}_m$.

There are a plethora of other ways to express the robustness results. For example, if the additive perturbation is used, the

singular value inequality changes to:

$$\sigma_{max} \, [\underline{E}_a \underline{K} \, (\underline{I} + \underline{GK})^{-1} (j\omega)] < 1 \qquad \text{for all } \omega$$

$$\leq \sigma_{max} \, [\underline{E}_a (j\omega)] < \sigma_{min} \, [\underline{K}^{-1} (j\omega) + \underline{G}(j\omega)] \qquad \text{for all } \omega \qquad (2.23)$$

It is not always obvious which of the various results is best to use. For a method to derive these results and for some guidance on which to use see Lehtomaki [3].

2.2.7 Phase and Gain Margins

These terms have been handed down to us from classical control theory and are used to characterize the uncertainty of SISO plants. Let the nominal and actual SISO plants be related by

$$\tilde{g}(s) = g(s) \, \tilde{e}(s) \qquad (2.24)$$

To verify a phase margin specification let $\tilde{e}(s) = e^{j\phi}$. If the closed loop system is stable for all $\tilde{g}(s)$ such that $|\phi| < 45°$ then the closed loop system has a phase margin of 45°. Similarly, to verify a gain margin specification let $\tilde{e}(s) = \ell$. If the closed loop system is stable for all $\tilde{g}(s)$ such that $\ell_1 < \ell < \ell_2$ then it has a gain margin of $[\ell_1, \ell_2]$. The gain margin is usually expressed in terms of decibels: $[20 \, \log_{10}(\ell_1),$ $20 \, \log_{10}(\ell_2)]$.

Phase and gain margins can be expressed as multiplicative perturbations. For SISO plants the multiplicative perturbation is

$$\tilde{g}(s) = g(s) \, [1 + e_m(s)] \qquad (2.25)$$

which is related to $\tilde{e}(s)$ by

$$e_m(s) = \tilde{e}(s) - 1 \qquad (2.26)$$

A phase margin specification of 45° corresponds to the following bound on the multiplicative perturbation:

$$|e_m(j\omega)| < |e^{j45°} -1| = \ell_m(\omega) = .77 \tag{2.27}$$

Thus, if the closed loop system is nominally stable and if

$$|1 + (gk)^{-1}(j\omega)| > .77 \quad \text{for all } \omega \tag{2.28}$$

then the closed loop system has at least a 45° phase margin.

The correspondence can be turned around. Suppose that

$$|1 + (gk)^{-1}(j\omega)| > \ell_m(\omega) = \alpha \quad \text{for all } \omega \tag{2.29}$$

Then the closed loop system has the following guarantees[1]:

$$\text{guaranteed phase margin} = \pm \arccos\left(1 - \frac{\alpha^2}{2}\right)$$

$$\text{guaranteed gain margin} = \left[\frac{1}{1+\alpha}, \frac{1}{1-\alpha}\right] \tag{2.30}$$

These are guarantees - the actual margins may be better.

The phase and gain margins cannot be simultaneously achieved. They indicate robustness with respect to pure phase or pure gain perturbations. It is possible, however, to analyze robustness with respect to simultaneous phase and gain changes [16]. Let $\tilde{e}(s) = \ell e^{j\phi}$, and then find regions in the $20 \log_{10}(\ell) \times \phi$ space where $|\ell e^{j\phi} -1| < \alpha$. These regions are plotted in Figure 2.2. Suppose that $\alpha = .8$. Then any combination of ℓ and ϕ inside of the ellipse marked $\alpha = .8$ will not affect closed loop stability.

---

[1] This is shown by finding ϕ such that $|e^{j\phi}-1| < \alpha$ and by finding ℓ such that $|\ell-1| < \alpha$.
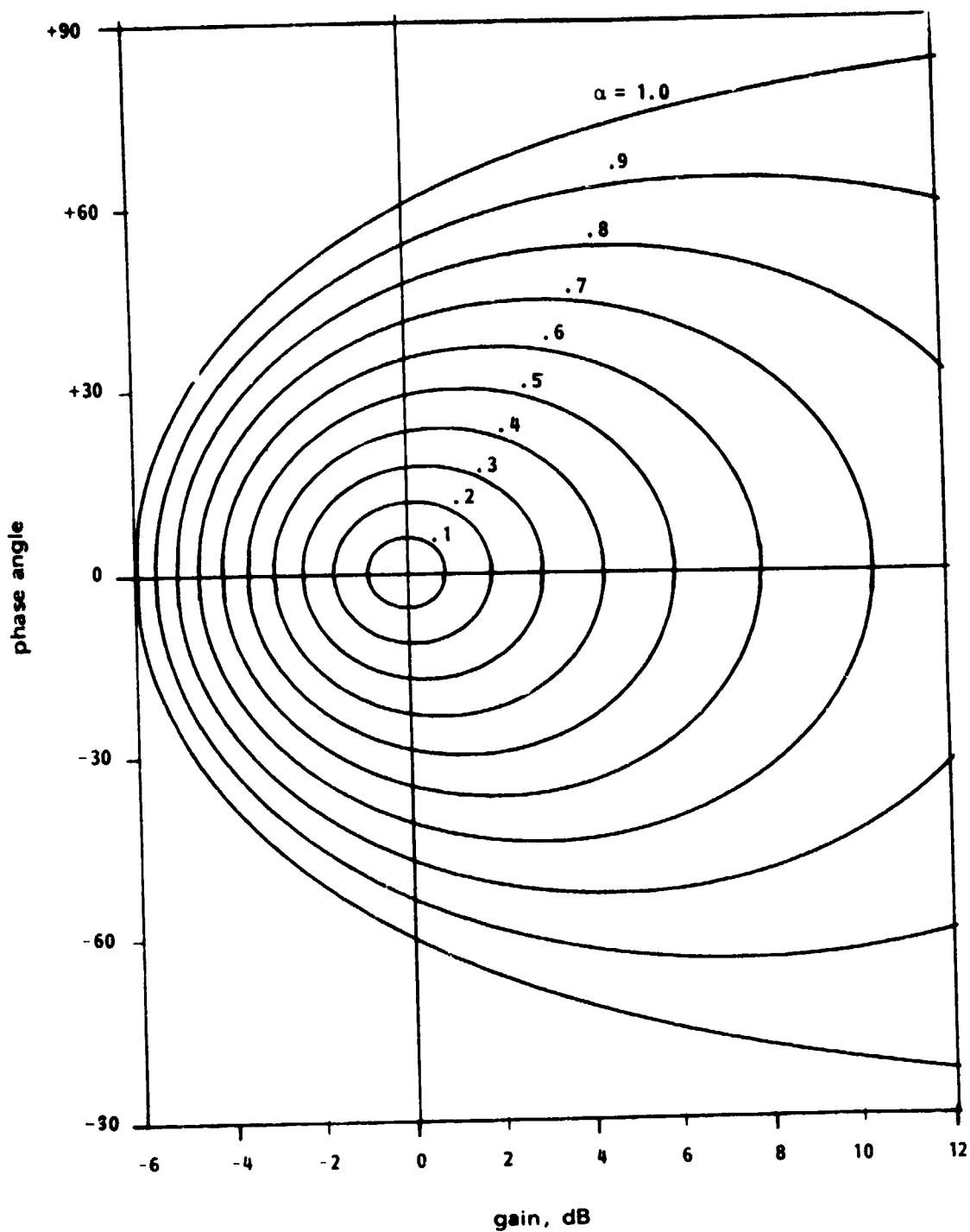
Figure 2.2: Simultaneous phase and gain changes that correspond
to a constant multiplicative perturbation of $\ell_m(\omega) = \alpha$

The guaranteed phase and gain margins lie on the boundary of the ellipse.

Phase and gain margins can be generalized to multivariable systems [7, 3]. This is done by inserting the diagonal perturbation

$$\underline{\tilde{E}}(s) = \text{diag } \{\tilde{e}_i(s)\} \tag{2.31}$$

In which case, if

$$\sigma_{\min} \ [\underline{I} + (\underline{GK})^{-1}(j\omega)] < \alpha \tag{2.32}$$

then the $\tilde{e}_i$'s can simultaneously undergo phase and gain changes as indicated in Figure 2.2.

The generalizations of phase and gain margins are sometimes subject to misinterpretation. The danger lies in restricting attention to diagonal perturbations. The closed loop system may be very robust with respect to diagonal perturbations, but sensitive to off diagonal perturbations. When this happens then α of (2.32) will be small, leading to conservative guarantees for perturbations that are restricted to be diagonal.

2.3 Conventional Analysis of Hybrid Feedback Systems

2.3.1 The Hybrid Compensator

A hybrid compensator consists of a prefilter, sampler, digital computer, and hold. A block diagram is shown in Figure 2.3. The word "hybrid" emphasizes that the compensator has both analog and digital parts. Both the input and output are analog signals, so from an input-output point of view the hybrid compensator is an analog device. Internally the signals are represented by discrete sequences, so from this point of view the hybrid compensator is a digital device.

It is the sampler that converts an analog signal into a digital sequence, and it is the sampler that complicates the analysis of hybrid feedback systems. Associated with the sampler are the signals $\underline{e}_d(t)$, $\underline{e}_d(nT)$, $\underline{e}_d^*(t)$, and their respective transforms $\underline{e}_d(s)$, $\underline{e}_d(z)$, and $\underline{e}_d^*(s)$. We show below how they are related.

The input to the sampler is the analog signal $\underline{e}_d(t)$. The sampler is periodic and outputs a sample every T seconds, so the output is the discrete sequence $\underline{e}_d(nT)$. Another way to represent the output is the input multiplied by a train of impulses:

$$\underline{e}_d^*(t) \;=\; \sum_n \underline{e}_d(t)\,\delta(t-nT) \tag{2.33}$$

where $\delta(t)$ is an impulse at time t=0. The following identities are well known, and are derived in [4]:

$$\underline{e}_d^*(s) \;=\; \frac{1}{T}\sum_n \underline{e}_d(s-j\omega_s n), \text{ where } \omega_s \;=\; \frac{2\pi}{T} \tag{2.34}$$

$$\underline{e}_d^*(s) \;=\; \underline{e}_d(z)\Big|_{z=e^{sT}} \tag{2.35}$$
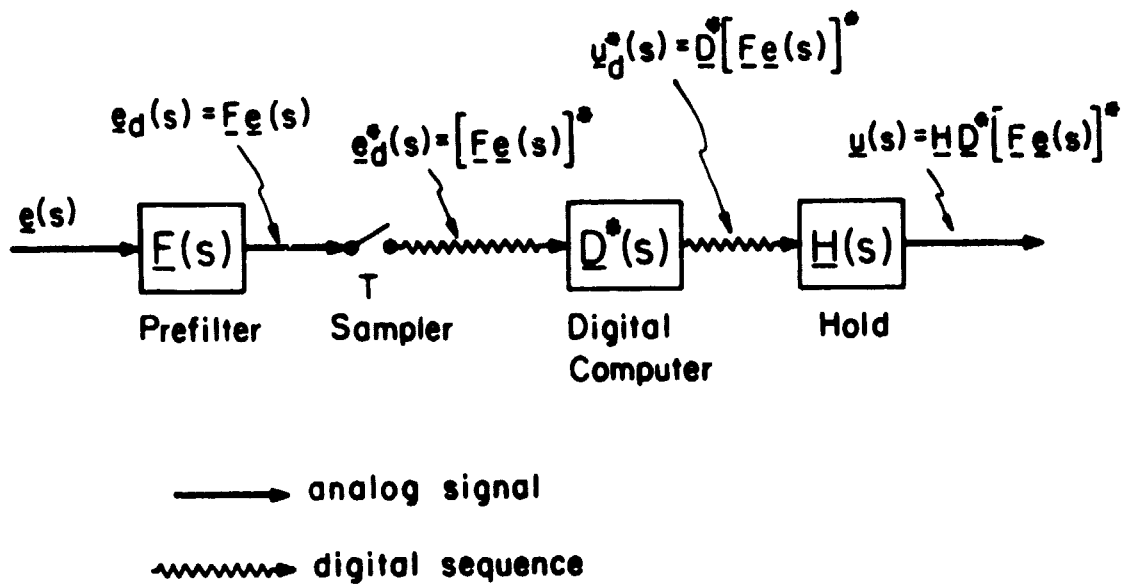
Figure 2.3: The hybrid compensator

The star operation may be considered a mathematical operation independent of its above use with samplers. Its definition for Laplace transform matrices is

$$\underline{A}^*(s) \triangleq \frac{1}{T} \sum_n \underline{A}(s-j\omega_s n) \tag{2.36}$$

Two of the properties of the star operation are

$$\underline{A}^*(s-j\omega_s n) = \underline{A}^*(s) \quad \text{for any integer } n \tag{2.37}$$

$$[\underline{A}^*(s) \underline{B}(s)]^* = \underline{A}^*(s) \underline{B}^*(s) \tag{2.38}$$

Every z-transform matrix $\underline{A}(z)$ has associated with it on $\underline{A}^*(s)$ defined by

$$\underline{A}^*(s) \triangleq \underline{A}(z)\Big|_{z=e^{sT}} \tag{2.39}$$

An $\underline{A}^*(s)$ matrix defined by (2.39) obeys properties (2.37) and (2.38), and can be used interchangeably with an $\underline{A}^*(s)$ defined by (2.36). In this thesis the star notation is preferred to the z-transform rotation (e.g. Figure 2.3).

The first part of the hybrid compensator is the prefilter. It is a linear time invariant (LTI) system which has the Laplace transform matrix $\underline{F}(s)$. Its main purpose is to low pass filter the input and reduce aliasing. If $\underline{F} \underline{e}(j\omega)$ is nonzero for $|\omega| > \pi/T$ then aliasing will occur, as readily seen from (2.34).[1]

---

[1] Aliasing occurs if $|(Fe)^*(j\omega)| > |Fe(j\omega)|$ for $0 < \omega < \pi/T$. Aliasing is undesirable phenomina for control systems. One of the effects of aliasing is that high frequency inputs are interpreted as low frequency inputs, which is particularly true of high frequency noise.

The digital computer is a linear shift invariant[1] device with the z-transform $\underline{D}(z)$. How the z-transform is derived is a synthesis problem and is not the main concern of this thesis. The two basic approaches are (1) to discretize an analog compensator and (2) to discretize the plant and synthesize $\underline{D}(z)$ by a direct method.

In the examples of Chapter 5 the Tustin with prewarping method [4, p. 59] is used to discretize $\underline{K}(s)$. The z-transform for the computer is set equal to

$$\underline{D}(z) = \underline{K}(s)\Big|_{s = \alpha \frac{z-1}{z+1}} \tag{2.40}$$

$$\text{where} \quad \alpha = \frac{\omega_1}{\tan\left(\frac{\omega_1 T}{2}\right)}$$

Tustin with prewarping has the property that (respectively):

$$\underline{D}(z)\Big|_{z=1,\ e^{j\omega_1 T}} = \underline{K}(s)\Big|_{s=0,\ j\omega_1} \tag{2.41}$$

The analog compensator is perfectly matched at $s=0$ and $s=j\omega_1$. The prewarped frequency ω_1 should in some respect be a "special" frequency, such as the natural frequency of a pole or zero, the frequency of maximum phase lag or lead, or the closed loop bandwidth.

_____

[1] Linear shift invariance is the discrete equivalent of linear time invariance. It the input sequence is shifted an integer number of sample periods then the output is the same except for being shifted the same number of sample periods. Only linear shift invariant operators have z-transforms defined for them.

Tustin with prewarping has the advantage of being easy to compute.
Suppose that $\underline{K}(s)$ has the state space realization

$$\left.\begin{array}{l} \underline{\dot{x}} = \underline{A}\,\underline{x} + \underline{B}\,\underline{u} \\[2mm] \underline{y} = \underline{C}\,\underline{x} + \underline{D}\,\underline{u} \end{array}\right\} \tag{2.42}$$

Then the state space realization of $\underline{D}(z)$ is

$$\left.\begin{array}{l} \underline{x}(n+1) = \underline{F}\,\underline{x}(n) + \underline{G}\,\underline{u}_d(n) \\[2mm] \underline{y}_d(n) = \underline{H}\,\underline{x}(n) + \underline{K}\,\underline{u}_d(n) \end{array}\right\} \tag{2.43}$$

where

$$\left.\begin{array}{l} F = (\alpha\underline{I}-\underline{A})^{-1}\,(\alpha\underline{I}+\underline{A}) \\[3mm] G = 2\alpha(\alpha\underline{I}-\underline{A})^{-2}\,\underline{B} \\[3mm] \underline{H} = \underline{C} \\[3mm] \underline{K} = \underline{C}\,(\alpha\underline{I}-\underline{A})^{-1}\,\underline{B} + \underline{D} \\[3mm] \alpha = \dfrac{\omega_1}{\tan\left(\dfrac{\omega_1 T}{2}\right)} \end{array}\right\} \tag{2.44}$$

The hold device transforms a digital sequence into an analog signal.
The hold is modelled as a LTI system with the Laplace transform $\underline{H}(s)$.
The input to the hold is a train of impulses $\underline{u}_d^*(t)$ with Laplace transform $\underline{u}_d^*(s)$, and the output of the hold has the Laplace transform

$H(s)\underline{u}_d^*(s)$

The most common type of hold is the zero-order-hold. Its impulse response and Laplace transform (for the SISO case) are

$$h_i t) = \begin{cases} 1 & 0 \le t \le T \\ 0 & \text{elsewhere} \end{cases} \tag{2.45}$$

$$h(s) = \frac{1}{s} (1 - e^{-sT}) \tag{2.46}$$

A first order analog approximation of $h(s)$ is

$$h_a(s) = \frac{2}{s + 2/T} \tag{2.47}$$

Magnitude and phase Bode plots of $h(j\omega)$ and $h_a(j\omega)$ are shown in Figure 2.4 (for $T = .6283$, $\omega_s = 10$). Below $\frac{1}{4}\omega_s$ rad/sec the approximation is very good.

2.3.2 The Hybrid Operator

An operator transforms input signals (belonging to a set of allowable input signals) to unique output signals.[1] An operator is a mathematical model, as opposed to a physical system. The hybrid operator is a mathematical model of a hybrid compensator. It is given the symbol K, and the transformation from an input signal e to an output signal u is represented by

$$\underset{\sim}{u} = K \underset{\sim}{e} \tag{2.48}$$

---

[1] A more precise definition is given in Section 2.4.
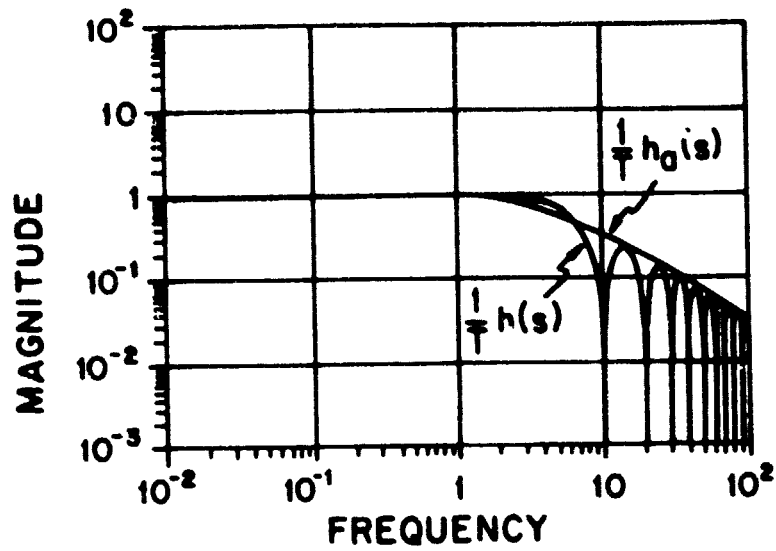
Figure 2.4a: Magnitude Bode plot of zero-
order-hold
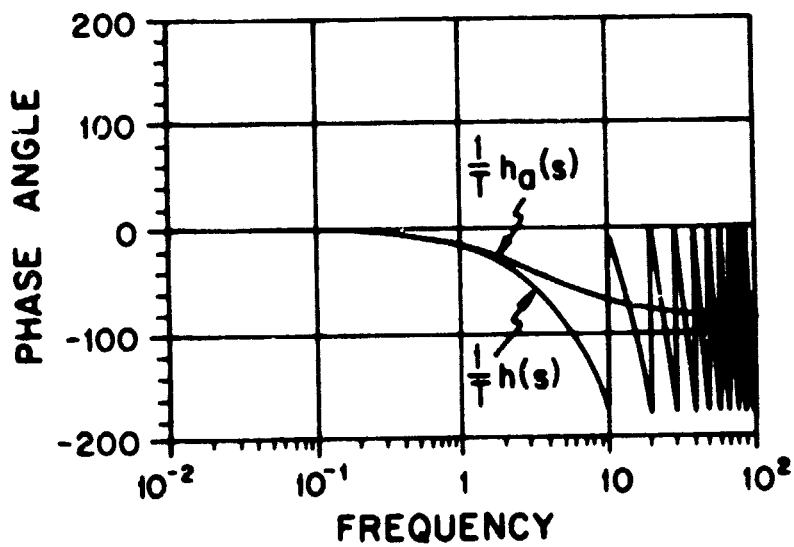
Figure 2.4b: Phase angle Bode plot of
zero-order-hold

The hybrid operator is a linear time varying (LTV) operator. The time variations are due to the sampler. The same input signal shifted in time by a fraction of sample period results in a different sequence of samples.

A time domain description of the hybrid operator is given by the convolution

$$\underline{u}(t) = \int_{-\infty}^{\infty} \underline{K}(t,\theta)\underline{e}(\theta)d\theta \qquad (2.49)$$

where $\underline{K}(t,\theta)$ is an impulse response matrix. It is periodic in the sense that

$$\underline{K}(t+Tn, \theta+nT) = \underline{K}(t,\theta) \quad \text{for any integer n} \qquad (2.50)$$

The same input shifted by an integer number of sample periods results in the same output shifted by the same integer number of sample periods.

It is this time domain description that was used by Kostovetsky [17] (see also [18]) to investigate some properties of hybrid operators. He was able to show that the gain of the hybrid operator is unbounded as the prefilter approaches an impulse ($\underline{F}(s) \rightarrow \underline{I}$). Also, he showed how to select a prefilter, digital computer, and hold such that $\underline{K}(t,\theta)$ is optimally close to a specified LTI impulse matrix $\underline{K}(t)$.

This thesis uses the following frequency domain description of the hybrid operator. If the input signal has the Laplace transform $\underline{e}(s)$ then the output signal has the Laplace transform

$$\underline{u}(s) = \underline{H}(s) \underline{D}^*(s) [\underline{F}(s) e(s)]^* \qquad (2.51)$$

This equation is crucial to the conic sector results of Chapter 3.
Note that (2.51) does not define a transfer function. Only LTI operators
can be represented by transfer functions.

One of the properties of the hybrid compensator that distinguishes
it from LTI compensators is that the hybrid compensator spreads out the
power spectrum of the input. This property is due to the sampler, which
when viewed in the frequency domain shifts and adds the power spectrum
of the sampled signal. An example is shown in Figure 2.5. The plots are
magnitude versus frequency for signals at different points in the hybrid
compensator. The input signal is bandlimited, but the output signal
has energy outside of this bandlimited region. A LTI compensator would
have energy only in the same bandlimited region as the input.

2.3.3 The Hybrid Feedback System

The hybrid compensator is one part of the hybrid feedback system
of Figure 2.6a. The plant $\underline{G}(s)$ is the same as in the analog feedback
system in Section 2.2.1 and Figure 2.1. As with the analog feedback
system, closed loop properties are determined by how signals pass
around the loop. The difference is that loop transfer operators must
be used instead of loop transfer functions.

Consider the loop broken at point (1) in Figure 2.6a. Inject the
input signal $\underline{e}_{in}$ and let $\underline{e}_{out}$ be the signal that returns after passing
around the loop. Their Laplace transforms are related by

$$\underline{e}_{out}(s) = \underline{G}(s) \, \underline{H}(s) \, \underline{D}^*(s) \, [\underline{F}(s) \, \underline{e}_{in}(s)]^* \qquad (2.52)$$

This transformation can be represented by the loop transfer operator
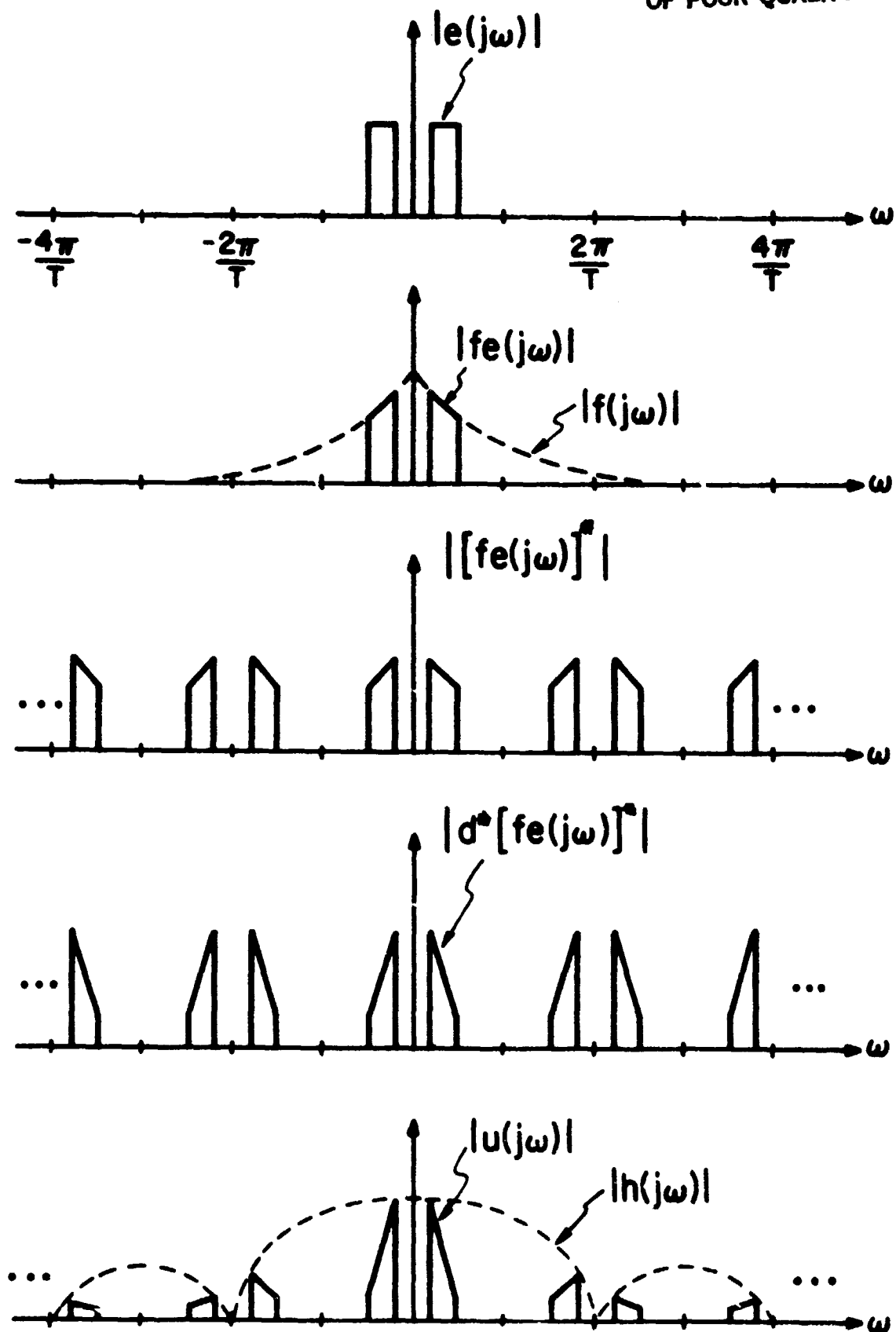
Figure 2.5: Magnitude of signals at different points in the hybrid compensator
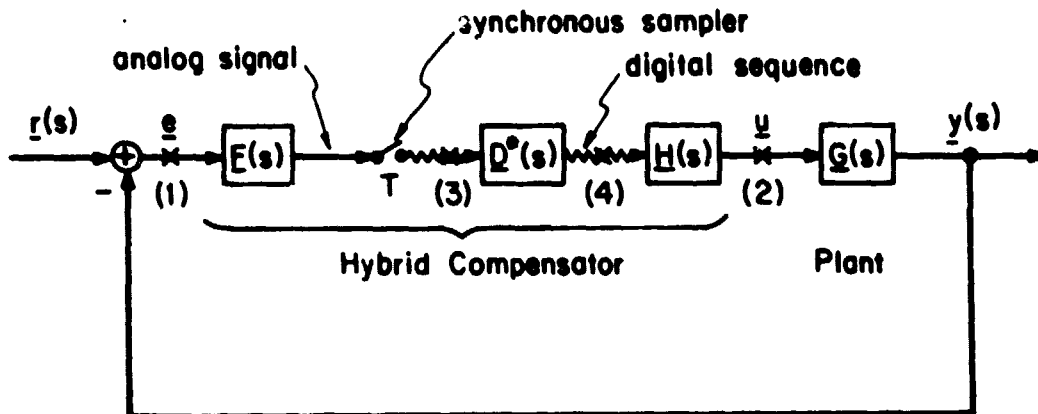
Figure 2.6a: The hybrid feedback system.
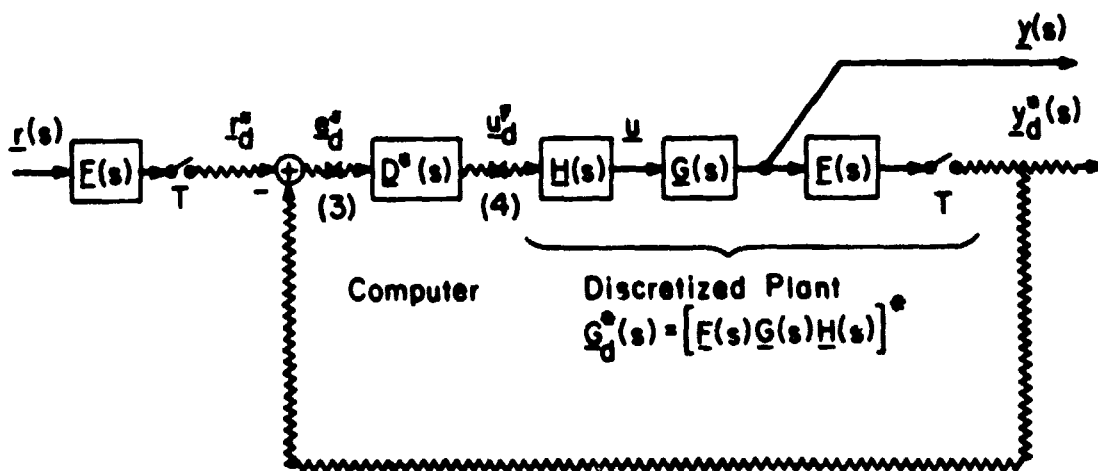
Figure 2.6b: A transformed version of the hybrid
feedback system.

$$\underline{r}_d(z) \quad \underline{e}_d \qquad \underline{u}_d \qquad \underline{y}_d(z)$$

$$\boxed{\underline{D}(z)} \qquad \boxed{\underline{G}_d\ (z)}$$

$$-\qquad (3) \qquad (4)$$
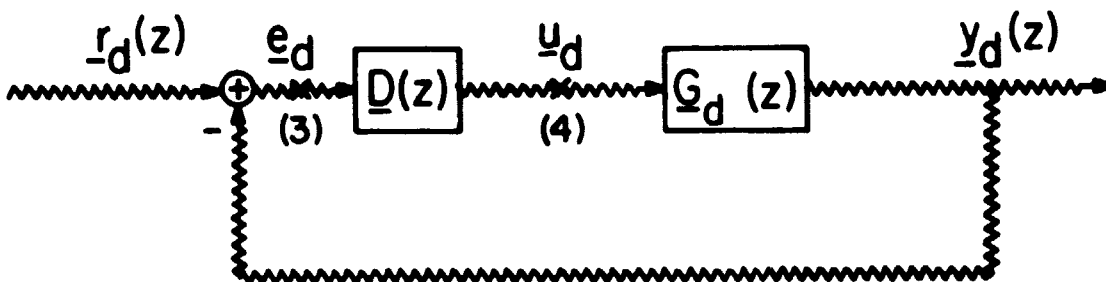
Figure 2.6c: The digital feedback system

$$e_{out} = T_1 e_{in} \tag{2.53}$$

but it is not possible to define a loop transfer function. The same is true for the loop broken at point (2) in Figure 2.6a.

The conventional analysis of hybrid feedback systems avoids the problems of dealing with LTV operators by analyzing the system at points (3) and (4) of Figure 2.6a. Here the loop transfer operators T_3 and T_4 are linear shift invariant and can be represented by the z-transforms $T_3(z)$ and $T_4(z)$. This simplifies the analysis, but at the cost of only examining the system at the sample times.

The conventional analysis proceeds by transforming the hybrid feedback system to a discrete feedback system. An intermediate step is shown in Figure 2.6b. The block diagram maniupulation used to derive Figure 2.6b is to pass the prefilter and sampler backwards across the sum. The prefilter and hold can be grouped with the plant to form the discretized plant

$$G_d^*(s) = [F(s) \, G(s) \, H(s)]^* \tag{2.54}$$

which can also be represented by the z-transform $G_d(z)$.

The discrete portion of Figure 2.6b is extracted to form the digital feedback system of Figure 2.6c. The output $y_d(z)$ and the error $e_d(z)$ are related to the command input $r_d(z)$ by

$$y_d(z) = G_d(z) \, D(z) \, [I + G_d(z)D(z)]^{-1} \, r_d(z) \tag{2.55}$$

$$e_d(z) = [I + G_d(z) \, D(z)]^{-1} \, r_d(z) \tag{2.56}$$

It is possible to compute the analog output $\underline{y}(s)$ given a command input $r(s)$:

$$\underline{y}(s) = \underline{G}(s)\ \underline{H}(s)\ \underline{D}^*_{c\ell}(s)\ [\underline{F}(s)\underline{r}(s)]^* \qquad (2.57)$$

where $\underline{D}^*_{c\ell}(s) = \underline{D}^*(s)\ [I + \underline{G}_d^*(s)\ \underline{D}^*(s)]^{-1} \qquad (2.58)$

The closed loop operator is a linear time varying operator with the same structure as the hybrid operator defined by (2.51).

2.3.4 Command Response, Stability, and Robustness

The discrete loop transfer function and the discrete return difference equation can be used to analyze the command response, stability, and robustness of the digital feedback system of Figure 2.6c. These results are analogous to those for the analog feedback system of Figure 2.1. One of the differences is that the results in this subsection apply to discrete sequences - not to the analog signals - that appear in the hybrid feedback system.

The command response is considered to be good if the discrete output $\underline{y}_d(nT)$ tracks the discrete input $\underline{r}_d(nT)$ with small error over some frequency range. As seen from (2.56), this will be the case if the return difference equation (similarly the loop transfer function) is large over the frequency range where the discrete input has significant energy. A command response specification can be stated

$$\sigma_{min}\ [\underline{G}_d^*(j\omega)\ \underline{D}^*(j\omega)] \geq p(\omega) \quad \text{for} \quad \omega_o \leq \omega \leq \omega_1 \qquad (2.59)$$

The loop transfer function is periodic, and the specification should only be given over a portion of the frequency range 0 to π/T rad/sec. A discrete sequence $\underline{r}_d(nT)$ is said to have significant energy over some frequency range if $\underline{r}_d(z)$ evaluated at $z = e^{j\omega T}$ has large magnitude for ω in the specified frequency range.

The digital closed loop system is stable if all of the digital closed loop poles have magnitude less than unity. The digital closed loop poles can be found by various frequency domain and state space techniques [4].

Another way to determine stability is to use the discrete version of the multivariable Nyquist theorem. It will be stated here, using the same notation as in [3]. Let $N(\Omega, f(s), C)$ denote the "number of clockwise encirclements of the point Ω by the locus $f(s)$ as s traverses the closed contour C in the complex plane in a clockwise sense" [3, p. 76]. Let the contour $\mathcal{D}$ be the unit circle, with small expansions to include the open loop poles of $\underline{G}_d(z)\underline{D}(z)$ with unit magnitude (these are considered open loop stable). Let P be the number of open loop unstable poles of $\underline{G}_d(z)\underline{D}(z)$. The multivariable Nyquist theorem states that the discrete closed loop system is stable (has no poles with magnitude > 1). if and only if

$$N (-1, -1 + \det [I + \underline{G}_d^*(s)\underline{D}^*(s)], \mathcal{D}) = - P \qquad (2.60)$$

An important point to note is that the hybrid feedback system is stable if and only if the discrete feedback system is stable. Hence, the two stability tests just mentioned are useful for the hybrid feedback system.

The model of the plant is not exact, and closed loop stability must be preserved for all possible perturbations of the plant. Robustness results similar to those for analog systems can be derived. The starting point is a z-transform description of the additive perturbation:

$$\tilde{G}_d(z) = \underline{G}_d(z) + \underline{E}_{da}(z) \tag{2.61}$$

It is assumed that $\tilde{\underline{G}}_d(z)$ and $\underline{G}_d(z)$ have the same number of open loop unstable poles, and that the magnitude of $\underline{E}_{da}(z)$ is bounded by

$$\sigma_{max}[\underline{E}_{da}{}^*(j\omega)] \leq \ell_{da}(\omega) \quad \text{for} \quad 0 \leq \omega \leq \omega_s \tag{2.62}$$

The digital closed loop system is stable if it is nominally closed loop stable and if

$$\sigma_{max}[\underline{E}_{da}{}^* \; \underline{D}^* \; (\underline{I} + \underline{G}_d{}^*\underline{D}^*)^{-1}(j\omega)] < 1 \quad \text{for} \quad 0 \leq \omega \leq \omega_s$$

$$<= \sigma_{max}[\underline{E}_{da}{}^*(j\omega)] < \sigma_{min}[\underline{D}^*(j\omega)^{-1} + \underline{G}_d{}^*(j\omega)] \quad \text{for} \quad 0 \leq \omega \leq \omega_s$$

$$\tag{2.63}$$

The singular value inequality need only be checked over the fundamental frequency range.

A digital robustness analysis can also be performed using the discrete multiplicative perturbation:

$$\tilde{\underline{G}}_d(z) = \underline{G}_d(z) [\underline{I} + \underline{E}_{dm}(z)] \tag{2.64}$$

It is assumed that $\underline{G}_d(z)$ and $\underline{\tilde{G}}_d(z)$ have the same number of open loop unstable poles, and it is assumed that

$$\sigma_{max} \; [\underline{E}_{dm}{}^*(j\omega)] \leq \ell_{dm}(\omega) \quad \text{for} \quad 0 \leq \omega \leq \omega_s \tag{2.65}$$

The closed loop system is stable if the nominal system is closed loop stable and if

$$\sigma_{max} \; [\underline{E}_{dm}{}^* \; \underline{G}_d{}^* \; \underline{D}^* \; (\underline{I} + \underline{G}_d{}^* \; \underline{D}^*)^{-1}(j\omega)] < 1 \quad \text{for} \quad 0 \leq \omega \leq \omega_s \tag{2.66}$$

$$<= \quad \sigma_{max} \; [\underline{E}_{dm}{}^*(j\omega)] < \sigma_{min} \; [\underline{I} + (\underline{G}_d{}^* \; \underline{D}^*)^{-1}(j\omega)] \quad \text{for} \quad 0 \leq \omega \leq \omega_s \tag{2.67}$$

A digital robustness analysis starts with a discrete perturbation. This is not a natural place to start, however, for a robustness analysis of a hybrid system. It is the analog plant $\underline{G}(s)$ that is uncertain, and its uncertainty is expressed by an analog perturbation. The analog perturbation must be discretized in order to obtain a discrete perturbation.

Consider when the actual plant is $\underline{\tilde{G}}(s) = \underline{G}(s) + \underline{E}_a(s)$. The actual discretized plant is

$$\underline{\tilde{G}}_d{}^*(s) = \underline{G}_d{}^*(s) + \underline{E}_{da}{}^*(s) \tag{2.68}$$

$$\text{where} \quad \underline{E}_{da}{}^*(s) = [\underline{F} \; \underline{E}_a \; \underline{H}(s)]^* \tag{2.69}$$

The additive perturbation is discretized the same way as the analog plant.

When multiplicative perturbations are used then the actual plant

is $\tilde{G}(s) = G(s)\ [I + E_m(s)]$ and its discretized version is

$$\tilde{G}_d{}^*(s) = G_d{}^*(s) + [F\ G\ E_m\ H(s)]^* \tag{2.70}$$

This cannot easily be expressed as a discrete multiplicative pertur-

bation except when E_m is a constant that commutes with $H(s)$[1], in which

case

$$\tilde{G}_d{}^*(s) = G_d{}^*(s)\ [I + E_{dm}],\ \text{where } E_{dm} = E_m \tag{2.71}$$

The analog and discrete multiplicative perturbations are equal.

Constant E_{dm}'s can be used to find guarenteed phase and gain margins

(see Subsection 2.2.7). By the argument of the above paragraph the phase

and gain margins of the digital system are also phase and gain margins

of the hybrid system.

Discretizing analog perturbations is one way to analyze the ro-

bustness of closed loop hybrid control systems. This is not, however,

the approach that is persued in this thesis. Rather, the approach is

to approximate the hybrid operator by a LTI operator and then to use

analog techniques to analyze robustness (Theorems 3.4, 3.5, and 3.7).

The "analog techniques" are conic sector techniques. They are

now reviwed, using a precise mathematical format.

---

[1] For SISO systems any constant $E_m = e_m$ satisfies this condition. For multivariable systems the easiest example is when both E_m and $H(s)$ are diagonal matrices.

2.4 Results from General Feedback Theory

The hybrid compensator is modelled with a LTV operator which is called a hybrid operator. The analysis techniques described so far make no direct use of this hybrid operator. In order to do so, this thesis makes use of a feedback theory that is more general than the analog or digital feedback theory of the previous two sections. Components of a feedback system are modelled with mathematical entities called "relations." Hybrid compensators and the LTI plants are special cases of relations, so analysis techniques for general feedback systems can be applied to hybrid feedback systems.

The description given here of the general feedback system follows the work of Zames, Safonov, Athans, Desoer, and Vidyasagar [5] to [9]. The most general part of the description is contained in the subsections on relations and conic sectors. The subsections on the feedback systems are less general because they assume that the feedback system is causal and well-posed.[1] Even with this restriction the components can be nonlinear and time varying. It is not until specific conic sectors are developed that further restrictions are needed.

2.4.1 Extended Normed Linear Spaces

The analog signals in a feedback system are members of an extended normed linear space. A "linear space" is a basic concept of analysis. Definitions and properties can be found in many textbooks [e.g. 19]. A "normed linear space" is a linear space with a norm defined for it. The norm introduces the concepts of "size" and "distance". Elements

---

[1] A feedback system is causal if its output at time t is independent of its input after time t. It is well-posed if for every possible input there exists an output.

of a normed linear space must have finite norm. This restriction can
be removed by extending the normed linear space. The result is called
an "extended normed linear space."

In this thesis the only normed linear space that will be extensively
used is L_2^n, the space of square integrable n-dimensional functions.
Elements of L_2^n are functions $\underset{\sim}{x}: R_+ \rightarrow R^n$ (from the set of real numbers
≥ 0 to the set of n-dimensional vectors) that have finite norm. The
norm is defined

$$\| \underset{\sim}{x} \|_{L_2} \triangleq \left[\int_0^\infty \| \underset{\sim}{x}(t) \|_E^2 \, dt \right]^{1/2} \tag{2.72}$$

L_2^n has engineering significance as being the set of signals with finite
energy. The square of the norm, $\| \underset{\sim}{x} \|_{L_2}^2$ is proportional to the energy of
the signal $\underset{\sim}{x}(t)$.

The extension of L_2^n is the extended normed linear space L_{2e}^n.
Elements are functions $\underset{\sim}{x}: R_+ \rightarrow R^n$ that have finite truncated norm $\| \underset{\sim}{x} \|_\tau$
for all $\tau \in R_+$, where

$$\| \underset{\sim}{x} \|_\tau \triangleq \left[\int_0^\tau \| \underset{\sim}{x}(t) \|_E^2 \, dt \right]^{1/2} \tag{2.73}$$

Elements of L_2^n are automatically in the extension L_{2e}^n and have the
property that the limit as $\tau \rightarrow \infty$ of $\| \underset{\sim}{x} \|_\tau = \| \underset{\sim}{x} \|_{L_2}$. Examples of
functions that are in L_{2e}^n but not L_2^n are $x(t) = t$ and $x(t) = \exp(t)$.
Examples of functions in neither space are $x(t) = \tan(t)$ and $x(t) = 1/(1-t^2)$.

2.4.2 Relations, Operators, Gain, and Stability

A relation H is any subset of the product space $L_{2e}^n \times L_{2e}^m$. The range and domain of H are defined by

$$Ra(H) \triangleq \{\underset{\sim}{y} | (\underset{\sim}{x}, \underset{\sim}{y}) \in H \quad \text{for some } \underset{\sim}{x} \in L_{2e}^n\} \tag{2.74}$$

$$Do(H) \triangleq \{\underset{\sim}{x} | (\underset{\sim}{x}, \underset{\sim}{y}) \in H \quad \text{for some } \underset{\sim}{y} \in L_{2e}^m\} \tag{2.75}$$

The inverse of the relation H is a set with the elements $\underset{\sim}{x}$ and $\underset{\sim}{y}$ arranged in the reverse order. This inverse relation always exists and is defined by

$$H^I \triangleq \{(\underset{\sim}{y}, \underset{\sim}{x}) \in L_{2e}^m \times L_{2e}^n | (\underset{\sim}{x}, \underset{\sim}{y}) \in H\} \tag{2.76}$$

The composition product HK and the sum $H + K$ are relations defined by

$$HK \triangleq \{(\underset{\sim}{x}, \underset{\sim}{z}) \in L_{2e}^n \times L_{2e}^r | \text{ there e: ..s a } \underset{\sim}{y} \in L_{2e}^m \text{ such that}$$

$$(\underset{\sim}{x}, \underset{\sim}{y}) \in K \text{ and } (\underset{\sim}{y}, \underset{\sim}{z}) \in H\} \tag{2.77}$$

$$H + K \triangleq \{(\underset{\sim}{x}, \underset{\sim}{y}) \in L_{2e}^n \times L_{2e}^m | \underset{\sim}{x} \in L_{2e}^n \text{ and } \underset{\sim}{y} = \underset{\sim}{y}_1 + \underset{\sim}{y}_2 \text{ for some}$$

$$\underset{\sim}{y}_1 \in Ra(H) \text{ and } \underset{\sim}{y}_2 \in Ra(K)\} \tag{2.78}$$

An operator H is a relation which satisfies two conditions: 1) $Do(H) = L_{2e}^n$, and 2) for each $\underset{\sim}{x} \in L_{2e}^n$ there exists a unique $\underset{\sim}{y} \in L_{2e}^m$ such that $(\underset{\sim}{x}, \underset{\sim}{y}) \in H$. The same notation is used for both relations and operators. It is usually not important to distinguish between them, and when it is, it is usually apparent. For the thesis, it would not have been necessary to define relations, except that the inverse of

operators are not necessarily operators.

The relation H can be considered to be a transformation from the input space L_{2e}^n to the output space L_{2e}^m, in which case the notation $\underset{\sim}{y} = H\underset{\sim}{x}$ indicates that $(\underset{\sim}{x},\underset{\sim}{y}) \in H$. This transformation is somewhat dangerous to use, however, because there may be none, one, or several $\underset{\sim}{y}$'s for which $(\underset{\sim}{x},\underset{\sim}{y}) \in H$. If H is an operator then the transformation is well defined (it exists for every $\underset{\sim}{x} \in L_{2e}^n$ and is unique).

The gain (or norm) of the relation H is defined by

$$\| H \|_{L_2} \triangleq \sup \frac{\| H\underset{\sim}{x} \|_\tau}{\| \underset{\sim}{x} \|_\tau} \tag{2.79}$$

where the suprenum is taken over all nonzero $\underset{\sim}{x} \in \text{Do}(H)$, all corresponding $H\underset{\sim}{x} \in \text{Ra}(H)$, and all $\tau \in R_+$. In other words, for all possible input-output pairs and for all possible truncations. Note that the ratio is always finite, and only the suprenum can be infinite.

The relation H is defined to be L_{2e}-stable if $\| H \|_{L_2} < \infty$, in which case there exists a constant k such that

$$\| H\underset{\sim}{x} \|_\tau < k \| \underset{\sim}{x} \|_\tau \tag{2.80}$$

for all $\underset{\sim}{x} \in \text{Do}(H)$, all corresponding $H\underset{\sim}{x} \in \text{Ra}(H)$, and all $\tau \in R_+$. This type of stability is usually called "bounded input bounded output" stability.

It may not be immediately apparent why an extended spaces are needed. The reason is that unstable relations cannot be defined on the unextended product space $L_2^n \times L_2^m$. A relation that is L_{2e}-stable maps L_2^n into L_2^m, but an unstable relation maps L_2^n into L_{2e}^m. Therefore, to consistently define L_{2e}-stable and unstable relations it is

necessary to use extended normed linear spaces.

2.4.3 Conic Sectors

In this section the concept of conic sectors is defined and discussed. Necessary and sufficient conditions for relations to belong to a conic sector are presented. The reason for using conic sectors will become apparent later - when sufficient conditions for closed loop stability are stated in terms of conic sectors.

Let H be a relation, and let C and R be operators. If

$$\| \underset{\sim}{y} - C\underset{\sim}{x} \|_T^2 \leq \| R\underset{\sim}{x} \|_T^2 - \epsilon \| \underset{\sim}{x} \|_T^2 \tag{2.81}$$

for all $(\underset{\sim}{x}, \underset{\sim}{y}) \in H$, $\tau \in R_+$, and for some $\epsilon > 0$ then H is said to be "strictly inside the conic sector with center C and radius R;" which is equivalently stated "strictly inside cone (C,R)." If (2.81) is true for some $\epsilon \geq 0$ then H is "inside cone (C,R)."

Now turn around the inequality sign. If

$$\| \underset{\sim}{y} - C\underset{\sim}{x} \|_T^2 \geq \| R\underset{\sim}{x} \|_T^2 + \epsilon \| \underset{\sim}{x} \|_T^2 \tag{2.82}$$

for all $(\underset{\sim}{x}, \underset{\sim}{y}) \in H, \tau \in R_+$, and for some $\epsilon > 0$ then H is "strictly outside cone (C,R)," and if (2.82) is true for some $\epsilon \geq 0$ then H is "outside cone (C,R)."

The easiest visual example of conic sectors is obtained from relations H which are memoryless nonlinear operators $y = h(x)$. For example, consider the function $y = h(x)$ plotted in Figure 2.7. function is bounded by lines with slopes c-r and c+r, which can be used to show

$$|y - cx| < |rx| \tag{2.83}$$
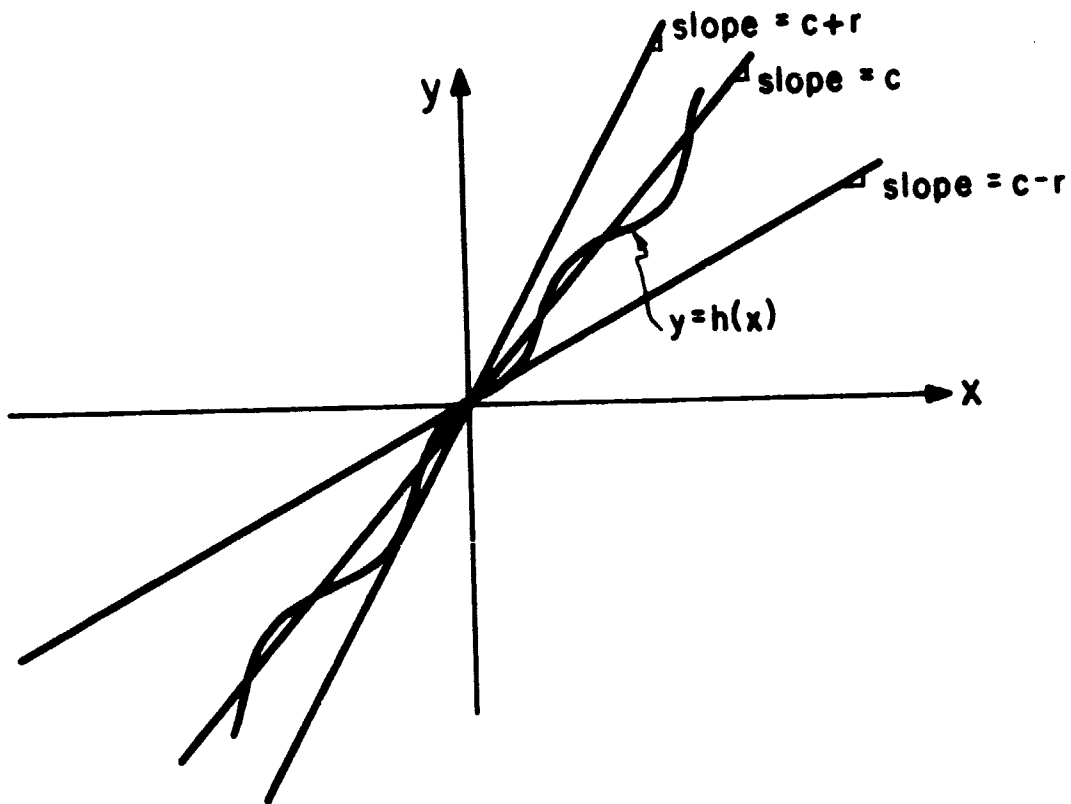
Figure 2.7: A memoryless nonlinearity inside conic sector (c,r)

This inequality implies (2.81) with $\varepsilon=0$, and therefore H is inside of cone (C,R), where C and R are memoryless __linear__ operators defined by $y = cx$ and $y = rx$.

One way to interpret H being inside of a cone (C,R) is to think of the center C as an approximation of H and to think of the radius R as a bound on the errors due to this approximation. Presumably if the approximation is to be of any use then R must in some sense be small. At the very least it should be the case that for a certain class of inputs $\underset{\sim}{x} \in S$ that $\|R\underset{\sim}{x}\|_\tau << \|C\underset{\sim}{x}\|_\tau$.

Another way to interpret conic sectors is to think of them as a bound on the energy of various signals. Consider the case[1] when for all $\underset{\sim}{x} \in L_2$

$$\|(H-C)\ \underset{\sim}{x}\|_{L_2} < \|R\underset{\sim}{x}\|_{L_2}^2 \tag{2.84}$$

The L_2 norm is a measure of energy, so this inequality states that the energy of $(H-C)\underset{\sim}{x}$ is less than or equal to the energy of $R\underset{\sim}{x}$. Let $\underset{\sim}{x} \in S$ be a set of signals that are in some way special. For example, inputs that have $> 99\%$ of their energy below 10 Hz. Then the center is a good approximation of H if the energy of $(H-C)\underset{\sim}{x}$ is small for all $\underset{\sim}{x} \in S$. One possible way to be quantitative about the approximation is to require for all $\underset{\sim}{x} \in S$ that $R\underset{\sim}{x}$ has $< 1\%$ of the energy of $C\underset{\sim}{x}$.

Two lemmas are now presented that give necessary and sufficient conditions for an operator to be either inside or outside of a cone. The

---

[1] The assumptions for this case are that $H, C,$ and R are operators, $H-C$ is stable, R is stable, and H is inside cone (C,R).

conic sector inequalities (2.81) and (2.82) are satisfied if and only if certain composite operators have gain $\leq$ 1. Safonov[1] states the results [9, p. 420], which to him fall into the "it can be shown" category. Here the attitude is not so cavalier, and proofs are included in the Appendix to Chapter 2.

Lemma 2.1 Let H, C, R, and R^I be operators such that $H-C$, R, and R^I are L_{2e}-stable. Then the following are equivalent:

(a) H is strictly inside cone (C,R)

(b) $\quad \| (H-C) \, R^I \|_{L_2}^2 \leq 1 - \epsilon \quad$ for some $\epsilon > 0$ ■ (2.85)

Lemma 2.2 Let H, C, R, R^I, and $(I + CH)^I$ be operators such that R, R^I, and $H(I + CH)^I$ are L_{2e}-stable. Then the following are equivalent

(a) $\quad -H^I$ is outside cone (C,R)

(b) $\| RH \, (I + CH)^I \|_{L_2}^2 \leq 1$ ■ (2.86)

The radius R is a very special type of operator. In these two lemmas, and everywhere else in this thesis, it is assumed that R and R^I are L_{2e}-stable operators. The assumption that they are operators is enough to imply a one-to-one mapping between functions in the domain and range of R. The additional assumption that R and R^I are L_{2e}-stable implies a one-to-one mapping between the finite norm parts of the domain and range.

What all of this means for LTI operators is that the Laplace

---

[1] See also Zames [5] and Desoer and Vidyasagar [8].

transform matrix $\underline{R}(s)$ is proper[1] and have no poles or zeros with real parts $\geq$ o, and in addition, $R^{-1}(s)$ is proper and has no poles or zeros with real parts $\geq$ o. Examples are $r(s) = 1$, $r(s) = (s+1)/(s + 10)$, and $r(s) = (1 - .5e^{-sT})/(1 - .9e^{-sT})$.

One of the subtle interpretations of Lemma 2.2 is that being outside of a cone is an inherently closed loop property[2]. If $-H^I$ is outside of cone (C,R) then it is not useful to think of C as an approximation of $-H^I$. It is better to think of C as any operator that stabilizes the feedback system

$$\left.\begin{array}{l} \underline{y} = H\underline{x} \\ \underline{x} = \underline{u} - C\underline{y} \end{array}\right\} \tag{2.87}$$

The assumption that $(I + CH)^I$ is an operator guarantees that the feedback system is well-posed (see Willems [20]). The additional assumption that $H(I + CH)^I$ is stable is another way of saying that the feedback system of (2.87) is closed loop stable.

2.4.4 The General Feedback System and the Small Gain Theorem

The general feedback system is shown in Figure 2.8. It will be referred to as System 1. The equations that define System 1 and the assumptions that the components satisfy are

$$\left.\begin{array}{l} \underline{u} = K\underline{e} \\ \underline{e} = \underline{r} - G\underline{u} \\ \underline{r}, \ \underline{e} \in L_{2e}^r, \ \underline{u} \in L_{2e}^m \\ G, \ K, \text{ and } (I + GK)^I \text{ are causal operators} \end{array}\right\} \tag{2.88}$$

---

[1] $\underline{R}(s)$ is proper if $\sigma_{max}[R(\infty)] < \infty$, ie # poles = # zeros, ie $R(j\omega)$ does not roll-off or grow as $\omega \to \infty$.

---

[2] In contrast to outside conic sectors being closed loop properties, inside conic sectors are inherently open loop properties.
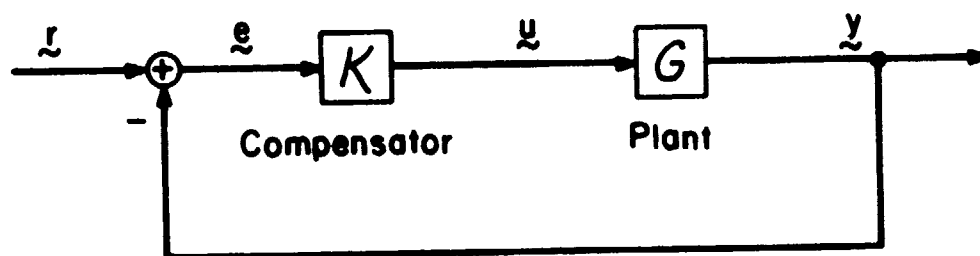
Figure 2.8: System 1, the general feedback system

Any mathematical model that represents a physical system should be well-posed and causal. The assumptions in (2.88) guarantee this. The stability theory of Zames [5,6] and Safonov [7,9] does not require well-posedness and causality. These assumptions are made here because the extra level of generality is not needed to analyze hybrid control systems.

The closed loop operators of System 1 are E and U, where

$$E \triangleq \{(\underset{\sim}{r},\underset{\sim}{e}) \mid (\underset{\sim}{r},\underset{\sim}{e}) \in L_{2e}^r \times L_{2e}^r \text{ and there exists } \underset{\sim}{u} \text{ such that}$$
$$(2.88) \text{ is satisfied}\} \tag{2.89}$$

and where U is defined in a similar way. The closed loop system is stable if E and U are L_{2e}-stable. Hence, closed loop stability is proved by showing that $\|E\|_{L_2}$ and $\|U\|_{L_2}$ are bounded.

The Small Gain Theorem is used to show that a certain class of systems is closed loop stable. The proof differs little from those of [5, Theorem 1] and [8, Theorem III.2.1].

Lemma 2.3 (The Small Gain Theorem) Consider System 1. If

$$\|K\|_{L_2} \cdot \|G\|_{L_2} < 1$$

then E and U are L_{2e}-stable. ∎

The Small Gain Theorem has a nice interpretation using the SISO Nyquist Theorem. Assume GK is SISO, LTI, L_{2e}-stable, and that

$$\|GK\|_{L_2} = \max_{\omega} |gk(j\omega)| < 1 \tag{2.90}$$

The sufficient condition of the Small Gain Theorem is satisfied and therefore the closed loop system is stable. The Nyquist plot is inside

the unit circle and cannot encircle the (-1, 0) point. Hence, by the Nyquist Theorem the same conclusion is reached that the closed loop system is stable.

Unfortunately, any system that satisfied (2.90) is of little practical use, because good command response (and other performance specifications) generally require that $|gk(j\omega)| \gg 1$ over some frequency range. The Small Gain Theorem would likewise be of little practical use if it were not for the Loop Transformation Theorem, which is discussed next.

2.4.5 Sufficient Conditions for Closed Loop Stability

If the operators G and K of System 1 satisfy certain conic sector conditions then the system is closed loop stable. This result is an extension of the Small Gain Theorem.

The extension is made possible by the Loop Transformation Theorem. A system is transformed to another system in such a way that the stability of the transformed system implies the stability of the original system. If G and K satisfy certain conic sector conditions then by the Small Gain Theorem the transformed system is stable, and by the Loop Transformation Theory the original system is stable.

This approach is due to Zames [5, 6]. His results are less general because the cone center and radius are constant multipliers. The generalization presented here, which allows the center and radius to be operators, is due to Safonov [7]. He goes even further in his generalizations, and the main results presented in this preliminary chapter (Lemmas 2.5, 2.6, and 2.7) are special cases of [7, Theorem 2.1].

The transformations of System 1 are shown in Figure 2.9a. After a few block diagram manipulations the result in System 2 of Figure 2.9b. The defining equations and the assumptions for System 2 are:

$$
\left.
\begin{aligned}
&\underset{\sim}{u}_2 = K_2 \, \underset{\sim}{e}_2 + C\underset{\sim}{r} \\[2mm]
&\underset{\sim}{e}_2 = R\underset{\sim}{r} - G_2 \, \underset{\sim}{u}_2 \\[2mm]
&\underset{\sim}{r}, \; \underset{\sim}{e}_2 \in L_{2e}^r, \; \underset{\sim}{u}_2 \in L_{2e}^m \\[2mm]
&G_2, \; K_2, \text{ and } (I + G_2 K_2)^I \text{ are causal operators}
\end{aligned}
\right\} \qquad (2.91)
$$

The transformations from System 1 are described algebraically by:

$$
\left.
\begin{aligned}
&K_2 = (K-C) \, R^I \\[2mm]
&G_2 = RG \, (I + CG)^I \\[2mm]
&\underset{\sim}{u}_2 = (I + CG) \, \underset{\sim}{u} \\[2mm]
&\underset{\sim}{e}_2 = R\underset{\sim}{e}
\end{aligned}
\right\} \qquad (2.92)
$$

The closed loop operators E_2 and U_2 respectively relate $\underset{\sim}{r}$ to $\underset{\sim}{e}_2$ and $\underset{\sim}{u}_2$.

Lemma 2.4   (Loop Transformation Theorem)

(a) $\underset{\sim}{r}$, $\underset{\sim}{u}$, and $\underset{\sim}{e}$ are solutions of System 1 if and only if $\underset{\sim}{r}$, $\underset{\sim}{u}_2$, and $\underset{\sim}{e}_2$ are solutions of System 2.

(b)   Furthermore if $(I + CG)^I$ and R^I are L_{2e}-stable then the stability of System 2 implies the stability of System 1.   ∎

The proof of part (a) differs little from those of [5, Theorem 2] and [8, Theorem III.6.3]. Part (b) follows after a few steps from (2.92).
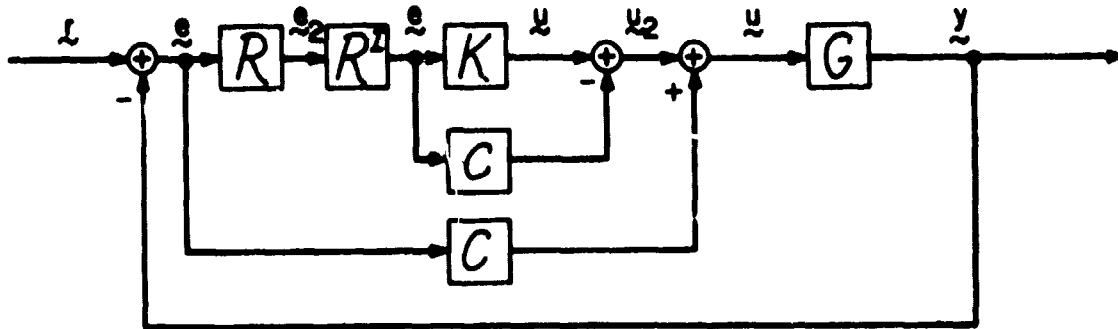
Figure 2.9a: Transformations of System 1

$$K_2 = (K-C)R^I \qquad G_2 = RG(I+CG)^I$$
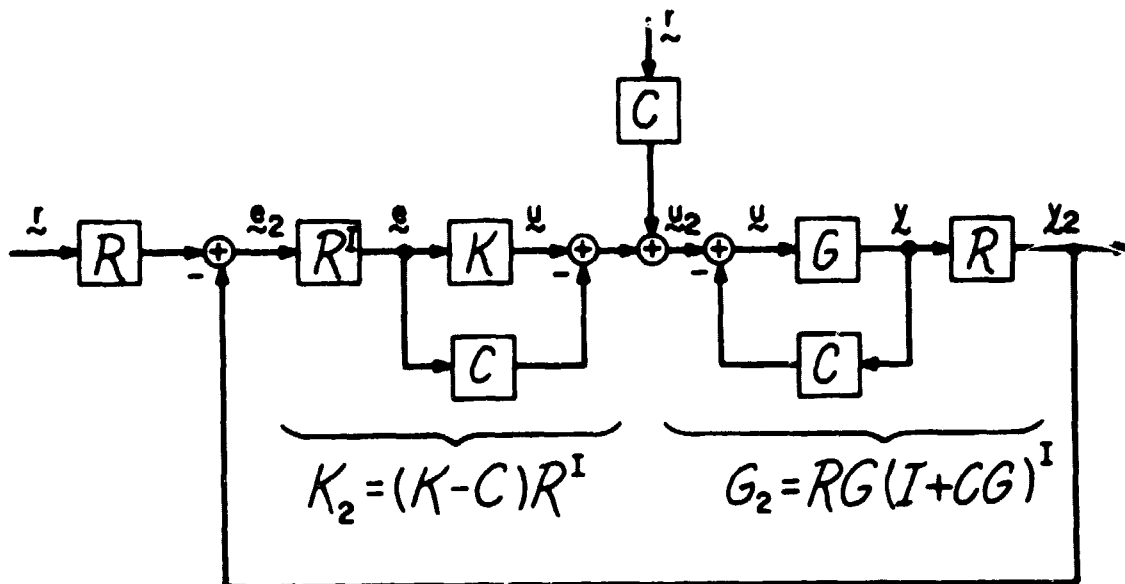
Figure 2.9b: System 2

<u>Lemma 2.5</u> (Sufficient Conditions for Closed Loop Stability, K Inside of a Cone). Consider System 1. Let C and R be operators such that $(I + CG)^I$, $G(I + CG)^I$, $K-C$, R, and R^I are L_{2e}-stable. Then System 1 is closed loop stable if

    (i) K is strictly inside cone (C,R)

    (ii) $-G^I$ is outside cone (C,R) ■

The proof is now sketched out. If the conic sector conditions (i) and (ii) are true then (by Lemmas 2.1 and 2.2) it follows that

$$\|K_2\|_{L_2} \cdot \|G_2\|_{L_2} \leq 1 - \epsilon \quad \text{for some } \epsilon > o \tag{2.93}$$

By the Small Gain Theorem (Lemma 2.3) it follows that System 2 is closed loop stable, and by the Loop Transformation Theorem (Lemma 2.4) it follows that System 1 is closed loop stable.

The major restriction of Lemma 2.5 is that $K-C$ must be L_{2e}-stable. Whatever is placed inside of the conic sector must be bounded by a stable radius.

Lemma 2.5 is a robustness as well as a stability result. The closed loop system will be stable not just for a particular K and G but for <u>any</u> K that satisfies (i) and <u>any</u> G that satisfies (ii).

Condition (i) of Lemma 2.5 states that the compensator K is inside of a cone. Sometimes it is more convenient to think of the plant G as being inside of a cone. Sufficient conditions for closed loop stability can also be derived when this is the case. A different transformation of System 1 is required, as shown in Figures 2.10a and 2.10b; and a different version of the Loop Transformation Theorem is required, so that stability of System 3 in Figure 2.10b implies the stability of
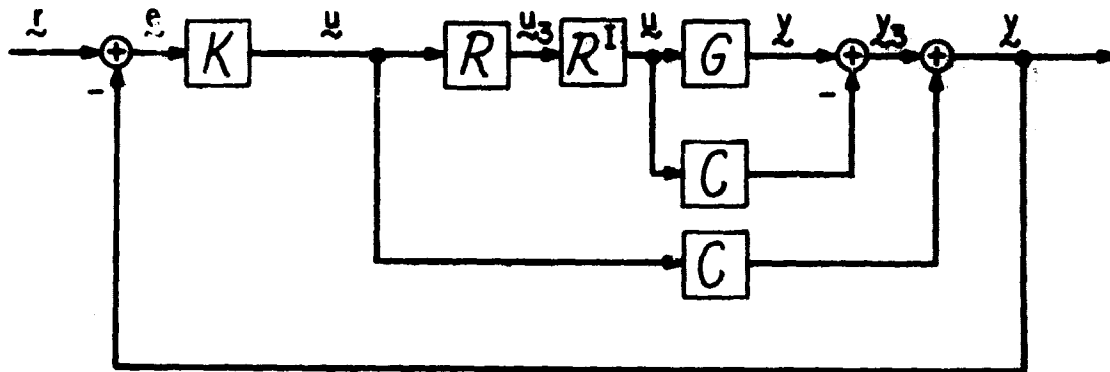
Figure 2.10a: Alternate transformation of system 1

$$K_3 = RK(I+CK)^I \qquad G_3 = (G-C)R^I$$
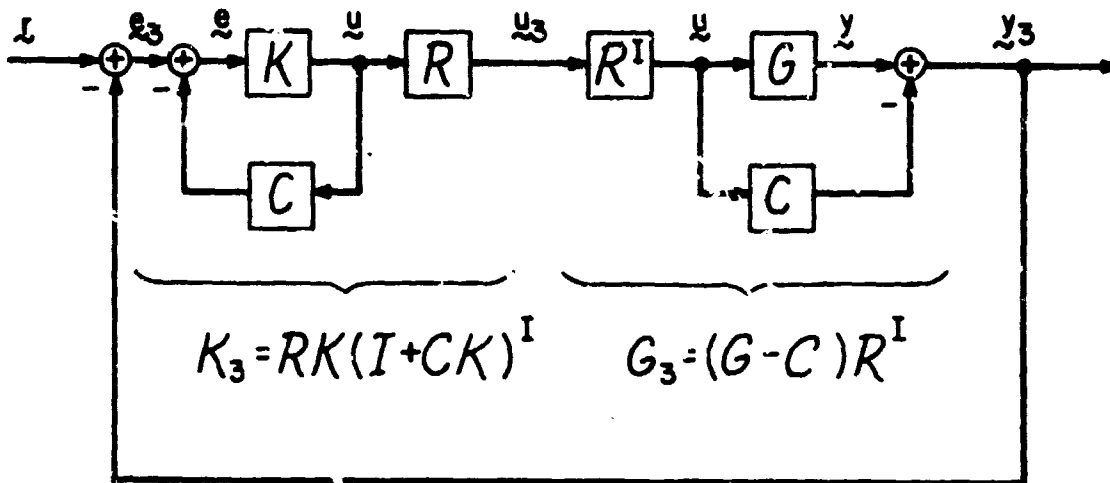
Figure 2.10b: System 3

System 1. The final result is shown below.

Lemma 2.6 (Sufficient Conditions for Closed Loop Stability, $-K^I$ Outside of a Cone). Consider System 1. Let C and R be operators such that $(I + CK)^I$, $K(I + CK)^I$, $G-C$, R, and R^I are L_{2e}-stable. Then System 2 is closed loop stable if

   (i) $-K^I$ is outside cone (C,R)

   (ii) G is strictly inside cone (C,R) ∎

The major restriction of Lemma 2.6 is that $G-C$ must be L_{2e}-stable. Just as is the case for Lemma 2.5, Lemma 2.6 is a robustness as well as a stability result.

Some of the references for t. e general feedback theory set up a version of System 1 that has symmetric inputs, thereby avoiding separate derivations for inside and outside conic sector conditions for closed loop stability. Symmetric inputs are not usual for hybrid control systems, however, and therefore for this thesis it was decided to include the two derivations.

One more set of sufficient conditions for closed loop stability is included. The difference here is that the loop transfer operator $T_1 = GK$ is placed inside of a cone. The general feedback system can still be considered to have two elements - one is T_1 and the other is I.

Lemma 2.7 (Sufficient conditions for closed loop stability. T_1 inside of a cone). Consider System 1. Let C and R be operators such that $(I + C)^I$, $T_1 - C$, R, and R^I are L_{2e}-stable. System 1 is closed loop stable if

   (i) T_1 is strictly inside cone (C,R)

   (ii) $\| R (I + C)^I \|_{L_2} < 1$ ∎

If condition (ii) is true then $-I$ is outside of cone (C,R). The major restriction of Lemma 2.7 is that $T_1 - C$ must be L_{2e}-stable.

2.4.6 Conic Sector Analysis of Command Response

Conic sectors can be used to analyze the response to signals that enter the feedback loop. The only signal that enters the general feedback system of Figure 2.8 is the command input r, which enters just before the prefilter.

In this thesis we will be interested in the steady state response to commands that belong to a set of command signals $S \subset L_{2e}^r$. In particular, we will be interested in the steady state response of low frequency sinusoidal inputs. Transient errors (overshoot, risetime, settling time, etc.) are not analyzed in this thesis.

The error signal is

$$\underline{e} = (I + GK)^I \underline{r} \qquad (2.94)$$

and the steady state command response specification is

$$\lim_{\tau \to \infty} \frac{\| \underline{e} \|_\tau}{\| \underline{r} \|_\tau} \leq q \quad \text{for all } \underline{r} \subset S \qquad (2.95)$$

The constant "q" is called the "quality measure". By letting the transient time τ approach infinity the transient errors become insignificant, and therefore the quality measure is a measure of the steady state error. It is in general difficult to compute the quality measure. As will be shown, conic sectors can be used to find an upperbound for q.

There are two approaches. The first is to place the loop transfer operator GK inside of a cone, and the second is to place the closed loop

operator $(I + GK)^I$ inside of a cone. The first approach is due to Stein [18][1], and the second approach is new.

Placing GK Inside of a Cone

Assume that the operators GK and C are L_{2e}-stable, and assume that GK is inside of the cone (C, R_1). Expand the error equation (2.94) as follows:

$$
\begin{aligned}
e &= (I + GK)^I \, r \\
&= (I + C + GK - C)^I \, r \\
&= (I + C)^I \, [I + (GK - C)(I + C)^I]^I \, r \\
&= (I + C)^I \left(I - [I + (GK - C)(I + C)^I]^I \, (GK - C)(I + C)^I \right) r
\end{aligned}
$$

$$(2.96)$$

Take the truncated norm of each side of (2.96), and then use singular value and conic sector inequalities to obtain

$$
\| e \|_\tau < \| (I + C)^I \, r \|_\tau + \frac{\| (I + C)^I \|_{L_2}}{1 - \| R_1 (I + C)^I \|_{L_2}} \, \| R_1 (I + C)^I \, r \|_\tau
$$

$$
\text{for all } r \in L_{2e}^r \text{ and all } \tau \in R_+ \qquad (2.97)
$$

---

[1]Stein [18] defines the quality measure by

$$
\frac{\| e \|_\tau}{\| r \|_\tau} < q \quad \text{for all } r \in S \text{ and for all } \tau \in R_+
$$

This quality measure is valid for transient as well as steady state errors.

An upperbound for the quality measure is

$$q \leq q_o \left(1 + \frac{s^*}{m^*} r_1\right) \quad \text{for all } r \in S \qquad (2.98)$$

where

$$q_o \leq \lim_{\tau \to \infty} \frac{\left\| (I + C)^I r \right\|_\tau}{\left\| r \right\|_\tau} \quad \text{for all } r \in S$$

$$m^* = 1 - \left\| R_1 (I + C)^I \right\|_{L_2}$$

$$s^* = \left\| (I + C)^I \right\|_{L_2} \qquad \qquad (2.99)$$

$$r_1 q_o \leq \lim_{\tau \to \infty} \frac{\left\| R_1 (I + C)^I r \right\|_\tau}{\left\| r \right\|_\tau} \quad \text{for all } r \in S$$

The constant "q_o" is the "nominal quality measure," which is obtained when the operator GK is replaced by C. The constant $\left(1 + \frac{s^*}{m^*} r_1\right)$ is the amount by which q_o must be raised to obtain an upperbound for q. If the set S is sinewaves with frequencies less then ω_o, and if C and R_1 are LTI operators, then the constants in (2.99) are

$$q_o = \max_{o < \omega < \omega_o} \sigma_{max} \left[(I + C)^{-1} (j\omega) \right]$$

$$m^* = 1 - \max_{\omega} \sigma_{max} \left[R_1 (I + C)^{-1} (j\omega) \right]$$

$$s^* = \max_{\omega} \sigma_{max} \left[(I + C)^{-1} (j\omega) \right] \qquad (2.100)$$

$$r_1 q_c = \max_{o < \omega < \omega_o} \sigma_{max} \left[R_1 (I + C)^{-1} \ \ \right]$$

Two restrictions to the use of (2.98) are (1) that GK must be open
loop stable and (2) that the cone around GK must meet the sufficient
conditions for closed loop stability.[1] In addition to these restrictions
there is also the problem that (2.98) may give a conservative upperbound
for q. By "conservative" it is meant that the upperbound for q is higher
than it needs to be. If the cone around GK is not very tight, then m* will
be small and r_1 will be large - both of which lead to conservativeness.
Two more sources of conservativeness are that both m* and s* use operator
norms, and hence must be true for all input signals and not just $\underset{\sim}{r} \in S$

Despite the problems mentioned above, equation (2.98) is a natural
generalization of LTI results - specifically (2.21) and [1, equation (19)].
It is a first attempt at using conic sectors to analyze command response
(as opposed to the more common uses of conic sectors to analyze closed
loop stability and robustness). One advantage of working with GK instead
of $(I + GK)^I$ is that the perturbations of G and K are easier to separate.
For example, a multiplicative perturbation of G is also a multiplicative
perturbation of GK, but not of $(I + GK)^I$.

Placing $(I + GK)^I$ Inside of a Cone

Assume that the operators $(I + GK)^I$ and $(I + C)^I$ are L_{2e}-stable,
and assume that $(I + GK)^I$ is inside of the cone $[(I + C)^I, R_2]$.[2] Expand

---

[1] It must be true that $\| R_1 (I + C)^I \|_{L_2} < 1$, which is the sufficient
condition for closed loop stability given in Lemma 2.7. If this in-
equality is not satisfied then m* < o.

[2] The operator C is an approximation of GK. The open loop stability
assumptions of C and GK are replaced by the less restrictive assumptions
of closed loop stability.

the error equation (2.94) by adding and then subtracting $(I + C)^I \underset{\sim}{r}$:

$$\underset{\sim}{e} = (I + GK)^I \underset{\sim}{r}$$

$$= (I + C)^I \underset{\sim}{r} + [(I + GK)^I - (I + C)] \underset{\sim}{r} \qquad (2.101)$$

An upperbound for the quality measure is

$$q \leq q_o (1 + r_2) \quad \text{for all } \underset{\sim}{r} \in S \qquad (2.102)$$

where

$$q_o \leq \lim_{\tau \to \infty} \frac{\| (I + C)^I \underset{\sim}{r} \|_\tau}{\| \underset{\sim}{r} \|_\tau} \quad \text{for all } \underset{\sim}{r} \in S \qquad (2.103)$$

$$r_2 q_o \leq \lim_{\tau \to \infty} \frac{\| (I + GK)^I - (I + C)^I \underset{\sim}{r} \|_\tau}{\| \underset{\sim}{r} \|_\tau} \quad \text{for all } \underset{\sim}{r} \in S \qquad (2.104)$$

As before, the constant q_c is the nominal quality measure. The constant $(1 + r_2)$ is the amount that q_o must be raised to obtain an upperbound tor q.

One way to compute the constant r_2 is to construct a cone $[(I + C)^I, R_2]$ that contains $(I + GK)^I$. It follows that

$$r_2 q_o < \frac{\| R_2 \underset{\sim}{r} \|_\tau}{\| \underset{\sim}{r} \|_\tau} \quad \text{for all } \underset{\sim}{r} \in L_{2e}^r \text{ and all } \tau \in R_+ \qquad (2.105)$$

Equation (2.105) may result in a conservative (i.e. large) estimate for $r_2 q_o$ because (1) the conic sector does not take advantage of the restricted set $\underset{\sim}{r} \in S$ and (2) the conic sector must be valid for all possible truncations of the input signal.

An alternate form of (2.104) is

$$r_2 q_o \leq \lim_{\tau \to \infty} \frac{\| [GK (I + GK)^I - C(I + C)^I] \underset{\sim}{r} \|_\tau}{\| \underset{\sim}{r} \|_\tau} \quad \text{for all } \underset{\sim}{r} \in S$$

(2.106)

which is derived from (2.104) by use of the identity

$$(I + A)^I = I - A (I + A)^I$$

(2.107)

This alternate form is easier to use for hybrid operators. It is interesting to note that conic sectors that contain $(I + GK)^I$ and $GK (I + GK)^I$ have the same radius.

In this subsection two different approaches have been discussed for using conic sectors to analyze the steady state response to commands. Either the loop transfer operator GK or the closed loop operator $(I + GK)^I$ can be placed inside of a cone.

2.5 Conic Sector Analysis of Analog Feedback Systems

The general feedback theory is just that - general. It is only when specific assumptions are made about the feedback system that the results from the general feedback theory can be applied.

In this section the conic sector analysis techniques are applied (for better or for worse) to the analog feedback system of Section 2.2. The feedback system is briefly described, sufficient conditions for LTI operators to be inside or outside of a cone are presented, and then sufficient conditions for robust closed loop stability are presented.

The conic sector analysis techniques are not as general as the analysis techniques of Section 2.2. The distinction is that conic sectors cannot be used for unstable perturbations of the analog plant.

The compensator and nominal plant are modelled, respectively, by K and G. The uncertainty of the nominal plant is modelled by the additive perturbation E_a, where

$$\tilde{G} = G + E_a \tag{2.108}$$

and where E_a is a L_{2e}-stable LTI operator. The only other information known about E_a is a bound on the magnitude of its Fourier transform matrix:

$$\sigma_{max} [E_a(j\omega)] \leq \ell_a(\omega) \quad \text{for all } \omega \tag{2.109}$$

The uncertainty of the nominal plant can also be modelled by the multiplicative perturbation E_m, where

$$\tilde{G} = G(I + E_m) \tag{2.110}$$

$$\sigma_{max} [E_m(j\omega)] < \ell_m(\omega) \quad \text{for all } \omega \tag{2.111}$$

and where $E_a = GE_m$ is L_{2e}-stable.[1]

Three Lemmas are now presented: Lemma 2.8 gives sufficient conditions for $\tilde{G}$ to be strictly inside of a cone, Lemma 2.9 gives sufficient conditions for $-K^I$ to be outside of a cone, and Lemma 2.10 combines the previous two and gives sufficient conditions for robust closed loop stability.[2]

__Lemma 2.8__ Let $\tilde{G}$, G, R, and R^I be LTI operators such that $\tilde{G}-G$, R, and R^I are L_{2e}-stable. $\tilde{G}$ is strictly inside cone (G, R) if

$$\sigma_{min} \ [\underline{R}(j\omega)] \geq \frac{1}{(1-\epsilon)^{1/2}} \ \sigma_{max} \ [\underline{\tilde{G}}(j\omega) - \underline{G}(j\omega)] \qquad (2.112)$$

for all ω and some $\epsilon > 0$ ■

__Lemma 2.9__ Let K, G, R, and R^I be LTI operators such that $K(I + GK)^I$, R, and R^I are L_{2e}-stable. $-K^I$ is outside cone (G,R) if

$$\sigma_{max} \ [\underline{RK} \ (\underline{I} + \underline{GK})^{-1} \ (j\omega)] \leq 1 \quad \text{for all } \omega \qquad ■(2.113)$$

__Lemma 2.10__ Consider the analog feedback system containing the LTI operators K, G, and $\tilde{G}$. Let R and R^I be L_{2e}-stable LIT operators. The closed loop system is stable for all possible $\tilde{G}$'s if there exists an $\underline{R}(j\omega)$ such that

---

[1] The requirement that E_a is L_{2e}-stable means that the exact number and the exact location of unstable poles of $\underline{G}(s)$ must be known. The less restrictive requirement in Section 2.2 is that $\underline{G}(s)$ and $\underline{\tilde{G}}(s)$ must have the same number of unstable poles, which means that only the exact number of unstable poles must be known.

---

[2] Lemmas 2.8, 2.9, and 2.10 (for analog systems) correspond, respectively, to Theorems 3.2, 3.6, and 3.7 (for hybrid systems). Lemmas 2.8 and 2.9 are due to Safonov [9, Lemmas A4 and A2]. He gives necessary and sufficient conditions to be conic. Only the sufficient conditions are presented here, to facilitate comparison with the results for hybrid systems.

(i) $K(I + GK)^I$ is L_{2e}-stable

(ii) $\sigma_{max} [RK (I + GK)^{-1} (j\omega)] \leq 1$ for all ω (2.114)

(iii) $\sigma_{min} [R(j\omega)] > \ell_a(\omega)$ for all ω ■   (2.115)

The proof for Lemma 2.10 can be quickly sketched out. Conditions (i) and (ii) guarantee that $-K^I$ is outside of cone (G , R). Condition (iii) guarantees that $\tilde{G}$ is strictly inside cone (G , R). Hence, by Lemma 2.6, the analog system is closed loop stable.

The first step in applying conic sectors to analog feedback systems is to construct a cone (G, R) such that all possible $\tilde{G}$'s are strictly inside of it. By Lemma 2.8, this is true if

$$\sigma_{min} [R(j\omega) \geq \frac{1}{(1-\epsilon)^{1/2}} \ell_a(\omega)$$ (2.116)

for all ω and some $\epsilon > o$

The ϵ term is a nuisance. It suffices to repace (2.115) with the strict inequality:

$$\sigma_{min} [R(j\omega)] > \ell_a(\omega)$$ uniformly in ω (2.117)

If the uncertainty is modelled by a multiplicative perturbation then (2.117) is replaced by

$$\sigma_{min} [R(j\omega)] > \ell_m(\omega) \cdot \sigma_{max} [G(j\omega)]$$ uniformly in ω (2.118)

Note that the additive perturbation E_a cannot in general be used as the radius of the cone. A radius must have the property that both it and its inverse are L_{2e}-stable. This is not assumed about E_a - only that E_a is stable. The problem is that $E_a(j\omega)$ may roll off, whereas $R(j\omega)$ must eventually flatten out (or become periodic). This distinction

is not cf practical importance, however, because the radius can be
arbitrarily close to bound $\ell_a(\omega)$ out to arbitrarily high frequencies.

Appendix to Chapter 2

This appendix contains proof of Lemmas 2.1 and 2.2.

Proof of Lemma 2.1 Here it is shown that H is strictly inside of cone (C, R) if and only if the operator $(H - C) R^I$ has gain $\leq 1 - \epsilon$ for some $\epsilon > 0$. The operators are defined on the cross product spaces:

$$
\left.
\begin{array}{l}
H, C \subset L_{2e}^n \times L_{2e}^m \\[2ex]
R \subset L_{2e}^n \times L_{2e}^n \\[2ex]
(H-C)R^I \subset L_{2e}^n \times L_{2e}^m
\end{array}
\right\}
\tag{2.A.1}
$$

Each step in the proof is equivalent. Explanations are enclosed in parenthesis.

H is strictly inside cone (C, R) (2.A.2)

$\Longleftrightarrow \quad \| y - Cx \|_\tau^2 < \| Rx \|_\tau^2 - \epsilon \| x \|_\tau^2$ (2.A.3)

   for all $(x, y) \in H$, all $\tau \in R_+$, and some $\epsilon > 0$
   (definition of strictly inside)

$\Longleftrightarrow \quad \| (H-C) x \|_\tau^2 < \| Rx \|_\tau^2 - \epsilon \| x \|_\tau^2$ (2.A.4)

   for all $x \in L_{2e}^n$, all $\tau \in R_+$, and some $\epsilon > 0$
   (because H, C, and R are operators with the same
   domains)

$\Longleftrightarrow \quad \| (H-C)R^I \xi \|_\tau^2 < \| \xi \|_\tau^2 - \epsilon \| R^I \xi \|_\tau^2$ (2.A.5)

   for all $\xi \in L_{2e}^n$, and $\tau \in R_+$, and some $\epsilon > 0$

   where $\xi \triangleq Rx$

   (because R and R^I are operators)

$$\Longleftrightarrow \quad \| (H-C)R^I \underset{\sim}{\xi} \|_\tau^2 \leq \| \underset{\sim}{\xi} \|_\tau^2 (1-\epsilon') \tag{2.A.6}$$

for all $\underset{\sim}{\xi} \in L_{2e}^n$, all $\tau \in R_+$, and some $\epsilon' > 0$

where $\epsilon' = \alpha^2 \epsilon$ and

$$\alpha \leq \frac{\| R^I \underset{\sim}{\xi} \|_\tau}{\| \underset{\sim}{\xi} \|_\tau} \quad \text{for all } \| \underset{\sim}{\xi} \|_\tau \neq 0$$

($\alpha < \infty$ because R^I is L_{2e}-stable)

$$\Longleftrightarrow \quad \| (H-C)R^I \|_2^2 \triangleq \sup \frac{\| (H-C)R^I \underset{\sim}{\xi} \|_\tau^2}{\| \underset{\sim}{\xi} \|_\tau} < 1 - \epsilon' \tag{2.A.7}$$

suprenum taken over all $\underset{\sim}{\xi} \in L_{2e}^n$ with

$\| \underset{\sim}{\xi} \|_\tau^2 \neq 0$ and all $\tau \in R_+$

(only possible if $H-C$ and R^I are L_{2e}-stable)

This complete the proof.

Proof of Lemma 2.2 Here it is shown that $-H^I$ is outside of a cone if and only if the operator $RH(I + CH)^I$ has gain ≤ 1. The operators are defined on the following cross product spaces:

$$
\left.
\begin{array}{l}
-H^I \cdot C \subset L_{2e}^m \times L_{2e}^n \\[2mm]
R \subset L_{2e}^m \times L_{2e}^m \\[2mm]
RH(I + CH)^I \subset L_{2e}^n \times L_{2e}^m
\end{array}
\right\}
\qquad (2.A.8)
$$

Note that the center and radius differ from those of Lemma 2.1. Each step in the following is equivalent:

$$-H^I \text{ is outside cone } (C,R) \qquad (2.A.9)$$

$$\Longleftrightarrow \| \underset{\sim}{x} - C\underset{\sim}{y} \|_\tau^2 \geq \| R\underset{\sim}{y} \|_\tau^2 \qquad (2.A.10)$$

for all $(\underset{\sim}{y},\underset{\sim}{x}) \in -H^I$ and all $\tau \in R_+$

(by definition)

$$\Longleftrightarrow \| (I + CH) \underset{\sim}{x} \|_\tau^2 \geq \| RH\underset{\sim}{x} \|_\tau^2 \qquad (2.A.11)$$

for all $\underset{\sim}{x} \in L_{2e}^n$ and all $\tau \in R_+$

(because H is an operator)

$$\Longleftrightarrow \| \underset{\sim}{\xi} \|_\tau^2 \geq \| RH(I + CH)^I \underset{\sim}{\xi} \|_\tau^2 \qquad (2.A.12)$$

for all $\underset{\sim}{\xi} \in L_{2e}^n$ and all $\tau \in R_+$

(because $(I + CH)$ and $(I + CH)^I$ are operators)

$$\iff \quad \| RH(I + CH)^I \|_2^2 = \sup \frac{\| RH(I + CH)^I \underset{\sim}{\xi} \|_\tau^2}{\| \underset{\sim}{\xi} \|_\tau^2} \leq 1 \qquad (2.A.13)$$

suprenum taken over all $\underset{\sim}{\xi} \in L_{2e}^n$ with $\| \underset{\sim}{\xi} \|_\tau^2 \neq o$

and all $\tau \in R_+$.

(only possible if R and $H(I + CH)^I$ are L_{2e}-stable)

This completes the proof.

3. CONIC SECTORS FOR HYBRID OPERATORS

3.1 Introduction

The major theoretical results of this thesis are presented in this chapter. It is here that the conic sector analysis techniques developed for general feedback systems are applied to hybrid feedback systems. The results are condensed into eight theorems, which are now briefly described:

Theorem 3.1: An upper bound for the gain of the hybrid operator.

Theorem 3.2: Sufficient conditions for a hybrid operator to be inside of a cone.

Theorem 3.3: Sufficient conditions for closed loop stability when the hybrid operator is inside of a cone.

Theorem 3.4: First approach to sufficient conditions for robust closed loop stability when the hybrid operator is inside of a cone.

Theorem 3.5: Second approach to sufficient conditions for robust closed loop stability when the hybrid operator is inside of a cone.

Theorem 3.6: Sufficient conditions for a hybrid operator to be outside of a cone.

Theorem 3.7: Sufficient conditions for robust closed loop stability when the hybrid operator is outside of a cone.

Theorem 3.8: Use of the closed loop hybrid operator to analyze command response.

The theorems about closed loop stability and command response (3.3, 3.4, 3.5, 3.7, and 3.8) all begin with the statement: "Consider the hybrid feedback system." This refers to the hybrid feedback system of Section 2.3, which is a special case of System 1 of Section 2.4. For the hybrid feedback system:

- The compensator is modelled with the casual hybrid operator K, which relates the Laplace transforms of its input and output by $\underline{u}(s) = \underline{H}(s) \underline{D}^*(s) [\underline{F}(s)\underline{e}(s)]^*$.

- The nominal and actual plants are modelled by the causual LTI operators G and $\tilde{G}$, which are related by either the additive perturbation E_a or the multiplicative perturbation E_m, as described by equations (2.108) to (2.111).

- Associated with the hybrid feedback system are the LTI operators C, R, and R^I; which form the center and radius of various conic sectors. It is always assumed that R and R^I are L_{2e}-stable. This, and any other assumptions of open loop or nominal closed loop stability, are explicitly stated in the Theorems.

- The hybrid feedback system is assumed to be well-posed and causal, in other words it is assumed that $(I+GK)^I$ is a casual operator. For Theorems 3.3, 3.4, and 3.5 it is also assumed that $(I+CG)^I$ is a casual operator.

A distinction is made between "closed loop stability" (Theorem 3.3) and "robust closed loop stability" (Theorems 3.4, 3.5, and 3.7). The former applies only to the nominal plant G, and the latter to all possible plants $\tilde{G}$. A distinction is also made as to whether the hybrid operator is inside of a cone (Theorems 3.2 to 3.5) or outside of a cone (Theorems 3.6 and 3.7). When the hybrid operator is inside of a cone, then the center C can be viewed as a LTI approximation of K. On the other hand, when the hybrid operator is outside of a cone, the center C can be viewed as an approximation of the plant, and is usually set equal to the nominal plant G.

3.2   The Gain of the Hybrid Operator

One of the properties of an operator is its gain [see (2.79)].

It is the maximum ratio of output norm to input norm. An upperbound

for the gain of the hybrid operator K is presented in Theorem 3.1.

When K is SISO then an input signal can be constructed which achieves

the upperbound, hence the upperbound actually is the gain.

Theorem 3.1   Let K be a stable hybrid operator.

(a) An upperbound for the gain of K is

$$\|K\|_{L_2} \leq \max_{0 \leq \omega \leq \frac{\pi}{T}} \left\{ \frac{1}{T} \left[\sum_k \|\underline{H}_k\|^2 \right]^{1/2} \cdot \|\underline{D}^*\| \cdot \left[\sum_n \|\underline{F}_n\|^2 \right]^{1/2} \right\} \qquad (3.1)$$

(b) Furthermore, if K is SISO then (3.1) is true with equality. ∎

The proof is presented in the Appendix to Chapter 3. Included in

the proof of part (b) is a signal which achieves the upperbound.   At

the end of the proof a conjecture is made about the actual gain in the

multivariable case.

After some thought (possibly after considerable thought), Theorem

3.1 should be as intuitively reasonable as the corresponding result for

a LTI operator H, which is

$$\|H\|_{L_2} = \max_{\omega} \|\underline{H}(j\omega)\| \qquad (3.2)$$

The input signal that achieves the maximum gain for LTI operators is a

sinewave at the frequency ω_0 that maximizes (3.2). The corresponding

input signal for hybrid operators is an infinite series of sinewaves.

The fundamental frequency is the ω_0 that maximizes (3.1), and the other

frequencies are shifted away from ω_0 by integer multiples of ω_s.

The gain of the hybrid compensator depends on how fast the pre-filter rolls off. Consider when the impulse response of the SISO pre-filter approaches an impulse, i.e. when $f(j\omega) \to 1$. The infinite sum $\sum_n \|f_n\|^2$ approaches infinity, which implies that the gain of the hybrid operator approaches infinity. Spurious inputs such as noise will be greatly amplified. Hence, Theorem 3.1 can be used to justify the need for adequate prefiltering. This duplicates a result of Kostovetsky [17].

The gain also depends on how fast the hold rolls off. In fact, the hold is treated exactly the same way as the prefilter. This results in the intuitively pleasing symmetry of equation (3.1). This symmetry is important when the hybrid compensator is included in a feedback system, in which case it is not obvious which parts of the loop should be included in the prefilter and which parts should be included in the hold.

3.3 A Cone that Contains the Hybrid Operator

3.3.1 Existence

For any stable hybrid operator K there exists a cone (C,R) such that K is strictly inside of the cone. This result is presented in Theorem 3.2.

Theorem 3.2 Let K be a stable hybrid operator, let C be **any** LTI l_{2e}-stable operator, and let R and R^I be LTI l_{2e}-stable operators.

(a) K is strictly inside cone (C,R) if

$$\sigma_{min} \left[\underline{R}(j\omega)\right] \geq \frac{1}{(1-\epsilon)^{1/2}} \left[r_1(\omega) - r_2(\omega) + r_3(\omega)\right]^{1/2} \tag{3.3}$$

for all ω and some $\epsilon > 0$

where

$$r_1(\omega) = \frac{1}{T^2} \left[\sum_k \|\underline{H}_k\|^2\right] \cdot \|\underline{D}^*\|^2 \cdot \left[\sum_n \|\underline{F}_n\|^2\right] \tag{3.4}$$

$$r_2(\omega) = \frac{1}{T^2} \sum_k \|\underline{H}_k \underline{D}^* \underline{F}_k\|^2 \tag{3.5}$$

$$r_3(\omega) = \sum_k \|\frac{1}{T} \underline{H}_k \underline{D}^* \underline{F}_k - \underline{C}_k\|^2 \tag{3.6}$$

(b) Furthermore, the optimal center

$$\underline{C}(s) = \frac{1}{T} \underline{H}(s) \underline{D}^*(s) \underline{F}(s) \tag{3.7}$$

minimizes the lower bound for $\sigma_{min} [\underline{R}(j\omega)]$. ∎

The proof of this result is in the Appendix to Chapter 3. A few remarks are now made to highlight the theorem. A conic sector exists for any **stable** hybrid operator. The stability requirement is the major

limitation of this theorem, in fact it is the major limitation of all the inside conic sector results. Unstable hybrid operators (which includes hybrid operators with digital integrators) cannot be bounded by finite radii.

The conic sector is not unique - and not always useful. The choice of center determines to a large extent how useful the conic sector is. The center should be a good approximation of the low frequency behavior of the hybrid operator.

Usually, but not always, the optimal center (3.7) is a good choice. It has the distinct advantage of minimizing the radius. Also, since this choice makes $r_3(\omega) = 0$, there is one less term to compute. The optimal center is an infinite dimensional LTI operator. If a low order rational polynominal center is desired then use

$$\underline{C}(s) = \frac{1}{T} \underline{H}_a(s) \ \underline{K}(s) \ \underline{F}(s) \tag{3.8}$$

where $\underline{H}_a(s)$ is an approximation of a zero-order-hold, such as (2.47). If the objective is to compare different discretization techniques then use

$$\underline{C}(s) = \frac{1}{T} \underline{H}(s) \ \underline{K}(s) \ \underline{F}(s) \tag{3.9}$$

The magnitude of the radius will rise or fall depending on how well $\underline{D}^*(s)$ approximates $\underline{K}(s)$ at low frequencies.

An alternate equation for the radius uses a double summation:

$$\sigma_{\min}\left[\underline{R}(j\omega)\right] \geq \frac{1}{(1-\epsilon)^{1/2}} \left[r_4(\omega) + r_3(\omega)\right]^{1/2} \tag{3.10}$$

where

$$r_4(\omega) = \frac{1}{T^2} \sum_k \sum_{n \neq k} \| \underline{H}_k \underline{D}^* \underline{F}_n \|^2 \tag{3.11}$$

and wher. $r_3(\omega)$ is given by (3.6). For SISO systems $r_4(\omega) = r_1(\omega) - r_2(\omega)$, and for multivariable systems $r_4(\omega) \leq r_1(\omega) - r_2(\omega)$. Whether to use (3.3) or (3.10) to compute the radius is primarily a computational issue, as discussed in Section 4.3.

Theorem 3.2 only gives a lower bound for the radius. It is always best to choose $\underline{R}(j\omega)$ so that it actually equals the lower bound, because this choice gives the least conservative stability and robustness results. If $\underline{R}(j\omega)$ is multivariable then all of its singular values should be set equal to the lower bound. This is done by making $\underline{R}(j\omega)$ a diagonal matrix with equal diagonal entries.

An important point to make about the radius is that it is computable. In the examples of Chapter 5 the radius is computed for many different values of ω and then plotted on a magnitude Bode plot. The radius is periodic with period ω_s, and need only be computed over the frequency range 0 to $\omega_s/2$.

The radius $\underline{R}(j\omega)$ corresponds to an additive perturbation, whereas the quantity $\underline{R}(j\omega)\underline{C}^{-1}(j\omega)$ corresponds to a multiplicative perturbation. The quantity $\underline{R} \ \underline{C}^{-1}(j\omega)$ is called the "multiplicative radius." It contains information about the size of the radius relative to the center, which is usually more important than the absolute size of the radius. The center $\underline{C}(j\omega)$ is a good approximation of the hybrid operator K over the frequency range where $\sigma_{max}\left[\underline{R} \ \underline{C}^{-1}(j\omega) \right] << 1$.

If the hybrid operator is SISO and if the optimal center is used for the cone then the multiplicative radius is independent of the

computer transform d*(s). In this case the multiplicative radius depends only on the prefilter and hold. All of the closed loop stability, robustness, and performance results do depend (of course) on the computer z-transform.

The last comment is that Theorem 3.1 is a special case of Theorem 3.2. If the choice of center is $\underline{C}(s)=\underline{0}$, then $r_2(\omega) = r_3(\omega)$, which means that $-r_2(\omega) + r_3(\omega) = 0$. What remains of (3.3) can be used in place of (3.1) of Theorem 3.1.

3.3.2 Closed Loop Stability

The hybrid operator K is one part of a hybrid feedback system. Sufficient conditions for closed loop stability are now presented.

Theorem 3.3 Consider the hybrid feedback system (see Section 3.1). Assume K, C, R, and R^I are L_{2e}-stable. The hybrid feedback system is closed loop stable if a C and R exist such that

   (i) K is strictly inside cone (C,R)

   (ii) $G(I+CG)^I$ is L_{2e}-stable

   (iii) $\sigma_{max}\left[\underline{R}\ \underline{G}(\underline{I} + \underline{C}\ \underline{G})^{-1}(j\omega)\right] \leq 1$ for all ω ■ (3.12)

The proof can be quickly sketched out. If condition (i) is true then K is strictly inside cone (C,R). Such a cone always exists (by Theorem 3.2), because it is assumed that K is L_{2e}-stable. If conditions (ii) and (iii) are true then $-G^I$ is outside of the same cone (by Lemma 2.8). The fact that K is strictly inside and $-G^I$ is outside of the same cone implies that the hybrid system is closed loop stable (by Lemma 2.5).

Theorem 3.3 is applied by first constructing a $\underline{C}(j\omega)$ and $\underline{R}(j\omega)$ such that condition (i) is true, and then by using $\underline{C}(j\omega)$ and $\underline{R}(j\omega)$ to check conditions (ii) and (iii). The major restriction of this theorem is that the hybrid operator must be open loop stable. This guarantees

the existence of a $\underline{C}(j\omega)$ and $\underline{R}(j\omega)$ such that condition (i) is true. If the hybrid operator is not open loop stable then Theorem 3.3 cannot be used to determine closed loop stability.

Condition (ii) is a check for nominal closed loop stability. The nominal system is an analog LTI system, and therefore standard techniques can be used to determine closed loop stability (see Subsection 2.2.5).

The singular value inequality (3.12) can be graphically checked on a magnitude Bode plot. This is done in the examples of Chapter 5. The inequality (3.12) is implied by either of the following:[1]

$$\sigma_{max}\left[\underline{R}(j\omega)\right] \cdot \sigma_{max}\left[\underline{G}\ (\underline{I} + \underline{C}\ \underline{G})^{-1}(j\omega)\right] \leq 1 \quad \text{for all } \omega \quad (3.13)$$

$$\sigma_{max}\left[\underline{R}\ \underline{C}^{-1}(j\omega)\right] \leq \sigma_{min}\left[\underline{I} + (\underline{C}\ \underline{G})^{-1}(j\omega)\right] \quad \text{for all } \omega \quad (3.14)$$

It is (3.13) that is used in the examples. The problem with (3.14) is that it cannot be used if $\underline{C}(j\omega) = \underline{0}$ for some ω. This happens whenever the hold $\underline{H}(j\omega)$ is a zero-order-hold and the center that is chosen includes $\underline{H}(j\omega)$. The only way that (3.14) can be used is if the center includes an approximation to $\underline{H}(j\omega)$, such as $\underline{H}_a(j\omega)$ of (2.47).

3.3.3 Robust Closed Loop Stability

One of the problems with Theorem 3.3 is that plant uncertainties are not explicitly included in the sufficient conditions for closed loop stability. The closed system should be stable not just for the nominal plant G but for all possible plants $\tilde{G}$ in a defined set.

---

[1] Note the similarity of (3.13) and (3.14) to the robustness conditions (2.23) and (2.22) for analog feedback systems.

Two robustness results are now derived. The first result uses the fact that conditions (ii) and (iii) are true for a set of linear operators, of which G is one element. This set will contain all possible $\tilde{G}$'s if the condition of Theorem 3.4 is satisfied.

Theorem 3.4 Consider the hybrid feedback system. Assume that all of the assumptions and conditions of Theorem 3.3 are satisfied. The hybrid feedback system is closed loop stable for all possible $\tilde{G}$'s if

$$\ell_m(\omega) < \frac{\sigma_{min}[\underline{I} + \underline{G}\,\underline{C}(j\omega)] - \sigma_{max}[\underline{R}\,\underline{G}(j\omega)]}{\sigma_{max}[\underline{G}\,\underline{C}(j\omega)] + \sigma_{max}[\underline{R}\,\underline{G}(j\omega)]} \qquad \text{for all } \omega \qquad \blacksquare \ (3.15)$$

The proof of Theorem 3.4 is included in the Appendix to Chapter 3. Theorem 3.4 is set up to be used when the uncertainty of the nominal plant G is characterized by a multiplicative perturbation. The hybrid operator K is inside of the cone (C, R), and if the conditions of Theorem 3.3 are satisfied then $-G^I$ is outside of this cone. If in addition the condition of Theorem 3.4 is satisfied then all possible $-\tilde{G}^I$'s are outside of this cone.

The next robustness result uses a different approach. The perturbation of the nominal plant is used to increase the size of the radius (the radius of the cone that the hybrid operator is inside of). This is accomplished by grouping $(\underline{I} + \underline{E}_m)$, the multiplicative perturbation, with the hold.[1]

Theorem 3.5 Consider the hybrid feedback system. Assume that K, G, E_m, C, R, and R^I are L_{2e}-stable. Choose the center

---

[1] Similar results are possible by grouping the multiplicative perturbation with the prefilter.

$$\underline{C}(s) = \frac{1}{T} \underline{H}(s) \ \underline{D}^*(s) \ \underline{F}(s) \tag{3.16}$$

(a) The composite operation $(I+\xi_m)K$ is strictly inside cone (C,R) if

$$\sigma_{min}\left[\underline{R}(j\omega)\right] \geq \frac{1}{(1-\epsilon)^{1/2}} \left[r_5(\omega) - r_6(\omega) + r_7(\omega)\right]^{1/2} \tag{3.17}$$

for all ω and some $\epsilon > 0$

where

$$r_5(\omega) = \frac{1}{T^2}\left[\sum_k (1+\ell_{mk})^2 \cdot \|\underline{H}_k\|^2\right] \cdot \|\underline{D}^*\|^2 \cdot \left[\sum_n \|\underline{F}_n\|^2\right] \tag{3.18}$$

$$r_6(\omega) = \frac{1}{T^2} \sum_k (1 + \ell_{mk})^2 \cdot \|\underline{H}_k \ \underline{D}^* \ \underline{F}_k\|^2 \tag{3.19}$$

$$r_7(\omega) = \frac{1}{T^2} \sum_k \ell_{mk}^2 \cdot \|\underline{H}_k \ \underline{D}^* \ \underline{F}_k\|^2 \tag{3.20}$$

(b) The hybrid system is closed loop stable for all possible $\tilde{G}$'s if

(i) $(I+\xi_m)K$ is strictly inside cone (C,R)

(ii) $G(I + CG)^I$ is L_{2e}-stable

(iii) $\sigma_{max}\left[\underline{R} \ \underline{G} \ (\underline{I} + \underline{C} \ \underline{G})^{-1}(j\omega)\right] \leq 1$ for all ω $\blacksquare$ (3.21)

The proof of Theorem 3.5 is a composition of the proofs of Theorems 3.2 and 3.3. The proof of part (a) differs from the proof of Theorem 3.2 only in that $\underline{H}(s)$ is replaced by $(\underline{I} + \underline{E}_m)\underline{H}(s)$, and the following inequality is inserted in the appropriate place in the proof:

$$\|(\underline{I}+\underline{E}_m)\underline{H}(j\omega)\| \leq \|(\underline{I}+\underline{E}_m)\| \cdot \|\underline{H}(j\omega)\|$$

$$\leq \left(1 + \|\underline{E}_m\|\right) \cdot \|\underline{H}(j\omega)\|$$

$$\leq \left(1 + \ell_m\right) \cdot \|\underline{H}(j\omega)\| \tag{3.22}$$

The proof of (b) differs from the proof of Theorem 3.3 only in that K is replaced by $(I+E_m)K$. The hybrid operator $(I+E_m)K$ is strictly inside of cone (C,R) if condition (bi) is true, and $-G^I$ is outside of the same cone if conditions (bii) and (biii) are true. Hence, the closed loop system is stable for all possible $\tilde{G}$'s in the set defined by E_m.

An alternate expression for the radius (3.17) uses a double summation:

$$\sigma_{min}\left[\underline{R}(j\omega)\right] \geq \frac{1}{(1-\epsilon)^{1/2}} \left[r_8(\omega) + r_7(\omega)\right]^{1/2} \tag{3.23}$$

$$\text{for all } \omega \text{ and some } \epsilon > 0$$

where

$$r_8(\omega) = r_5(\omega) - r_6(\omega) = \frac{1}{T^2} \sum_k \sum_{n \neq k} (1 + \ell_{mk})^2 \cdot \|\underline{H}_k\underline{D}^*\underline{F}_n\|^2$$

$$\tag{3.24}$$

and where $r_7(\omega)$ is defined by (3.20)

Constant values of $\ell_m(\omega)$ are useful for phase and gain margin analysis (see Subsection 2.2.\`\)   Suppose

$$\ell_m(\omega) = \alpha \quad \text{for all } \omega \tag{3.25}$$

Then the various components of the radii of Theorems 3.3 and 3.5 are related by

$$
\left.
\begin{aligned}
r_5(\omega) &= (1+\alpha)^2\, r_1(\omega) \\[2mm]
r_6(\omega) &= (1+\alpha)^2\, r_2(\omega) \\[2mm]
r_7(\omega) &= \alpha^2\, r_2(\omega) \\[2mm]
r_8(\omega) &= (1+\alpha)^2\, r_4(\omega)
\end{aligned}
\right\}
\qquad (3.26)
$$

The significance of (3.26) is that the same computations for Theorem 3.3 suffice for Theorem 3.5.

It is possible to systematically find the maximum value of α such that the robustness condition (3.21) is satisfied. Let $\ell_m(\omega) = \alpha$ and substitute parts of (3.26) into (3.21) to obtain:

$$
\left[(1+\alpha)^2 r_4^2 + \alpha^2 r_3^2\right]^{1/2} g(1+cg)^{-1} \le 1 \quad \text{for all } \omega \qquad (3.27)
$$

Change the inequality to an equality, and manipulate (3.27) to obtain

$$
\alpha^2 + \tilde{b}\alpha + \tilde{c} = 0 \qquad (3.28)
$$

where $\tilde{b}$ and $\tilde{c}$ are functions of r_3, r_4, c, and g. If the stability condition (3.12) is true (i.e. if (3.21) is true when $\alpha=0$) then $\tilde{c} < 0$ and (3.28) has one negative and one positive real root. Let the positive real root be $\alpha_1(\omega)$, which is a function of ω. The maximum value of α that satisfies (3.21) is

$$\alpha \;=\; \min_{\omega} \; \alpha_1(\omega) \tag{3.29}$$

Note that $\alpha_1(\omega)$ is <u>minimized</u> over ω

As just shown, Theorem 3.5, equations (3.28) and (3.29), can be used to find a guaranteed phase and gain margin. Minimizing over ω the positive real root of the quadratic equation (3.28) is not diffi- cult, but it is nevertheless easier to use Theorem 3.4, equation (3.15), to find a guaranteed phase and gain margin. As will be seen later, Theorem 3.7, equation (3.40) can also be used to find a guaranteed phase and gain margin. In general, Theorems 3.4, 3.5, and 3.7 will give different margins.

3.4 A Cone that Contains the Loop Transfer Operator

The entire loop transfer operator can be placed inside of a cone.[1] This will usually result in less conservative sufficient conditions for closed loop stability and robustness. The size of the radius depends on the amount of aliasing of both the prefilter and the hold. Including the plant with the compensator will usually help because the rolloff of the plant reduces the amount of aliasing of the prefilter and/or the hold.

There are some pitfalls, however, the most important of which is where to include the plant. There are three choices:

Case 1: with the hold

Case 2: with the prefilter

Case 3: with a combination of the hold and prefilter

The three cases are illustrated in Figure 3.1.

Case 1 corresponds to breaking the feedback loop before the prefilter. The loop transfer operator at this point can be used to analyze the response to signals injected there (such as r).

Case 2 corresponds to breaking the loop before the plant. The loop transfer operator at this point can be used to analyze the response to signals injected at this point.

Case 3 does not correspond to breaking the loop at any physical point. Both the prefilter and the hold are replaced by $(\underline{F}\ \underline{G}\ \underline{H})^{1/2}$.

Case 3 is the best to use to analyze closed loop stability and robustness.[2]

---

[1] Whatever is placed inside of a cone must be open loop stable. If the plant is open loop unstable it can be split into a stable part and a unit magnitude unstable part, and then the stable part can be included in the cone. See Section 5.4 for an example.

[2] Nowhere does the square root actually have to be computed, because
$$\|(\underline{F}\ \underline{G}\ \underline{H})^{1/2}\|^2 = \|\underline{F}\ \underline{G}\ \underline{H}\|.$$

Case 1: Plant included with the hold

Case 2: Plant included with the prefilter
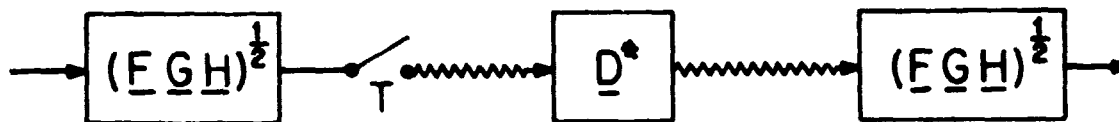
Case 3: Plant included with a combination of the hold and prefilter

Figure 3.1: Three cases of including the plant with the hybrid compensator.

Theorems 3.1 to 3.5 are used when the hybrid operator is inside of a cone. With appropriate modifications these theorems can also be used when the loop transfer operator is inside of a cone. The modifications are described in the following paragraph.

In each of the theorems the hybrid operator K is replaced by the appropriate loop transfer T. Depending on where the plant is included:

Case 1: Replace $\underline{H}$ by $\underline{G}\ \underline{H}$

Case 2: Replace $\underline{F}$ by $\underline{F}\ \underline{G}$

Case 3: Replace $\underline{H}$ and $\underline{F}$ by $(\underline{F}\ \underline{G}\ \underline{H})^{1/2}$

In Theorem 3.3 replace G by I, and the three conditions for closed loop stability become

(i) T is strictly inside cone (C,R)

(ii) $(I+C)^{I}$ is L_{2e}-stable

(iii) $\sigma_{max}\left[\underline{R}(\underline{I+C})^{-1}(j\omega)\right] \leq 1$ for all ω (3.30)

In Theorem 3.4 replace the condition for robust closed loop stability by

$$\ell_m(\omega) < \frac{\sigma_{min}\ [\underline{I}\ +\ \underline{C}(j\omega)]\ -\ \sigma_{max}\ [\underline{R}(j\omega)]}{\sigma_{max}\ [\underline{C}(j\omega)]\ +\ \sigma_{max}\ [\underline{R}(j\omega)]} \qquad (3.31)$$

In Theorem 3.5 replace G by I and replace the three conditions for robust closed loop stability by

(i) $(I+E_m)T$ is strictly inside cone (C,R)

(ii) $(I+C)^{I}$ is L_{2e}-stable

(iii) $\sigma_{max}\left[\underline{R}(\underline{I+C})^{-1}(j\omega)\right] \leq 1$ for all ω (3.32)

The significance of case 3 is that for SISO systems the radius is smaller (for each ω) than the radii for cases 1 and 2. Hence, case 3 gives the least conservative sufficient conditions for closed loop stability and robustness. The Cauchy-Schwartz inequality is used to show this.

The equation for the radius in Theorem 3.3 is[1]

$$r(\omega) = \left[r_1(\omega) - r_2(\omega) + r_3(\omega) \right]^{1/2} \qquad (3.33)$$

For SISO systems $r_2(\omega)$ and $r_3(\omega)$ do not change for the three cases. Therefore, whatever differences exist in $r(\omega)$ are due to differences in $r_1(j\omega)$.[2] The equations for $r_1(\omega)$ are:

$$
\left.
\begin{aligned}
\text{Case 1:} \quad r_1(\omega) &= \frac{1}{T^2} \left[\sum_k |g_k h_k|^2 \right] \cdot |d*|^2 \cdot \left[\sum_n |f_n|^2 \right] \\
\text{Case 2:} \quad r_1(\omega) &= \frac{1}{T^2} \left[\sum_k |h_k|^2 \right] \cdot |d*|^2 \cdot \left[\sum_n |f_n g_n|^2 \right] \\
\text{Case 3:} \quad r_1(\omega) &= \frac{1}{T^2} \left[\sum_k |f_k g_k h_k| \right]^2 \cdot |d*|^2
\end{aligned}
\right\} \quad (3.34)
$$

By the Cauchy-Schwartz inequality:

---

[1] Without loss of generalty the ε term has been ignored.

[2] For multivariable systems both $r_2(\omega)$ and $r_3(\omega)$ differ for the three cases, because matrices do not commute.

$$\left[\sum_k |f_k g_k h_k| \right]^2 \leq \left[\sum_k |g_k h_k|^2 \right] \cdot \left[\sum_n |f_n|^2 \right]$$

$$\left[\sum |f_k g_k h_k| \right]^2 \leq \left[\sum_k |h_k|^2 \right] \cdot \left[\sum_n |f_n g_n|^2 \right]$$

(3.35)

Therefore $r_1(\omega)$ for case 3 is less (for each ω) then $r_1(\omega)$ for the other

cases. It follows that $r(\omega)$ for case 3 is less (for each ω) then $r(\omega)$

for cases 1 and 2.

Without further information about $h(s)$ and $f(s)$ it is not possible

to tell which of the radii for cases 1 and 2 is smaller. Some indica-

tion of which radii is smaller can be gleaned by comparing the relative

magnitudes of $\frac{1}{T^2} \sum_k |h_k|^2$ and $\sum_n |f_n|^2$, but the best way is just to graphically

compare the radii. In general, neither will be smaller for all ω.

3.5 A Cone that the Inverse Hybrid Operator is Outside of

3.5.1 Existence

Just as there exists a conic sector that K is inside of, there also exists a conic sector that $-K^I$ is outside of. This result is presented in Theorem 3.6. It is proved in the Appendix to Chapter 3.

Theorem 3.6 Let K be a hybrid operator, let C be any LTI operator such that $K(I+CK)^I$ is L_{2e}-stable, and let R and R^I be LTI L_{2e}-stable operators. $-K^I$ is outside cone (C,R) if

$$\sigma_{max}\left[\underline{R}(j\omega)\right] \leq \frac{1}{\sqrt{r_9(\omega)}} \quad \text{for all } \omega \tag{3.36}$$

$$\text{where} \quad r_9(\omega) = \frac{1}{T^2}\left[\sum_k \|\underline{H_k}\|^2\right] \cdot \|\underline{D^*_{c\ell}}\|^2 \cdot \left[\sum_n \|\underline{F_n}\|^2\right] \tag{3.37}$$

$$\underline{D^*_{c\ell}}(s) = \underline{D}^*(s)\left[\underline{I} + [\underline{F}\,\underline{C}\,\underline{H}(s)]^* \,\underline{D}^*(s)\right]^{-1} \quad \blacksquare \tag{3.38}$$

The outside conic sector conditions do not require open loop stability of the hybrid compensator. This removes the major restriction of the inside conic sector conditions. Taking its place is a requirement that $K(I+CK)^I$ is L_{2e}-stable. The composite operator $K(I+CK)^I$ is a hybrid operator (see the proof). It is stable if all of the poles of $D_{c\ell}(z)$ have magnitude < 1 (see Subsection 2.3.4).

3.5.2 Robust Closed Loop Stability

Sufficient conditions are presented for the hybrid feedback system to be closed loop stable for all possible plants $\tilde{G}$. The robustness result follows much more naturally than in Subsection 3.3.3. Here the

hybrid operator $-K^I$ is outside of a cone and the plant operator $\tilde{G}$ is inside of a cone. This is more natural because the nominal plant G and its additive or multiplicative perturbation can be used to place $\tilde{G}$ inside of a cone.

<u>Theorem 3.7</u> Consider the hybrid feedback system. Assume R and R^I are L_{2e}-stable. The hybrid feedback system is closed loop stable for all possible $\tilde{G}$'s if an $\underline{R}(j\omega)$ exists such that

(i) $K(I+GK)^I$ is L_{2e}-stable

(ii) $-K^I$ is outside cone (G,R)

(iii) $\sigma_{min} [\underline{R}(j\omega)] > \ell_a(\omega)$ for all ω.   ∎ (3.39)

The proof is sketched out here. If condition (i) is true then a $\underline{R}(j\omega)$ can be constructed such that condition (ii) is true (by Theorem 3.6). If condition (iii) is true then $\tilde{G}$ is strictly inside of cone (G,R). Hence, the hybrid system is closed loop stable for all possible $\tilde{G}$'s (by Lemma 2.6).

If the uncertainty of the nominal plant G is modelled by a multiplicative perturbation then (3.39) has the alternate form:

$$\ell_m(\omega) < \sigma_{min} [\underline{R}(j\omega)]/\sigma_{max} [\underline{G}(j\omega)]   \text{ for all } \omega \qquad (3.40)$$

If $\ell_m(\omega) = \alpha$ then the maximum value of α such that (3.40) is true can be used to find guarenteed phase and gain margins.

3.6 Command Response of Hybrid Feedback Systems

Conic sectors can be used to analyze the steady state command response of a hybrid feedback system. The objective is to find an upperbound for the quality measure "q", which is defined by equation (2.95) of Subsection 2.4.6. Either the loop transfer operator GK or the closed loop operator $(I + GK)^I$ can be placed inside of a cone.

The first approach uses Theorem 3.2 or Theorem 3.5 to place the loop transfer operator GK inside of a cone.[1] The loop is broken where the command signal enters the loop, which is just before the prefilter, and the plant is grouped with the hold (case 1 of Section 3.4). The cone is placed around either GK (if the nominal plant is used) or $\tilde{GK}$ (if the perturbed plant is used). The center and radius are used via (2.98) and (2.99) to compute an upperbound for q.

The second approach to computing an upperbound for q is to place the closed loop operator $GK(I + GK)^I$ inside of a cone. The center of the cone is $C(I + C)^I$, where C is a LTI approximation of GK.[2] The closed loop operator $GK(I + GK)^I$ has the same structure as a hybrid operator. The input-output transformation of $GK(I + GK)^I$ is given by (2.57), which is repeated here:

$$\underline{y}(s) = \underline{G}(s)\ \underline{H}(s)\ \underline{D}^*_{c\ell}(s)\ [\underline{F}(s)\ \underline{r}(s)]^* \tag{3.41}$$

where

$$\underline{D}^*_{c\ell}(s) = \underline{D}^*(s)\ [\underline{I} + \underline{G}_{\tilde{a}}^*\ \underline{D}^*(s)]^{-1} \tag{3.42}$$

---

[1] Theorems 3.2 and 3.5 must be modified as discussed in Section 3.4.

[2] This is equivalent to placing $(I + GK)^I$ inside of a cone with center $(I + C)^I$. See (2.106) and (2.107).

$$\underset{\sim d}{G}{}^{*}(s) = [\underset{\sim\sim\sim}{HGF}(s)]^{*} \tag{3.43}$$

Theorem 3.2 (appropriately modified) can be used to construct a cone that contains $GK(I + GK)^{I}$. The radius of this cone can then be used, via (2.105), to compute an upperbound for q.

Significant improvements can be made to the second approach by taking advantage of the fact that the command signals are restricted to a set $S \subset L_{2e}^{r}$. Rather than meet the conic sector inequality

$$\| [GK(I + GK)^{I} - C(I + C)^{I}]\underset{\sim}{r} \|_{\tau} \leq \| R_{2}\underset{\sim}{r} \|_{\tau}$$

$$\text{for all } \underset{\sim}{r} \subset L_{2e}^{r} \text{ and } \tau \in R_{+} \tag{3.44}$$

it is only necessary that

$$\lim_{\tau \to \infty} \frac{\| [GK(I + GK)^{I} - C(I + C)^{I}]\underset{\sim}{r} \|_{\tau}}{\| \underset{\sim}{r} \|_{\tau}} \leq \lim_{\tau \to \infty} \frac{\| R_{3}\underset{\sim}{r} \|_{\tau}}{\| \underset{\sim}{r} \|_{\tau}}$$

$$\text{for all } \underset{\sim}{r} \in S \tag{3.45}$$

By virtue of the fact that $S \subset L_{2e}^{r}$ it follows that

$$\lim_{\tau \to \infty} \frac{\| R_{3}\underset{\sim}{r} \|_{\tau}}{\| \underset{\sim}{r} \|_{\tau}} \leq \lim_{\tau \to \infty} \frac{\| R_{2}\underset{\sim}{r} \|_{\tau}}{\| \underset{\sim}{r} \|_{\tau}} \quad \text{for all } \underset{\sim}{r} \in S \tag{3.46}$$

A particular set $S_{a} \subset L_{2e}^{r}$ is now defined:

$$S_{a} = \{\text{sinewaves with frequency} < \frac{\pi}{T}\} \tag{3.47}$$

An important property of signals in this set is that they do not cause any aliasing when they are sampled.

The following theorem can be used to analyze the steady state response to commands that are members of S_a. The proof of Theorem 3.8 is in the Appendix to Chapter 3.

Theorem 3.8 Consider the hybrid feedback system. Assume that $GK(I + GK)^I$ and $C(I + C)^I$ are L_{2e}-stable. Then

$$\lim_{\tau \to \infty} \frac{\|[GK(I + GK)^I - C(I + C)^I]\underset{\sim}{r}\|_\tau}{\|\underset{\sim}{r}\|_\tau} \leq \lim_{\tau \to \infty} \frac{\|R_3 \underset{\sim}{r}\|_\tau}{\|\underset{\sim}{r}\|_\tau}$$

$$\text{for all } r \in S_a \tag{3.48}$$

if

$$\sigma_{min}[\underline{R}(j\omega)] \geq [r_{10}(\omega) + r_{11}(\omega)]^{1/2} \quad \text{for } |\omega| < \frac{\pi}{T} \tag{3.49}$$

where

$$r_{10}(\omega) = \frac{1}{T^2} \sum_{k \neq o} \|\underline{G}_k \underline{H}_k \underline{D}_{c\ell} \underline{F}\|^2$$

$$r_{11}(\omega) = \|\frac{1}{T} \underline{G} \underline{H} \underline{D}_{c\ell} \underline{F}(j\omega) - \underline{C}(\underline{I} + \underline{C})^{-1}(j\omega)\|^2 \qquad \blacksquare \tag{3.50}$$

Theorem 3.8 can be used to find an upperbound for the quality measure q. Let the set of command signals be sinewaves with frequency less than ω_o (which is a subset of S_a). Then it follows that

$$q \leq q_o (1 + r_3) \tag{3.51}$$

where

$$q_o = \max_{o \leq \omega \leq \omega_o} \sigma_{max} [(I + C)^{-1}(j\omega)] \tag{3.52}$$

$$r_3 q_o = \max_{o \leq \omega \leq \omega_o} \sigma_{max} [R_3(j\omega)] \tag{3.53}$$

This completes the section on using conic sectors to analyze the steady state response of the hybrid feedback system to command signals. The suggested approaches are (1) use Theorem 3.2 to construct a cone that contains GK, (2) use Theorem 3.2 to construct a cone that contains $GK(I + GK)^I$, and (3) use Theorem 3.8 to construct a cone that contains $GK(I + GK)^I$ but is only valid for command signals $\underset{\sim}{r} \in S_a$. In the example of Subsection 5.2.11 the third approach is shown to give the least conservative (lowest) upperbound for the quality measure q.

Appendix to Chapter 3

This appendix contains proofs for Theorems 3.1, 3.2, 3.4, 3.6, and 3.8. The proofs of the remaining theorems of Chapter 3 are sketched out in the text.

This appendix begins by stating and proving a lemma which is an intermediate step used in the proofs of Theorems 3.1, 3.2, and 3.6. The lemma is a frequency domain inequality that is used for signals that are inputs of hybrid compensators. The proof uses the Cauchy-Schwartz inequality [19, p. 30] and Lebesque Dominated Convergence [21, p. 44].

Lemma 3.A Let $\underline{K}_n(s)$ be Laplace transform matrices for all integers n, and let $\underline{e}(s)$ be the Laplace transform of $\underline{e} \in L_2$. Furthermore (to assure Lebesque Dominated Convergence) assume for $|\omega|$ sufficiently large that

$$\sum_n \left\| \underline{K}_n(j\omega) \right\|^2 \leq \frac{\alpha}{|\omega|^{1+\beta}} \qquad \text{for some } \alpha, \beta > 0 \qquad (3.A.1)$$

Then

$$\frac{1}{2\pi} \int_{-\infty}^{\infty} \left\| \sum_n \underline{K}_n(j\omega)\underline{e}(j\omega - j\omega_s n) \right\|_E^2 d\omega \leq$$

$$\frac{1}{2\pi} \int_{-\infty}^{\infty} \left[\sum_k \sum_n \left\| \underline{K}_n(j\omega - j\omega_s k) \right\|^2 \right] \cdot \left\| \underline{e}(j\omega) \right\|_E^2 d\omega \qquad \blacksquare \qquad (3.A.2)$$

<u>Proof of Lemma 3.A</u> The proof is a long series of equalities and inequalities. Justification for each step is included in parenthesis.

$$\frac{1}{2\pi} \int_{-\infty}^{\infty} \left\| \sum_n \underline{K}_n(j\omega)\underline{e}(j\omega-j\omega_s n) \right\|_E^2 d\omega$$

$$\leq \frac{1}{2\pi} \int_{-\infty}^{\infty} \left[\sum_n \left\| \underline{K}_n(j\omega)\underline{e}(j\omega-j\omega_s n) \right\|_E \right]^2 d\omega \qquad (3.A.3)$$

(because $\|\underline{a}+\underline{b}\|_E \leq \|\underline{a}\|_E + \|\underline{b}\|_E$)

$$\leq \frac{1}{2\pi} \int_{-\infty}^{\infty} \left[\sum_n \left\| \underline{K}_n(j\omega) \right\| \cdot \left\| \underline{e}(j\omega-j\omega_s n) \right\|_E \right]^2 d\omega \qquad (3.A.4)$$

(because $\|\underline{A}\,\underline{b}\|_E \leq \|\underline{A}\| \cdot \|\underline{b}\|_E$)

$$\leq \frac{1}{2\pi} \int_{-\infty}^{\infty} \left[\sum_n \left\| \underline{K}_n(j\omega) \right\|^2 \right] \cdot \left[\sum_k \left\| \underline{e}(j\omega-j\omega_s k) \right\|^2 \right] d\omega \qquad (3.A.5)$$

(By the Cauchy-Schwartz inequality. Let $a_n = \left\| \underline{K}_n(j\omega) \right\|^2$ and $b_n = \left\| \underline{e}(j\omega-j\omega_s n) \right\|_E^2$. For each ω, a_n and b_n are non-negative real numbers. Let $\underline{a}$ and $\underline{b}$ be ℓ_2 vectors (of infinite length) containing the a_n's and b_n's. The Cauchy-Schwartz inequality states that $|\underline{a}^T\underline{b}| \leq \|\underline{a}\|_E \cdot \|\underline{b}\|_E$).

$$= \frac{1}{2\pi} \sum_k \int_{-\infty}^{\infty} \left[\sum_n \| \underline{K}_n(j\omega) \|^2 \right] \cdot \| \underline{e}(j\omega - j\omega_s k) \|_E^2 \, d\omega \qquad (3.A.6)$$

(move sum over k outside integral, which is valid

by Lebesque Dominated Convergence).

$$= \frac{1}{2\pi} \sum_k \int_{-\infty}^{\infty} \left[\sum_n \| \underline{K}_n(j\tilde{\omega} + j\omega_s k) \|^2 \right] \cdot \| \underline{e}(j\tilde{\omega}) \|^2 \, d\tilde{\omega} \qquad (3.A.7)$$

(for each k change the variable of integration

to $\tilde{\omega} = \omega - \omega_s k$).

$$= \frac{1}{2\pi} \int_{-\infty}^{\infty} \left[\sum_k \sum_n \| \underline{K}_n(j\tilde{\omega} + j\omega_s k) \|^2 \right] \cdot \| \underline{e}(j\tilde{\omega}) \|_E^2 \, d\tilde{\omega} \qquad (3.A.8)$$

(move sum over k back inside the integral).

This completes the proof.

<u>Proof of Theorem 3.1</u> The objective is to show that equation (3.1)
is an upperbound for the gain of a hybrid operator. The proof essentially
boils down to an application of the frequency domain inequality of
Lemma 3.A. Some extra work is required, however, both before and
after this lemma can be applied. The operator gain is defined in the
time domain using truncated norms [see (2.79)]. A truncated function
is defined so that L_2 function norms can be used in place of the trun-
cated norms. L_2 function norms are needed so that Parseval's Theorem
can be used to switch from the time to the frequency domain. While
in the frequency domain Lemma 3.A is applied. Parseval's Theorem is
then used to switch back to the time domain, and finally the truncated
function is used to switch back to truncated norms.

The truncated function is defined by

$$
\underline{e}_\tau(t) \triangleq
\begin{cases}
\underline{e}(t) & t \le \tau \\
\\
\underline{0} & t > \tau
\end{cases}
\tag{3.A.9}
$$

The proof uses the notation:

$$
\underline{K}_n(j\omega) \triangleq \underline{H}(j\omega)\underline{D}^*(j\omega)\,\underline{F}(j\omega - j\omega_s n)
\tag{3.A.10}
$$

and the following:

$$
\sum_k \sum_n \left\| \underline{K}_n(j\omega - j\omega_s k) \right\|^2
= \sum_k \sum_n \left\| \underline{H}_k \underline{D}^* \underline{F}_{n+k} \right\|^2
\tag{3.A.11}
$$

$$\leq \sum_{k} \sum_{n} \left[\|\underline{H}_{k}\|^2 \cdot \|\underline{D}^*\|^2 \cdot \|\underline{F}_{n+k}\|^2 \right] \qquad (3.A.12)$$

$$= \left[\sum_{k} \|\underline{H}_{k}\|^2 \right] \cdot \|\underline{D}^*\|^2 \cdot \left[\sum_{n} \|\underline{F}_{n}\|^2 \right] \qquad (3.A.13)$$

The last step, (3.A.13), is possible because $\sum_{n} \|\underline{F}_{n}\|^2$ is periodic with period ω_s.

The main part of the proof is now presented. Fo. all $\underline{e} \in L_{2e}$ and all $\tau \in R_+$:

$$\|K\underline{e}\|_{\tau}^2 = \|K\underline{e}_{\tau}\|_{\tau}^2 \qquad \text{(because } K \text{ is causal)} \qquad (3.A.14)$$

$$\leq \|K\underline{e}_{\tau}\|_{L_2}^2 \qquad \text{(norm increases as } \tau \to \infty) \qquad (3.A.15)$$

$$= \int_{-\infty}^{\infty} \|(K\underline{e}_{\tau})(t)\|_{E}^2 \, dt \qquad \text{(by definition)} \qquad (3.A.16)$$

$$= \frac{1}{2\pi} \int_{-\infty}^{\infty} \|(K\underline{e}_{\tau})(j\omega)\|_{E}^2 \, d\omega \qquad \text{(Parseral's Theorem)} \qquad (3.A.17)$$

$$= \frac{1}{2\pi} \int_{-\infty}^{\infty} \|\sum_{n} \underline{K}_{n}(j\omega)\underline{e}_{\tau}(j\omega-j\omega_s n)\|_{E}^2 \, d\omega \qquad (3.A.18)$$

[where $\underline{K}_{n}$ is defined by (3.A.10)]

$$\leq \frac{1}{2\pi} \int_{-\infty}^{\infty} \left[\sum_k \sum_n \|\underline{K}_{-n}(j\omega - j\omega_s k)\|^2 \right] \cdot \|\underline{e}_\tau(j\omega)\|^2 \; d\omega \qquad (3.A.19)$$

(by Lemma 3.A)

$$\leq \frac{1}{2\pi} \int_{-\infty}^{\infty} \frac{1}{T^2} \left[\sum_k \|\underline{H}_{-k}\|^2 \right] \cdot \|\underline{D}*\|^2 \cdot \left[\sum_n \|\underline{F}_n\|^2 \right] \cdot \|\underline{e}_\tau(j\omega)\|^2 \; d\omega$$

$$\qquad (3.A.20)$$

[by (3.A.13)]

$$\leq g^2 \frac{1}{2\pi} \int_{-\infty}^{\infty} \|\underline{e}_\tau(j\omega)\|^2 \; d\omega \qquad (3.A.21)$$

$$\text{where } g = \max_{0 \leq \omega \leq \frac{\pi}{T}} \left\{ \frac{1}{T} \left[\sum_k \|\underline{H}_{-k}\|^2 \right]^{1/2} \cdot \|\underline{D}*\| \cdot \left[\sum_n \|\underline{F}_{-n}\|^2 \right]^{1/2} \right\}$$

$$\qquad (3.A.22)$$

(restricted frequency range used because

the bracketed term is periodic with period

ω_s and is symmetric about $\omega = 0$)

$$= g^2 \|\underline{e}_\tau\|^2_{L_2} \qquad \text{(Parseval's theorem)} \qquad (3.A.23)$$

$$= g^2 \|\underline{e}\|^2_\tau \qquad [\underline{e}_\tau(t) = 0 \text{ for } t > \tau] \qquad (3.A.24)$$

By definition of the gain of an operator:

$$\|K\|_{L_2} = \sup \frac{\|K\underline{e}\|_\tau}{\|\underline{e}\|_\tau} \leq g \qquad (3.A.25)$$

This completes the proof of part (a).

Part (b) of Theore 3.1 is proved by showing that the following input (for the SISO case) achieves the upperbound:

$$e(t) = \sum_n |a_n| \cdot \cos\left[(\omega_o - \omega_s n)t + \text{Arg}(a_n)\right] \qquad (3.A.26)$$

where $\quad a_n = d^*(-j\omega_o) \; f(-j\omega_o + j\omega_s n)$

ω_o = frequency the maximizes (3.A.22)

The norm of this function, expressed as a limit, is:

$$\lim_{\tau \to \infty} \frac{1}{\tau} \cdot \|\underset{\sim}{e}\|_\tau = \left[\sum_n |a_n|^2\right]^{1/2} = |d^*(j\omega_o)| \cdot \left[\sum_n |f(j\omega_o - j\omega_s n)|^2\right]^{1/2}$$

$$(3.A.27)$$

The output of the hybrid compensator is

$$u(t) = \frac{1}{T} \sum_k |b_k| \cdot \cos\left[(\omega_o - \omega_s k)t + \text{Arg}(b_k)\right] \qquad (3.A.28)$$

where $\quad b_k = h(j\omega_o - j\omega_s k) \cdot \left[\sum_n |a_n|^2\right]$

and the norm of this output signal is

$$\lim_{\tau \to \infty} \frac{1}{\tau} \|\underset{\sim}{u}\|_\tau = \frac{1}{T}\left[\sum_k |h(j\omega_o - j\omega_s k)|^2\right]^{1/2} \cdot \left[\sum_n |a_n|^2\right] \qquad (3.A.29)$$

The gain for this input signal is

$$\lim_{\tau \to \infty} \frac{\|\underset{\sim}{u}\|_\tau}{\|\underset{\sim}{e}\|_\tau} = g \tag{3.A.30}$$

This completes the proof.

Remark The input (3.A.26) and the output (3.A.28) have sinewaves at the same frequencies. The a_n's in (3.A.26) are chosen so that the Cauchy-Schwartz inequality is met with equality [see (3.A.5)].

Conjecture (Multivariable version of Theorem 3.1, part (b)).
The gain of the multivariable hybrid operator is

$$\|K\|_{L_2} = \max_{0 \le \omega \le \frac{\pi}{T}} \frac{1}{T^2} \left\{ \sum_k \sum_n \|\underset{\sim}{H}_k \underset{\sim}{D}^* \underset{\sim}{F}_n\|^2 \right\} \tag{3.A.31}$$

Proof of Theorem 3.2   The objective is to show that the hybrid operator K is strictly inside cone (C, R). This proof is similar to the proof of Theorem 3.1, and again essentially boils down to an application of Lemma 3.A. Parseval's Theorem is used to pass between the time and frequency domain, and the following truncated input is used to pass between the truncated norm and the L_2 function norm:

$$\underline{e}_\tau(t) = \begin{cases} (R\underline{e})(t) & t \geq \tau \\ \\ \underline{0} & t < \tau \end{cases} \tag{3.A.32}$$

The input is truncated only after it is convolved with the radius. Rather than show that $\| (K-C)\underline{e}\|_\tau < \| R\underline{e}\|_\tau$, the main part of the proof shows that $\| (K-C)R^I\underline{e}_\tau\|_{L_2} < \| \underline{e}_\tau\|_{L_2}$. Yet another complicating factor is that the ϵ term must be manipulated to show strict inequality. This is possible because R is L_{2e}-stable. The middle part of this proof [steps (3.A.45) to (3.A.50), which includes the application of Lemma 3.A] is the only part that differs significantly from [9, Theorem A.4].

It is convenient to introduce the notation

$$\underline{K}_n(s) \triangleq \begin{cases} \dfrac{1}{T} \underline{H}(s) \; \underline{D}^*(s) \; \underline{F}(s) - \underline{C}(s) & n=0 \\ \\ \dfrac{1}{T} \underline{H}(s) \; \underline{D}^*(s) \; \underline{F}(s-j\omega_s n) & n \neq 0 \end{cases} \tag{3.A.33}$$

which is used to express the Laplace transform of $(K-C)\underline{e}$ as

$$\underline{u}(s) - \underline{C}(s)\underline{e}(s) = \sum_n \underline{K}_n(s)\underline{e}(s-j\omega_s n) \tag{3.A.34}$$

Midway through the proof the following inequality is used:

$$\sum_k \sum_n \|\underline{K}_n(j\omega - j\omega_s k)\|^2 = \sum_k \sum_{n \neq 0} \|\underline{K}_n(j\omega - j\omega_s k)\|^2 + \sum_k \|\underline{K}_o(j\omega - j\omega_s k)\|^2$$

$$(3.A.35)$$

$$= \sum_k \sum_n \frac{1}{T^2} \|\underline{H}_k \underline{D}^* \underline{F}_{n+k}\|^2$$

$$- \sum_k \frac{1}{T^2} \|\underline{H}_k \underline{D}^* \underline{F}_k\|^2$$

$$+ \sum_k \|\frac{1}{T} \underline{H}_k \underline{D}^* \underline{F}_k - \underline{C}_k\|^2 \qquad (3.A.36)$$

$$\leq \frac{1}{T^2} \left[\sum_k \|\underline{H}_k\|^2\right] \cdot \|\underline{D}^*\|^2 \cdot \left[\sum_n \|\underline{F}_n\|^2\right] - r_2(\omega) + r_3(\omega)$$

$$(3.A.37)$$

$$= r_1(\omega) - r_2(\omega) + r_3(\omega) \qquad (3.A.38)$$

$$= r(\omega) \qquad (3.A.39)$$

Part (a) is now proved. For all $\underset{\sim}{e} \in L_{2e}$ and all $\tau \in R_+$:

$$\|(K-C)\underset{\sim}{e}\|_\tau^2 = \|(K-C)R^I R \underset{\sim}{e}\|_\tau^2 \qquad \text{(because } R^I \text{ exists)} \qquad (3.A.40)$$

$$= \|(K-C)R^I \underset{\sim}{e}_\tau\|_\tau^2 \qquad \text{(because } R \text{ is causal)} \qquad (3.A.41)$$

$$\leq \|(K-C)R^I \underset{\sim}{e}_\tau\|_{L_2}^2 \qquad \text{(norm increases as } \tau \to \infty) \qquad (3.A.42)$$

$$= \int_0^\infty \left\| (K-C) R^I \underline{e}_\tau(t) \right\|_E^2 \, dt \tag{3.A.43}$$

(by definition of the L_2 norm, the integral

exists because $K, C,$ and R^I are L_{2e}-stable)

$$= \frac{1}{2\pi} \int_{-\infty}^\infty \left\| (K-C) R^I \, \underline{e}_\tau(j\omega) \right\|_E^2 \, d\omega \qquad \text{(Parseval's)} \tag{3.A.44}$$

$$= \frac{1}{2\pi} \int_{-\infty}^\infty \left\| \sum_n \underline{K}_n \, \underline{R}^{-1} \, \underline{e}_\tau(j\omega) \right\|_E^2 \, d\omega \qquad \text{[by (3.A.33)]} \tag{3.A.45}$$

$$\leq \frac{1}{2\pi} \int_{-\infty}^\infty \left[\sum_k \sum_n \left\| \underline{K}_n(j\omega - j\omega_s k) \right\|^2 \right] \cdot \left\| \underline{R}^{-1} \underline{e}_\tau(j\omega) \right\|_E^2 \, d\omega \tag{3.A.46}$$

(by Lemma 3.A)

$$\leq \frac{1}{2\pi} \int_{-\infty}^\infty r(\omega) \cdot \left\| \underline{R}^{-1} \underline{e}_\tau(j\omega) \right\|_E^2 \, d\omega \qquad \text{[by (3.A.39)]} \tag{3.A.47}$$

$$\leq \frac{1}{2\pi} \int_{-\infty}^\infty r(\omega) \cdot \left\| \underline{R}^{-1}(j\omega) \right\|^2 \cdot \left\| \underline{e}_\tau(j\omega) \right\|_E^2 \, d\omega \tag{3.A.48}$$

$$= \frac{1}{2\pi} \int_{-\infty}^\infty r(\omega) \cdot \sigma_{min}^{-2} \left[\underline{R}(j\omega) \right] \cdot \left\| \underline{e}_\tau(j\omega) \right\|_E^2 \, d\omega \tag{3.A.49}$$

$$\leq \frac{1}{2\pi} \int_{-\infty}^\infty (1-\varepsilon) \cdot \left\| \underline{e}_\tau(j\omega) \right\|_E^2 \, d\omega \qquad \text{[by (3.3)]} \tag{3.A.50}$$

$$= (1-\epsilon) \, \|\underset{\sim}{e}_\tau\|^2_{L_2} \qquad\qquad (3.A.51)$$

$$= (1-\epsilon) \, \|\underset{\sim}{e}_\tau\|^2_\tau \qquad\qquad (3.A.52)$$

$$= (1-\epsilon) \, \|R\underset{\sim}{e}\|^2_\tau \qquad\qquad (3.A.53)$$

$$\leq \|R\underset{\sim}{e}\|_\tau - \epsilon'\|\underset{\sim}{e}\|^2_\tau \qquad\qquad (3.A.54)$$

$$\text{where } \epsilon' = \epsilon \, \|R\|_{L_2}$$

It has been shown that K is strictly inside cone (C,R). This completes the proof of part (a).

The objective of the proof of part (b) is to show that the optimal $\underline{C}(s)$ of (3.7) minimizes the lower bound of $\sigma_{min} \, [\underline{R}(j\omega)]$. Note that $\underline{C}(j\omega)$ enters only in $r_3(\omega)$; and that $r_1(\omega)$, $r_2(\omega)$, and $r_3(\omega)$ are all nonnegative real numbers. If the optimal center is used then $r_3(\omega)=0$, which minimizes $r_1(\omega) - r_2(\omega) + r_3(\omega)$. This completes the proof of Theorem 3.2.

Proof of Theorem 3.4   This theorem gives sufficient conditions for robust closed loop stability when the hybrid operator is inside of a conic sector. The objective of the proof is to show that conditions (ii) and (iii) of Theorem 3.3 are true for all possible $\tilde{G}$'s.

The first part of this proof uses the LTI robustness result (2.22). Conditions (ii) of Theorem 3.3 is that $\tilde{G}(I+C\tilde{G})^I$ is L_{2e}-stable for all possible $\tilde{G}$'s. The assumption is made that $G(I+CG)^I$ is L_{2e}-stable. It follows from (2.22) that $\tilde{G}(I+C\tilde{G})^I$ is L_{2e}-stable for all possible $\tilde{G}$'s if

$$\ell_m(\omega) < \frac{\sigma_{min}\ [\underline{I} + \underline{G}\ \underline{C}(j\omega)]}{\sigma_{max}\ [\underline{G}\ \underline{C}(j\omega)]} \qquad \text{for all } \omega \qquad (3.A.55)$$

This inequality is implied by (3.15) of Theorem 3.4. Hence, if (3.15) is true then condition (ii) of Theorem 3.3 is true for all possible $\tilde{G}$'s.

The second part of the proof uses the following string of inequalities:

$$\sigma_{max}\ [\underline{R}\ \tilde{\underline{G}}\ (\underline{I} + \underline{C}\ \tilde{\underline{G}})^{-1}] \leq \sigma_{max}\ [\underline{R}\ \tilde{\underline{G}}]/\sigma_{min}\ [\underline{I} + \underline{C}\ \tilde{\underline{G}}] \qquad (3.A.56)$$

$$\leq \sigma_{max}\ [\underline{R}\ \underline{G}]\ (1+\ell_m)/\sigma_{min}\ [\underline{I} + \underline{C}\ \tilde{\underline{G}}]$$

$$(3.A.57)$$

(by the triangle inequality)

$$\leq \sigma_{max} [\underline{R}\ \underline{G}]\ (1+\ell_m)/\left\{\sigma_{min}\ [\underline{I} + \underline{C}\ \underline{G}] - \sigma_{max}\ [\underline{C}\ \underline{G}]\ \ell_m\right\}$$

$$(3.A.58)$$

(by property 10 of Table 2.1)

$$\leq 1 \quad \text{(if (3.15) is true)} \quad (3.A.59)$$

Hence, if (3.15) is true then conditions (iii) of Theorem 3.4 is true for all possible $\tilde{G}$. This completes the proof.

<u>Proof of Theorem 3.6</u> The objective is to show that $-K^I$ is outside of cone (C,R). This will be true (by Lemma 2.2) if and only if $\|RK(I+CK)^I\|_{L_2} \leq 1$. The proof of Theorem 3.6 is basically an application of Lemma 3.A to show that the composite operator has gain ≤ 1.

Condition (i) of Theorem 3.6 assumes that the following feedback system is closed loop stable:

$$
\left.
\begin{aligned}
\underline{e} &= \underline{e}_3 - C\underline{u} \\[8pt]
\underline{u} &= K\underline{e} \\[8pt]
\underline{u}_3 &= R\underline{u}
\end{aligned}
\right\}
\tag{3.A.60}
$$

A block diagram of this feedback system[1] is shown in Figure 3.A.1. The closed loop operator is $RK(I+CK)^I$.

Given the Laplace transform $\underline{e}_3(s)$ of the input, the Laplace transform of the output is

$$
\underline{u}_3(s) = \underline{R}(s)\,\underline{H}(s)\,\underline{D}^*_{c\ell}(s)\,\frac{1}{T}\sum_n \underline{F}(s-j\omega_s n)\underline{e}_3(s-j\omega_s n)
\tag{3.A.61}
$$

An alternate expression for (3.A.61) is obtained by defining

$$
\underline{K}_n(s) \overset{\Delta}{=} \frac{1}{T}\underline{R}(s)\,\underline{H}(s)\,\underline{D}^*_{c\ell}(s)\,\underline{F}(s-j\omega_s n) \quad \text{for all } n
\tag{3.A.62}
$$

---

[1]The subscript "3" is used to be consistent with Figure 2.10b of Subsection 2.4.5.

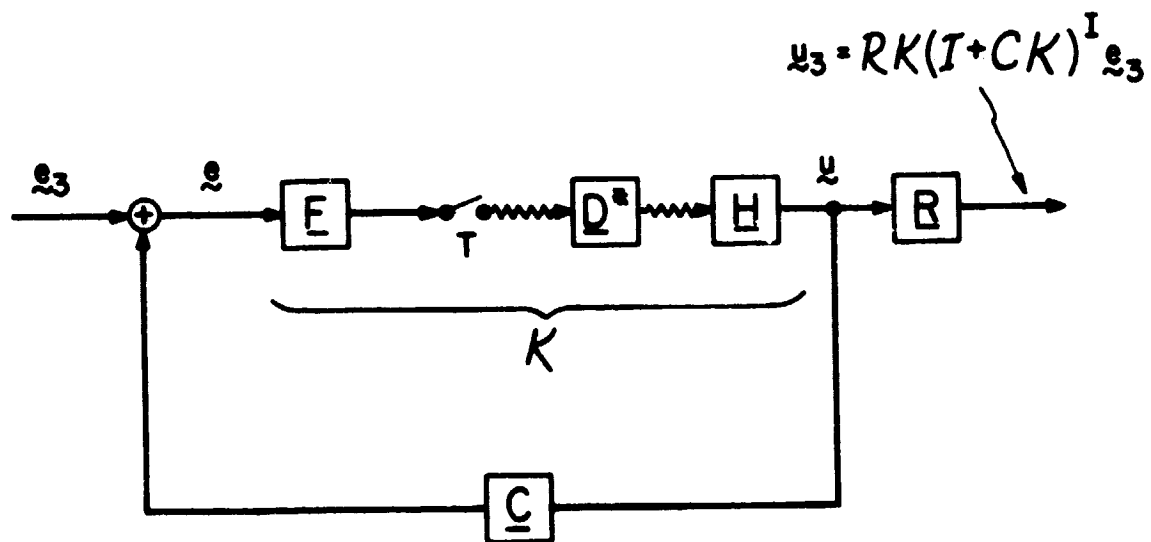$$\underset{\sim}{u}_3 = RK(I+CK)^I \underset{\sim}{e}_3$$

Figure 3.A.1: Feedback system used in proof of
Theorem 3.6.

and then by substituting (3.A.62) into (3.A.61) to obtain

$$\underline{u}_3(s) = \sum_n \underline{K}_n(s)\underline{e}(s-j\omega_s n) \tag{3.A.63}$$

The closed loop system has the same structure as a hybrid compensator, except that $\underline{D}^*(s)$ is replaced by its closed loop counterpart $\underline{D}^*_{c\ell}(s)$.

Define the truncated input

$$\underline{e}_\tau(t) = \begin{cases} \underline{e}(t) & t \leq \tau \\ \\ \underline{0} & t > \tau \end{cases} \tag{3.A.64}$$

The main part of the proof now follows. For all $\underline{e} \in L_{2e}$ and all $\tau \in R_+$:

$$\left\| RK(I+CK)^I \underline{e} \right\|_\tau = \left\| RK(I+CK)^I \underline{e}_\tau \right\|_\tau^2 \tag{3.A.65}$$

$$\leq \left\| RK(I+CK)^I \underline{e}_\tau \right\|_{L_2}^2 \tag{3.A.66}$$

$$= \frac{1}{2\pi} \int_{-\infty}^{\infty} \left\| \sum_n \underline{K}_n(j\omega)\underline{e}_\tau(j\omega-j\omega_s n) \right\|_E^2 d\omega \tag{3.A.67}$$

$$\leq \frac{1}{2\pi} \int_{-\infty}^{\infty} \left[\sum_k \sum_n \left\| \underline{K}_n(j\omega-j\omega_s k) \right\|^2 \right] \cdot \left\| \underline{e}_\tau(j\omega) \right\|_E^2 d\omega$$

$$\tag{3.A.68}$$

(by Lemma 3.A)

$$\leq \frac{1}{2\pi} \int_{-\infty}^{\infty} \frac{1}{T^2}\left[\sum_k \|\underline{R}\|^2 \cdot \|\underline{H}_k\|^2\right] \cdot \|\underline{D}_{c\ell}^*\|^2 \cdot \left[\sum_n \|\underline{F}_n\|^2\right] \cdot \|\underline{e}_\tau(j\omega)\|_E^2 \, d\omega$$

$$(3.A.69)$$

$$(\underline{R}_k = \underline{R} \text{ because } \underline{R} \text{ is periodic})$$

$$= \frac{1}{2\pi} \int_{-\infty}^{\infty} \|\underline{R}\|^2 \cdot r_9(\omega) \cdot \|\underline{e}_\tau(j\omega)\|_E^2 \, d\omega \qquad (3.A.70)$$

$$[r_9(\omega) \text{ defined in } (3.37)]$$

$$\leq \frac{1}{2\pi} \int_{-\infty}^{\infty} \|\underline{e}_\tau(j\omega)\|_E^2 \, d\omega \qquad [\text{by } (\ .3\ ?)] \qquad (3.A.71)$$

$$= \|\underline{e}_\tau\|_{L_2}^2 \qquad (3.A.72)$$

$$= \|\underline{e}\|_\tau^2 \qquad (3.A.73)$$

It has been shown that the operator $RK(I+CK)^I$ has gain ≤ 1, and therefore that $-K^I$ is outside of cone (C,R). This completes the proof.

<u>Proof of Theorem 3.8</u> The objective is to show that the inequality

(3.48) is satisfied for all $\underset{\sim}{r} \in S_a$. The property of signals $\underset{\sim}{r} \in S_a$ that

is exploited in this proof is that these signals are not aliased when

they are sampled. This lack of aliasing eliminates the need to shift and

add the prefilter $\underset{\sim}{F}(j\omega)$.

The following is valid as $\tau \to \infty$ and for all $\underset{\sim}{r} \in S_a$:

$$\| [GK(I + GK)^I - C(I + C)^I]\underset{\sim}{r} \|^2_{\tau}$$

$$= \| [GK(I + GK)^I - C(I + C)^I]\underset{\sim}{r} \|^2_{L_2} \qquad (3.A.74)$$

$$= \frac{1}{2\pi} \int_{-\infty}^{\infty} \| \underset{---cl}{GHD}^* \frac{1}{T} \sum_n F_{-n}r_n - C(I + C)^{-1}\underset{\sim}{r} \|^2_E d\omega \qquad (3.A.75)$$

$$= \frac{1}{2\pi} \sum_k \int_{(2k-1)\frac{\pi}{T}}^{(2k+1)\frac{\pi}{T}} \| \underset{---cl}{GHD}^* \frac{1}{T} \sum_n F_{-n}r_n - C(I + C)^{-1}\underset{\sim}{r} \|^2_E d\omega \qquad (3.A.76)$$

$$= \frac{1}{2\pi} \sum_k \int_{-\pi/T}^{\pi/T} \| \underset{-k-k-cl}{G_k H_k D}^* \frac{1}{T} \sum_n F_{-n+k}r_{n+k} - C_k(I + C_k)^{-1}\underset{-k}{r_k} \|^2_E d\omega \qquad (3.A.77)$$

$$= \frac{1}{2\pi} \int_{-\pi/T}^{\pi/T} \left[\sum_{k \neq 0} \| \underset{-k-k-cl}{G_k H_k D}^* \frac{1}{T} F\underset{\sim}{r} \|^2_E \right.$$

$$\left. + \| \underset{---cl}{GHD}^* \frac{1}{T} Fr - C(I + C)^{-1}\underset{\sim}{r} \|^2_E \right] d\omega \qquad (3.A.78)$$

(because there is no aliasing)

$$\leq \frac{1}{2\pi} \int_{\pi/T}^{\pi/T} \left[\sum_{k \neq 0} \| \underset{-k-k-cl}{G_k H_k D}^* \frac{1}{T} F \|^2 \right.$$

$$\left. + \| \underset{---cl}{GHD}^* \frac{1}{T} F - C(I + C)^{-1} \|^2 \right] \| \underset{\sim}{r} \|^2_E d\omega \qquad (3.A.79)$$

$$\leq \frac{1}{2\pi} \int_{\pi/T}^{\pi/T} \| \underline{R}_3 \underline{r} \|_E^2 \; d\omega \qquad \text{[by (3.49)]} \qquad (3.A.80)$$

$$= \| R_3 \underline{r} \|_{L_2}^2 \qquad (3.A.81)$$

$$= \| R_3 \underline{r} \|_{\tau}^2 \qquad (3.A.82)$$

This completes the proof.

4. NUMERICAL CONSIDERATIONS FOR THE COMPUTATION OF THE CONE RADIUS

4.1 Introduction

The previous chapter contains many different cones that the hybrid operator is either inside of or outside of. For each of these cones the radius must be computed. In this chapter it is shown how to compute the different radii.

Equations for the radius are given in Theorems 3.2, 3.5, and 3.6. The equations contain several parts that are combined in straightforward ways. What is $\underline{not}$ straightfoward is that each of the parts contain infinite series that must be summed. The infinite series take the form

$$s(\omega) = \sum_k \| \underline{A}_k \|^2 \tag{4.1}$$

$$r_4(\omega) = \frac{1}{T^2} \sum_k \sum_{n \neq k} \| \underline{H}_k \underline{D}^* \underline{F}_n \|^2 \tag{4.2}$$

The "$\underline{A}$" matrix is either the prefilter, the hold, or any of several different combinations of the prefilter, hold, and plant. Equation (4.2) has appeared earlier as equation (3.11).

The computational results of this chapter are grouped into three sections. In Section 4.2 the infinite sum (4.1) is approximated by summing a finite number of terms. Sufficient conditions are given for the remainder to be bounded. In Section 4.3 the double infinite sum (4.2) is approximated by summing a finite number of terms. Analysis of the double infinite sum is aided by splitting it into several single infinite sums. The double infinite sum is finite if the single infinite sums are finite. In Section 4.4 analytical solutions for $s(\omega)$ of (4.1) are presented. Analytical solutions have been found when $\underline{A}(s) = a(s)$ is single input single output (SISO). The major

results of this chapter are summerized in three theorems:

Theorem 4.1: Upperbound for the remainder of the truncated
infinite series for $s(\omega)$.

Theorem 4.2: Analytical solution for $s(\omega)$ when $a(s)$ has a state
space realization.

Theorem 4.3: Analytical solution for $s(\omega)$ when $a_o(s) = h(s) a(s)$,
where $h(s)$ is a zero-order-hold and $a(s)$ has a state
space realization.

It is helpful to understand some of the qualitative behavior of the

infinite series for $s(\omega)$. The sum is even [i.e. $s(\omega) = s(-\omega)$] and periodic

with period ω_s [i.e. $s(\omega) = s(\omega-k\omega_s)$ for any interger k].   Because of

these two facts it is only necessary to compute $s(\omega)$ for points between

0 and $\omega_s/2 = \pi/T$ (the foldover frequency). If $\underline{A}(j\omega)$ is small above the

foldover frequency then the aliasing is insignificant and $s(\omega)^{1/2}$ will

be approximately equal to $\| \underline{A}(j\omega) \|$ for $|\omega| < \pi/T$.

An example will help to clarify this qualitative behavior. Consider

the first order lag

$$a(s) = \frac{1}{s + 1} \qquad\qquad (4.3)$$

A magnitude Bode plot of $a(j\omega)$ is shown in Figure 4.1. The same Bode

plot contains several different plots of $s(\omega)^{1/2}$, each for a different

sample interval T.

The break point of $a(j\omega)$ is at $\omega = 1$. If $1 << \omega_s$ then $s(\omega)^{1/2} \approx$

$|a(j\omega)|$ for $o \leq \omega \leq \omega_s/2$. On the other hand, if $\omega_s << 1$ then $s(\omega) \approx$

$(T/2)^{1/2}$ for all ω. At high frequencies ($\omega_s << \omega$) it is always true

that $|a(j\omega)| << s(\omega)^{1/2}$, because $|a(j\omega)|$ rolls off and $s(\omega)^{1/2}$ is
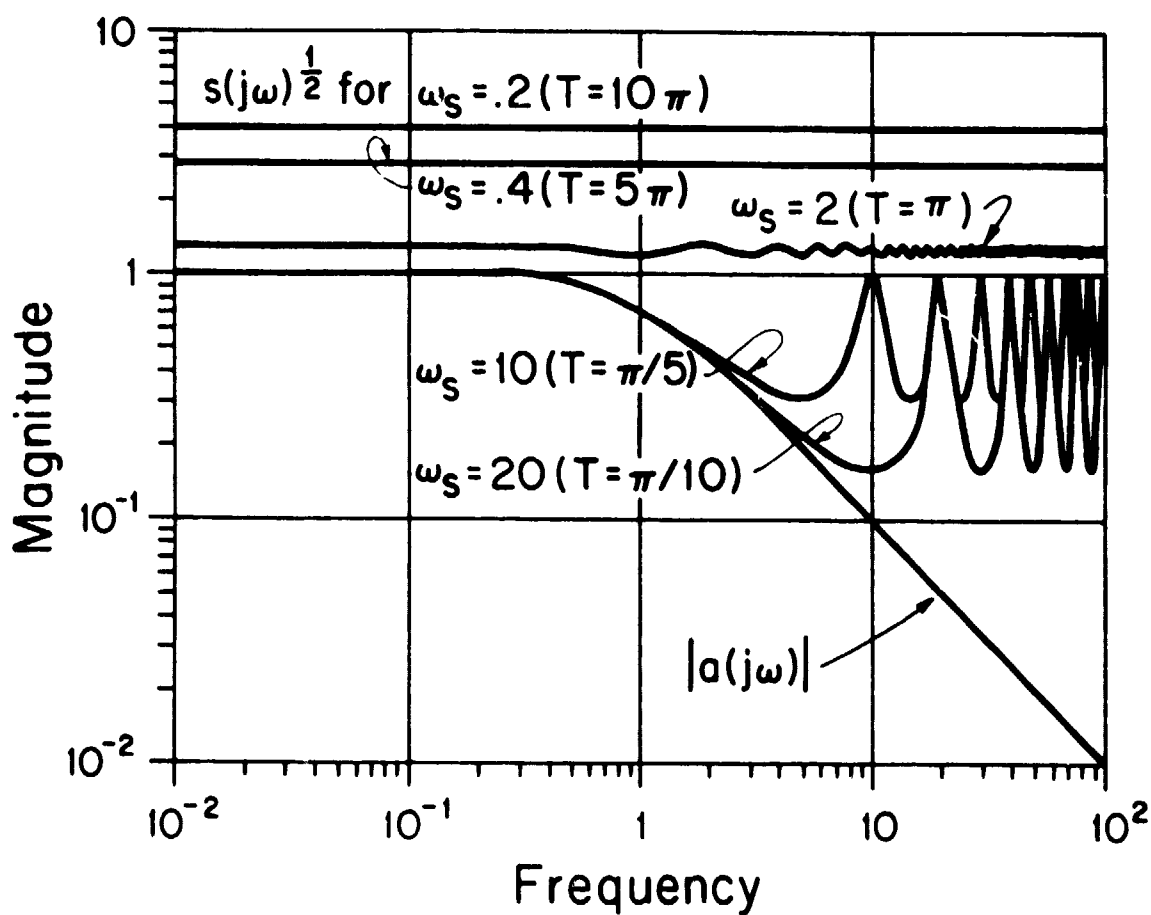
periodic.

Figure 4.1: Comparison of $|a(j\omega)|$ and $s(\omega)^{1/2}$

4.2 Truncating an Infinite Series

One way to compute $s(\omega)$ is to sum a finite number of terms of the infinite series (4.1). Whether or not this is feasible depends on the behavior of the remainder.

In this section sufficient conditions are presented for the remainder to be bounded. One example of these sufficient conditions is that the remainder is bounded if $\underline{A}(j\omega)$ has an one pole rolloff. These sufficient conditions show that the remainder approaches zero as the number of terms of the truncated series increases. This information can be used to determine where to truncate the infinite series so that the remainder is less than a specified amount.

Some new notation is needed. Let the truncated series and its remainder be defined by

$$s_N(\omega) \triangleq \sum_{k=-N}^{N} \| \underline{A}_k \|^2 \tag{4.4}$$

$$r_N(\omega) \triangleq s(\omega) - s_N(\omega) \tag{4.5}$$

Two assumptions are made about $\underline{A}(j\omega)$. It is assumed that above some frequency ω_o that $\| \underline{A}(j\omega) \|$ lies below a straight line asymptote:

$$\| \underline{A}(j\omega) \| \leq b(\omega) \quad \text{for } \omega \geq \omega_o \tag{4.6}$$

$$\text{where} \quad b(\omega) = \left(\frac{\omega_o}{\omega}\right)^p \tag{4.7}$$

This assumption is illustrated in Figure 4.2. On a log-log scale the straight line asymptote has a slope of $-p$. If $p = 1$ then $\underline{A}(j\omega)$ is said to have at least an one pole rolloff.
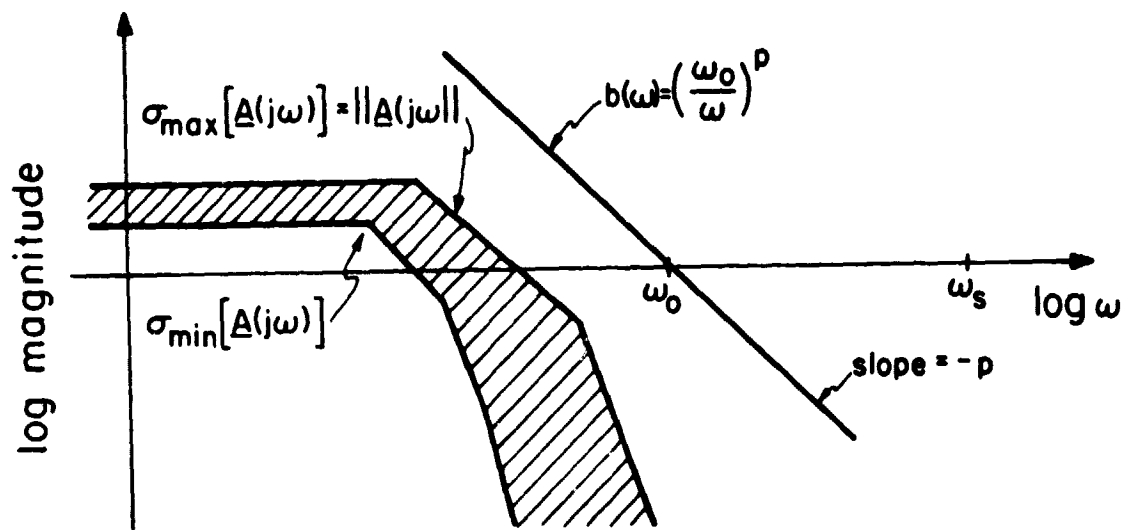
Figure 4.2: Assumption that $\|\underline{A}(j\omega)\|$ lies below a straight
line asymptote

The second assumption about $\underline{A}(j\omega)$ is that

$$\| \underline{A}(j\omega) \| < \infty \quad \text{for all } \omega \tag{4.8}$$

If this assumption is true then the boundedness of $r_N(\omega)$ implies the boundedness of $s(\omega)$.

The main result of this section is now presented. The proof is in the Appendix to Chapter 4.

<u>Theorem 4.1</u> Consider the Laplace transform matrix $\underline{A}(s)$.

(a) If (4.6) is true for $p > \frac{1}{2}$ then

$$r_N(\omega) \leq \left(\frac{2}{2p-1}\right) \left(\frac{\omega_o}{\omega_s}\right)^{2p} \left(\frac{1}{N-1}\right)^{2p-1} \tag{4.9}$$

$$\text{for } o < \omega < \omega_s \text{ and } N \geq \left(\frac{\omega_o}{\omega_s}\right)$$

(b) Furthermore, if (4.8) is true then

$$s(\omega) \leq g \quad \text{for all } \omega \text{ and some } g < \infty \qquad \blacksquare \tag{4.10}$$

The upperbound on $r_N(\omega)$ is only valid over the fundamental frequency range. Only at the cost of considerable notation can the result be extended to other frequency ranges (see the remark in the Appendix to Chapter 4). The lower bound on N, which is one of the conditions of (4.9), assures that all of the terms of the remainder are bounded by $b(\omega)$ of (4.7).

When $\underline{A}(j\omega)$ has an one-pole rolloff then (4.6) is true for $p = 1$. The upperbound on the remainder is given by

$$r_N(\omega) \leq 2 \left(\frac{\omega_o}{\omega_s}\right)^2 \left(\frac{1}{N-1}\right) \tag{4.11}$$

The remainder is (approximately) proportional to $\frac{1}{N}$, which is characteristic

of an incredibly slow rate of convergence.[1] Each extra decimal point of accuracy requires 10 times as many terms in $s_N(\omega)$.

Theorem 4.1 can be used to determine the value of N such that the upperbound of $r_N(\omega)$ is less than a specified amount.[2] If this is important then it should be recognized that the upperbound (4.9) can be tightened, and may result in a value of N larger than necessary.

The best use of Theorem 4.1 is to help understand the qualitative behavior of the remainder (such as when it is bounded and, if bounded, what is its rate of convergence).

---

[1] Slow compared to exponential convergence.

---

[2] For example, if $p = 1$ then $N > (2/\epsilon)\,(\omega_0/\omega_s)^2$ guarantees that $r_N(\omega) < \epsilon$ for $o < \omega < \omega_s$.

4.3 Truncating a Double Infinite Series

The double infinite series (4.2) can be decomposed into several single infinite series:

$$r_4 (\omega) = \frac{1}{T^2} \sum_k \sum_{n \neq k} \| \underline{H}_k \underline{D}^* \underline{F}_n \|^2 \tag{4.12}$$

$$= \frac{1}{T^2} \sum_k \sum_n \| \underline{H}_k \underline{D}^* \underline{F}_n \|^2 - \frac{1}{T^2} \sum_k \| \underline{H}_k \underline{D}^* \underline{F}_k \|^2 \tag{4.13}$$

$$\leq \left[\frac{1}{T^2} \sum_k \| \underline{H}_k \|^2 \right] \cdot \| \underline{D}^* \|^2 \cdot \left[\sum_n \| \underline{F}_n \|^2 \right] - \frac{1}{T^2} \sum_k \| \underline{H}_k \underline{D}^* \underline{F}_k \|^2 \tag{4.14}$$

The inequality in (4.14) can be replaced by an equality if the matrices are replaced by scalars.

The double infinite series (4.12) is finite for each ω if $\sum_k \| \underline{H}_k \|^2$, $\| \underline{D}^* \|^2$, and $\sum_n \| \underline{F}_n \|^2$ are all finite for each ω. Each term of (4.12) is nonnegative, so (4.12) is lower bounded by zero. The subtraction in (4.14) cannot result in a negative number.

A truncated version of (4.12) is defined:[1]

$$r_{4N} (\omega) = \frac{1}{T^2} \sum_{k=-N}^{N} \sum_{\substack{n=-N \\ n \neq k}}^{N} \| \underline{H}_k \underline{D}^* \underline{F}_n \|^2 \tag{4.15}$$

The remainder $r_4 (\omega) - r_{4N} (\omega)$ can be analyzed by using the remainders of the single infinite series of (4.14). This analysis is cumbersome and will not be attempted here. The endpoint of this analysis is clear - if $\underline{H}(j\omega)$ and $\underline{F}(j\omega)$ both have at least a one pole rolloff then

---

[1] Equation (4.15) with N = 20 was used in the examples of Chapter 5.

the remainder $r_4(\omega) - r_{4n}(\omega)$ is bounded and approaches zero as $N \to \infty$.

Truncating the double infinite series is often prefereable to truncating the various single infinite series of (4.14). For multivariable systems the double infinite series has the distinct advantage of being less than or equal to (4.14).

The double infinite series has another advantage in that it avoids a common numerical problem. The double infinite series [which sums to $r_4(\omega)$] is converted to (4.14) by adding and substracting $\frac{1}{T^2} \sum_k \|\underline{H}_{-k} \underline{D}^* \underline{F}_{-n}\|^2$. For some values of ω this term may be orders of magnitude larger than $r_4(\omega)$. This introduces numerical problems when finite precision arithmetic is used, because (4.14) involves the substraction of two large numbers, which results in a loss of accuracy. An example of this loss of accuracy is shown in Subsection 5.2.6.

4.4 Analytic Solutions

In some cases an analytic solution can be found for $s(\omega)$ of (4.1). The Laplace transform matrix $\underline{A}(s)$ must be a scalar, in other words $\underline{A}(s) = a(s)$.

Equation (4.19) is used to find analytic solutions for $s(\omega)$. This equation is now derived. Let $b(s)$ be a Laplace transform, $b(t)$ the inverse Laplace transform, and $b(z)$ the z-transform of the samples $b(kT)$[1]. It is well known [4, pp. 77-80] that

$$\sum_k b_k = T \cdot b(z)\Big|_{z=e^{j\omega T}} \tag{4.16}$$

Define

$$b(s) \stackrel{\Delta}{=} a(-s)\, a(s) \tag{4.17}$$

and then it follows that

$$b(j\omega) = a(-j\omega)\, a(j\omega) = \left| a(j\omega) \right|^2 \tag{4.18}$$

$$s(\omega) = \sum_k \left| a_k \right|^2 = \sum_k b_k = T \cdot b(z)\Big|_{z=e^{j\omega T}} \tag{4.19}$$

Whether or not (4.19) is useful depends on how easy it is to derive an expression for $b(z)$. Given an expression for $a(s)$ the way to find $b(z)$ is to respectively find $a(-s)$, $b(s)$, $b(t)$, $b(nT)$, and then $b(z)$. This procedure will be followed for the following cases:

1) Zero-order-hold
2) First order lag
3) Cascaded zero-order-hold and first order lag
4) $a(s)$ given by a state space representation

---

[1] Any region of convergence (ROC) can be used. If the ROC of $b(s)$ is $s_o < \mathrm{Re}(s) < s_1$ then the corresponding ROC of $b(z)$ is $e^{s_o T} < |z| < e^{s_1 T}$.

5) a(s) given by a state space representation cascaded with a zero-order-hold.

The last two cases are sufficiently general to present them as theorems.

<u>Case 1</u> If the hold device is a zero-order-hold then $a_1(s) = h(s)$ has the following Laplace transform:[1]

$$a_1(s) = \frac{1-e^{-sT}}{s} \qquad\qquad (4.20)$$

It is straightforward but tedious to compute $b_1(s) = a_1(-s)\, a_1(s)$ and then to compute the inverse Laplace transform to obtain $b_1(t)$. A shortcut is to recognize that the inverse Laplace transform of $a_1(-s)$ is $a_1(-t)$, and that $b_1(t) = a_1(t) * a_1(-t)$. This convolution is shown in Figure 4.3. There is only one nonzero sample of $b_1(t)$, which is $b_1(o) = T$. The z-transform of $b_1(nT)$ is

$$b_1(z) = T \qquad\qquad (4.21)$$

Therefore the analytical solution for $s(\omega)$ is

$$s(\omega) = \sum_n \left| a_{1n} \right|^2 = T^2 \qquad\qquad (4.22)$$

which is a remarkable simplification!

<u>Case 2</u> If the prefilter is a first order lag then $a_2(s) = f(s)$ has the following Laplace transform:

$$a_2(s) = \frac{a_o}{s + a_o} \qquad\qquad (4.23)$$

Unlike the previous case there is no shortcut around the page or two of mathematical tedium which results in the desired expression

---

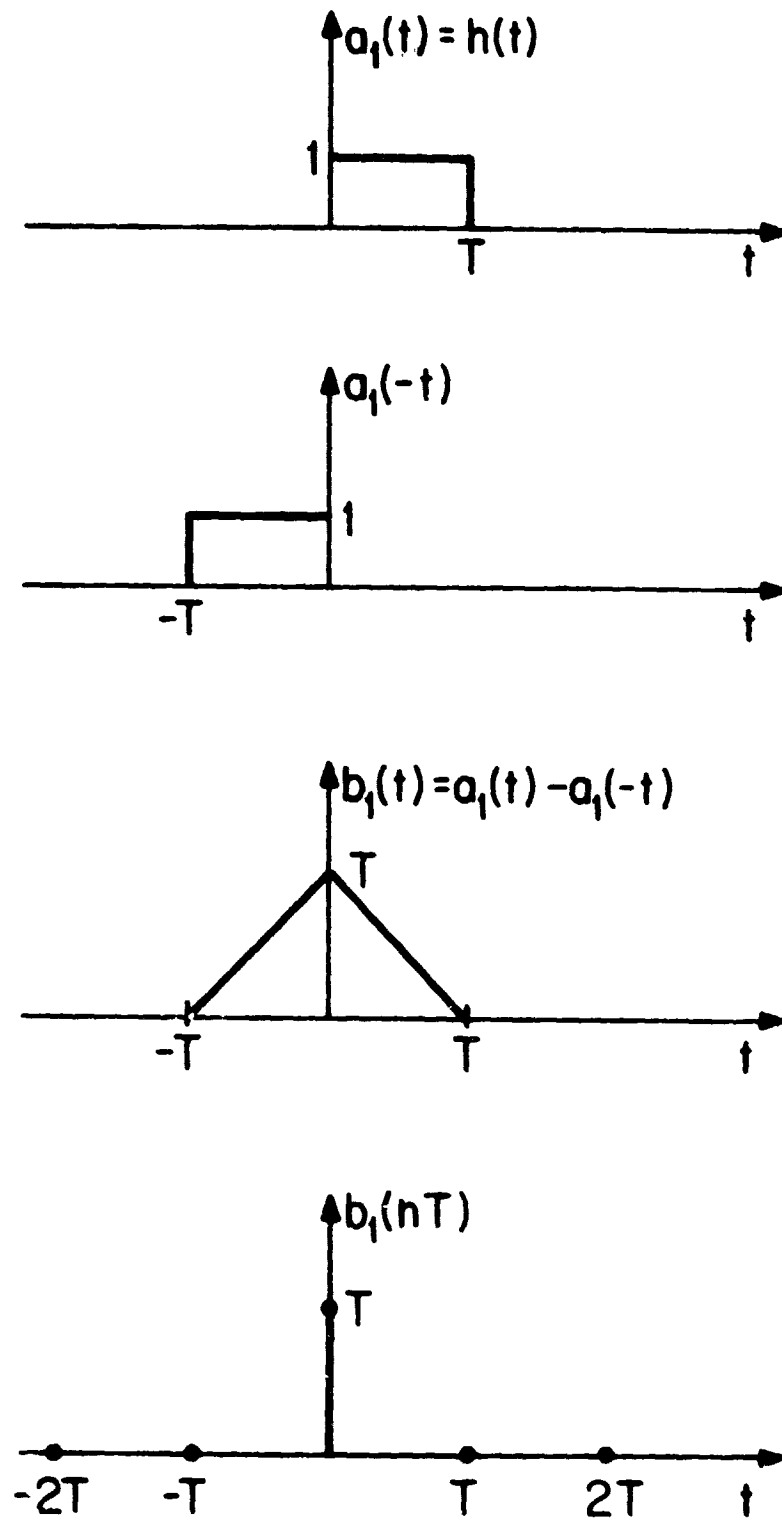[1] The subscripts "1" through "5" are used to distinguish the a's and b's of the five cases.

Figure 4.3: Zero-order-hold

$$b_2(z) = \frac{a_o}{2} \quad \frac{\alpha z}{z^2 - \beta z + 1} \tag{4.24}$$

where

$$\alpha = \exp(-a_o T) - \exp(a_o T)$$

$$\beta = \exp(-a_o T) + \exp(a_o T)$$

Case 3 Part of the radius calculation has the hold and prefilter in the same infinite sum [e.g. $r_2(\omega)$ of Theorem 3.2]. In this case a zero-order-hold is cascaded with a first order lag:

$$a_3(s) = \frac{1 - e^{-sT}}{s} \quad \frac{a_o}{s + a_o} \tag{4.24}$$

Again the intermediate steps are left to the reader. The final result is

$$b_3(z) = \frac{1}{2a_o} \quad \frac{\alpha(z-1)^2}{z^2 - \beta z + 1} + T \tag{4.25}$$

The α and β are the same as for the case 2. The denominators of $b_2(z)$ and $b_3(z)$ are the same.

Example Consider a SISO hybrid compensator with a first order lag and a zero-order-hold. The digital computer z-transform is arbitrary. The results of the first three cases of this section can be used to place this hybrid compensator inside of a cone.

Choose the optimal center of the cone:

$$c(s) = \frac{1}{T} h(s) d^*(s) f(s) \tag{4.26}$$

From Theorem 3.2 the radius r(s) must satisfy the inequality:

$$|r(j\omega)| \geq [r_1(\omega) - r_2(\omega)]^{1/2} \tag{4.27}$$

After a few substitutions it follows that

$$r_1(\omega) - r_2(\omega) = |d(z)|^2 \{b_1(z)\ b_2(z) - \frac{1}{T}\ b_3(z)\}\Big|_{z=e^{j\omega T}} \quad (4.28)$$

<u>Case 4</u> If $a_4(s)$ has a state space realization then an analytical solution can be found for $s(\omega)$. This case is useful when the prefilter is more complicated than the first order lag of case 2.

Let the state space realization of $a_4(s)$ be

$$\left.\begin{array}{l} \dot{x} = \underline{A}\underline{x} + \underline{b}u \\ y = \underline{c}\underline{x} \end{array}\right\} \quad (4.29)$$

The Laplace transform of (4.29) is

$$a_4(s) = \underline{c}\ (s\underline{I} - \underline{A})^{-1}\ \underline{b} \quad (4.30)$$

and the Laplace transform of $a_4^T(-s)$ is

$$a_4^T(-s) = -\underline{b}^T\ (s\underline{I} + \underline{A}^T)^{-1}\ \underline{c}^T \quad (4.31)$$

which has the state space realization

$$\left.\begin{array}{l} \dot{\underline{x}} = -\ \underline{A}^T\underline{x} + \underline{c}^T u \\ y = -\underline{b}^T\ \underline{x} \end{array}\right\} \quad (4.32)$$

The cascade of the two systems (4.29) and (4.32) has the Laplace transform $b_4(s) = a_4^T(-s)\ a_4(s)$. The state space realization of $b_4(s)$ is[1]

$$\left.\begin{array}{l} \dot{\underline{x}} = \hat{\underline{A}}\underline{x} + \hat{\underline{b}}u \\ y = \hat{\underline{c}}\underline{x} \end{array}\right\} \quad (4.33)$$

---

[1] The transpace $a^T(-s)$ is used so that $\hat{\underline{A}}$ has the form of a Hamiltonian matrix.

where

$$\hat{\underline{A}} = \begin{bmatrix} \underline{A} & \underline{o} \\ -\underline{c}^T\underline{c} & -\underline{A}^T \end{bmatrix} \qquad \hat{\underline{b}} = \begin{bmatrix} \underline{b} \\ \underline{o} \end{bmatrix} \Bigg\}$$

$$\hat{\underline{c}} = [\underline{o} \quad \underline{b}^T] \qquad\qquad\qquad\qquad \Bigg\}$$

(4.34)

The causal impulse response of $b_4(s)$ is

$$b_4(t) = \hat{\underline{c}}\, e^{\hat{A}t}\, \hat{\underline{b}} \qquad \text{for } t \geq o \tag{4.35}$$

and the z-transform $b_4(z)$ of the samples $b_4(nT)$ is

$$b_4(z) = \sum_{n=o}^{\infty} b_4(nT)\, z^{-n} \tag{4.36}$$

$$= \underline{h}\, (z\underline{I} - \underline{F})^{-1}\, \underline{g} \tag{4.37}$$

where

$$\left.\begin{aligned} \underline{F} &= \exp\,(\hat{\underline{A}}T) \\ \underline{g} &= \underline{F}\hat{\underline{b}} \\ \underline{h} &= \hat{\underline{c}} \end{aligned}\right\}$$

(4.38)

The result just derived is presented as a Theorem.

Theorem 4.2   If $a_4(s)$ has the state space realization (4.29) then

$$s(\omega) = \sum_{n} \left|a_{4n}\right|^2 = T \cdot b_4(z)\Big|_{z=e^{j\omega T}} \tag{4.39}$$

where $b_4(z)$ is given by (4.37) and (4.38).   ∎

Case 5   In this case $a_5(s)$ is a zero-order-hold cascaded with $a_4(s)$ of the previous case. This case is a generalization of case 3. It is useful when a prefilter that is more complicated then first order lag is cascaded with a zero-order-hold. This case is also useful when the plant is cascaded with a zero-order-hold.

State space realizations of $a_4(s)$, $a_4^T(-s)$, and $b_4(z)$ are given in the previous case. Let $h(s)$ be a zero-order-hold and let

$$b_1(s) = h(-s) \; h(s) \tag{4.40}$$

$$b_5(s) = b_4(s) \; b_1(s) \tag{4.41}$$

The impulse response $b_5(t)$ is a convolution of $b_4(t)$ [the causal impulse response of (4.35)] and $b_1(t)$ [the non-causal impulse response in Figure 4.3]. Sample $b_5(t)$ and compute the z-transform of these samples. The result is

$$b_5(z) = \underline{h}_5(z\underline{I} - \underline{F}_5)^{-1} \; \underline{g}_5 + k_5 \tag{4.42}$$

where

$$F_5 = \exp{(\hat{\underline{A}}T)}$$

$$\underline{g}_5 = \int_0^T \exp{(\hat{\underline{A}}\tau)} \; \underline{\hat{b}}\tau \; d\tau$$

$$+ \underline{F}_o \int_0^T \exp{(\hat{\underline{A}}\tau)} \; \underline{\hat{b}} \; (T-\tau) \; d\tau \tag{4.43}$$

$$\underline{h}_5 = \hat{\underline{c}}$$

$$k_5 = \hat{\underline{c}} \int_0^T \exp{(\hat{\underline{A}}\tau)} \; \underline{b}(T-\tau) \; d\tau$$

One more step is needed to avoid the integrations of (4.43). The trick is to use the augmented matrix.

$$\underline{C} = \begin{bmatrix} \underline{A} & \underline{b} & \underline{0} \\ \underline{0} & 0 & 1 \\ \underline{0} & 0 & 0 \end{bmatrix} \begin{matrix} \updownarrow 2n \\ \updownarrow 1 \\ \updownarrow 1 \end{matrix} \tag{4.44}$$

$$\begin{matrix} \leftrightarrow & \leftrightarrow & \leftrightarrow \\ 2n & 1 & 1 \end{matrix}$$

The dir ensions of each of the sub-matrices are indicated, where n is the order of $a_4(s)$. As shown by Van Loan [22], the matrix exponential has the form:

$$\exp\ (\underline{C}T)\ =\ \begin{bmatrix} \underline{F}_1 & \underline{g}_1 & \underline{h}_1 \\ \underline{0} & f_2 & g_2 \\ \underline{0} & 0 & f_3 \end{bmatrix} \tag{4.45}$$

where

$$\left. \begin{aligned} \underline{F}_1 &= \exp\ (\hat{\underline{A}}T) \\[1em] f_2 &= 1 \\[1em] f_3 &= 1 \\[1em] \underline{g}_1 &= \int_0^T \exp\ (\hat{\underline{A}}\tau)\ \hat{\underline{b}}\ d\tau \\[1em] \underline{g}_2 &= T \\[1em] \underline{h}_1 &= \int_0^T \exp\ (\hat{\underline{A}}\tau)\ \underline{b}(T-\tau)\ d\tau \end{aligned} \right\} \tag{4.46}$$

Hence, by substituting (4.46) into (4.43)

$$\left. \begin{aligned} \underline{F}_5 &= \underline{F}_1 \\[1em] \underline{g}_5 &= T\underline{g}_1 + (\underline{F}_1 - \underline{I})\ \underline{h}_1 \\[1em] \underline{h}_5 &= \hat{\underline{c}} \\[1em] k_5 &= \hat{\underline{c}}\underline{h}_1 \end{aligned} \right\} \tag{4.47}$$

The result just derived for case 5 is summarized in the following theorem.

Theorem 4.3 Let $a_5(s) = h(s) \, a_4(s)$, where $h(s)$ is a zero-order-hold and $a_4(s)$ has the state space realization (4.29). Then

$$s(\omega) = \sum_n \left| a_{5n} \right|^2 = T \cdot b_5(z) \Big|_{z=e^{j\omega T}} \qquad (4.48)$$

where $b_5(z)$ is given by (4.42) and (4.47).   ∎

This completes the section on analytical solutions of (4.1). The Fourier transform matrix $\underline{A}(j\omega)$ must be a scalar $\underline{A}(j\omega) = a(j\omega)$. The matrix exponential is used for the analytical solutions of Theorems 4.2 and 4.3. The $a(j\omega)$ of Theorem 4.2 is represented by a state space description, and the $a(j\omega)$ of Theorem 4.3 is represented by a state space description cascaded with a zero-order-hold.

Appendix to Chapter 4

This appendix contains the following proof:

Proof of Theorem 4.1   The objective of part (a) is to show the validity of (4.9), which is an upperbound for the remainder $r_N(\omega)$ of the truncated series (4.4). An upperbound is found for each term of the infinite series for $r_N(\omega)$, and then an upper bound is found for the sum of the infinite series of upperbounds.

An intermediate step in the proof is to find an upperbound for

$$\hat{r}_N = \sum_{k=N}^{\infty} \left(\frac{1}{k}\right)^{2p} \tag{4.A.1}$$

This series is known to converge[1] if and only if $p > \frac{1}{2}$. An upper bound is

$$r_N < \int_{N-1}^{\infty} \left(\frac{1}{x}\right)^{2p} dx = \left(\frac{1}{2p-1}\right)\left(\frac{1}{N-1}\right)^{2p-1} \tag{4.A.2}$$

This inequality is illustrated in Figure 4.A.1. The sum $\hat{r}_N$ is the area of the rectangular boxes, which is less than the area under the curve.

The main part of the proof now follows. For $o \leq \omega \leq \omega_s$ and $N \geq (\omega_o/\omega_s)$:

$$r_N(\omega) = \sum_{k=-\infty}^{-(N+1)} \left\| \underline{A}(j\omega-j\omega_s k) \right\|^2 + \sum_{k=N+1}^{\infty} \left\| \underline{A}(-j\omega+j\omega_s k) \right\|^2 \tag{4.A.3}$$

(by definition)

---

[1] An analytical solution is known for the case

$$\sum_{k=1}^{\infty} \left(\frac{1}{k}\right)^2 = \frac{\pi^2}{6}$$

$$= \sum_{k=N+1}^{\infty} \| \underline{A}(j\omega+j\omega_s k) \|^2 + \sum_{k=N+1}^{\infty} \| \underline{A}(-j\omega+j\omega_s k) \|^2 \qquad (4.A.4)$$

(In the first series replace k by -k. In
the second series use the identity
$\| \underline{A}(j\tilde{\omega}) \| = \| \underline{A}(-j\tilde{\omega}) \|$).

$$\leq \sum_{k=N+1}^{\infty} [b(\omega+\omega_s k)^2 + b(-\omega+\omega_s k)^2] \qquad (4.A.5)$$

(for all k both $\omega+\omega_s k$ and $-\omega+\omega_s k$ are $> \omega_o$).

$$= \sum_{k=N+1}^{\infty} \left[\left(\frac{\omega_o}{\omega+\omega_s k} \right)^2 + \left(\frac{\omega_o}{-\omega+\omega_s k} \right)^2 \right] \qquad (4.A.6)$$

[substitute (4.7) for b(ω)]

$$\leq 2 \sum_{k=N+1}^{\infty} \left[\frac{\omega_o}{\omega_s(k-1)} \right]^{2p} \qquad (4.A.7)$$

(This step removes the dependence on ω.
Hence, the convergence is uniform for
$o < \omega < \omega_s$)

$$= 2 \left(\frac{\omega_o}{\omega_s} \right)^{2p} \sum_{k=N}^{\infty} \left(\frac{1}{k} \right)^{2p} \qquad (4.A.8)$$

$$\leq 2 \left(\frac{\omega_o}{\omega_s} \right)^{2p} \left(\frac{1}{2p-1} \right) \left(\frac{1}{N-1} \right)^{2p-1} \qquad (4.A.9)$$

[if $p > \frac{1}{2}$, by (4.A.2)]

This completes the proof of part (a).

Part (b) is true if $s_N(\omega)$ is finite for all ω, which is in turn
true if $\| \underline{A}(\omega) \|$ is bounded for all ω. This completes the proof.

$$f(x) = \left(\frac{1}{x}\right)^{2p}$$

$$\hat{r}_N = \sum_{k=N}^{\infty} \left(\frac{1}{k}\right)^{2p} \leq \int_{N-1}^{\infty} f(x)\, dx$$
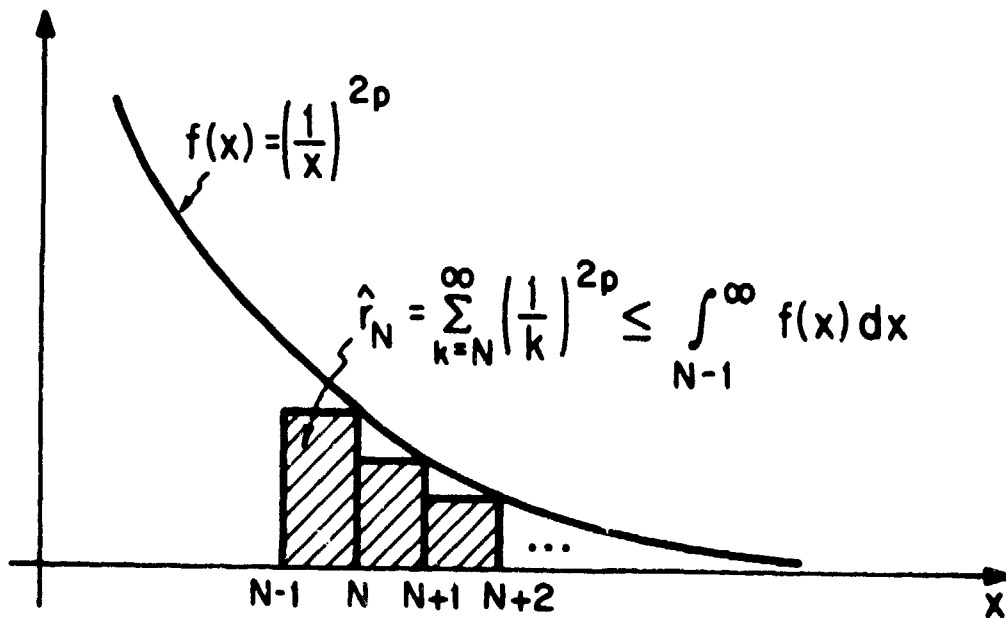
N-1   N   N+1   N+2

x

Figure 4.A.1: An upperbound for an infinite series

<u>Remark</u> The upperbound for $r_N(\omega)$ is only valid for ω in the fundamental frequency range $c \leq \omega < \omega_s$. This is a consequence of the fact that $s_N(\omega)$ and $r_N(\omega)$ are not periodic. The finite sum $s_N(\omega)$ is centered around the fundamental frequency range. To extend the upperbound to other frequency ranges then $s_N(\omega)$ must be defined to be centered around the other frequency ranges.

There is no need to go through this trouble, because $s(\omega)$ is periodic. Compute $s_N(\omega)$ over the fundamental frequency range and then shift it as needed by multiples of ω_s.

5. ANALYSIS OF HYBRID SYSTEMS AND NUMERICAL EXAMPLES

5.1 Introduction

The examples in this chapter show how conic sectors can be used to analyze hybrid feedback systems. In the first example the plant is a SISO open loop stable system. An analog lead-lag compensator is designed by classical control techniques. The analog compensator is discretized, a prefilter and hold are chosen, and then the resulting hybrid system is analyzed by conventional z-transform techniques. The first new technique is the use of Theorem 3.1 to compute the gain of the hybrid operator. Theorems 3.2 to 3.7 are then used to analyze closed loop stability and robustness. The analysis techniques based on these theorems are grouped according to whether the hybrid operator is inside of a cone, the loop transfer operator is inside of a cone, or the hybrid operator is outside of a cone. The example continues with three more uses of conic sectors - selecting the sample rate, comparison of discretization techniques, and robustness with respect to extra delay. The example then shows how conic sectors can be used to analyze command response.

The second example is not as extensive as the first. The plant is SISO and open loop stable, and the hybrid compensator is a discretized version of an analog integrator. An attempt is made to place the hybrid compensator inside of a conic sector, but the attempt fails because the radius is not finite. The example then goes on to show that Theorems 3.6 and 3.7 (for which the $-K^I$ is outside of a cone) can be used to analyze the robustness of this integral control problem.

In the third example the plant is a linearized model of motion

in the pitch axis of a high performance aircraft. Both SISO and multi-variable analog compensators are designed using Linear Quadratic Guassian (LQG) methodology, and then the analog compensators are discretized to form hybrid compensators. For the SISO hybrid feedback system the compensator is open loop stable and the plant is unstable. The hybrid operator can be placed inside of a conic sector but the loop transfer operator cannot be. The example shows how to proceed by placing a stable version of the loop transfer operator inside of a conic sector. For the multivariable version of this example, Theorems 3.6 and 3.7 are used to analyze robustness. The margins are shown to be conservative.

Before starting with the examples the difference between the nominal and actual feedback systems should be made clear. The nomi-feedback system differs depending on how the conic sectors are applied. The actual feedback system is the same (of course) no matter how the conic sectors are applied.

If the hybrid operator (or loop transfer operator) is inside of a cone then the nominal feedback system is an analog LTI feedback system. The center of the cone is part of this nominal feedback system. Perturbations of the nominal feedback system have two causes: (1) due to the use of a hybrid as opposed to an analog compensator, and (2) due to the actual plant being different from the nominal plant. The robustness results (Theorems 3.4 and 3.5) assume that the nominal feedback system is closed loop stable (as determined by analog techniques) and then give sufficient conditions for all perturbations in a defined set to preserve closed loop stability.

On the other hand, if the hybrid operator is outside of a cone then the nominal feedback system is a **hybrid** feedback system. Perturbations are due to the actual plant being different from the nominal plant. The robustness result (Theorem 3.7) assumes that the nominal feedback system is closed loop stable (as determined by digital techniques) and then gives sufficient conditions for all perturbations in a defined set to be closed loop stable.

5.2 Lead-lag Compensator

5.2.1 Classical Control Design

This example begins as a standard classical control problem. The open loop plant has the following transfer function:

$$g(s) = \frac{150}{(s+1)(s+3)} \tag{5.1}$$

The plant is single-input-single-output, 2nd order, and open loop stable. There is no particular system that $g(s)$ is supposed to represent (this is an academic example), but such a transfer function is typical of some kinds of rotating mechanical systems.

The objective of the classical control design is to find a compensator $k(s)$ that meets the following specifications:

(i) steady state error < 2% to a step input (dc gain > 50)

(ii) phase margin > 45°

(iii) maximize crossover frequency, but not above the uncompensated value.

The dc gain of $g(s)$ is 50, so no extra gain is needed to meet the steady state error requirement. Phase lead is needed around crossover to meet the phase margin specification. A lead compensator provides the phase lead, but cannot be used because it would raise the crossover frequency and violate the third specification. So phase lag is added below crossover, followed by phase lead around crossover.

Having decided on the type of compensator (phase lag followed by phase lead) there are numerous systematic and unsystematic ways to select the parameters. This is fairly easily done using a Bode plot. The details don't concern us, only the final result:

$$k(s) = \frac{(s+3)^2}{(s+.4)(s+22.5)} \tag{5.2}$$

The magnitude and phase Bode plots of g(s) and gk(s) are shown in

Figure 5.1. The closed loop system is stable, with poles at s = -11.7,

-3.0, and -6.1 ± 1.2j. The bandwidth is 7 rad/sec (down from the

uncompensated bandwidth of 12 rad/sec), and the phase margin is 60°.

The phase margin specification has been exceeded by 15°, which is some-

what conservative, but is in anticipation of the unavoidable phase lag

due to the hybrid implementation.

5.2.2 Hybrid Implementation

The analog compensator is converted to a hybrid compensator. The

different parts of the hybrid compensator are:

$$
\left.
\begin{aligned}
f(s) &= \frac{2500}{s^2 + 70s + 2500} \quad \text{(poles at } s = -35 \pm 35j\text{)} \\[2em]
T &= .031416 \text{ sec} \quad \text{(foldover} = \frac{\pi}{T} = 100 \text{ rad/sec)} \\[2em]
d(z) &= \frac{.80498 \ (z-.90993)^2}{(z-.98750)(z-.47744)} \\[2em]
h(s) &= \frac{1-e^{-sT}}{s} \quad \text{(zero-order-hold)}
\end{aligned}
\right\} \tag{5.3}
$$

The sample rate is chosen so that the foldover frequency is about 14

times the bandwidth (100 versus 7 rad/sec).

The prefilter is a 2nd order Butterworth filter with a break

point at 50 rad/sec. It contributes 11° of phase lag at 7 rad/sec

and has a magnitude of .24 at 100 rad/sec.

The z-transform d(z) is a discretized version of k(s). The Tustin

with prewarping method was used (see Subsection 2.3.1). The prewarped

frequency is chosen to be ω_1 = 3 rad/sec, which is the natural frequency
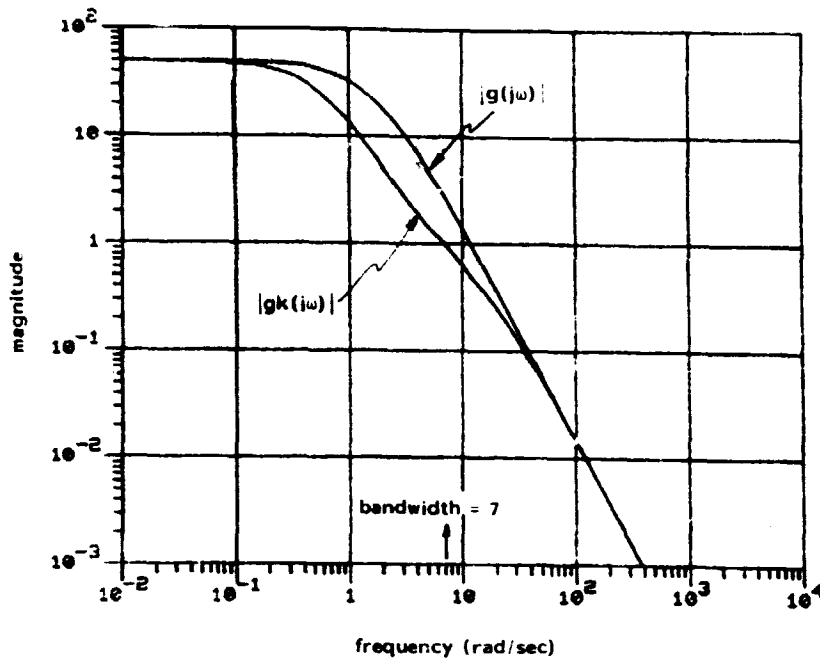
of the zeros at s = -3.

Figure 5.1a: Magnitude Bode plot of g(jω) and gk(jω)
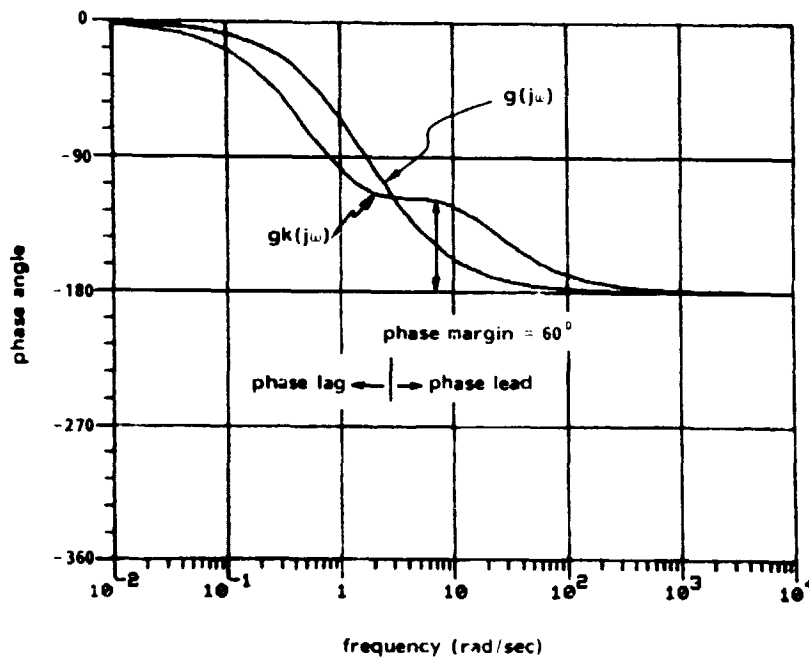

Figure 5.1b: Phase Bode plot of g(jω) and gk(jω)

A zero-order-hold is used to convert the digital sequence at the output of the computer to an analog signal. The zero-order-hold is a standard choice for control system design, and in this example it contributes 6° of phase lag at 7 rad/sec.

This completes the choice of the hybrid compensator. There are many different ways to choose the hybrid compensator, but it is not the intent of this thesis to recommend one way over another. Rather, the intent is to provide tools to analyze a particular choice of a hybrid compensator.

5.2.3 Digital Analysis

Before going on to the conic sector analysis techniques we do a quick digital analysis. The hold and prefilter are grouped with the plant and the combination is discretized[1]:

$$Z \{h(s)g(s)f(s)\} = g_d(z)$$

$$= \frac{.0094 \ (Z + 6.059)(z + .609) \ (z + .066)}{(z - .969) \ (z - .910) \ [(z - .145)^2 + (.3)^2]} \tag{5.4}$$

This combined with the computer z-transform [d(z) of (5.3)] gives the discrete loop transfer function:

$$t_3(z) = g_d(z) \ d(z) \tag{5.5}$$

Its discrete Nyquist plot ($t_3(z)$ evaluated for $z = e^{j\omega T}$) is shown in Figure 5.2. The number of clockwise encirclements (zero) of the 1 point equals the number of open loop unstable poles, so the digital closed loop system is stable. Closed loop stability can also be

---

[1] The script z indicates the z-transform of the samples of the inverse Laplace transform, see [4, Sections 3.4 and 6.2].
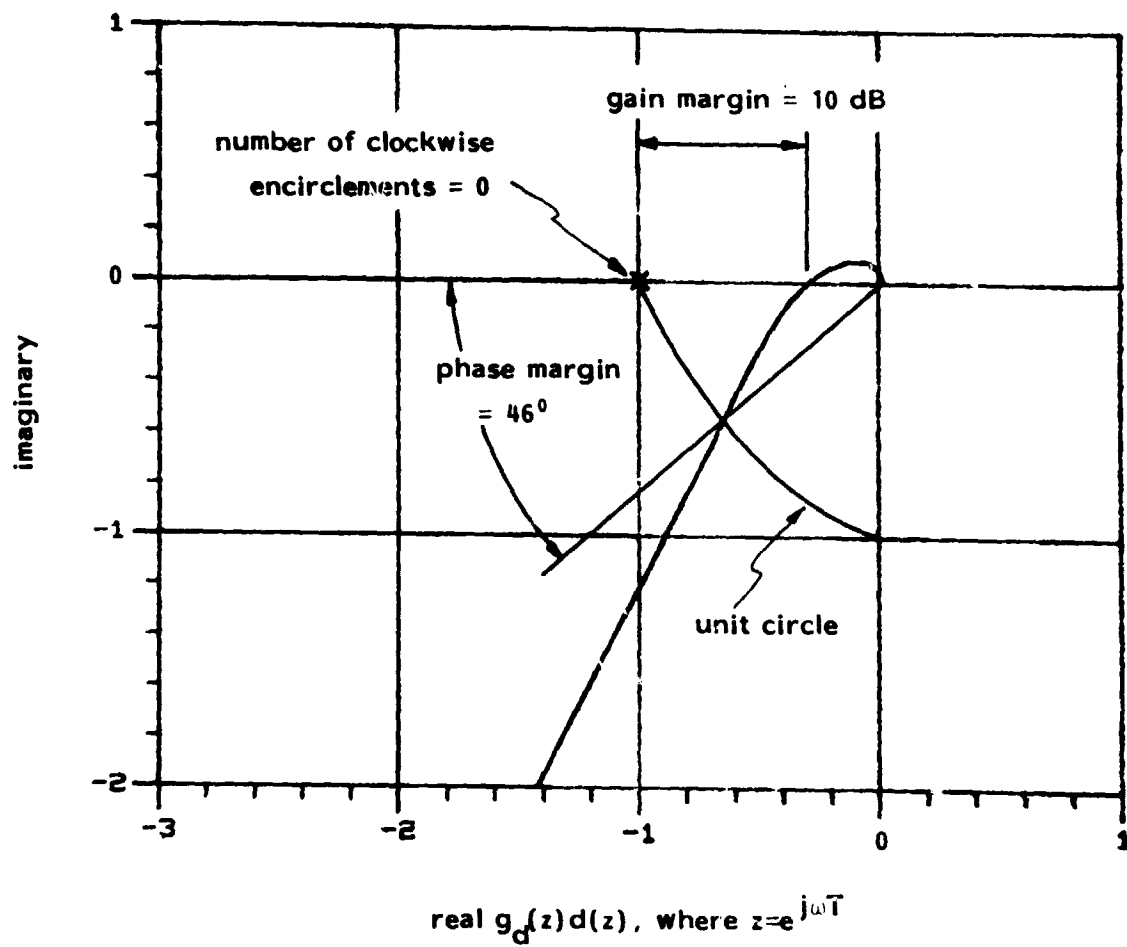
Figure 5.2:   Discrete Nyquist plot of $g_d(z)d(z)$,   where $z = e^{j\omega T}$

determined from the location of the digital closed loop poles, which all

have magnitude < 1: z = .910, .873, .812± .204j, and .109± .271j.

From the discrete Nyquist plot of Figure 5.2 it is seen that the

digital closed loop system has a phase margin of 46° and a gain margin

of 10dB. This implies that the hybrid closed loop system has these

same phase and gain margins (see Subsection 2.3.4). Therefore, the hybrid

closed loop system meets the phase margin specification of > 45°.

5.2.4 Gain of the Hybrid Operator

The first result of Chapter 3 (Theorem 3.1) is an upper bound on

the gain of the hybrid operator. For SISO hybrid operators (as in

this example) the upper bound actually is the gain.

The gain of the analog compensator is

$$\max_{\omega} \left| k(j\omega) \right| = \left| k(j0) \right| = 1 \tag{5.6}$$

and the gain of the hybrid operator is

$$\| K \|_{L_2} = \max_{0 < \omega < \frac{\pi}{T}} \underbrace{\frac{1}{T^2} \underbrace{\left[\sum_k |h_k|^2 \right]^{1/2}}_{= 1} \cdot \underbrace{|d*|}_{= 1} \cdot \underbrace{\left[\sum_n |f_n|^2 \right]^{1/2}}_{= 1.004}}_{\omega = 0} = 1.004 \tag{5.7}$$

The maximum for the hybrid operator occurs at $\omega = 0$. The hold term

is =1 at $\omega = 0$ (actually for all ω), and the computer term is =1

at $\omega = 0$ (z = 1). The extra gain is due to aliasing of the prefilter,

which, in this example, does not amount to much.

Different prefilters that cutoff less sharply or cutoff at higher

frequencies will result in a hybrid compensator with a larger gain.

For example, if f(s) = 50/(s+50) then $\| K \|_{L_2}$ = 1.094, and if f(s) =

100/(s+100) then $\| K \|_{L_2}$ = 1.309. As the gain gets higher the

compensator is more sensitive to noise. Thus, the higher gains are an indication of inadequate prefiltering.

5.2.5 Hybrid Operator Inside of Cone

Theorem 3.2 can be used to construct a conic sector that contains the hybrid operator. The choice of center is arbitrary. Here we choose the center that minimizes the radius:

$$c(s) = \frac{1}{T} h(s) \; d(e^{sT}) \; f(s) \tag{5.8}$$

The loop transfer function of the nominal feedback system is $cg(s)$.

At low frequencies $c(s)$ should be a good approximation of $k(s)$. This is checked with the magnitude and phase Bode plots of Figure 5.3. The magnitudes are close (within 1 dB) below 30 rad/sec, at which point the extra rolloff due to the prefilter and hold causes $c(s)$ to diverge from $k(s)$. The phase difference shows up at lower frequencies - the phases are close (within 5°) below 2 rad/sec. At 7 rad/sec the phase lead is reduced from 28° to 12° (which was anticipated). Above 100 rad/sec the phase of $c(s)$ rapidly swings over the entire 360° range.

The equation used to compute the radius is

$$r(j\omega) = \frac{1}{T} \left[\sum_{k=-20}^{20} \; \sum_{\substack{n=-20 \\ n\neq k}}^{20} \; |h_k d^* f_n|^2 \right]^{1/2} \qquad \text{for } o \leq \omega \leq \frac{\pi}{T} \tag{5.9}$$

which is a truncated version of (3.11). Because the optimal center is used, the $r_3(\omega)$ term of (3.6) is equal to zero. A plot of the radius is shown in Figure 5.2a. The radius is periodic with period $\omega_s = 200$ rad/sec.

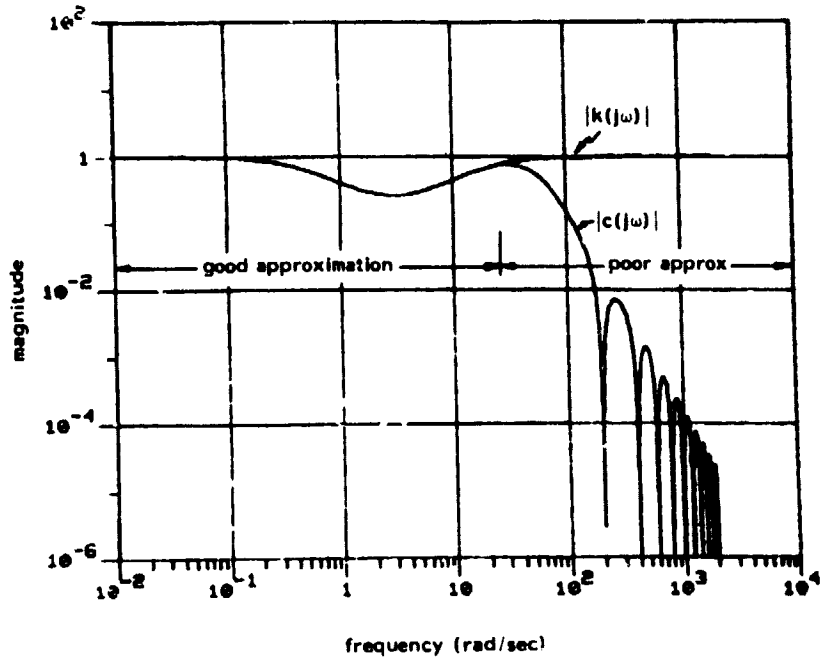More important than the magnitude of the radius is the relative

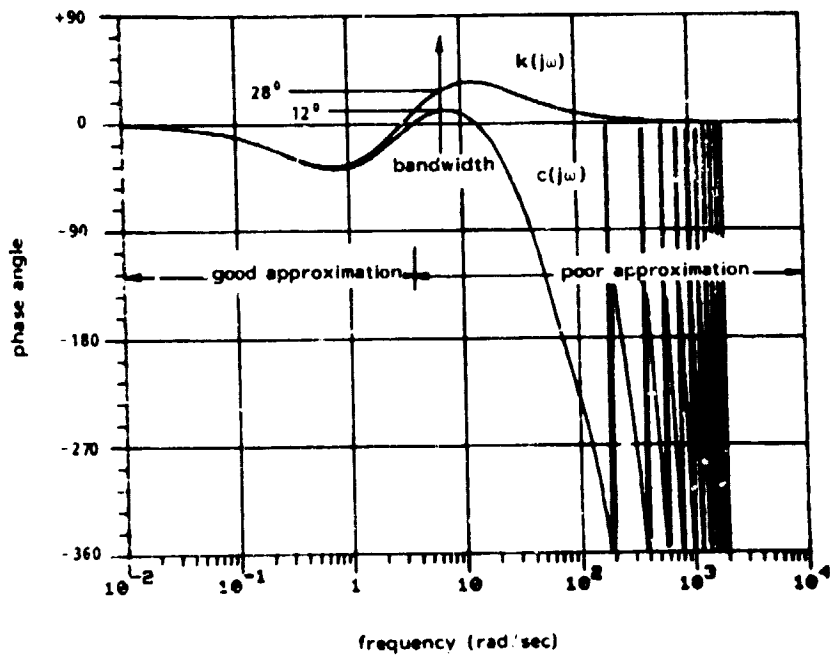Figure 5.3a: Magnitude Bod.. plot of $c(j\omega)$ and $k(j\omega)$.

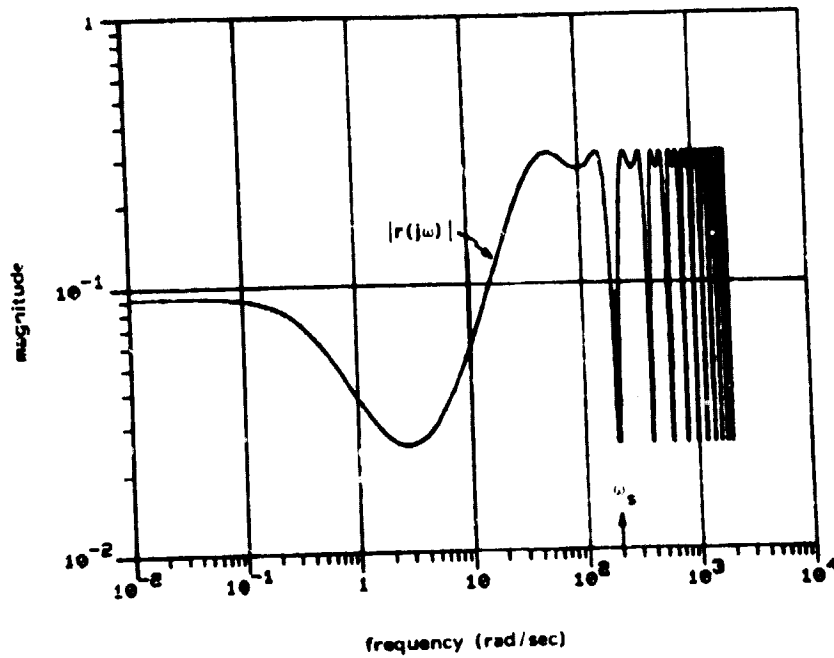Figure 5.3b: Phase Bode plot of $c(j\omega)$ and $k(j\omega)$.

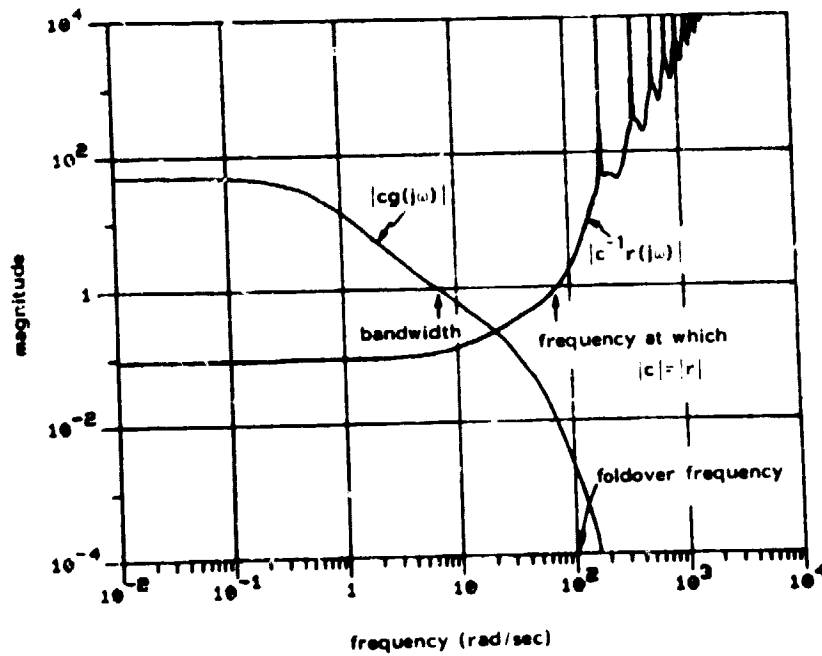Figure 5.4a: The radius of the cone that contains
K.

Figure 5.4b: The multiplicative radius.

magnitude of the center and radius. In Figure 5.4b the magnitude of $c^{-1}r$ is plotted. This is called the "multiplicative radius." When it is $<<1$ then the center can be considered a good approximation of the hybrid compensator.[1]

When the multiplicative radius is near unity or greater then the center is a poor approximation of hybrid compensator. Over this frequency range the analog loop transfer function $cg(j\omega)$ should be rolled off (have magnitude < 1) in order to meet the stability and robustness requirements of Theorems 3.3 to 3.5. In this example $|cg(j\omega)| < .1$ over the frequency range where $|c^{-1}r(j\omega)| > 1$, which should be considered "good".

Stability

Theorem 3.3 gives sufficient conditions for the hybrid feedback system to be closed loop stable. The three conditions of Theorem 3.3 will now be checked.

Condition (i) is that the hybrid operator K is strictly inside cone (C,R). The center and radius were constructed so that this is true. Condition (ii) is that the nominal system (with the loop transfer function cg) is closed loop stable. This is verified by the Nyquist diagram of Figure 5.5a.[2] The third and last condition is that

$$|rg\,(1 + cg)^{-1}\,(j\omega)| < 1 \quad \text{for all } \omega \qquad (5.15)$$

---

[1] For example, the center is a good approximation when $|c^{-1}r(j\omega)| < .1$, which is true in Figure 5.4b for $\omega < 6$ rad/sec.

---

[2] The number of open loop unstable poles is zero. The number of clockwise encirclements of the -1 point is zero. Since these two numbers are equal, the analog system is closed loop stable.
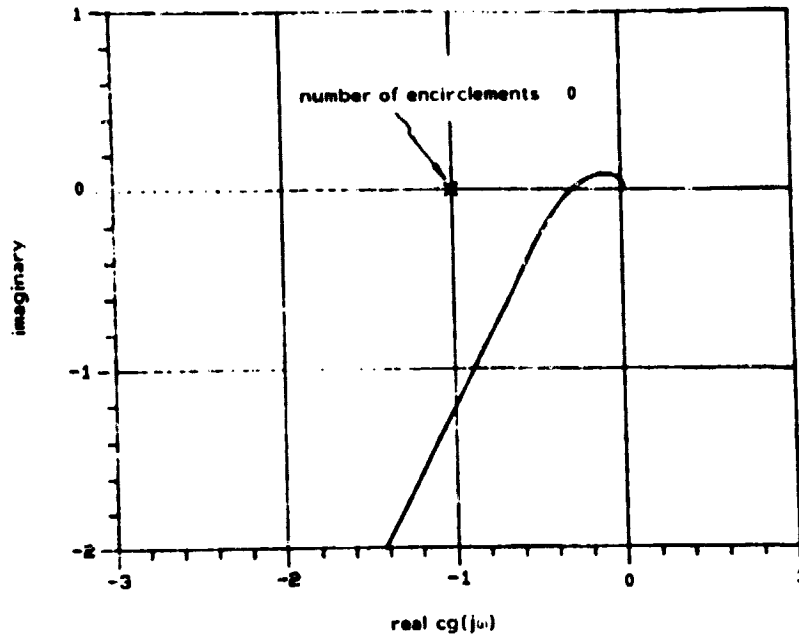
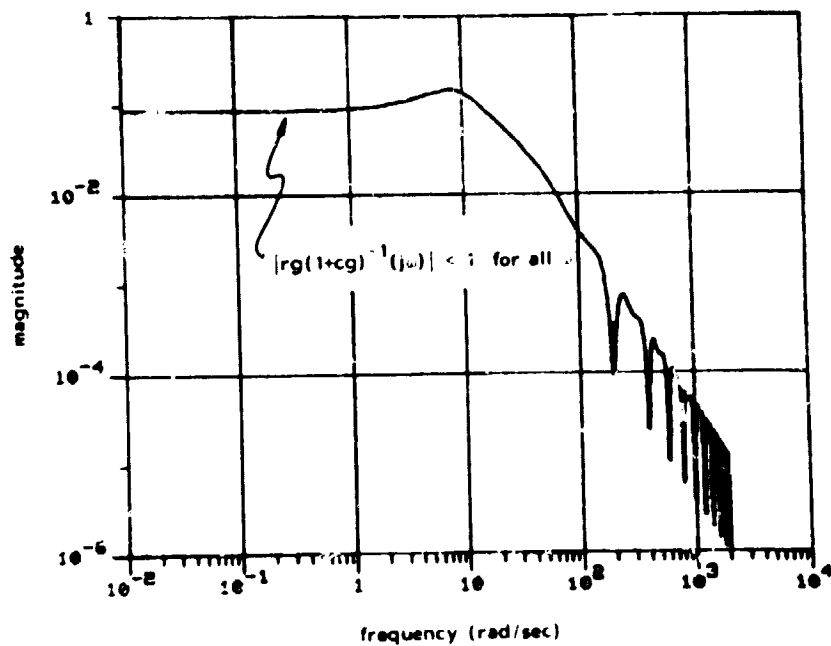Figure 5.5a: Nyquist plot of $cg(j\omega)$.

Figure 5.5b: Closed loop stability test of
Theorem 3.3 when hybrid operator
is inside of a cone.

This is verified in Figure 5.5b. Hence, the hybrid system is closed loop stable. Of course, we already know this from the earlier digital analysis.

Robustness - First Attempt

Beyond mere stability is robustness. Theorem 3.4 gives sufficient conditions for an entire set of plants to be closed loop stable. In this example the plant uncertainty is characterized as a phase uncertainty at the crossover frequency as high as 45°. The first step in applying Theorem 3.4 is to model this uncertainty as a multiplicative perturbation. As explained in Subsection 2.2.7, a multiplicative perturbation of

$$\ell_m(\omega) = \alpha = .77 \tag{5.16}$$

covers phase uncertainties up to ±45° (at all frequencies).

The robustness condition of Theorem 3.4 is graphically checked in Figure 5.6. It is seen that

$$\frac{\left|1+cg\right| - \left|rg\right|}{\left|cg\right| + \left|rg\right|} > .57 \quad \text{for all } \omega \tag{5.17}$$

This corresponds to a phase uncertainty at all frequencies of 33°, so based on Theorem 3.4 we cannot guarantee that the phase margin specifi- cation of 45° is actually satisfied. Because Theorem 3.4 gives only sufficient conditions, we know that the phase margin is > 33°, but we do not have enough information to say whether or not the actual phase margin is ≥ 45°.

Robustness - Second Attempt

Theorem 3.5 can be used to analyze robustness. The procedure is to (1) choose a multiplicative perturbation, (2) use part (a) of
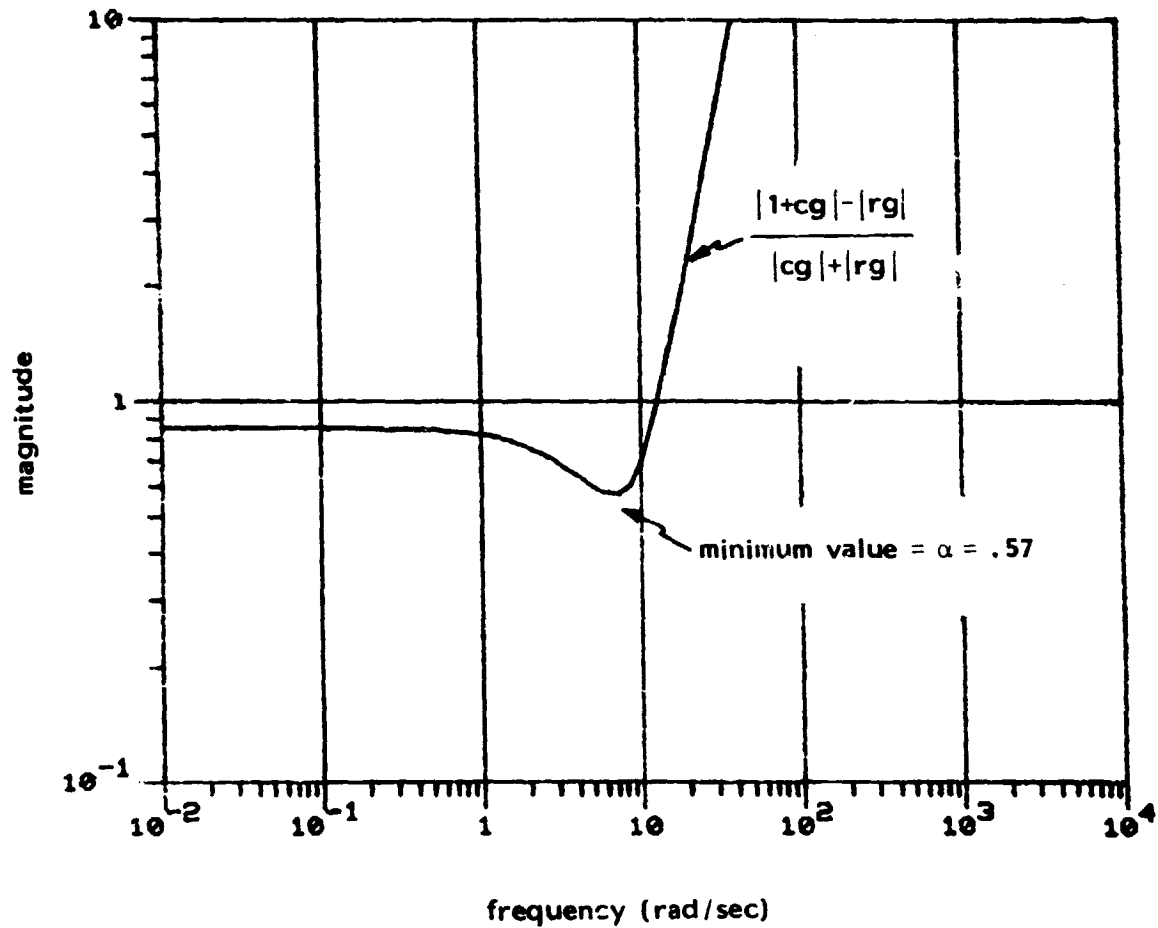
Figure 5.6: Robustness test of Theorem 3.4 when hybrid operator
inside of a cone.

Theorem 3.5 to construct a cone around $(I + E_m) K$, and (3) use part (b)

of Theorem 3.5 to check if $-G^I$ is outside of this cone. If part (b) of

Theorem 3.5 checks out then the closed loop system is stable for all

plants defined by $\tilde{G} = G (I + E_m)$.

In this example the multiplicative perturbation has already been

chosen ($\alpha = .77$). The center of the cone around $(I + E_m)K$ is given by

5.8)and is the same as the center of the cone around K. The radius of

the cone around $(I + E_m)K$ is computed via (3.23) and is plotted in Figure

5.7a. It is compared with the radius of the cone around K ($\alpha = o$).

The nominal plant will be outside of the cone that contains $(I + E_m)K$

if

$$\left| rg (1 + cg)^{-1} (j\omega) \right| < 1 \quad \text{for all } \omega \tag{5.18}$$

This inequality is checked in Figure 5.7b, and it is <u>not</u> satisfied. If

α is backed down to $\alpha = .72$ then the inequality <u>is</u> satisfied. Therefore,

we can say the guaranteed phase margin is 42°, which doesn't quite make

it to 45°, but is less conservative than the 33° of Theorem 3.4.

5.2.6 <u>Loop Transfer Operator Inside of Cone</u>

The entire loop transfer operator can be placed inside of a cone.

As discussed in Section 3.3, there are three ways that the plant can be

included with the compensator:

Case 1: with the hold (replace h with gh)

Case 2: with the prefilter (replace f with fg)

Case 3: with a combination of the hold and prefilter. (replace
both h and f with $(fgh)^{1/2}$)

For each of the three cases Theorem 3.2 will be used to construct a

cone. After this is done, Theorem 3.3 will be used to see which of the

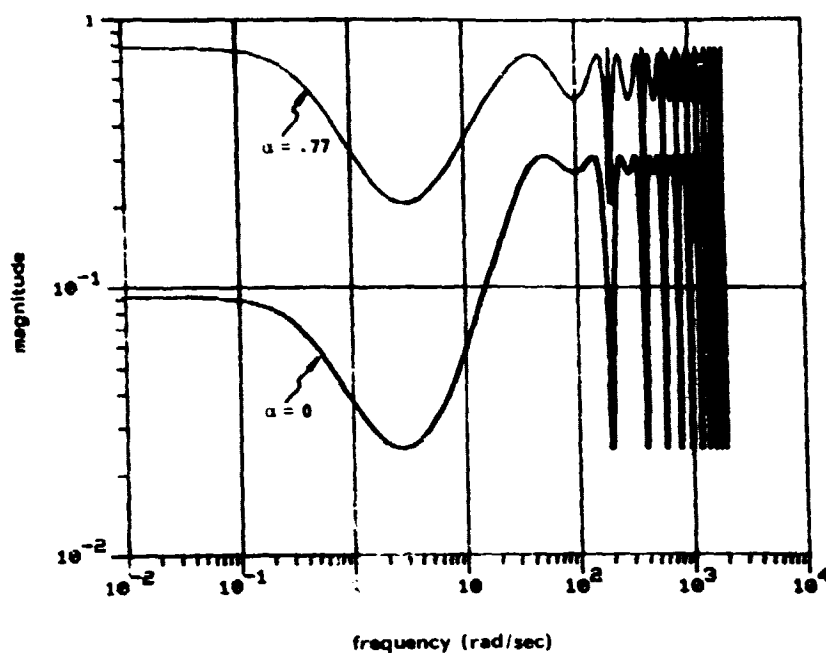three cases meet the sufficient conditions for closed loop stability.

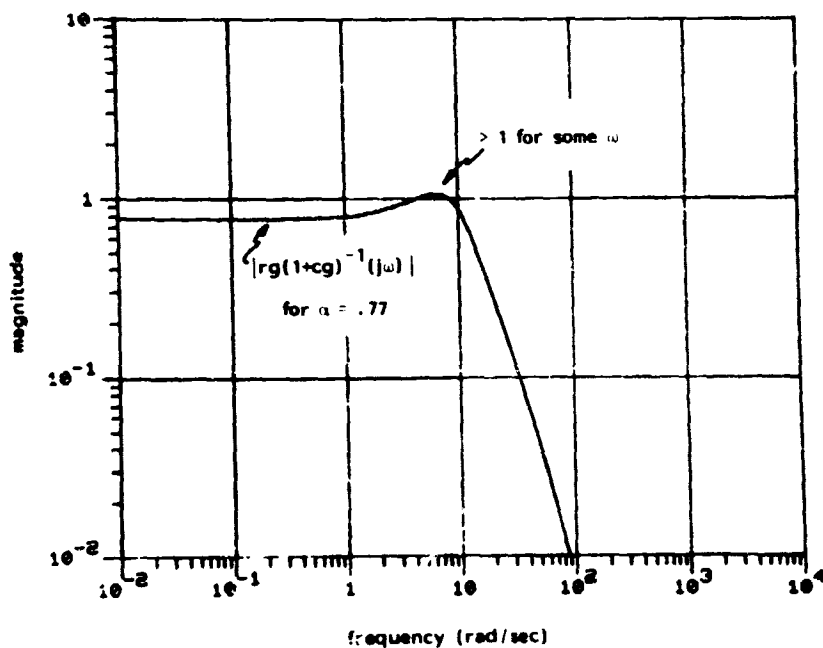Figure 5.7a: Comparison of radii as computed by
Theorem 3.5.

Figure 5.7b: Robustness test of Theorem 3.5
when hybrid operator is inside of
a cone.

A robustness analysis using Theorems 3.4 and 3.5 is then performed for case 3.

For each case the center of the cone is

$$c(s) = g(s) \frac{1}{T} h(s) d^*(s) f(s) \qquad (5.19)$$

The loop transfer function for the nominal feedback system is $c(s)$. In Figure 5.8 the magnitude and phase Bode plots of $c(s)$ and $gk(s)$ are compared. The center is a good approximation over the same frequency ranges as in Figure 5.3.

The radii for each of the three cases are shown in Figure 5.9a. As expected, the radius for case 3 is the smallest for each ω. At low frequencies the radii are significantly different, with the radius for case 1 (plant with hold) being the largest.

The significant differences came as a surprise, and further analysis was conducted to explain the differences. The detailed calculation for the radii at $\omega = .01$ (the leftmost points in Figure 5.9a) are shown in Table 5.1. The infinite series that are part of the equation for the radius were truncated at ± 100 terms. A large number of significant digits are needed in Table 5.1 because accuracy is lost when two large numbers are substracted (for case 3, $r = r_1 - r_2$, where $r \approx .001$ and both r_1 and r_2 are ≈ 2500).[1]

An indication that the radius for case 1 (plant with hold) is larger than the radius for case 2 (plant with prefilter) is given by the

---

[1] This problem with loss of accuracy does not occur when the double infinite sum, r_4 of (3.11), is used to compute the radius. The double infinite sum does not contain the large term ($r_2 \approx 2500$) which is added and then subtracted to convert the double sum to several single sums.
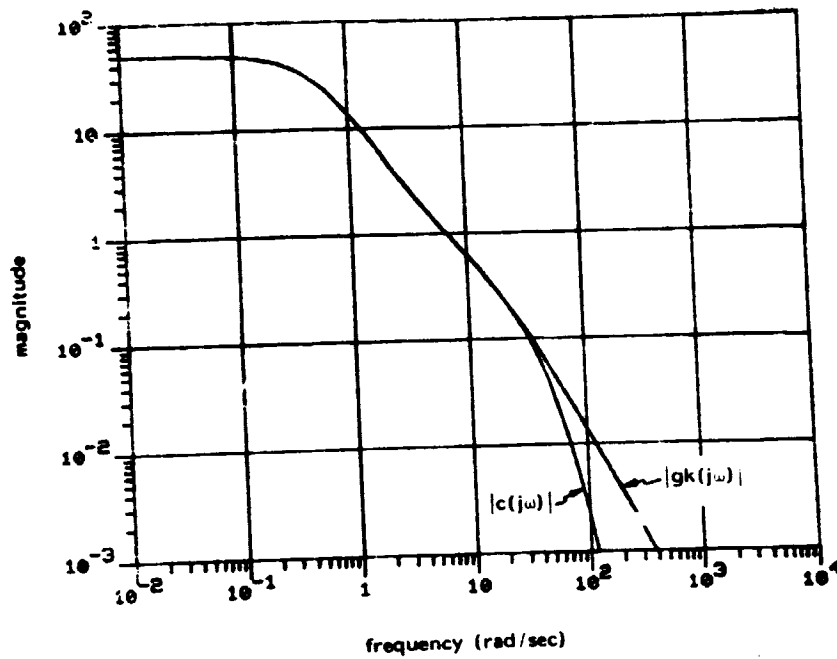
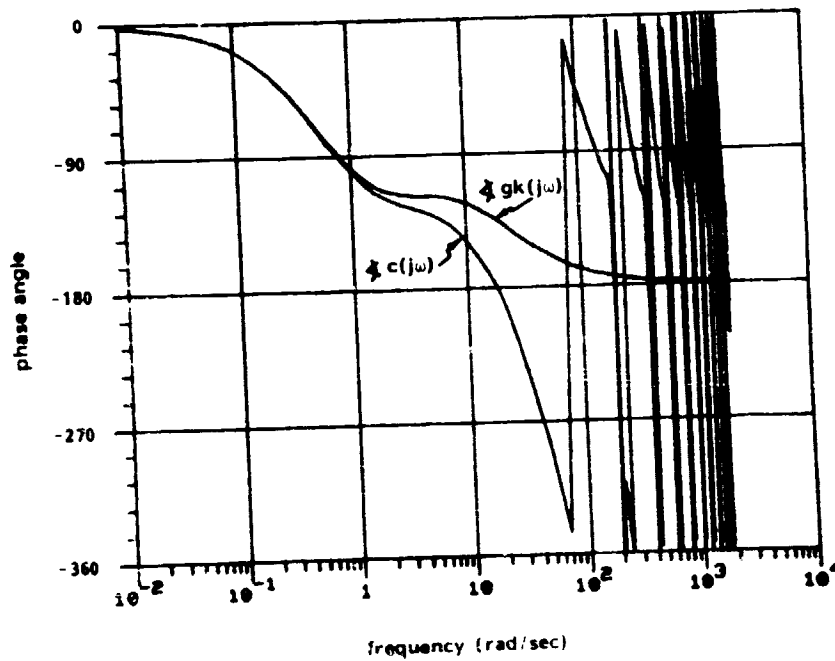Figure 5.8a: Magnitude Bode plot of $c(j\omega)$ and $gk(j\omega)$.

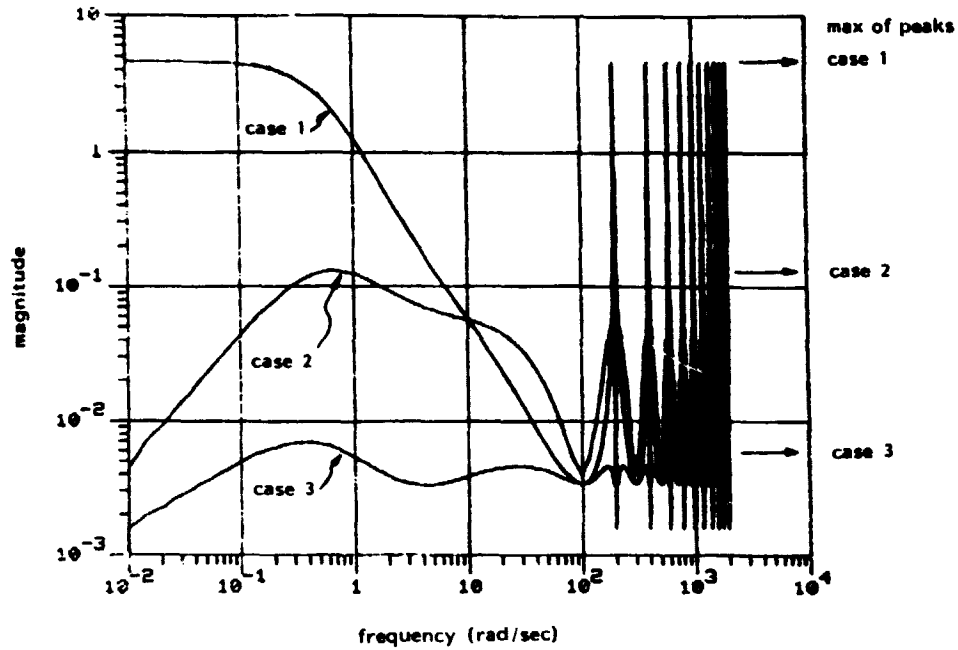Figure 5.8b: Phase Bode plot of $c(j\omega)$ and $gk(j\omega)$.

ORIGINAL PAGE IS
OF POOR QUALITY

Figure 5.9a: Radii of cones that contain 3 different
loop transfer operators.
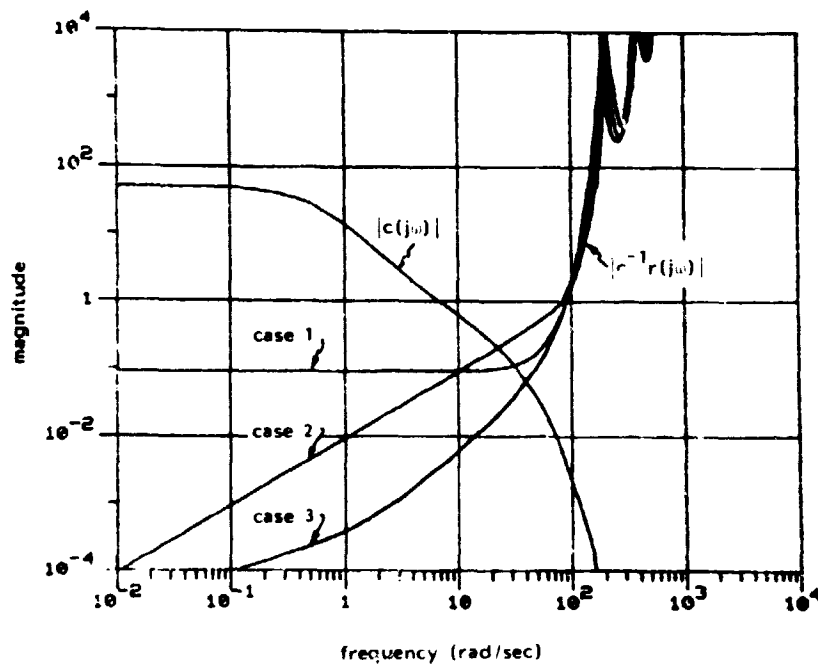
Figure 5.9b: Center and multiplicative radii.

Case 1

$$r(j.01) = |d| \cdot \left(\left[\frac{1}{T^2} \sum_k |h_k g_k|^2 \right] \cdot \left[\sum_n |f_n|^2 \right] - r_2 \right)^{1/2}$$

$$= .99970 \left([2499.72229] \; [1.00844497] - [2499.722234] \right)^{1/2}$$

$$= 4.29$$

Case 2

$$r(j.01) = |d| \cdot \left(\left[\frac{1}{T^2} \sum_k |h_k|^2 \right] \cdot \left[\sum_n |g_n f_n|^2 \right] - r_2 \right)^{1/2}$$

$$= .99970 \left([1] \; [2499.722254] - [2499.722234] \right)^{1/2}$$

$$= .00454$$

Case 3

$$r(j.01) = |d| \cdot \left(\left[\frac{1}{T} \sum_k |h_k g_k f_k| \right]^2 - r_2 \right)^{1/2}$$

$$= .99970 \left([49.997222284579]^2 - [2499.722233745] \right)^{1/2}$$

$$= .00156$$

where

$$r_2 = \frac{1}{T^2} \sum_k |h_k g_k f_k|^2$$

Table 5.1: Calculations for $r(j\omega)$ at $\omega = .01$

comparison;

$$\sum_n \left|f_n\right|^2 \doteq 1.008 > 1 = \frac{1}{T^2} \sum_k \left|h_k\right|^2 \quad \text{for } \omega = .01 \qquad (5.20)$$

The apparently small difference of .008 is amplified by a multiplication of 2500, which is approximately the difference (.008 x 2500 = 4) between the two radii at ω = .01.

The intuitive reason for including the plant with the compensator is that the extra rolloff of the plant will reduce aliasing and thereby make the radius smaller. The comparison (5.20) indicates that including the extra rolloff with the prefilter is better than including it with hold. The theoretical analysis of Section 3.4 indicates that it is even better to replace the prefilter and hold with $(hgf)^{1/2}$.

Moving on now to Figure 5.9b, the multiplicative radii $(c^{-1}r)$ are compared. Despite large differences at low frequencies, they cross unity at about the same frequency (ω = 80 rad/sec). All three are < .1 over the bandwidth of the analog loop transfer function (ω < 7 rad/sec).

Theorem 3.3 is used to check sufficient conditions for the hybrid system to be closed loop stable. The Nyquist plot of $c(j\omega)$ is shown in Figure 5.10a. The Nyquist plot indicates (for each of the three cases) that the nominal analog system is closed loop stable.

It is in the application of the stability test

$$\left| r(1+c)^{-1}(j\omega) \right| < 1 \quad \text{for all } \omega \qquad (5.21)$$

that the most significant differences in the three cases show up. As shown in Figure 5.10b, cases 2 and 3 meet the sufficient conditions but case 1 does not. Only one of the cases has to meet the sufficient
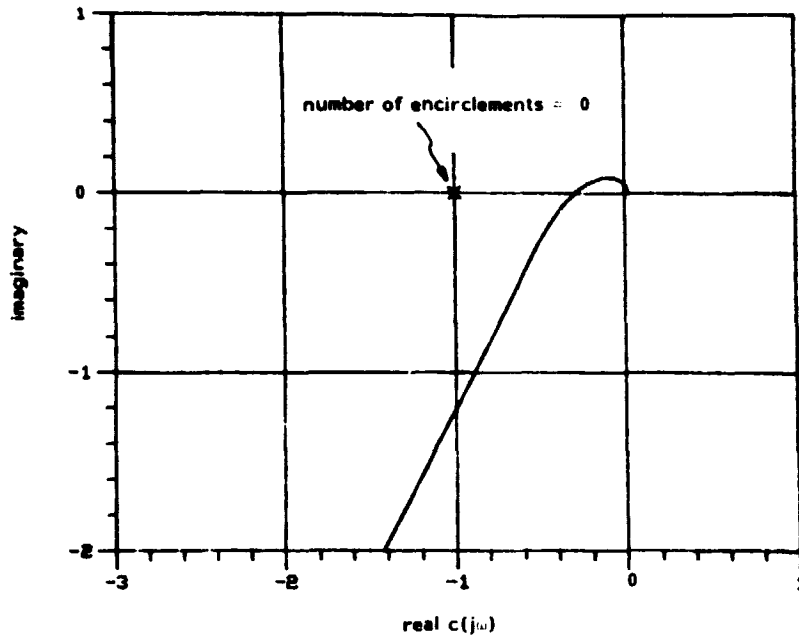
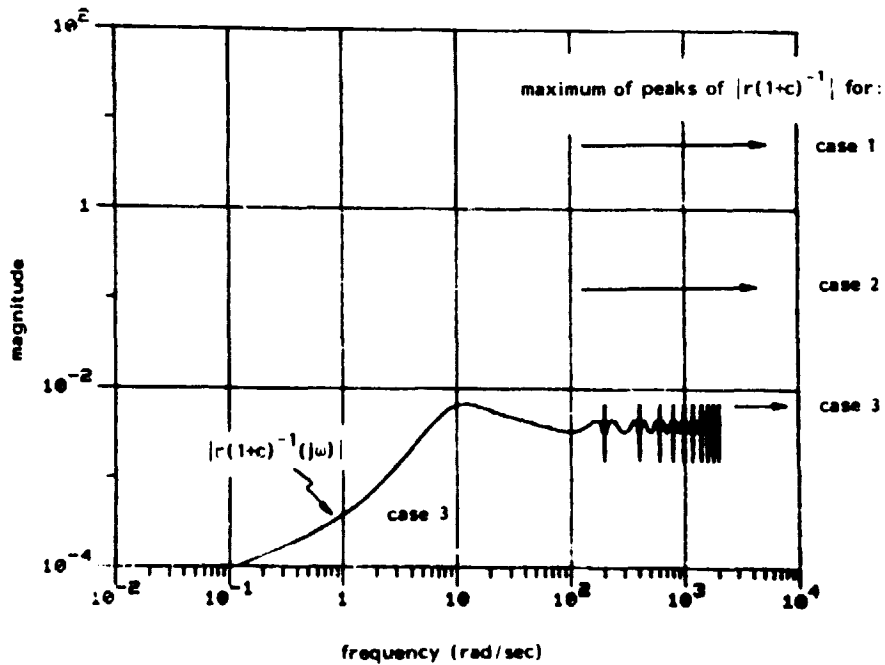Figure 5.10a: Nyquist plot of $c(j\omega)$, when loop transfer operator inside of a cone.

Figure 5.10b: Closed loop stability test of Theorem 3.3 when loop transfer operator is inside of a cone.

conditions in order to guarantee closed loop stability. It comes as some relief to know that case 3 will always be the least conservative.

An analysis of robustness is performed just for case 3. Figure 5.11 shows that

$$\frac{\left|1+c\right| - \left|r\right|}{\left|c\right| + \left|r\right|} > .74 \quad \text{for all } \omega \tag{5.22}$$

This is the single condition of Theorem 3.4 (appropriately modified for case 3). The bound on the multiplicative perturbation is $\ell_m(\omega) = \alpha = .74$, which corresponds to a guaranteed phase margin of 43°.

Theorem 3.5 can also be used to compute a guaranteed phase margin. A cone is constructed around $(I + E_m)T$. The largest α such that

$$\left| r(1+c)^{-1} \right| < 1 \quad \text{for all } \omega \tag{5.23}$$

is found to be $\alpha = .75$, which corresponds to a guaranteed phase margin of 44°. This is very close to the specification of 45°.

5.2.7 Hybrid Operator Outside of Cone

According to Theorem 3.6, a cone can be constructed such that $-K^I$ is outside of the cone if the hybrid operator $K I + GK)^I$ is L_{2e}-stable. From the digital analysis of Subsection 5.2.3 we know that this stability requirement is satisfied.

The center of the cone is the nominal plant $g(s)$. The radius is computed via (3.36) of Theorem 3.6. Rather than show a plot of the radius, a plot of the multiplicative radius $\left| g^{-1}r(j\omega) \right|$ is shown in Figure 5.12. The multiplicative radius is more useful for graphical tests of robustness margins. In this example the plot is almost identical to the plot of Figure 5.11. To two significant digits the minima are the same ($\alpha = .74$)
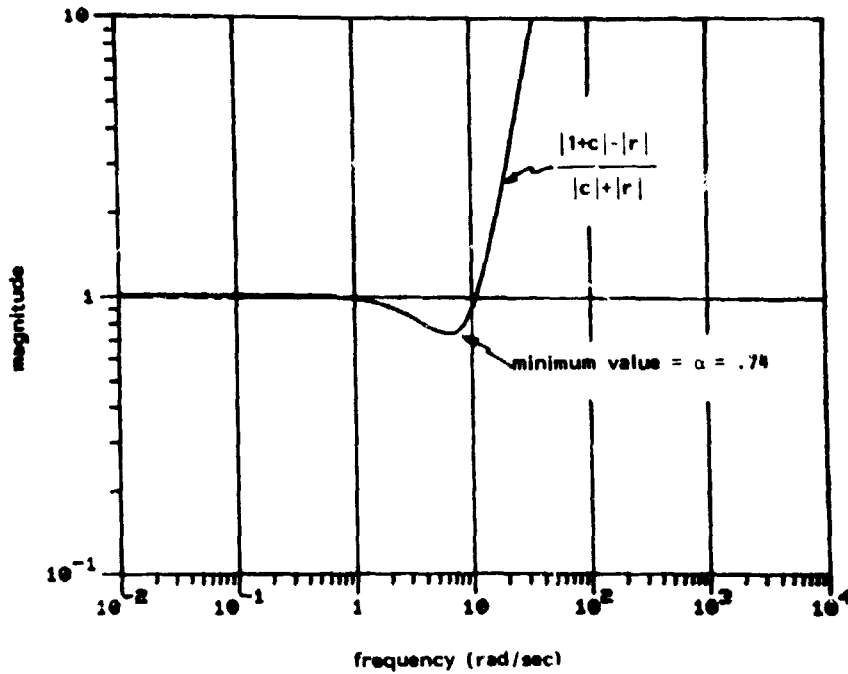
Figure 5.11: Robustness test of Theorem 3.4 when
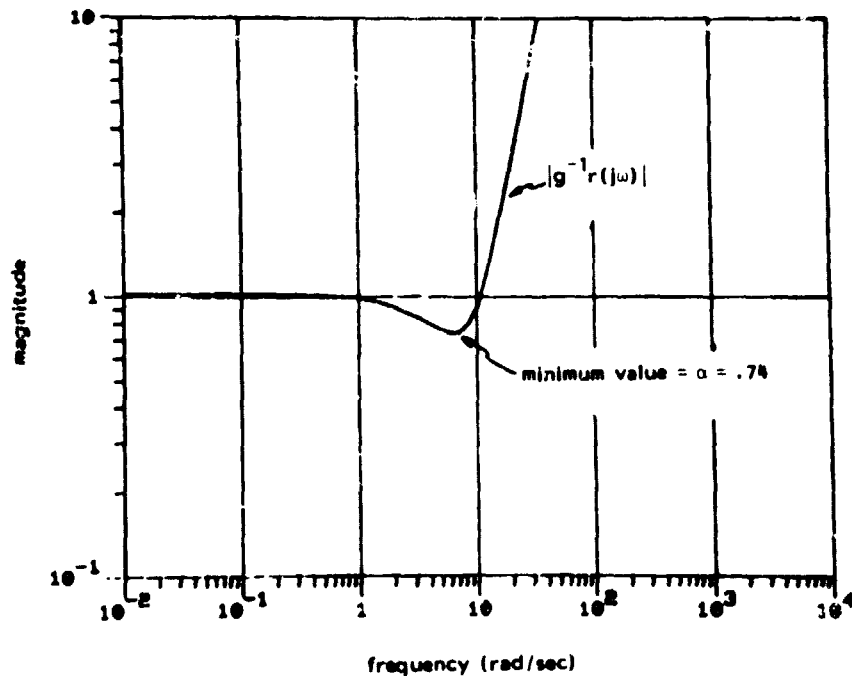the loop transfer operator is inside
of a cone.

Figure 5.12: Robustness test of Theorem 3.7 when
the hybrid operator is outside of a
cone.

From Theorem 3.7 we know that the minimum of $|g^{-1}r(j\omega)|$ can be used to guarantee that the hybrid closed loop system is robust with respect to a multiplicative perturbation of the form $\ell_m(\omega) = \alpha = .74$. This corresponds to a guaranteed phase margin of 43°.

In this lead-lag example there have been 5 separate tests for robustness. They are compared in Table 5.2. The actual phase margin (from the digital analysis) is 46°. The guaranteed phase margins of tests 2 through 5 are not significantly different. Only test 1 is conservative.

Table 5.2

Comparison of Guaranteed Phase Margins

Test		Theorem	α	Guaranteed phase margin
1	Compensator inside cone	3.4	.57	33°
2	" "	3.5	.72	42°
3	Loop operator inside cone	3.4	.74	43°
4	" "	3.5	.75	44°
5	Compensator outside cone	3.7	.74	43°

The major advantage of the outside conic sector analysis is that it can be used with open loop unstable compensators and plants. This advantage is not needed in this example.

5.2.8 Selecting the Sample Rate

The loop transfer operator can be placed inside of a cone (see Subsection 5.2.6). The idea now explored is that the multiplicative radius of this cone can be used to systematically select the sample rate.

The center is a good approximation of the loop transfer operator over the frequency range where the multiplicative radius has magnitude << 1. By varying the sample rate, this frequency range can be adjusted to correspond to the bandwidth of the analog system (i.e., adjust T so that $|c^{-1}r(j\omega)| << 1$ for ω such that $|gk(j\omega)| > 1$).

This procedure for selecting the sample rate is demonstrated for the lead-lag example. All of the components of the hybrid compensator must change as the sample rate is varied. The components are selected so that the sample rate is the only variable:

Prefilter: 2nd order Butterworth with break frequency $= \frac{\pi}{2T}$

Computer: Tustin prewarped version of $k(s)$, with $\omega_\lambda = 3$

Hold: Zero-order-hold.

For each of five sample rates a cone is constructed around the loop transfer operator.[1] The multiplicative radii are shown in Figure 5.13a, and compared with the center of the cone when T = .031416.

All but one of the multiplicative radii are < .1 over the bandwidth of the analog system (ω < 7 rad/sec). The conclusion based on Figure 5.13a is that all but the lowest sample rate (T = .31416) is acceptable. Further tests should be conducted, however, because the fact that $\left| c^{-1}r \right| \ll 1$ over the analog bandwidth is not by itself a guarantee of closed loop stability or adequate robustness margins.

The magnitude of the multiplicative radius can be compared with the magnitude of other multiplicative uncertainties. This comparison can also be used to help select the sample rate. The idea is to select the sample rate so that $\left| c^{-1}r(j\omega) \right| < \left| \ell_m(\omega) \right|$ over the bandwidth of the analog system. Lowering the sample rate (increasing T) will cause the errors due to sampling to dominate the other uncertainties, which is undesirable. On the other hand, increasing the sample rate (lowering T)

---

[1] The five sample rates are (T = .31416, .062832, .031416, .062832, and .0031416), which correspond to foldover frequencies of (π/T = 10, 50, 100, 500, and 1000). The case 3 loop transfer operator is used [prefilter and hold replaced by $(fgh)^{1/2}$].
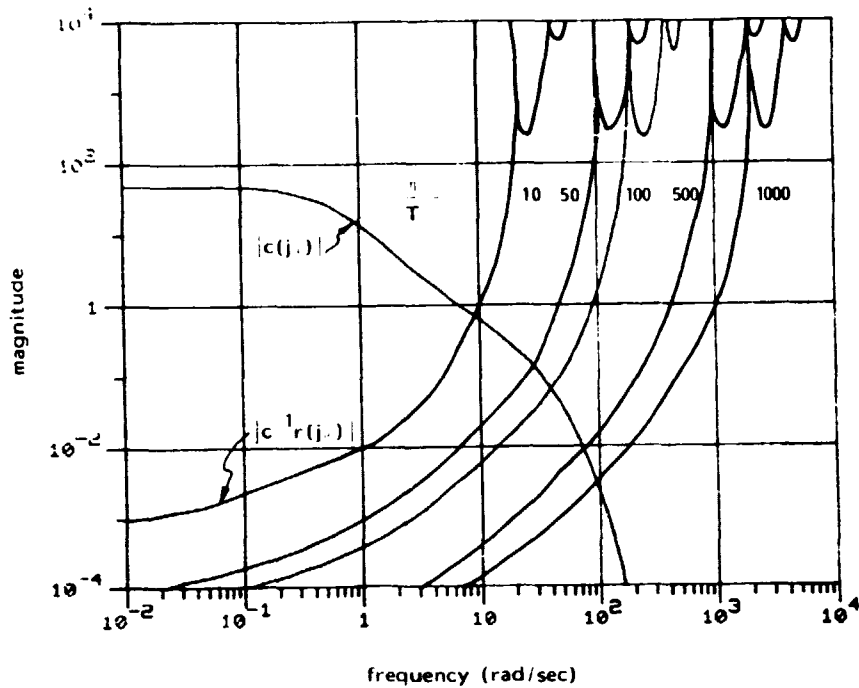
Figure 5.13a: Multiplicative radius of cone that
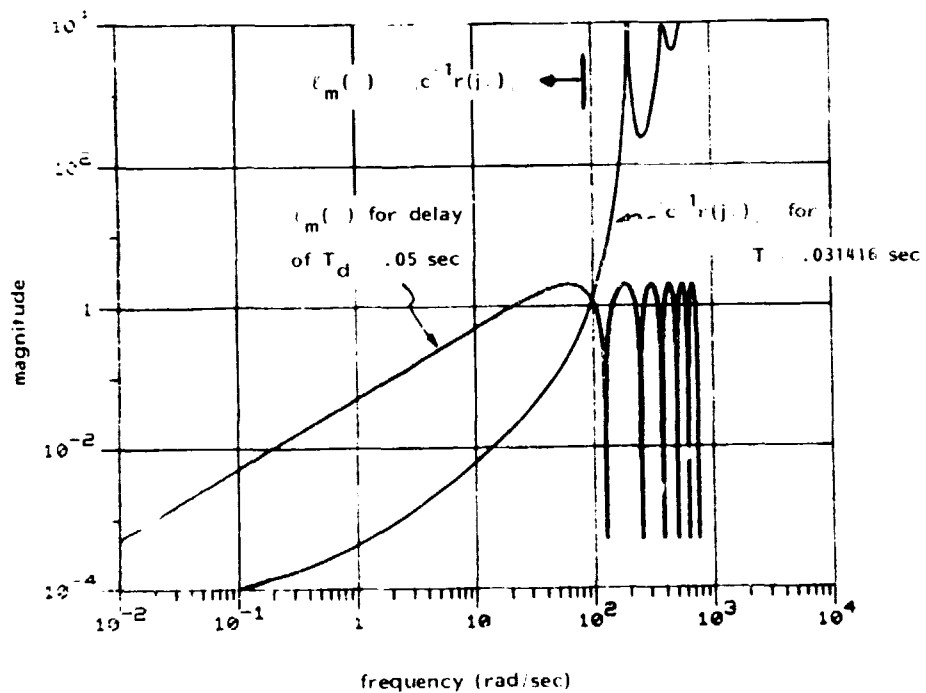loop transfer operator is inside of,
for each of 5 sample rates.

Figure 5.13b: Multiplicative radius compared with
multiplicative perturbation due to
extra delay

C - 3

will not result in any benefit, because the other errors (ℓ_m) are not affected and will dominate the errors due to sampling.

For example, suppose the following delay exists in the feedback loop:

$$\tilde{g}(s) = g\tilde{\ell}(s) \tag{5.24}$$

where $\tilde{\ell}(s) = e^{-sT_d}$, $T_d = .05$ seconds

The delay can be modelled as the multiplicative perturbation:

$$\tilde{g}(s) = g[1 + \ell_m(s)] \tag{5.25}$$

where $\ell_m(s) = e^{-sT_d} -1$, $T_d = .05$ seconds

In Figure 5.13b the magnitude of $\ell_m(\omega)$ is compared with the multiplicative radius when T = .031416. The magnitude of $\ell_m(\omega)$ dominates for ω < 100 rad/sec. The conclusion is that there is nothing to gain by increasing the sample rate (lowering T).

5.2.9 Comparison of Discretization Techniques

Another use of the multiplicative radius is to compare discretization techniques. Tustin with prewarping was used in this lead-lag example to transform k(s) into d(z), but this is only one of many techniques. The following discretization techniques are compared:

Tustin with prewarping: (see Subsection 2.3.1)

Forward rectangle rule: $d(z) = k(s)\Big|_{s=(z-1)/T}$

Backward rectangle rule: $d(z) = k(s)\Big|_{s=(z-1)/(zT)}$

Pole-zero mapping [4, p. 61]:

If p_i is a pole of k(s) then $e^{p_i T}$ is a pole of d(z)

If z_i is a zero of k(s) then $e^{z_i T}$ is a zero of d(z)

If ∞ is a zero of k(s) then -1 is a zero of d(z)

Choose constant so that $k(s)\Big|_{s=0} = d(z)\Big|_{z=1}$

The standard by which they are compared is the magnitude of the multiplicative radius. Each of the loop transfer operators (case 3) are placed in cones. In order to make a comparison the center of the cone is chosen to be the same for each of the discretization techniques:

$$c(s) = \frac{1}{T} h(s) k(s) f(s) \tag{5.26}$$

Note that $c(s)$ is not the optimal center. The center and the different multiplicative radii are shown in Figure 5.14.

The multiplicative radius is smallest when the Tustin with prewarping technique is used, following by the pole-zero, backward rectangle, and forward rectangle techniques. All of the techniques, however, should be considered "good enough" for this example, because all of the multiplicative radii have magnitudes < .1 over the bandwidth of the system (ω < 7 rad/sec).

There is a great deal of freedom in how to discretize $k(s)$. This example demonstrates that to a large extent it does not matter what discretization technique is used.

5.2.10 Extra Delay

Suppose an extra delay exists in the feedback loop. The delay can be modelled as a multiplicative perturbation of the plant, and then any of the robustness results (Theorems 3.4, 3.5, and 3.7) can be used to determine if the closed loop system is robust with respect to this multiplicative perturbation.

The delay may be a computational delay, in which case it will be a fraction of a sample period. On the other hand, the delay may be characteristic of the plant, such as a transport delay for mechanical systems. In this example the delay is chosen to be T_d = .05 seconds.
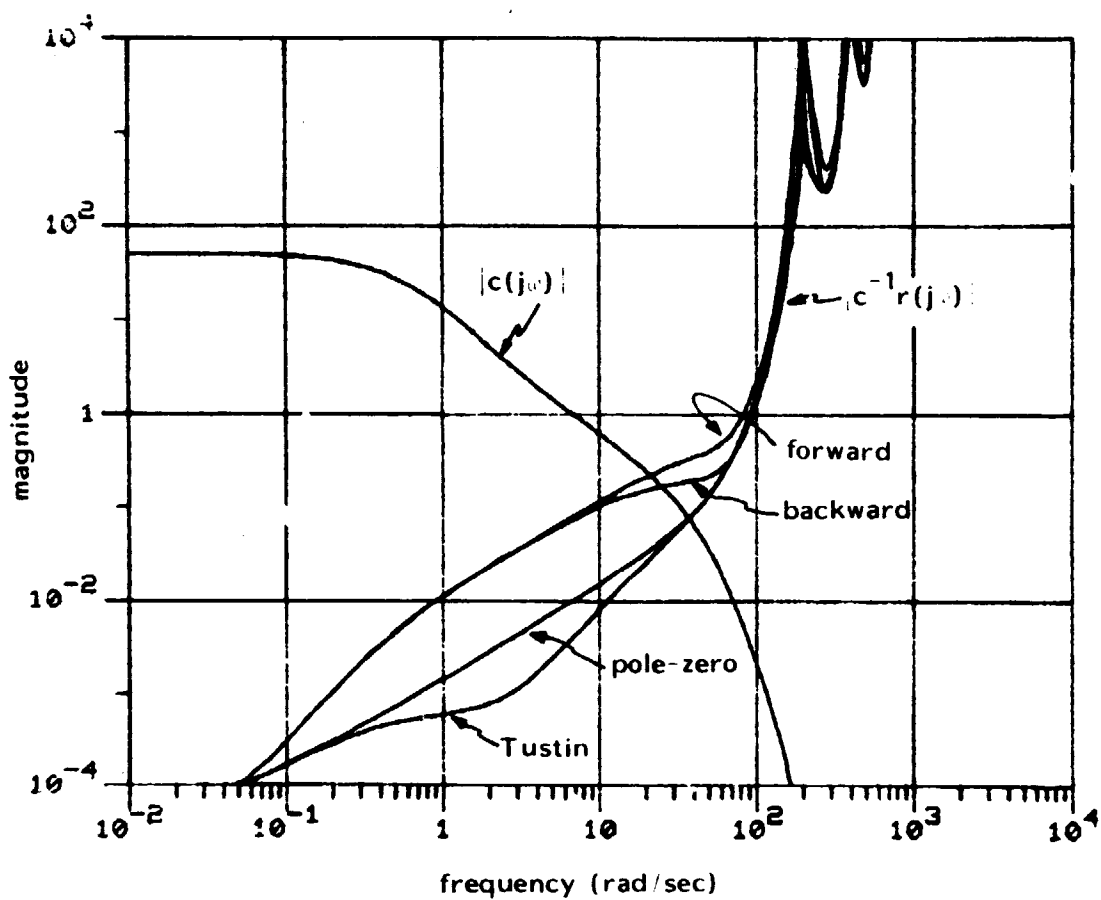
Figure 5.14: Comparison of discretization techniques.

It is between one and two sample periods, to emphasize that there is no need for the delay to be an integer number of sample periods.

Theorems 3.6 and 3.7 will be used to analyze robustness. The basic idea is to construct a cone such that the hybrid operator is outside of the cone, and then to show that all perturbations of the plant in a defined set are inside of this cone. The delay is modelled as a multiplicative perturbation, as shown in equations (5.24) and (5.25). The robustness analysis consists of checking the three conditions of Theorem 3.7.

Condition (i) is that $K(I+GK)^I$ is L_{2e}-stable. This is true because the discrete closed loop system is stable, as shown in Subsection 5.2.3.

Condition (ii) is that $-K^I$ is outside cone (G,R). The existence of such a cone is guaranteed by the fact that condition (i) is true. The radius is computed as shown in Theorem 3.6. The multiplicative version of this radius, $\left|g^{-1}r(j\omega)\right|$, is plotted in Figure 5.15.

Condition (iii) is that

$$\ell_m(\omega) < \left|\underline{g}^{-1}r(j\omega)\right| \qquad \text{for all } \omega \qquad (5.27)$$

This is shown to be true in Figure 5.15. Hence, all perturbations of the plant in a defined set are inside of cone (G,R).

All three conditions of Theorem 3.7 are satisfied. Hence, the hybrid system is robust with respect to an extra delay of $T_d = .05$ seconds.
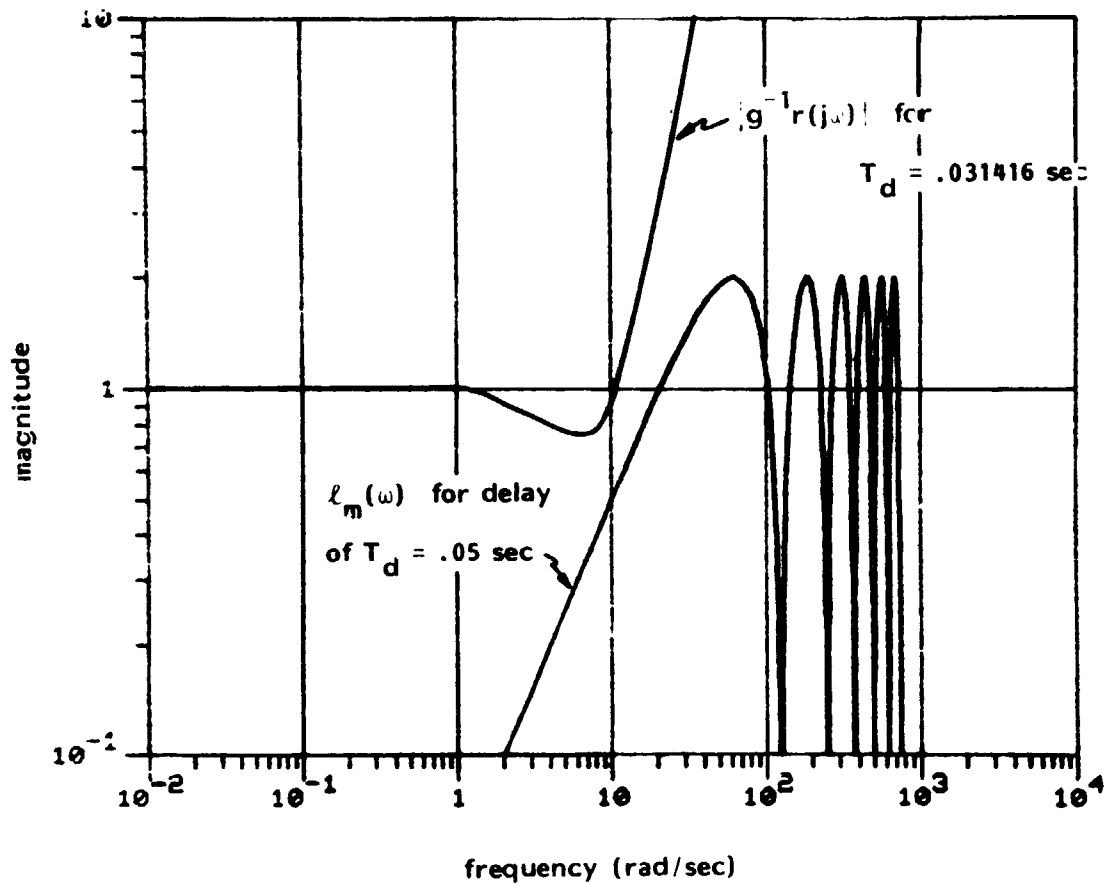
Figure 5.15: Test for robustness with respect to delay of $T_d = .05$ seconds.

5.2.11 Analysis of Command Response

Conic sectors can be used to analyze the steady state response to commands, as discussed in Subsection 2.4.6 and Section 5.6. The response to commands is good if the following error signal is small:

$$\underset{\sim}{e} = (I + GK)^{I} \underset{\sim}{r} \tag{5.28}$$

Conic sectors are used to find an upperbound for q, the quality measure defined by

$$\lim_{\tau \to \infty} \frac{\| \underset{\sim}{e} \|_{\tau}}{\| \underset{\sim}{r} \|_{\tau}} \leq q \quad \text{for all } \underset{\sim}{r} \in S \tag{5.29}$$

This inequality only has to be satisfied for input signals in the set $S \subset L_{2e}$, and by letting the truncation time tend to infinity the transient errors in the command response become insignificant.

Three attempts are made to find an upperbound for q:

(1) Theorem 3.2 is used to construct a cone that contains GK, and then (2.98) to (2.100) are used to compute the upperbound for q.

(2) Theorem 3.2 is used to construct a cone that contains $(I+GK)^{I}$, and then (2.102) and (2.105) are used to compute the upperbound for q.

(3) Theorem 3.8 and equations (3.51) to (3.53) are used to compute the upperbound for q.

The first attempt fails due to restrictions on its use. The second attempt is conservative, and the third attempt works well.

The first step for all three attempts is to define a nominal analog feedback system and then to compute the nominal quality measure q_o. In all of the attempts let the nominal loop transfer function be

$$c(s) = \frac{1}{T} g(s) \, h(s) \, d^*(s) \, f(s) \tag{5.30}$$

and let the set of command signals be

$$S = \{\text{sinewaves with frequency} < .1 \text{ rad/sec}\} \tag{5.31}$$

The nominal quality measure is

$$q_o = \max_{o < \omega < .1} \left| (1+c)^{-1} (j\omega) \right| = .02 \tag{5.32}$$

The magnitude Bode plot of $(1+c)^{-1}$ is shown in Figure 5.16a.

Earlier in this example[1] Theorem 3.2 was used to construct a cone that contains the loop transfer operator GK. The center and radius of this cone can be used via (2.98) to (2.100) to find an upperbound for the quality measure q. One of the restrictions of this first attempt is that the sufficient conditions for closed loop stability given by Theorem 3.3 must be satisfied. As shown in Figure 5.10b the sufficient conditions are not satisfied, and therefore the first attempt at finding an upperbound for q fails.

The second attempt uses Theorem 3.2 to construct a cone that contains the closed loop operator $(I+GK)^{I}$. The center is $(1+c)^{-1}$, where c(s) is given by (5.30). Both the center and radius are shown in Figure 5.16a. Equations (2.102) and (2.105) are now used to upperbound the quality measure:

$$r_2 q_o = \max_{o < \omega < .1} \left| r(j\omega) \right| = .09 \tag{5.33}$$

$$q \leq q_o (1+r_2) = .11 \tag{5.34}$$

This upperbound is significantly more than the nominal quality measure of $q_o = .02$.

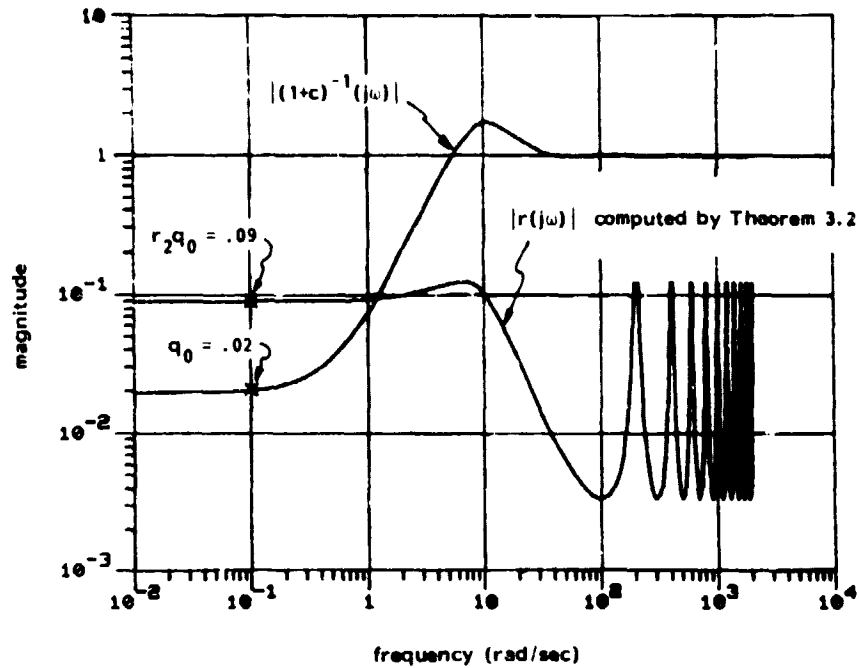[1]Case 1 of Subsection 5.2.6. The center and radius are shown in Figures 5.8 and 5.9.

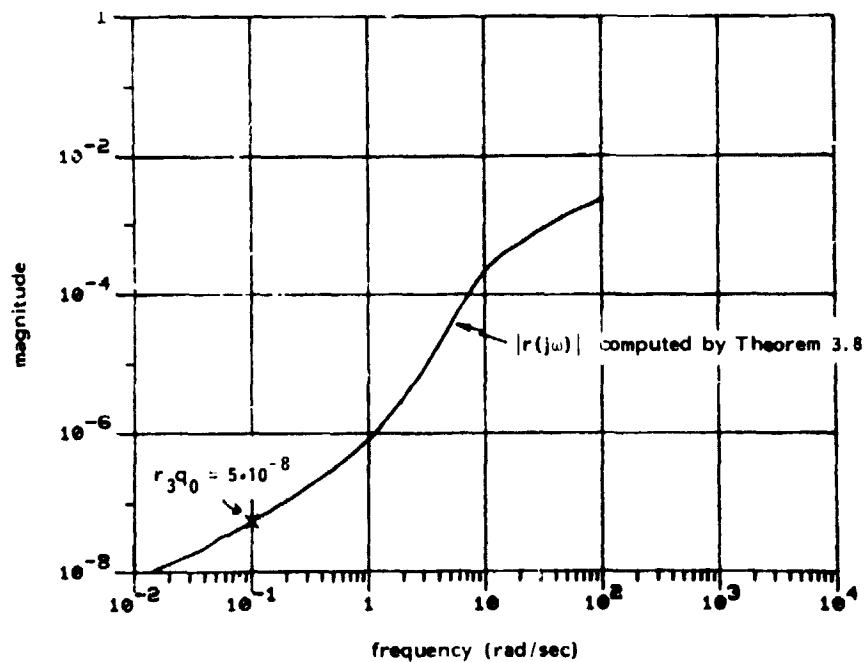Figure 5.16a: Center and radius of a cone that contains $(I+GK)^I$, when the radius is computed by Theorem 3.2.

Figure 5.16b: Radius of cone that contains $(I+GK)^I$, when the radius is computed by Theorem 3.8. This cone is only valid for input signals that are sinewaves with frequency $< \pi/T = 100$ rad/sec.

The second attempt at finding an upperbound for q is conservative because the radius computed by Theorem 3.2 does not take into account (1) the restricted set of input signals and (2) the truncation time of (5.29) which tends to infinity. Addressing the second point, the radius computed by Theorem 3.2 is valid for any truncation time [see (2.81)], and therefore the upperbound for q which uses (2.105) is likewise valid for any truncation time. One interpretation of this conservative upperbound is that it is conservative for steady state errors because it must also be valid for transient errors.

The third attempt at finding an upperbound for q makes use of Theorem 3.8, which explicitly takes into account the restricted set of input signals and the truncation time that tends to infinity. The radius computed by (3.49) of Theorem 3.8 is shown in Figure 5.16b. The upperbound for q is found by equations (3.51) to (3.53):

$$r_3 q_o = \max_{0 < \omega < .1} |r(j\omega)| = 5 \times 10^{-8} \tag{5.35}$$

$$q \leq q_o(1 + r_3) = .02 \tag{5.36}$$

The increase from the nominal value of $q_o = .02$ is insignificant!

The use of conic sectors to analyze command response is new with [16] and this thesis, and we must be careful not to make hasty generalizations about the very tight upperbound for the quality measure just demonstrated. Nevertheless the following statement appears to be justified – the nominal analog feedback system gives a very good approximation of the quality measure of a hybrid feedback system.

Three attempts were made to analyze command response. A straightforward use of the same conic sector used to analyze stability and robustness (Theorem 3.2) was shown to give a conservative upperbound

for the quality measure. Refinements of this conic sector (Theorem 3.8) significantly decrease the upperbound, and indicate that the nominal quality measure is a good approximation of the actual quality measure.

This analysis of command response completes this extensive lead-lag compensator example.

5.3 Integral Control Example

The next example demonstrates that the outside conic sector results can be used to analyze control systems with integrators in the forward loop. These types of control systems are used to achieve zero steady state error to constant inputs.

In this simple example the SISO plant is

$$g(s) = \frac{1}{s+1} \tag{5.37}$$

and the compensator is

$$k(s) = \frac{1}{s}$$

The analog system has closed loop poles at $s = .5 \pm j.87$. The bandwidth is $\omega = .8$ rad/sec, and the phase margin is $52°$.

The following hybrid implementation of $k(s)$ is used:

$$f(s) = \frac{25}{s^2+7s+25} \quad \text{(2nd order Butterworth, break frequency} = 5 \\ \text{rad/sec)}$$

$$T = .31416 \quad \text{(foldover frequency} = \frac{\pi}{T} = 10 \text{ rad/sec)}$$

$$d(z) = .1579 \frac{z+1}{z-1} \quad \text{(Tustin prewarped about } \omega_o = .8 \text{ rad/sec)}$$

$$h(s) = \frac{1-e^{-sT}}{s} \quad \text{(zero-order-hold)}$$

$$\tag{5.39}$$

At the crossover frequency ($\omega = .8$ rad/sec) the prefilter contributes $13°$ of phase lag and the hold contributes $7°$ of phase lag, so we expect the phase margin of the discrete closed loop system (i.e. the actual phase margin of the hybrid closed loop system) to drop from $52°$ to about $32°$.

Due to the digital integrator there does not exist a conic sector with a finite radius that contains the loop transfer operator. The

calculations for the radius[1] are performed to demonstrate this fact. The optimal center of the conic sector is chosen:

$$c(s) = \frac{1}{T} q(s) \; h(s) \; d^*(s) \; f(s) \qquad (5.40)$$

The radius is plotted in Figure 5.17a. The problem with the radius is immediately apparent - it has peaks of infinite height at frequencies that are multiples of $2\pi/T$.

A consequence of the infinite peaks is that the sufficient conditions for closed loop stability given by Theorem 3.3 cannot be met. This does not necessarily mean that the closed loop system is unstable, it may simply mean that the sufficient conditions are "infinitely" conservative. Condition (iii) of Theorem 3.3 (for the loop transfer operator inside of the cone) is that $|r(1+c)^{-1}(j\omega)| < 1$ for all ω. Due to the infinite peaks of $r(j\omega)$, this condition cannot be met.

The optimal center and the multiplicative radius are plotted in Figure 5.17b. The multiplicative radius, $c^{-1}r$, is independent of the computer z-transform $d(z)$. Hence, $c^{-1}r$ does not have the problem with the infinite peaks. From Figure 5.17b we see that $|c^{-1}r| \ll |c|$ over the bandwidth of the analog system $(\omega < .8$ rad/sec).

There are no open loop stability restrictions for the outside conic sector results of Theorems 3.6 and 3.7. The discrete closed loop system is stable, as demonstrated by the discrete Nyquist plot of Figure 5.18a. Therefore a cone can be constructed such that $-K^I$ is outside of the cone. The center is $q(j\omega)$, and the multiplicative radius is $|q^{-1}r(j\omega)|$, where $r(j\omega)$ is computed via equation (3.36). The multiplicative radius, $g^{-1}r$, is shown

---

[1] Case 3 is used, which means that the prefilter and hold are each replaced by $(fgh)^{1/2}$.

in Figure 5.18b. Its minimum value is α = .53, which corresponds to a guaranteed phase margin of 31°, and which is only 1° less than the actual phase margin of 32°.

In this short example it has been demonstrated for integral control problems that (1) there does not exist a conic sector with a finite radius that contains the loop transfer operator, (2) Theorem 3.3 <u>cannot</u> be used to determine closed loop stability, and (3) Theorems 3.6 and 3.7 <u>can</u> be used to determine guaranteed robustness margins.
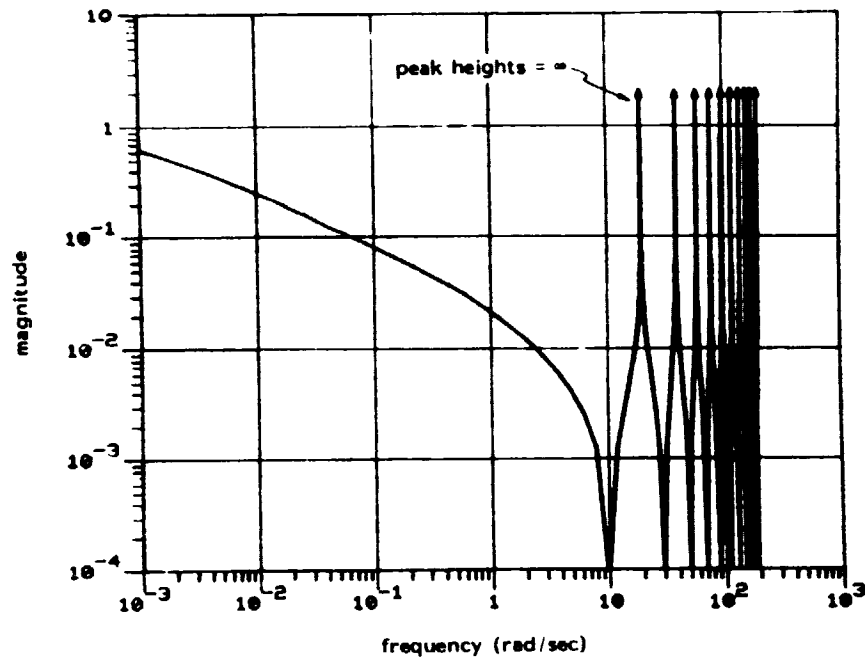
Figure 5.17a: Radius of cone that contains a loop
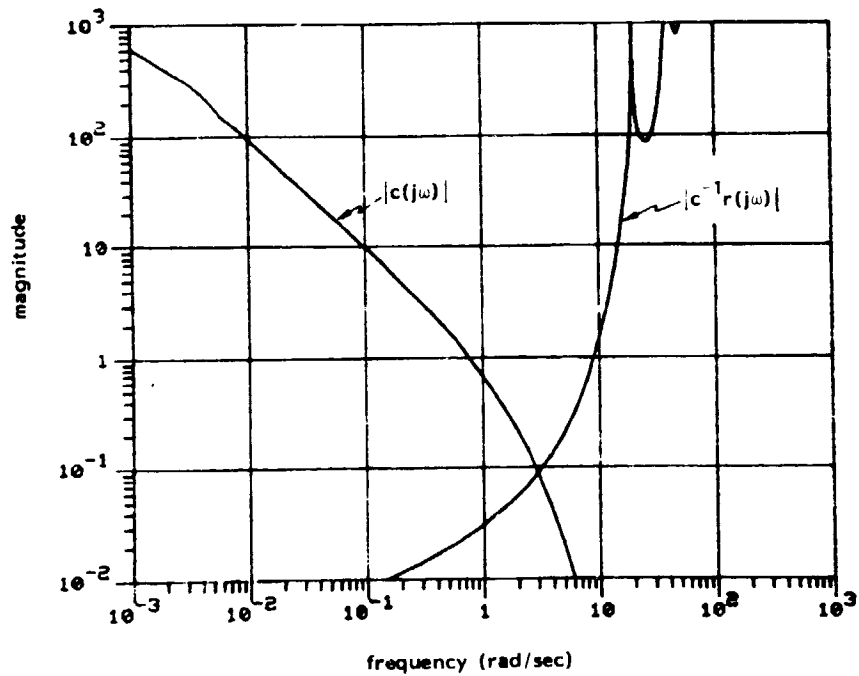transfer operator with a digital
integrator.
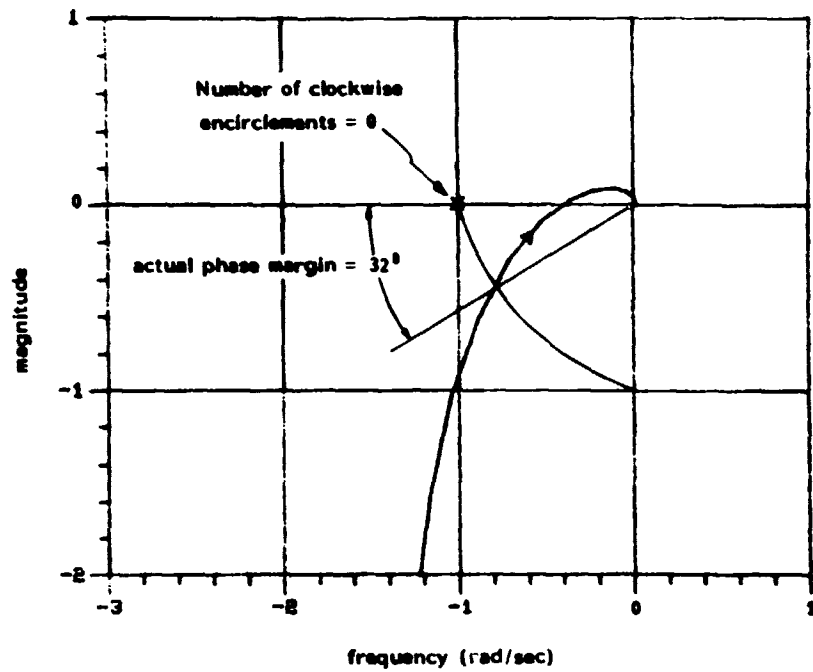

Figure 5.17b: Center and multiplicative radius.

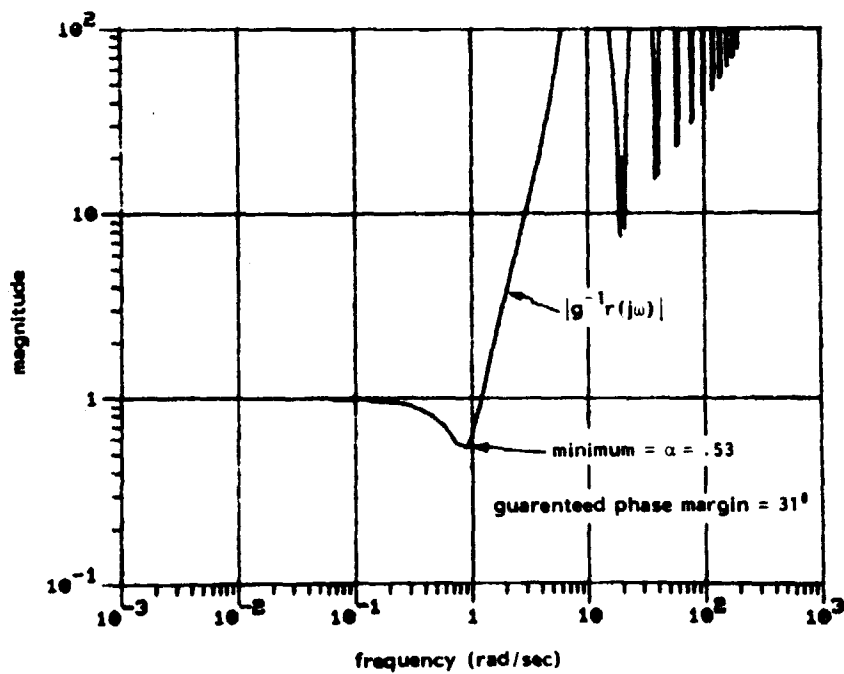Figure 5.18a: Discrete Nyquist of $dg_d(z)$, where $z = e^{j\omega T}$.

Figure 5.18b: Multiplicative radius of a cone such that $-K^I$ is outside of the cone

5.4 High Performance Aircraft

The next example contains both a SISO and a 2-input 2-output control system design for the pitch axis of a highly maneuverable aircraft. This aircraft has served as a test bed for multivariable design techniques [23, 24, 25, 26]. The analog compensators used in this example are designed using linear quadratic Guassian (LQG) methods, and are similar to the designs that appear in [26]. This example goes one step further and analyzes a hybrid implementation of these control laws.

The designs are based on a linearized model of motion in the vertical plane. The flight condition is Mach .9 at an altitude of 25,000 feet. A 4-state, 2-input, 2-output state space model is given in Table 5.3. The states and inputs are:

$$\underline{x} = \begin{bmatrix} \delta V \\ \alpha \\ q \\ \theta \end{bmatrix} = \begin{array}{l} \text{forward velocity} \\ \text{angle-of-attack} \\ \text{pitch rate} \\ \text{pitch attitude} \end{array}$$

$$\underline{u} = \begin{bmatrix} \delta_e \\ \delta_L \end{bmatrix} = \begin{array}{l} \text{elevator/elevon} \\ \text{canard} \end{array}$$

The model leaves out hydraulic actuators with time constants of 70 rad/ sec. The uncertainties in the model (data link time delays and bending modes) are such that the control loop should be rolled off before 10 rad/sec [26].

5.4.1 LQG Design of SISO Analog Compensator

In the first design the elevator/elevon input is used to command the pitch attitude. The transfer function of the open loop plant is

$$g(s) = \frac{-77.81 \ (s+.0232) \ (s+1.962)}{(s+.2576) \ (s+5.676) \ [(s-.6895)^2 + (.2484)^2]} \tag{5.41}$$

$$A = \begin{bmatrix} -.02257 & -36.62 & -18.9 & -32.0900 \\ .00009 & -1.90 & .9831 & -.0073 \\ .01233 & 11.72 & -2.6320 & 0 \\ 0 & 0 & 1 & 0 \end{bmatrix}$$

$$B = \begin{bmatrix} -.9821 & -.76260 \\ -.4144 & -.00496 \\ -77.81 & 22.4 \\ 0 & 0 \end{bmatrix}$$

$$C = \begin{bmatrix} 0 & 1 & 0 & 0 \\ 0 & 0 & 0 & 1 \end{bmatrix}$$

Table 5.3 State space model of highly maneuverable
aircraft

Due to its deliberate relaxed static stability design, the plant is open

loop unstable, with a pole pair at .6895 ± j.2484.

The Bode plot of g(s) is shown in Figure 5.19. The bandwidth of

g(s) is acceptable, but the magnitude Bode plot of g(s) has vo unde-

sirable features - low gain for ω < .1 rad/sec and a resonant peak around

ω = .5 rad/sec. The claim of LQG design methodology is that a k(s) can

be found that (1) "shapes the loop" to eliminate the undesirable features,

(2) guarantees closed loop stability, and (3) provides adequate robust-

ness margins.

The number of variations of LQG methods is somewhat greater than

the number of people who know what the abbreviation "LQG" stands for.

Here we step through a particular LQG design method and provide the

reader with enough information so that the design can be duplicated.

The steps are [35]:

(1)   Choose $\underline{h}$ to shape the magnitude Bode plot of $\underline{h}(s\underline{I}-\underline{A})^{-1}\underline{b}$.

(2)   Choose ρ to obtain desired bandwidth of $\underline{k}_c (s\underline{I}-\underline{A})^{-1}b$.

(3)   Solve LQ Riccati equation to obtain $\underline{k}_c$.

(4)   Choose process and measurement noise covariance matrices by
       the robustness recovery procedure [27].

(5)   Solve Kalman filter Riccati equation to obtain $\underline{k}_f$.

(6)   Use LQ and Kalman filter optimal gains to form analog
       compensator.

For the linear quadratic (LQ) regulator problem the open loop plant

is

$$\begin{matrix} \underline{\dot{x}} = \underline{A}\underline{x} + \underline{b}u \\ y = \underline{c}\underline{x} \end{matrix} \Bigg\}$$

(5.42)

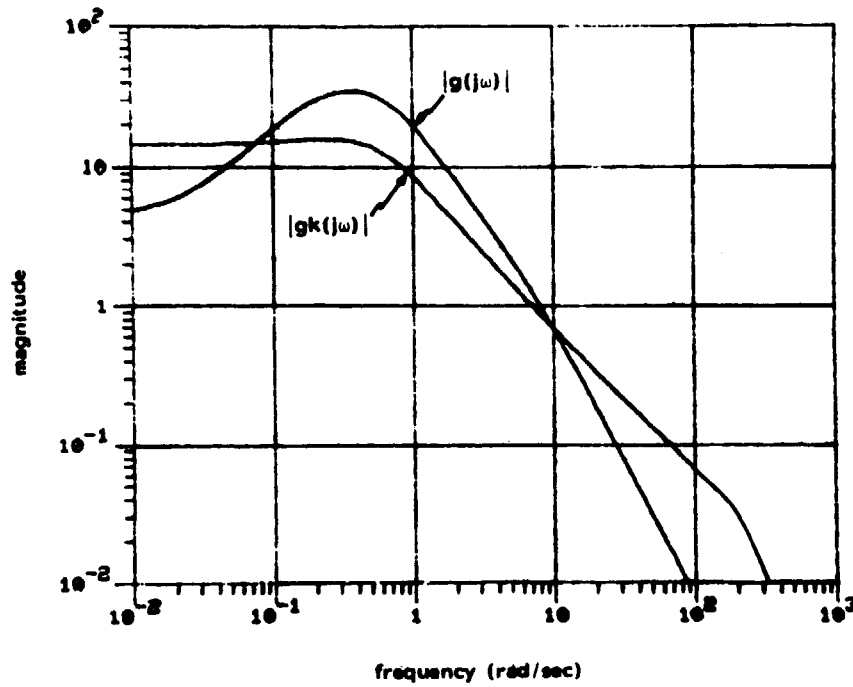In this example the plant is controllable and observable. The LQ

Figure 5.19a: Magnitude Bode plot of g(jω) and gk(jω).

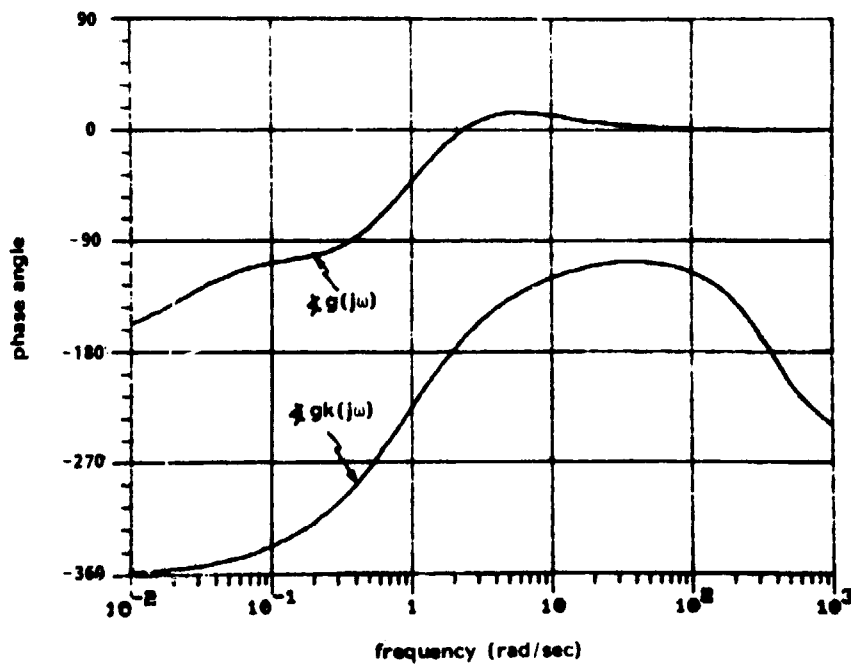Figure 5.19b: Phase Bode plot of g(jω) and gk(jω).

regulator cost function is

$$J = \int_0^\infty (\underline{x}^T \underline{h}^T \underline{h} \underline{x} + \rho \underline{u}^T \underline{u}) dt \tag{5.43}$$

The input that minimizes the cost function is

$$\underline{u} = -\underline{k}_c \underline{x} \tag{5.44}$$

where

$$\underline{k}_c = \frac{1}{\rho} \underline{b}^T \underline{K} \tag{5.45}$$

and where $\underline{K} > \underline{o}$ is the unique solution of the algebraic Riccati equation

$$\underline{o} = \underline{A}^T \underline{K} + \underline{K} \underline{A} + \underline{h}^T \underline{h} - \frac{1}{\rho} \underline{K} \underline{b} \underline{b}^T \underline{K} \tag{5.46}$$

For the Kalman filter problem the process and measurement noise enter the state space system as shown below:

$$\left. \begin{array}{l} \underline{\dot{x}} = \underline{A}\underline{x} + \underline{b}\underline{u} + \underline{\gamma}\xi \\[2mm] y = \underline{c}\underline{x} + \theta \end{array} \right\} \tag{5.47}$$

The noise sources have zero mean and intensities

$$\left. \begin{array}{l} E[\xi(t)\xi(s)] = \delta(t-s) \\[2mm] E[\theta(t)\theta(s)] = \mu\delta(t-s) \end{array} \right\} \tag{5.48}$$

The Kalman filter gains are

$$\underline{k}_f = \frac{1}{\mu} \underline{c}^T \underline{\Sigma} \tag{5.49}$$

where $\underline{\Sigma} > \underline{o}$ is the unique solution of

$$\underline{o} = \underline{A}\underline{\Sigma} + \underline{\Sigma}\underline{A}^T + \underline{\gamma}\underline{\gamma}^T - \frac{1}{\mu} \underline{\Sigma}\underline{c}^T \underline{c} \underline{\Sigma} \tag{5.50}$$

After solving the LQ regulator and Kalman filter problems the LQG

compensator is formed by

$$\dot{x}_k = (\underline{A} - \underline{bk}_c - \underline{k}_f\underline{c})\underline{x}_k + \underline{k}_f e$$

$$u = \underline{k}_c\underline{x}_k$$

(5.51)

The first step of the design procedure is to choose $\underline{h}$ to shape the magnitude Bode plot of $\underline{h}(s\underline{I}-\underline{A})^{-1}\underline{b}$. Let us look ahead a bit and explain why we want to do this. The LQ loop transfer function is $\underline{k}_c(s\underline{I}-\underline{A})^{-1}\underline{b}$, and for ω such that $|\underline{k}_c(j\omega\underline{I}-\underline{A})^{-1}\underline{b}| \gg 1$ the following approximation is valid:[1]

$$|\underline{k}_c(j\omega\underline{I} - \underline{A})^{-1}\underline{b}| \approx \alpha|\underline{h}(j\omega\underline{I}-\underline{A})^{-1}\underline{b}| \quad \text{for some } \alpha$$

(5.52)

The ultimate objective is to shape the magnitude Bode plot of $kg(s)$. If the robustness recovery procedure is used then for some finite region of ω:

$$kg(j\omega) \approx \underline{k}_c(j\omega\underline{I}-\underline{A})^{-1}\underline{b}$$

(5.53)

Therefore, the reason that we want to shape $|\underline{h}(j\omega\underline{I}-\underline{A})^{-1}\underline{b}|$ is that the magnitude of the loop transfer function $|kg(j\omega)|$ will approximate this shape.

The poles of $\underline{h}(s\underline{I}-\underline{A})^{-1}\underline{b}$ are the eigenvalues of $\underline{A}$. If the zeros are at $s = -.2$ and -2.5 then $|\underline{h}(j\omega\underline{I}-\underline{A})^{-1}\underline{b}|$ has a shape that corrects for the undesirable features of the shape of $|g(j\omega)|$. An $\underline{h}$ that places zeros at $s = -.2$ and -2.5 can be computed by the method of Harvey and Stein [28]:

---

[1] The constant "α" is used for scaling. It is the shape, not the magnitude, of $\underline{h}(s\underline{I}-\underline{A})^{-1}\underline{b}$ that is important.

$$\underline{h} = [9.3 \times 10^{-5} \quad 1.481 \times 10^{-3} \quad -9.061 \times 10^{-6} \quad -1.254 \times 10^{-2}] \qquad (5.54)$$

The bandwidth of $\underline{k}_c(s\underline{I}-\underline{A})^{-1}\underline{b}$ depends on the choice of the control weight ρ. A choice of

$$\rho = 1.6 \times 10^{-3} \qquad (5.55)$$

results in a bandwidth of 7 rad/sec.

The Kalman filter is designed by the robustness recovery procedure [27]. Choose

$$\underline{\gamma} = \underline{b} \qquad (5.56)$$

and adjust μ to select the frequency range over which kg(s) approximates $\underline{k}_c(s\underline{I}-\underline{A})^{-1}\underline{b}$. For this example use

$$\mu = 3.4 \times 10^{-7} \qquad (5.57)$$

For the choices given above of $\underline{h}$, ρ, $\underline{\gamma}$, and μ the LQG compensator has the transfer function

$$k(s) = \frac{-11,750 \ (s+.195)(s+1.395)(s+6.305)}{(s+.02319)(s+1.962)[(s+261.8)^2 + (261.8)^2]} \qquad (5.58)$$

The Bode plot of kg(s) is shown in Figure 5.19. The bandwidth is 7 rad/sec, the phase margin is 64°, and the gain margin is [-14.5dB, 37.8 dB]. The closed loop system is, of course, stable.

5.4.2 Conic Sector Analysis of SISO Design

The analog compensator is converted to a hybrid compensator. This is done in a way similar to the earlier examples in this chapter:

$$f(s) = \frac{2500}{s^2 + 70s + 2500} \quad \text{(2nd order Butterworth,}$$
$$\text{break frequency} = 50 \text{ rad/sec)}$$

$$T = .02 \quad \text{(foldover frequency} = \frac{\pi}{T} = 157 \text{ rad/sec)}$$

$$d(z) = \frac{-6.233 \ (z-.99611)(z-.97244) \ (z-.88119)(z+1)}{(z-.99954)(z-.96145)[(z+.63763)^2 + (.26229)^2]} \tag{5.59}$$

(Tustinized version of k(s), prewarped frequency = 7 rad/sec)

$$h(s) = \frac{1-e^{-sT}}{s} \quad \text{(zero-order-hold)}$$

The sample rate is 50 samples per second, which is typical for flight computers in fighter aircraft.

Closed Loop Stability by Theorem 3.3

Conic sector techniques will now be used to determine if the hybrid closed loop system is stable. A stable version of the loop transfer operator will be placed inside of a cone and then the sufficient conditions for closed loop stability given by Theorem 3.3 will be checked.

The hybrid operator is open loop stable, but the plant is not. The loop transfer operator is therefore unstable, and it is not possible to place an unstable operator inside of a cone. This problem is circumvented by separating the plant into a stable part multiplied by an allpass network. The stable part is created by mapping the unstable poles to their mirror images about the jω-axis. The allpass network has unit magnitude for all ω:

$$g(s) = g_s(s) \ g_{ap}(s) \tag{5.60}$$

where

$$g_{ap}(s) = \frac{[(s + .6895)^2 + (.2484)^2]}{[(s - .6895)^2 + (.2484)^2]} \tag{5.61}$$

The hybrid operator and the stable part of the plant are placed inside of a cone. The optimal center of the cone is used:

$$c(s) = \frac{1}{T} g_s hd*f(s) \tag{5.62}$$

The hold and prefilter are each replaced by $(hg_s f)^{1/2}$, and the radius of the cone is computed by

$$r(j\omega) = \frac{1}{T} \left[\sum_{k=-20}^{20} \sum_{\substack{n=-20 \\ n \neq k}}^{20} |(hg_s f)_k (hg_s f_n)| \right]^{1/2} |d*(j\omega)| \tag{5.63}$$

The radius is shown in Figure 5.20a. The center and the multiplicative radius are in Figure 5.20b.

The sufficient conditions for closed loop stability given by Theorem 3.3 are now checked. Condition (i) is that the hybrid operator and the stable part of the plant are strictly inside cone (C,R). This cone has just been constructed. Condition (ii) is that the analog system with the loop transfer operator $cg_{ap}(s)$ is closed loop stable. This is verified by the Nyquist diagram of $cg_{ap}(s)$ shown in Figure 5.21a.[1] Condition (iii) is that

$$|rg_{ap} (1 + cg_{ap})^{-1} (j\omega)| < 1 \quad \text{for all } \omega \tag{5.64}$$

This condition is verified in Figure 5.21b. Since all three conditions of (the appropriately modified) Theorem 3.3 are satisfied, the hybrid system is closed loop stable.

---

[1]The number of open loop unstable poles = 2, which equals the number of counter-clockwise encirclements of the -1 point.
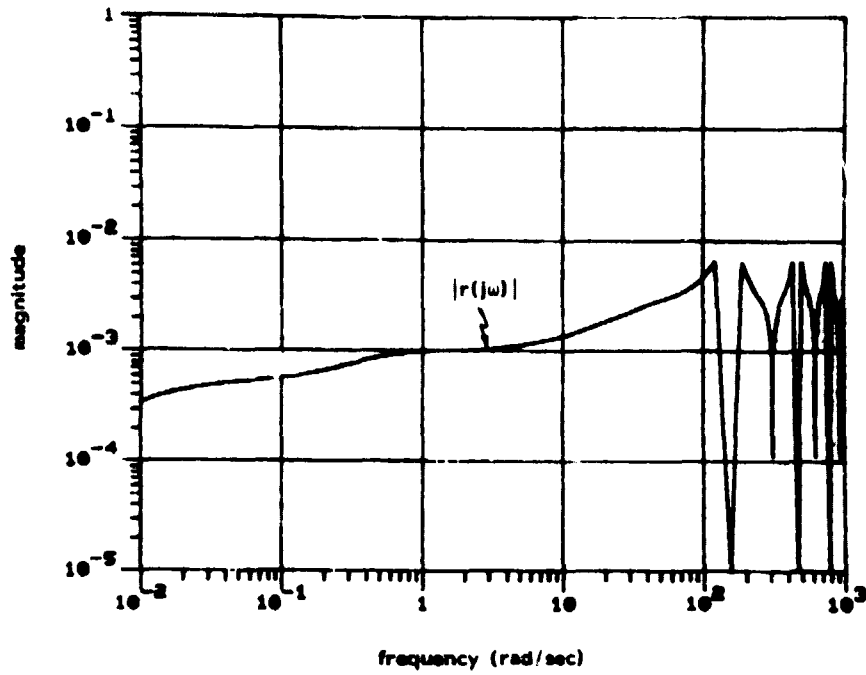
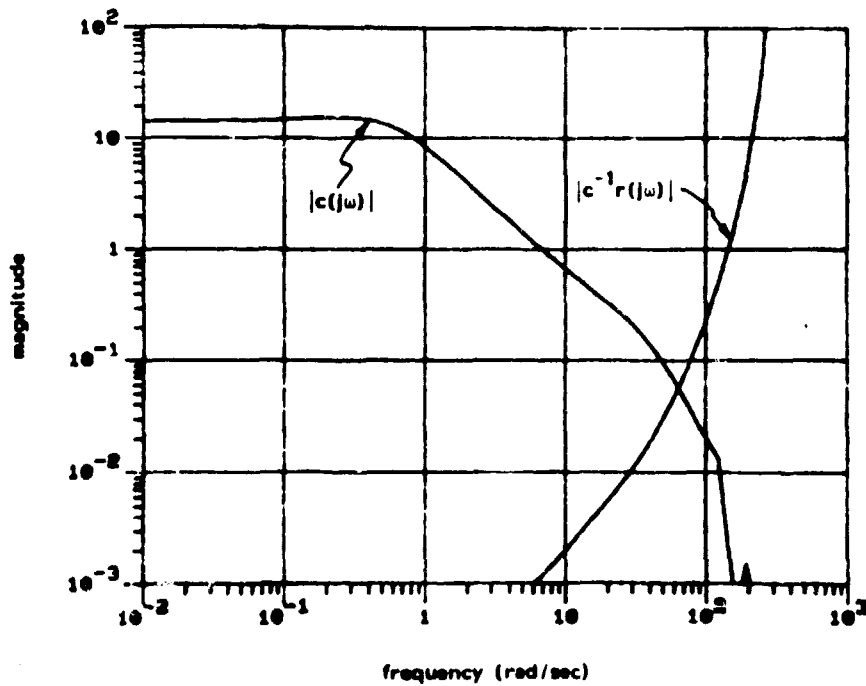Figure 5.20a: Radius of cone that contains a stable version of the loop transfer operator.

Figure 5.20b: Center and multiplicative radius.
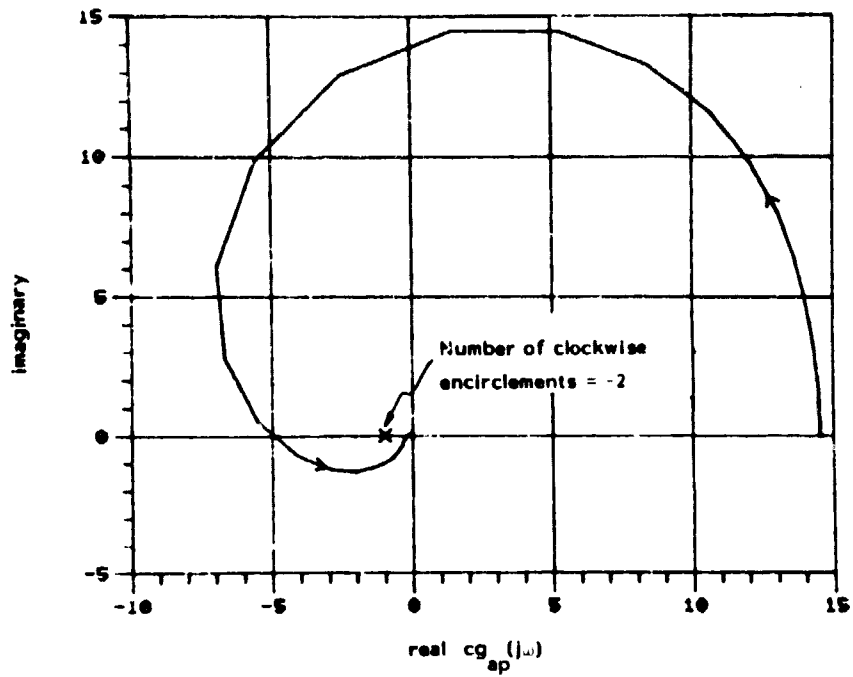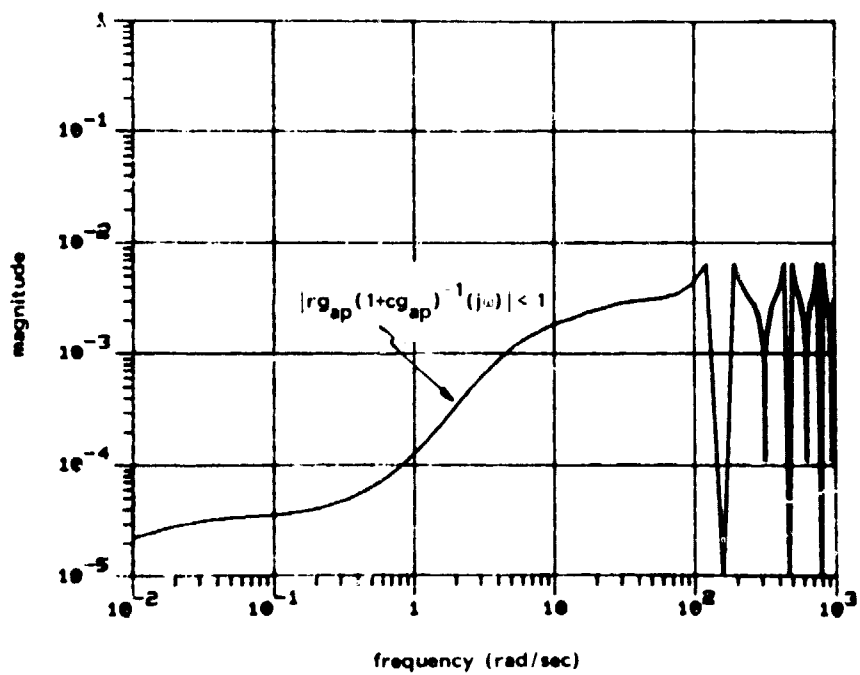
Figure 5.21a: Nyquist diagram of $cg_{ap}(j\omega)$.

Figure 5.21b: Stability test of Theorem 3.3.

Robust Closed Loop Stability by Theorem 3.5

The actual plant is $\tilde{g}(s) = g(s) [1 + e_m(s)]$. Assume that the multiplicative perturbation is bounded by the constant $|e_m(j\omega)| < \alpha$ for all ω. Theorem 3.5 can be used to find the maximum value of α such that $\tilde{g}(s)$ meets the sufficient conditions for closed loop stability. The maximum value is $\alpha = .36$, which corresponds to a guaranteed phase margin of $21°$.

Robust Closed Loop Stability by Theorem 3.7

If the discrete closed loop system is stable then a cone can be constructed such that $-K^I$ is outside of the cone. The condition of discrete closed loop stability is verified by the discrete Nyquist diagram of $d*g_d*(s)$ plotted in Figure 5.22a.

The center of the cone is $g(s)$, and the radius is computed by (3.36) of Theorem 3.6. The multiplicative radius $|g^{-1}r(j\omega)|$ is plotted in Figure 5.22b. By Theorem 3.7 the closed loop system is stable for $\tilde{g}(s) = g(s) [1 + e_m(s)]$ if $|e_m(j\omega)| < |g^{-1}r(j\omega)|$.

If the multiplicative perturbation is constrained to be constant for all ω then its magnitude must be less than the minimum value of $|g^{-1}r(j\omega)|$, which is $\alpha = .68$. This value of α corresponds to a guaranteed phase margin of $40°$, which is less conservative than the $21°$ obtained by Theorem 3.5. The actual phase margin is $46°$ (obtained from the discrete Nyquist diagram of Figure 5.22a).

This completes the SISO version of the high performance aircraft example. The analog compensator was designed using LQG methods and then
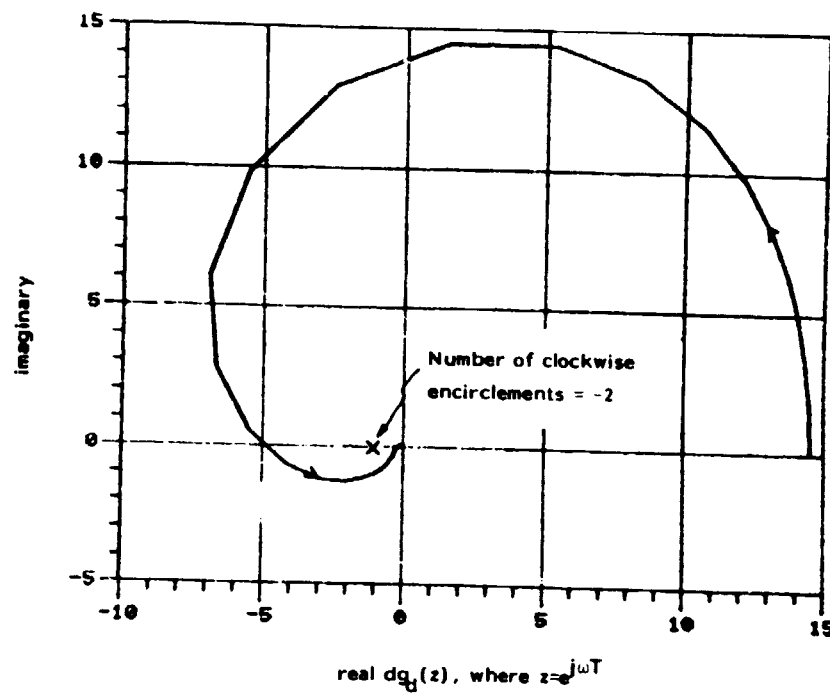
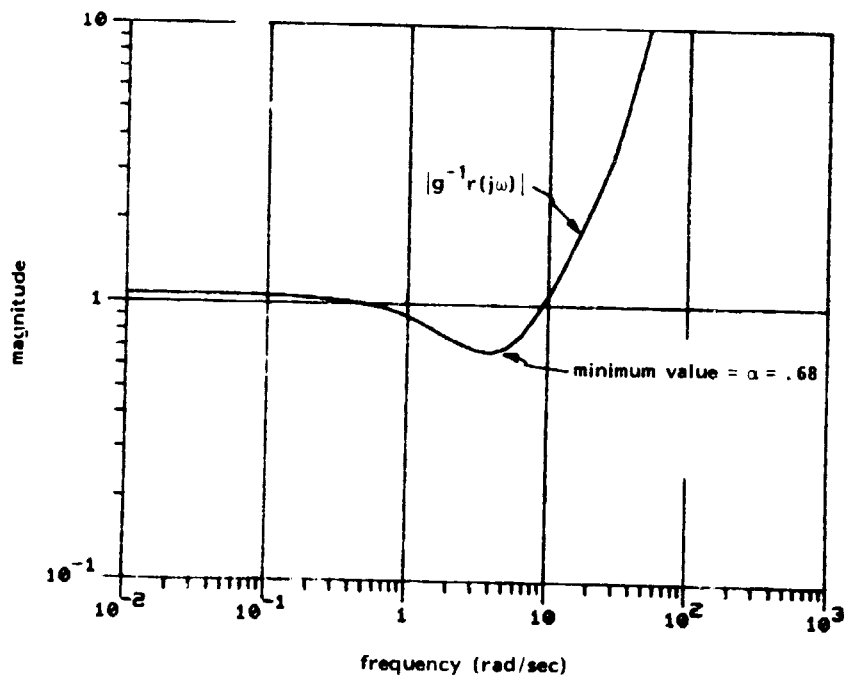Figure 5.22a: Discrete Nyquist diagram of $d*g_{d*}(j\omega)$.

Figure 5.22b: Multiplicative radius of cone such that $-K^I$ is outside of the cone.

converted to a hybrid compensator. A stable version of the loop transfer operator was created by multiplying the unstable plant by an all-pass network. Theorems 3.2, 3.3, 3.5, 3.6, and 3.7 were used in various ways to analyze closed loop stability and robustness properties.

5.4.3 LQG Design of Multivariable Analog Compensator

The high performance aircraft used in this example has multiple control surfaces (see [2,26]) that allow independent control of attitude and flight path motion. In the pitch axis the basic objective of the multivariable design is to achieve independent control of pitch attitude and angle-of-attack with approximately equivalent speeds of response. This objective is met in the analog design described in [26].

The analog design uses LQG techniques. The plant $\underline{G}(s)$ of Table 5.2 is augmented to $\underline{G}_a(s) = \frac{1}{s} \underline{G}(s) = \underline{C}_a(s\underline{I}-\underline{A}_a)^{-1} \underline{B}_a$ by appending integrators to the outputs (pitch attitude ang angle-of-attack). The Kalman filter noise covariance matrices are

$$\left.\begin{array}{l} \underline{\Gamma} = \underline{B}_a \, (\underline{V}\underline{\Sigma}^{-1}) \\ \\ \underline{N} = \underline{I} \end{array}\right\} \tag{5.65}$$

where

$$\left.\begin{array}{l} \underline{V} = \begin{bmatrix} .962 & -.274 \\ \\ -.274 & -.962 \end{bmatrix} \\ \\ \\ \underline{\Sigma} = \text{diag } [1.8 \quad .0077] \end{array}\right\} \tag{5.66}$$

The $\underline{V}$ and $\underline{\Sigma}$ matrices are, respectively, the right singular vectors and the singular values of $\underline{G}_a(j\omega_o)$ for $\omega_o = 10^{.5}$. They multiply the $\underline{B}_a$ matrix in (5.65) so that the singular values of $\underline{C}_a(s\underline{I}-\underline{A}_a)^{-1}\underline{\Gamma}$ are approximately equal at $\omega_o = 10^{.5}$.

The LQ regulator weighting matrices $\underline{Q}$ and $\underline{R}$ are chosen so that the loop transfer function $\underline{G}_a\underline{K}(s)$ approximates the Kalman filter loop transfer function $\underline{C}_a(s\underline{I}-\underline{A}_a)^{-1}\underline{K}_f$ over a finite frequency range:

$$\left.\begin{array}{l} \underline{Q} = \underline{c}^T\underline{c} \\[2em] \underline{R} = 10^{-6}\underline{I} \end{array}\right\} \tag{5.67}$$

The Kalman filter and LQ regulator problems are solved and used to form the LQG compensator $\underline{K}(s)$. The analog closed loop system is guaranteed to be closed loop stable. The singular values of $\underline{G}_a(j\omega)$ and $\underline{G}_a\underline{K}(j\omega)$ are shown in Figure 5.23a, and the "shape" of the loop transfer function $\underline{G}_a\underline{K}(j\omega)$ is used to analyze various performance measures (command response, bandwidth, disturbance rejection, and so on, see [1]). The singular values of $\underline{I} + (\underline{G}_a\underline{K})^{-1}(j\omega)$ are shown in Figure 5.23b and are used to analyze robustness with respect to perturbations inserted at the output of the plant [i.e. when $\underline{G}_a(j\omega)$ is replaced by $(\underline{I} + \underline{E}_m)\underline{G}_a(j\omega)$]. In Figure 5.23b it is shown that

$$\sigma_{min}[\underline{I} + (\underline{G}_a\underline{K})^{-1}(j\omega)] \geq \alpha = .54 \qquad \text{for all } \omega \tag{5.68}$$
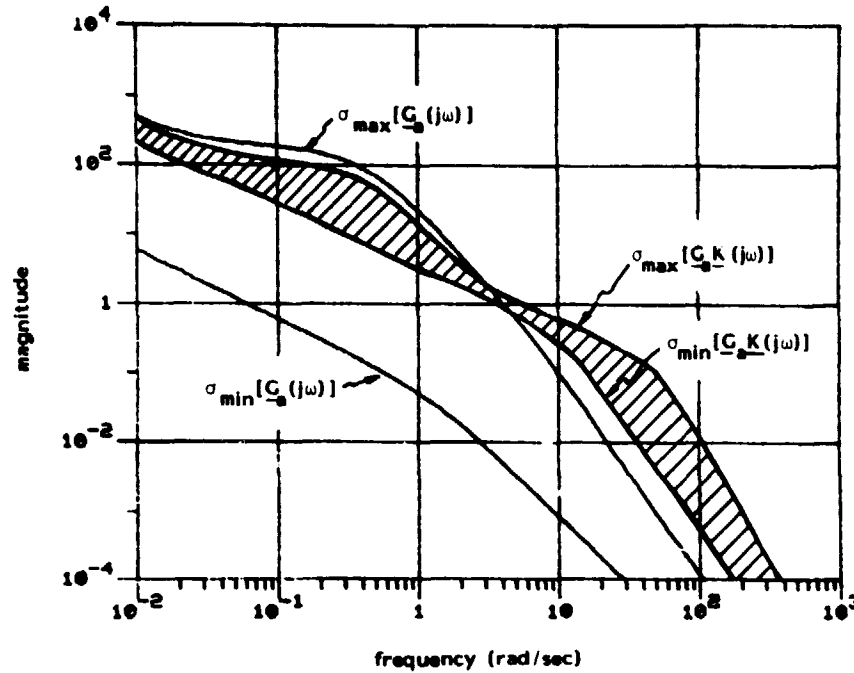
Figure 5.23a: Singular values of $\underline{G}_a(j\omega)$ and $\underline{G}_a\underline{K}(j\omega)$.
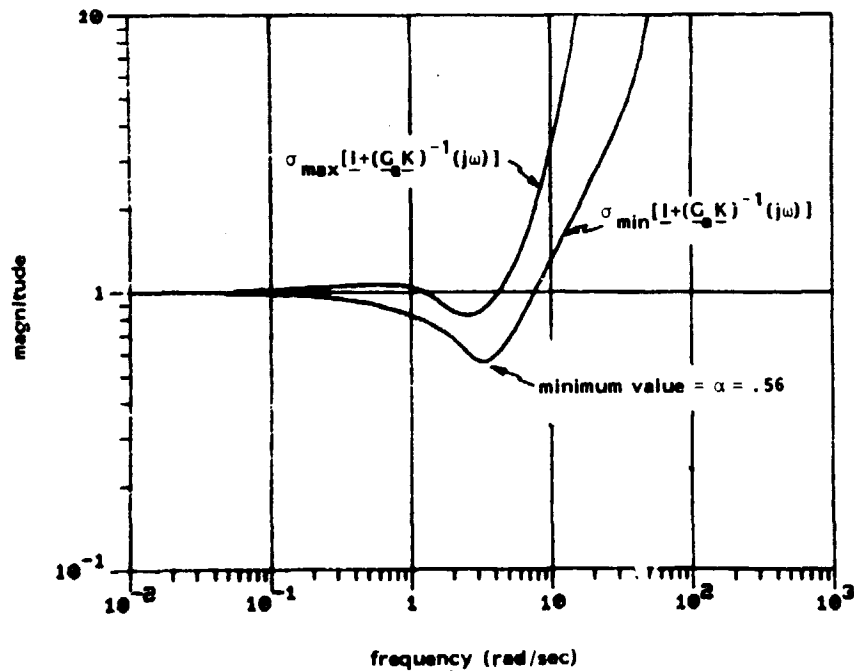

Figure 5.23b: Robustness test for multivariable
analog feedback systems.

which indicates that the analog closed loop system will remain stable

for phase uncertainties up to ±31°, at any frequency, simultaneously in

any output channel (see Subsection 2.2.7).

5.4.4 Conic Sector Analysis of Multivariable Design

The multivariable analog compensator is $\frac{1}{s} \underline{K}(s)$. The integrators

that were appended to the outputs of the plant are included with $\underline{K}(s)$.

The analog compensator $\frac{1}{s} \underline{K}(s)$ is now converted to a hybrid compensator.

The prefilters and holds are chosen to be the same in their respective

input and output channels:

$$
\left.
\begin{aligned}
\underline{F}(s) &= \left(\frac{2500}{s^2+70s+2500}\right) \cdot \underline{I} \\[1em]
T &= .02 \text{ seconds} \\[1em]
\underline{D}(z) &= \text{tustinized version of } \frac{1}{s}\underline{K}(s), \\
&\quad \text{ prewarped about 7 rad/sec} \\[1em]
\underline{H}(s) &= \left(\frac{1-e^{-sT}}{s}\right) \cdot \underline{I}
\end{aligned}
\right\}
\qquad (5.69)
$$

In this subsection closed loop stability and robustness margins will

be determined. The conic sector analysis techniques of Theorems 3.6 and

3.7 will be shown to give conservative robustness margins.

The discrete version of the multivariable Nyquist criterion is used

to determine the closed loop stability of the hybrid feedback system.

The discretized plant is $\underline{G}_d{}^*(j\omega) = [\underline{FGH}(j\omega)]^*$, and the discrete loop

transfer function is $\underline{G}_d^*\underline{D}^*(j\omega)$. The Nyquist plot of $-1 + \det [\underline{I} +$

$\underline{G}_d^*\underline{D}^*(j\omega)]$ is shown in Figures 5.24a and 5.24b. The first figure (which

is not to scale) shows the Nyquist plot as the frequency variable ω is

varied from $-\frac{\pi}{T}$ to $\frac{\pi}{T}$. The number of counterclockwise encirclements of

-1 point is 2, which is equal to the number of open loop unstable poles

of $\underline{G}_d(z)\underline{D}(z)$.[1] Therefore, the hybrid system is closed loop stable.

An exploded view of the Nyquist plot is shown in Figure 5.24b.
The nearness to the -1 point is a good robustness margin for SISO sys-
tems, but not for multivariable systems. Much better is the singular value
plot of Figure 5.25a,[2] where it is shown that

$$\sigma_{min}[\underline{I} + (\underline{G}_d^*\underline{D}^*)^{-1}(j\omega)] \geq \alpha = .48 \quad \text{for all } \omega \qquad (5.70)$$

Figure 5.25a is used to analyze robustness with respect to multiplicative

perturbations inserted in the feedback loop just before the digital

computer, where the physical signal is a discrete sequence. If the

multiplicative perturbation is a constant diagonal matrix then it can

be moved in the feedback loop to just after the analog plant. The lower

bound $\alpha = .48$ indicates that the hybrid closed loop system will remain

closed loop stable for phase uncertainties up to $\pm 28°$, at any frequency,

simultaneously in any output channel.

---

[1] The two integrators in $\underline{D}(z)$ account for the encirclement between $\omega = 0^-$
and $\omega = 0^+$.

[2] Singular values are better than determinants for indicating the nearness
to singularity of the return difference matrix $\underline{I} + \underline{G}_d^*\underline{D}^*(j\omega)$.
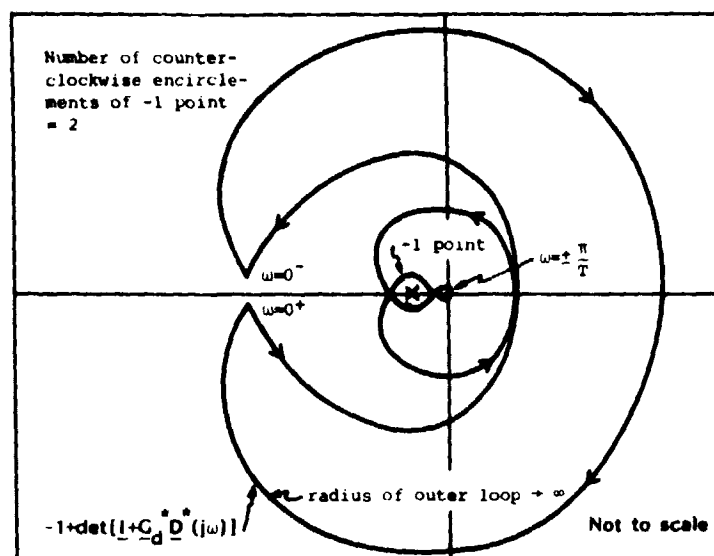
Figure 5.24a: Discrete multivariable Nyquist plot.
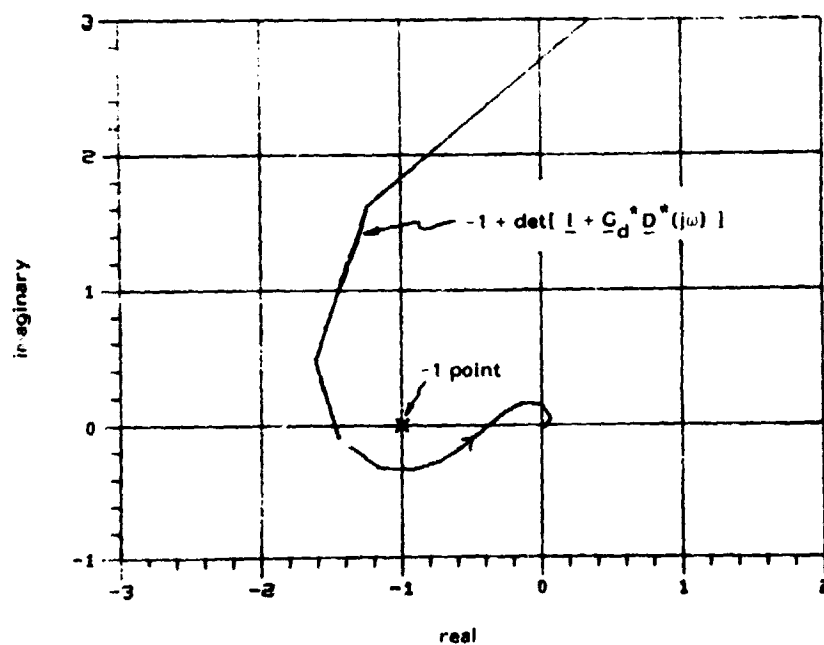

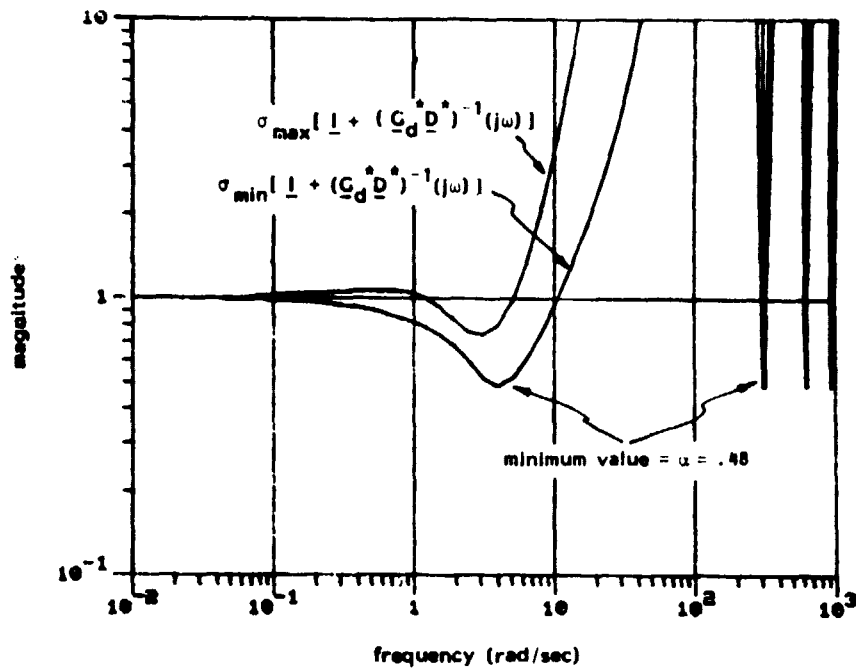Figure 5.24b: Exploded view of 5.24a.

Figure 5.25a: Robustness test for multivariable digital system.
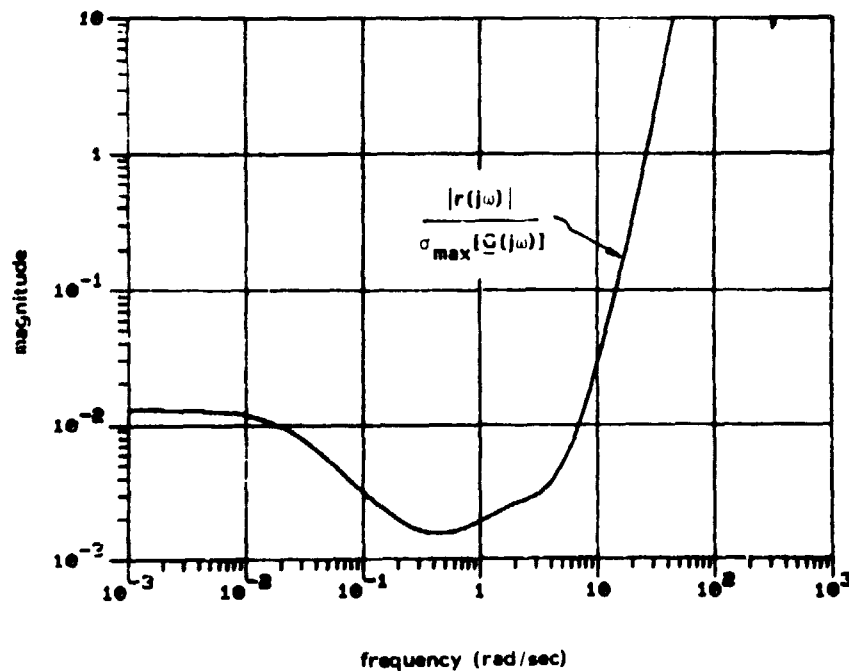
Figure 5.25b: Multiplicative radius of cone such that $-K^I$ is outside of the cone.

The conic sector analysis techniques of Theorems 3.6 and 3.7 will now be used to analyze robustness. Theorem 3.6 is used to construct a cone such that $-K^I$ is outside of the cone. The center of the cone is the nominal plant G, and the radius is the R computed by (3.36). The multiplicative radius is $r(j\omega)/\sigma_{max}[\underline{G}(j\omega)]$ and is shown in Figure 5.25b.

According to Theorem 3.7, the hybrid system will remain closed loop stable for a multiplicative perturbation of the nominal plant if

$$\ell_m(\omega) < \frac{r(j\omega)}{\sigma_{max}[\underline{G}(j\omega)]} \qquad \text{for all } \omega \qquad (5.71)$$

Unfortunately, this is a conservative result. In Figure 5.25b it is shown that

$$\ell_m(\omega) < \alpha = .002 \qquad \text{for all } \omega \qquad (5.72)$$

which corresponds to a guaranteed multivariable phase margin of $< 1°$.

More research is needed to remove this conservatism. Some indication of why this conservatism occurs is given by the following manipulation of the corresponding robustness result for multivariable analog systems:

$$\ell_m(\omega) < \sigma_{min}[\underline{I} + (\underline{GK})^{-1}(j\omega)] \qquad \text{for all } \omega \qquad (5.73)$$

$$\Longleftrightarrow \quad \ell_m(\omega) < \sigma_{max}^{-1}[\underline{GK}(\underline{I} + \underline{GK})^{-1}(j\omega)] \qquad \text{for all } \omega \qquad (5.74)$$

$$\Longleftarrow \quad \ell_m(\omega) < \sigma_{max}^{-1}[\underline{G}(j\omega)] \, \sigma_{max}[\underline{K}(\underline{I} + \underline{GK})^{-1}(j\omega)] \qquad \text{for all } \omega$$
$$(5.75)$$

If (5.75) is used instead of (5.73) then the analog robustness test will have approximately the same degree of conservatism as the result of Theorem 3.7. The problem occurs in (5.75) because the matrix product is split up, which is conservative when the minimum and maximum singular values of $\underline{G}(j\omega)$ are far apart.[1]

This completes the multivariable conic sector example. A multivariable analog compensator was transformed into a hybrid compensator. The resulting hybrid feedback system was analyzed with the use of the discrete loop transfer function $\underline{G}_d\underline{D}(z)$, and then was analyzed with the use of the conic sectors of Theorems 3.6 and 3.7. The conic sectors resulted in a conservative robustness margin, which occured because the multiplicative radius is conservative (small) when $\sigma_{min}[\underline{G}(j\omega)] \ll \sigma_{max}[\underline{G}(j\omega)]$.

---

[1] Note that $1 = \sigma_{max}(\underline{GG}^{-1}) \leq \sigma_{max}(\underline{G})/\sigma_{min}(\underline{G})$, which is conservative when $\sigma_{min}(\underline{G}) \ll \sigma_{max}(\underline{G})$.

6. MULTIRATE SAMPLING

6.1 Introduction

The hybrid feedback systems considered up until now have had one synchronous sampler. These are the most common types of hybrid feedback systems; however, there exist many applications where the hybrid feedback system contains more than one synchronous sampler, each operating at a different rate. These are called "multirate sampled-data systems".

Multirate sampling may occur because the measurements are discrete (e.g. radar tracking, sun sensors for dual spin satellites, or image processing algorithms for robot manipulators) and the digital computer used to implement the control law is separate and operates at a different sample rate. Multirate sampling may also be used if the plant has different time scales, in which case multirate sampling can be used to significantly decrease the required computer capacity, i.e. "slow" control loops are sampled at a slower rate as compared to "fast" ones.

A feedback system with two hybrid compensators in the same loop is shown in Figure 6.1. This is called a sinjle loop multirate hybrid (SLMRH) feedback system. The feedback loop is used for stability augmentation and contains a hybrid compensator (modelled by the hybrid operator K_2) with a sampling period of mT seconds (where m is an integer $\geq$ 1). The hybrid compensator in the forward loop (modelled by K_1) has the smaller sampling period of T seconds, which allows the output to respond faster to commands than to the feedback. The plant has the nominal model g(s) and the multiplicative perturbation $e_m(s)$, assumed bounded by $|e_m(j\omega)| < \ell_m(\omega)$ for all ω. All of the components in Figure 6.1 are single input single output (SISO).
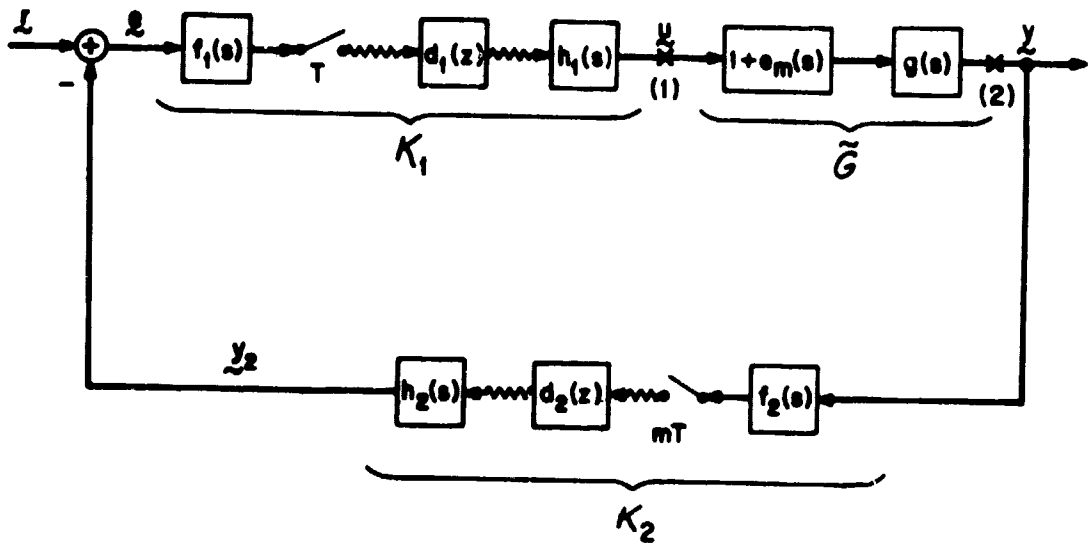
Figure 6.1: Single loop multirate hybrid feedback system

Conventional analysis techniques for single rate hybrid feedback systems have been extended to the multirate case. A survey with extensive references is by Walton [31]. A tutorial treatment of these techniques is by Konar and Mahesh [32]. The basic idea is to transform the multirate hybrid feedback system into an equivalent single rate hybrid feedback system and then apply standard z-transform techniques. The only multirate technique used in this chapter is called the "frequency decomposition" method [33, 34]. Using this method, the SLMRH feedback system in Figure 6.1 is broken at some point where the physical signal is a discrete sequence, and then a z-transform is derived for the linear shift invariant loop transfer operator.

Conic sector analysis techniques also can be extended from single rate to multirate hybrid feedback systems. In this chapter they are extended to the relatively simple SLMRH feedback systems. Further extensions to the much more difficult multiple loop case will not be attempted here.[1] The material in this chapter is simply a first step that demonstrates that further extensions of the conic sector analysis techniques are possible to more complicated multirate systems.

Conic sectors can be used for multirate hybrid feedback systems (either single or multiple loop) just as they can be used for single rate hybrid feedback systems and analog feedback systems - to analyze closed loop stability, command response, performance, disturbance rejection, and robustness with respect to plant uncertainties. If the

---

[1]Multiple loop multirate hybrid feedback systems are more common than the single loop case because different time scales of the plant naturally break down into multiple loops.

multirate hybrid operator is placed inside of a conic sector, then the

center can be used as a rigorous continuous time linear time invariant

(CTLTI) approximation.

Conic sector analysis techniques are potentially more important for

multirate than for single rate hybrid feedback systems. The feedback

loop is broken where the physical signal is analog and complexities due

to different sampling rates are subsumed by the use of conic sectors.

Techniques to analyze robustness do not currently exist, whereas conic

sector techniques are inherently robustness techniques (as discussed

in Subsection 2.4.5). The z-transform techniques used to convert multi-

rate to single rate systems have the problem of increased dimensionality

(proportional to the integer multiple of the sample rates). The conic

sector techniques do not suffer from this increased dimensionality.

In Section 6.2 the SLMRH feedback system is described and frequency

domain input-output transformations for the multirate hybrid operators

are presented. Theorems 3.1 to 3.7 for single rate hybrid feedback

systems are extended to SLMRH feedback systems. These extensions are

presented in the multiple-part Theorems 6.1 and 6.2. The new conic

sector analysis techniques can be used to analyze stability and robust-

ness, but the techniques for analyzing command response (as in Subsection

2.4.6 and Section 3.5) have not yet been extended. In Section 6.3 a

multirate version of the lead-lag compensator example of Section 5.2

is presented.

6.2 Conic Sectors for Multirate Hybrid Operators

Conic sector analysis techniques are used by first dividing a

feedback loop into two subsystems, and second by constructing a cone

such that it contains one of the subsystems and the other subsystem is outside of it. There are numerous ways to divide up the SLMRH feedback system of Figure 6.1. In this chapter the feedback loop is broken at points 1 and 2 (at the input and output of the plant). The two subsystems are (1) the multirate hybrid operator K_1K_2 and (2) the actual plant $\tilde{G}$. A conic sector is derived in Subsection 6.2.1 that contains K_1K_2, and in Subsection 6.2.2 that $-(K_1K_2)^I$ is outside of.

6.2.1 Existence of a Cone that Contains K_1K_2

The multirate hybrid operator K_1K_2 is shown in Figure 6.2. The analysis that follows assumes that the slower sampler is first[1]. The existence of a conic sector that contains K_1K_2 follows from the description of the input-output transformation from $\underset{\sim}{y}$ to $\underset{\sim}{u}$. The assumption is made that the two samplers are in synchronism, i.e. every mth sample the two samplers coincide.[2]

The transformation from $\underset{\sim}{y}$ to $\underset{\sim}{y}_2$ is described by[3]

$$y_2(j\omega) = h_2(j\omega)d_2(e^{j\omega mT})\ \frac{1}{mT}\ \underset{k}{\Sigma}\ f_2(j\omega - j\ \frac{2\pi}{mT}\ k)y(j\omega - j\ \frac{2\omega}{mT}\ k) \quad (6.1)$$

---

[1] A similar analysis can be performed if the faster sampler is first.

[2] If the samplers are not in synchronism then an extra delay term must be inserted between $h_2(s)$ and $f_1(s)$. This does not invalidate what follows. Simply replace $h_2(s)$ by $h_2(s)e^{-T_ds}$.

[3] To avoid confusion between sample times of T and mT seconds the star notation (see Subsection 2.3.1), the symbol "ω_s," and the subscripts indicating frequency shifts are not used. The notation $d_2(e^{j\omega mT})$ indicates $d_2(z)$ evaluated at $z = e^{j\omega mT}$.
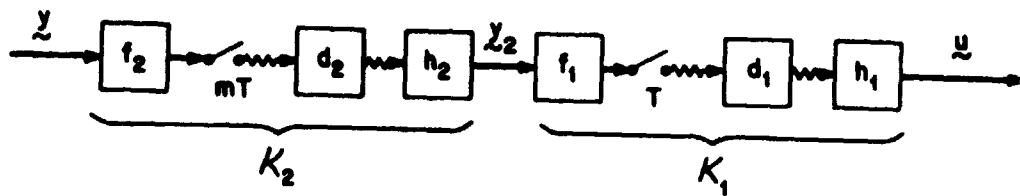
Figure 6.2: The multirate hybrid operator $K_1 K_2$

Similarly, the transformation from y_2 to u is described by

$$u(j\omega) = h_1(j\omega)d_1(e^{j\omega T}) \frac{1}{T} \sum_n f_1(j\omega - j \frac{2\pi}{T} n)y_2(j\omega - j \frac{2\omega}{T} n) \qquad (6.2)$$

Substitute (6.1) into (6.2) and change the variable of summation to obtain

$$u(j\omega) = \xi_1(j\omega)d_2(e^{j\omega m T}) \frac{1}{mT} \sum_k f_2(j\omega - j \frac{2\pi}{mT} k)y(j\omega - j \frac{2\pi}{mT} k) \qquad (6.3)$$

where

$$\xi_1(j\omega) = h_1(j\omega)d_1(e^{j\omega T}) \frac{1}{T} \sum_n f_1(j\omega - j \frac{2\pi}{T} n)h_2(j\omega - j \frac{2\pi}{T} n) \qquad (6.4)$$

The multirate hybrid operator described by (6.3) has the same structure as the single rate hybrid operator described by (2.51), except that the hold $h_2(j\omega)$ is replaced by $\xi_1(j\omega)$. It is precisely this similarity in structure that allows the conic sector results to be extended from the single to the multirate case.[1]

The following five part theorem is an extension of Theorems 3.1 to 3.4.

Theorem 6.1   Let $K_1 K_2$ be the multirate hybrid operator of Figure 6.2. Assume that $K_1 K_2$ is L_{2e}-stable. Let C be any LTI L_{2e}-stable operator, and let R and R^I be LTI L_{2e}-stable operators.

---

[1] The same structure is found if the higher rate sampler is first. The conjecture is made that the same structure will be found if the sample rates form a ratio that can be expressed as a rational number.

(a) $K_1 K_2$ is strictly inside cone (C,R) if

$$|r(j\omega)| \geq \frac{1}{(1-\varepsilon)^{1/2}} [r_4(\omega) + r_3(\omega)]^{1/2} \qquad (6.5)$$

for all ω and some $\varepsilon > 0$

where

$$r_4(\omega) = \frac{1}{(mT)^2} |d_2(e^{j\omega mT})|^2 \cdot \left[\sum_k \sum_{n \neq k} \left| \xi_1(j\omega - j\frac{2\pi}{mT}k) f_2(j\omega - j\frac{2\pi}{mT}n) \right|^2 \right] \qquad (6.6)$$

$$r_3(\omega) = \sum_k \left| \frac{1}{mT} \xi_1(j\omega - j\frac{2\pi}{mT}k) d_2(e^{j\omega mT}) f_2(j\omega - j\frac{2\pi}{mT}k) - c(j\omega - j\frac{2\pi}{mT}k) \right|^2 \qquad (6.7)$$

(b) The optimal center

$$c(s) = \frac{1}{mT} \xi_1(s) d_2(e^{smT}) f_2(s) \qquad (6.8)$$

minimizes the lower bound for $|r(j\omega)|$.

(c) The gain of the multirate hybrid operator is

$$\|K_1 K_2\|_{L_2} = \max_{0 \leq \omega \leq \frac{\pi}{mT}} \left\{ \left[\frac{1}{(mT)^2} \sum_k \left| \xi_1(j\omega - j\frac{2\pi}{mT}k) \right|^2 \right]^{1/2} \cdot \left| d_2(e^{j\omega mT}) \right| \cdot \right.$$

$$\left. \left[\sum_n \left| f_2(j\omega - j\frac{2\pi}{mT}n) \right|^2 \right]^{1/2} \right\} \qquad (6.9)$$

(d) The SLMRH feedback system of Figure 6.1 is closed loop stable

for $\tilde{G} = G$ (i.e. for the nominal plant with no perturbation) if

a C and R exist such that

(i) K_1K_2 is strictly inside cone (C,R)

(ii) $G(I+CG)^{-1}$ is L_{2e}-stable (i.e. the nominal analog system

is closed loop stable)

(iii) $|rg(1+cg)^{-1}(j\omega)| < 1$ for all ω (6.10)

(e) The SLMRH feedback system is closed loop stable for all pos-

sible $\tilde{G}$'s if in addition to the three conditions of part (d)

the following condition is true:

$$\ell_m(\omega) < \frac{|1+cg(j\omega)| - |rg(j\omega)|}{|cg(j\omega)| + |rg(j\omega)|} \quad \text{for all } \omega. \quad \blacksquare \quad (6.11)$$

The proof of Theorem 6.1 is similar to the proofs of Theorems 3.1

to 3.4. The following steps prove part (a) of Theorem 6.1 by showing

that the conic sector inequality (2.81) is satisfied for all input-

output pairs defined by K_1K_2.

(1) Define truncated function to convert from truncated to L_2
   function norm.

(2) Use Parseval's theorem to convert from time to frequency
   domain.

(3) Use frequency domain inequality of Lemma 3.A.

(4) Use Parseval's theorem again to convert from frequency to
   time domain.

(5) Convert from L_2 to truncated function norm.

Part (b) is proved by showing that the optimal center (6.8) makes $r_3(\omega)=0$ and therefore minimizes $r_4(\omega) + r_3(\omega)$ of (6.5). The proof of part (c) uses the center $c(s)=0$ to find an upperbound for the gain of K_1K_2 and then constructs an input signal that achieves the upperbound. Part (d) is an application of Lemma 2.5 to show closed loop stability. Conditions (ii) and (iii) of part (d) guarantee that $-G^I$ is outside cone (C,R). If inequality (6.11) of part (e) is satisfied then all possible $-\tilde{G}^I$'s are outside cone (C,R).

If Theorem 6.1 is used to analyze a SLMRH feedback system then the nominal feedback system is analog and has the loop transfer function $c(s)g(s)$. Stability and robustness properties of the SLMRH feedback system depend on the stability of the nominal feedback system. The radius of the conic-sector is treated as an additive perturbation of $c(s)$.

To reiterate, Theorem 6.1 has the following five parts:

(a) sufficient conditions for the existence of a cone that contains K_1K_2

(b) an optimal center for the cone

(c) the gain of K_1K_2

(d) sufficient conditions for closed loop stability

(e) sufficient conditions for robust closed loop stability

The analysis techniques laid out in Theorem 6.1 represent a new approach to the analysis of multirate hybrid feedback systems.

6.2.2 Existence of a Cone such that $-(K_1K_2)^I$ is Outside of the Cone

The alternative to constructing a cone that contains K_1K_2 is to construct a cone such that $-(K_1K_2)^I$ is outside of the cone. The best

choice for the center of this cone is G, the nominal plant. It follows
from Lemma 2.2 that $-(K_1 K_2)^I$ is outside of cone (G,R) if an R can be
found such that $\|R \, K_1 K_2 (I+G \, K_1 K_2)^I\|_{L_2} \leq 1$. The only restriction is
that the multirate hybrid operator $K_1 K_1 (I+G \, K_1 K_2)^I$ must be L_{2e}-stable.

The multirate hybrid feedback system that has the closed loop
operator $R \, K_1 K_2 (I+G \, K_1 K_2)^I$ is shown in Figure 6.3a. By breaking the
loop at point 1 and manipulating the block diagram the equivalent feed-
back system shown in Figure 6.3b is obtained. The feedback loop is
digital and operates at the slower sample period of mT seconds. The
multirate hybrid operator $K_1 K_2 (I+G \, K_1 K_2)^I$ is L_{2e}-stable if this digital
feedback loop is stable.

It is possible to obtain the z-transform of the loop transfer func-
tion of Figure 6.3b by the frequency decomposition method, see [31] to
[34]. Define the z-transform of the discretized plant as $g_d(z)$. The
loop transfer function is $d_2(z) g_d(z)$, and stability is checked by the
discrete Nyquist criterion, which uses a plot of $d_2(e^{j\omega mT}) g_d(e^{j\omega mT})$
from $\omega = 0$ to $\frac{\pi}{mT}$ rad/sec.

It is not necessary to go to the considerable trouble of finding
the z-transform $g_d(z)$. It is computationally easier to obtain $g_d(z)$,
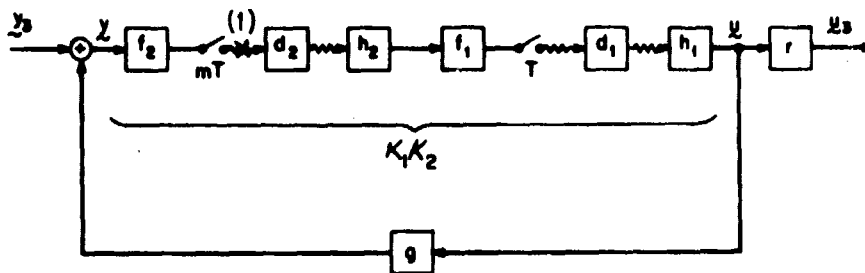evaluated at $z=e^{j\omega mT}$, by summing truncated versions of the following
infinite series:

Figure 6.3a: Multirate hybrid feedback system with the
closed loop operator $R\ K_1K_2(I+G\ K_1K_2)^I$
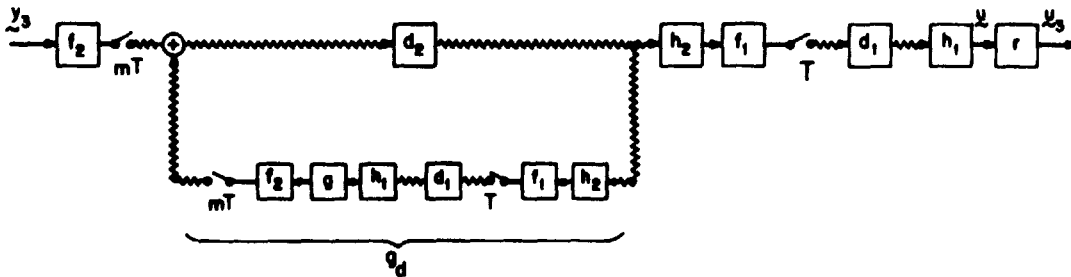

Figure 6.3b: Transformed version of 6.3a

$$g_d(e^{j\omega mT}) = \frac{1}{mT} \sum_k \xi_2(j\omega-j\frac{2\pi}{mT}k)f_1(j\omega-j\frac{2\pi}{mT}k)h_2(j\omega-j\frac{2\pi}{mT}k) \quad (6.12)$$

where

$$\xi_2(j\omega) = \left[\frac{1}{T}\sum_n f_2(j\omega-j\frac{2\pi}{T}n)g(j\omega-j\frac{2\pi}{T}n)h_1(j\omega-j\frac{2\pi}{T}n)\right]d_1(e^{j\omega T})$$

$$(6.13)$$

Before constructing a cone that $-(K_1K_2)^I$ is outside of, an input-output description of the multirate operator $K_1K_2(I+G\ K_1K_2)^I$ must be found. Using Figure 6.36b and equation (6.4), (6.12), and (6.13) we obtain

$$u(j\omega) = \xi_1(j\omega)d_{c\ell}(e^{j\omega mT})\frac{1}{mT}\sum_k f_2(j\omega-j\frac{2\pi}{mT}k)y_3(j\omega-j\frac{2\pi}{mT}k) \quad (6.14)$$

where

$$d_{c\ell}(e^{j\omega mT}) = d_2(1+g_d d_2)^{-1}(e^{j\omega mT}) \quad (6.15)$$

Equation (6.14) has the same form as the single rate hybrid compensator of (2.51), which makes possible the following extension of Theorems 3.6 and 3.7:

Theorem 6.2 Let K_1K_2 be the multirate hybrid operator of Figure 6.2, let G be any LTI operator such that $K_1K_2(I+G\ K_1K_2)^I$ is L_{2e}-stable, and let R and R^I be LTI L_{2e}-stable operators.

(a) $-(K_1K_2)^I$ is outside cone (G,R) if

$$|r(j\omega)| \leq \frac{1}{\sqrt{r_o(\omega)}} \qquad \text{for all } \omega \qquad (6.16)$$

where

$$r_g(\omega) = \frac{1}{(mT)^2} \left[\sum_k |\xi_1(j\omega-j\frac{2\pi}{mT}k)|^2 \right] \cdot |d_{c\ell}(e^{j\omega mT})|^2 \cdot$$

$$\left[\sum_n |f_2(j\omega-j\frac{2\pi}{mT}n)|^2 \right] \qquad (6.17)$$

(b) The multirate hybrid feedback system of Figure 5.1 is closed loop stable for all possible $\tilde{G}$'s if an $r(j\omega)$ exists such that

(i) $K_1K_2(I+G\ K_1K_2)^I$ is L_{2e}-stable

(ii) $-(K_1K_2)^I$ is outside cone (G,R)

(iii) $\ell_m(\omega) < |g^{-1}r(j\omega)|$ for all ω. ■ (6.18)

If $-(K_1K_2)^I$ is placed outside of a cone, then the nominal feedback system is the SLMRH feedback system with the nominal plant G. The stability of the nominal feedback system must be checked, which is done by constructing an equivalent single rate hybrid feedback system. It is not necessary to explicitly find a z-transform description of the single rate system. Instead, stability can be checked with the use of equations (6.12) and (6.13).

The center of the cone that $-(K_1K_2)^I$ is outside of is the nominal plant G. Part (a) of Theorem 6.2 gives a radius for this cone. Part (b) is a robustness result which gives sufficient conditions for all possible perturbations of the niminal plant to preserve closed loop stability.

6.3 Multirate Example

This example is a continuation of the lead-lag compensator example of Section 5.2. A second hybrid compensator, operating with twice the sample period, is added in the feedback loop. Theorem 6.1 is used to construct a cone that contains the multirate hybrid operator $K_1 K_2$ and to determine closed loop stability. Theorem 6.2 is then used to construct a cone such that $-(K_1 K_2)^I$ is outside of the cone and to determine a robustness margin.

This multirate example will appear to be similar to the single rate example of Section 5.2.[1] Though somewhat repetitious, this highlights the fact that conic sector analysis techniques are just as useful for multirate as for single rate hybrid feedback systems.

The SLMRH Feedback System

A block diagram of the SLMRH feedback system is shown in Figure 6.1. The transfer function of the nominal plant G is

$$g(s) = \frac{150}{(s+1)(s+3)} \tag{6.19}$$

and the hybrid compensator K_1 (in the forward loop) is a hybrid implementation of the analog compensator

$$k(s) = \frac{(s+3)^2}{(s+.4)(s+22.5)} \tag{6.20}$$

The prefilter, sample period (T = .031416 seconds), digital computer z-transform, and the hold are given in equation (5.3).

The components of the hybrid compensator K_2 (in the feedback loop) are

---

[1] Specifically, Subsections 5.2.5 and 5.2.7

shown below:

$$f_2(s) = \frac{625}{s^2+35s+625} \quad (2^{nd} \text{ order Butterworth with break at } 25 \text{ rad/sec})$$

$$2T = .062832 \text{ seconds } (m = 2, \frac{\pi}{T} = 50 \text{ rad/sec})$$

$$d_2(z) = \frac{1.2z}{z+.2} \quad (\text{digital lead compensator})$$

$$h_2(s) = \frac{1-e^{-2sT}}{s} \quad (\text{zero-order-hold})$$

(6.21)

In the single rate example a continuous estimate of the output signal was available. Here the estimate is undated every 2T seconds and held constant between updates. The prefilter $f_2(s)$ smooths the signal (prevents aliasing). The digital computer serves the purpose of adding phase lead around the crossover frequency to partially compensate for the phase lag due to the prefilter and hold.[1]

A Cone that Contains $K_1 K_2$

The feedback loop is broken before and after the analog plant, where the physical signals are analog, and the multirate hybrid operator $K_1 K_2$ transforms the output signal $\underset{\sim}{y}$ to the input signal $\underset{\sim}{u}$.

Part (a) of Theorem 6.1 is used to construct a cone that contains $K_1 K_2$. The optimal center is chosen:

$$c(s) = \frac{1}{T} \xi_1(s) \, d_2(e^{smT}) \, f_2(s)$$

(6.22)

---

[1] At $\omega = 7$ rad/sec the prefilter $f_2(s)$ decreases the phase by $23°$, the hold $h_2(s)$ decreases the phase by $13°$, and the computer $d_2(z)$ increases the phase by $4°$. The phase margin of the single rate system of Section 5.2 is $46°$, here we expect it to be about $46-23-13+4 = 14°$ (it turns out to be $11°$).

where $\xi_1(s)$ is defined by (6.1). In Figure 6.4 the magnitude and phase Bode plots of $cg(j\omega)$ and $kq(j\omega)$ are compared. The magnitude of $cg(j\omega)$ drops off sharply at about 20 rad/sec and has the expected extra phase lag at the crossover frequency of 7 rad/sec (phase margin = 14°).

The radius is computed by $(6.5)^1$ and is shown in Figure 6.5a. The multiplicative radius $c^{-1}r(j\omega)$ is shown in Figure 6.5b and is compared to $cg(j\omega)$. Over the bandwidth of the nominal analog system ($\omega < 7$ rad/sec) the multiplicative radius is $< .12$.

Closed loop stability is determined by the three conditions of part (d) of Theorem 6.1. Condition (i) is that K_1K_2 is strictly inside cone (C, R), which is true by the way that the cone was constructed. Condition (ii) is that the nominal analog system is closed loop stable, which is verified by the Nyquist plot of $cg(j\omega)$ in Figure 6.6a. Condition (iii) is that

$$\left| rg(1 + cg)^{-1}(j\omega) \right| < 1 \quad \text{for all } \omega \tag{6.23}$$

which is verified in Figure 6.6b. All three conditions are true, hence the SIMRH feedback system is closed loop stable.

A Cone such that $-(K_1K_2)^I$ is Outside of the Cone

The nominal feedback system differs depending on how the cone is applied. When K_1K_2 is inside of a cone then the nominal feedback system is analog. In this part of the example $-(K_1K_2)^I$ is outside of a cone, and the

---

[1] Because the optimal center was chosen $r_3(j\omega) = 0$. The infinite sum for $\xi_1(j\omega)$ was truncated at ± 30 terms, and the double infinite sum for $r_4(j\omega)$ was truncated at ± 20 terms.
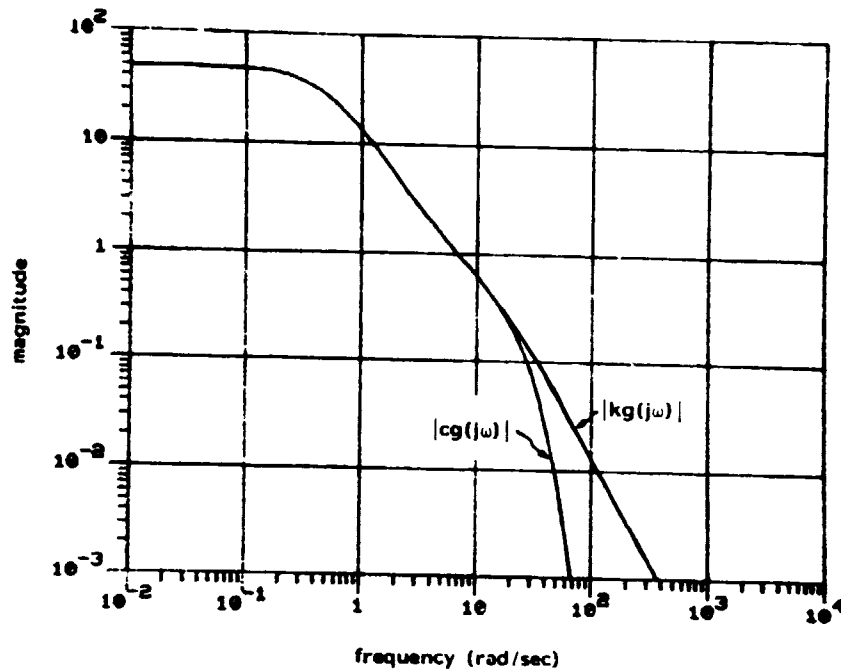
Figure 6.4a: Magnitude Bode plot of kg(jω) and eg(jω).

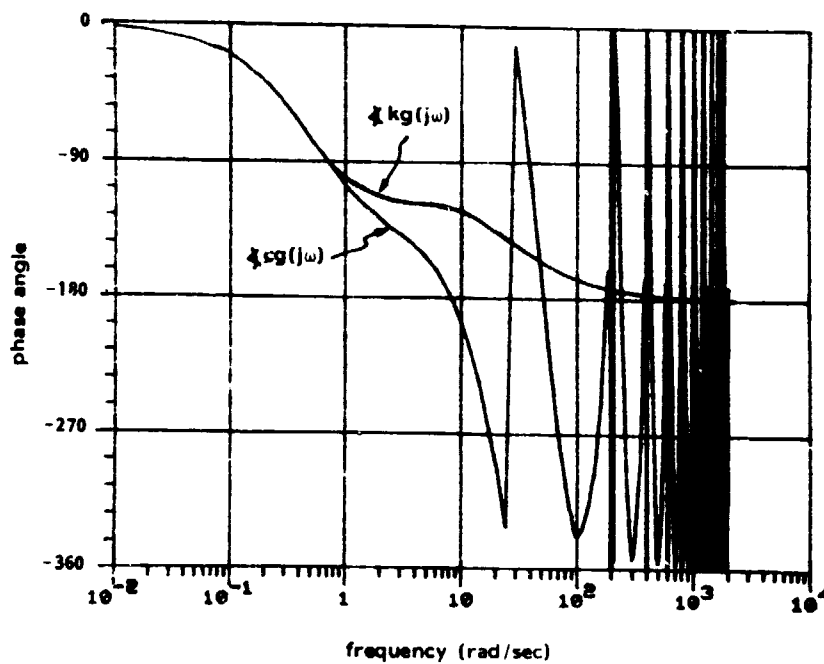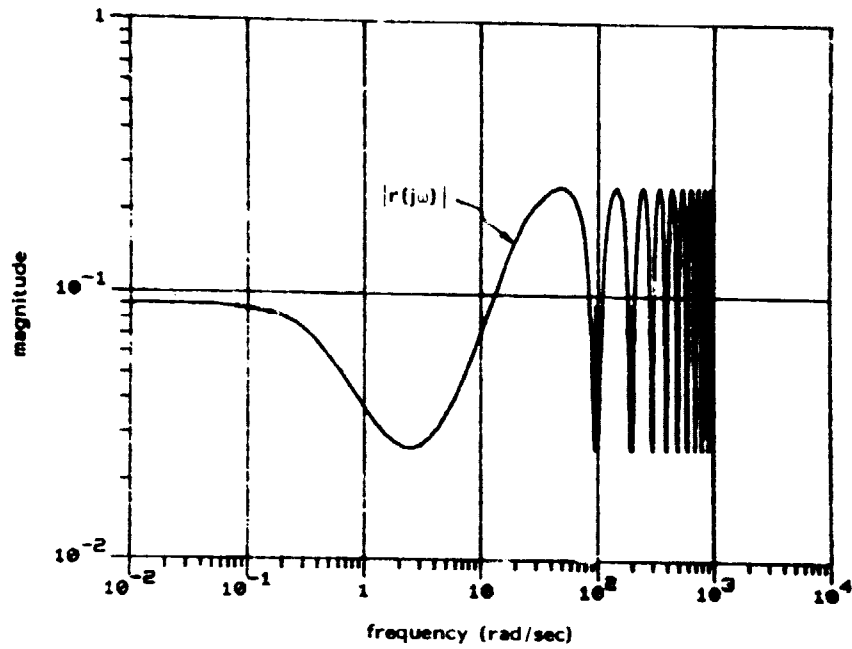Figure 6.4b: Phase Bode plot of kg(jω) and eg(jω).

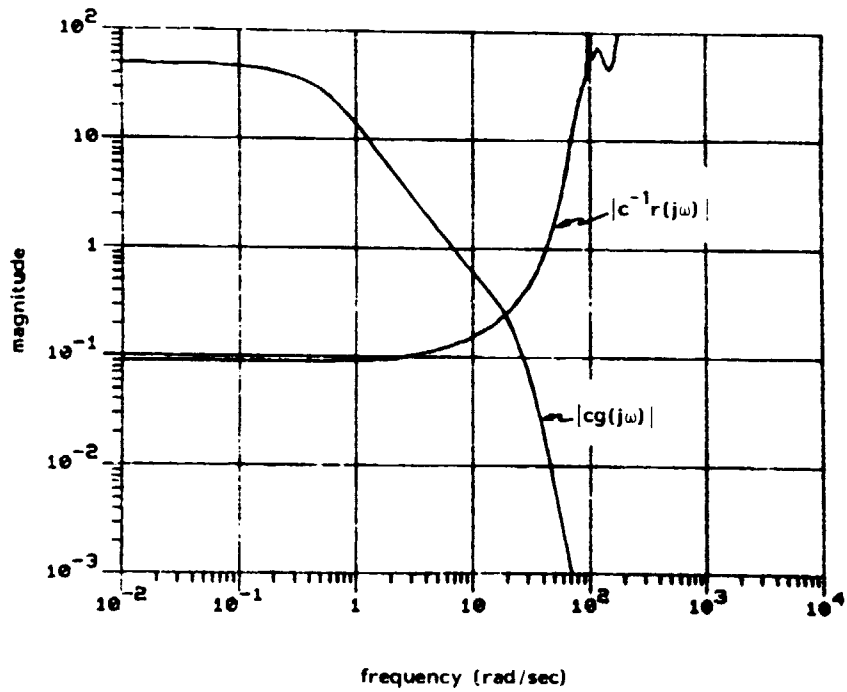Figure 6.5a: Radius of cone that contains $K_1 K_2$.

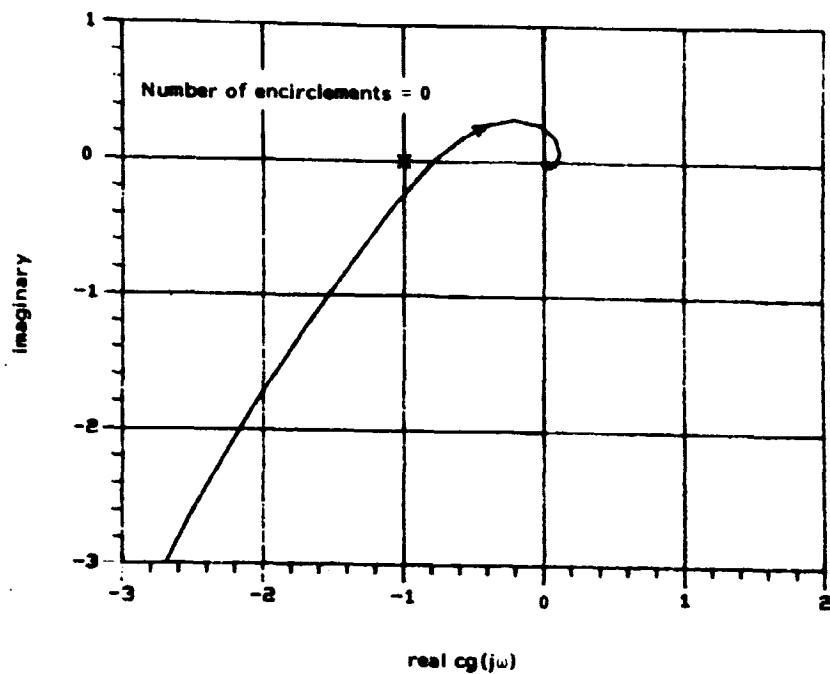Figure 6.5b: Multiplicative radius.

Figure 6.6a: Nyquist plot of $cg(j\omega)$
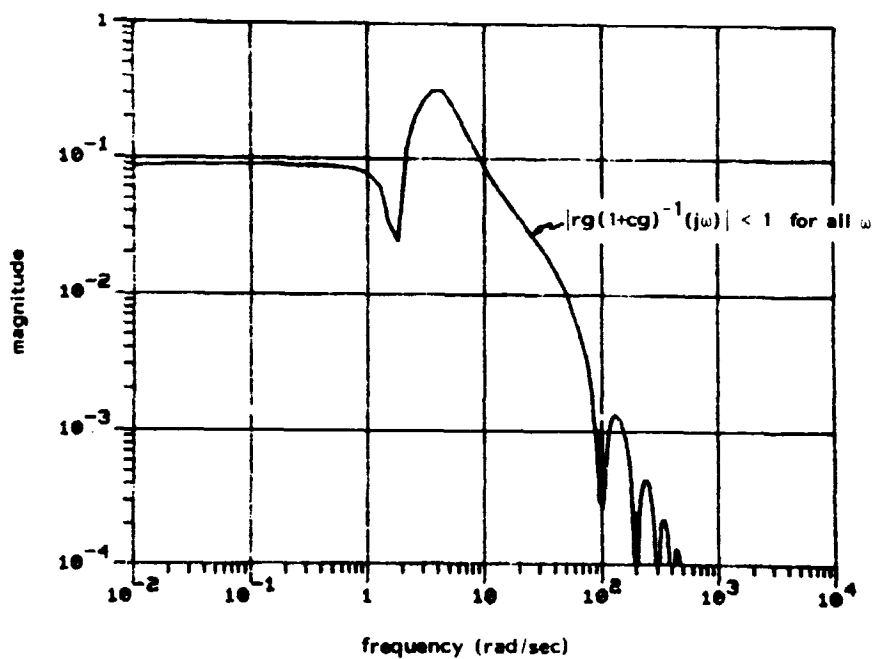
Figure 6.6b: Stability test of Theorem 6.1, part (d)

nominal feedback system is the SLMRH feedback system with the nominal

plant G. Its stability is verified by the discrete Nyquist plot of $d_2 g_d(z)$

shown in Figure 6.7a.[1] From this plot we obtain the discrete phase margin

of 11°.

Part (a) of Theorem 6.2 is used to construct the cone. The center

is the nominal plant G, the radius is computed by (6.16), and the multipli-

cative radius $q^{-1} r(j\omega)$ is shown in Figure 6.7b. According to part (b) of

Theorem 6.2, the SLMRH feedback system remains stable for any $\tilde{g} = g(1 + e_m)$

if

$$\ell_m(\omega) < |g^{-1} r(j\omega)| \quad \text{for all } \omega \tag{6.24}$$

and if $\ell_m(\omega)$ is constrained to be constant then

$$\ell_m(\omega) < \alpha = .19 \quad \text{for all } \omega \tag{6.25}$$

This constant corresponds to a phase uncertainty up to 11° at any frequency

(see Subsection 2.2.7).

This completes the multirate example. The conic sector analysis techni-

ques of Theorem 6.1 and 6.2 have been used to determine closed loop stability

and a robustness margin. These conic sector techniques are applied just as

were the corresponding techniques developed in Chapter 3 for single rate

hybrid feedback systems.[2]

---

[1] Of course we already knew the SLMRH feedback system is closed loop stable
form part (d) of Theorem 6.1.

---

[2] The second hybrid compensator has not affected closed loop stability, but has
significantly decreased the robustness margins. A step response will exhibit
large overshoot. This design is probably not acceptable, but can probably
be corrected by adjusting $d_1(z)$ and/or $d_2(z)$ to obtain more phase lead
around the crossover frequency.

Figure 6.7a: Discrete Nyquist plot of $d_2g_d(z)$, where $z = e^{j\omega mT}$
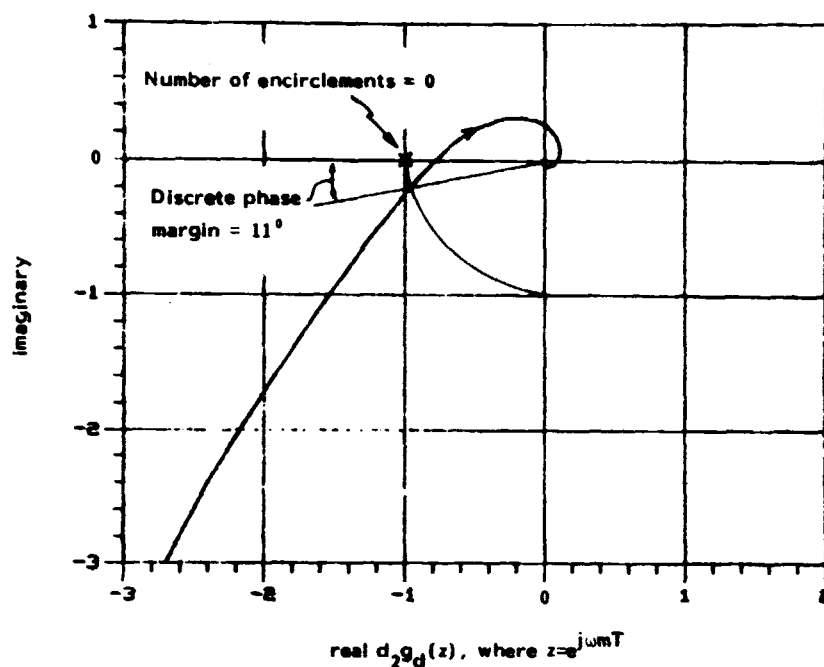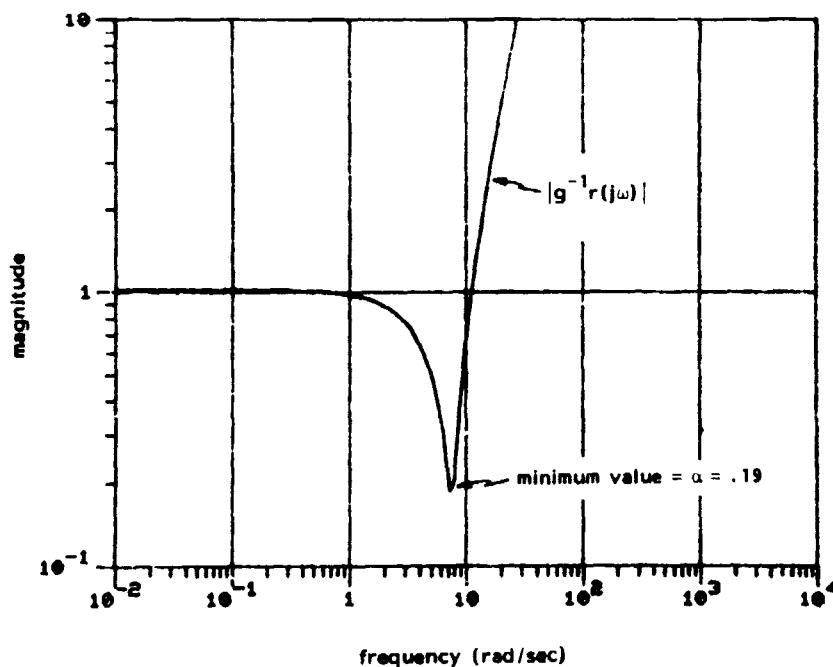

Figure 6.7b: Multiplicative radius of cone that $-(K_1K_2)^I$ is outside of

7. SUMMARY AND SUGGESTIONS FOR FUTURE RESEARCH

7.1 Summary

The major result of this thesis (Theorem 3.2) is the determination of a new conic sector which contains a stable hybrid operator. Everything else in this thesis leads up to, proves, modifies, constructs, demonstrates, and extends this basic result.

The mathematical preliminaries of Chapter 2 lead up to Theorem 3.2. Sections 2.2 and 2.3 contain a review of multivariable (singular value) analysis techniques for analog (CTLTI) and digital (DTLSI) feedback systems. A hybrid system with a single synchronous sampler is defined and its properties are discussed. In Section 2.4 a precise mathematical framework is set up for a conic sector analysis of nonlinear time varying feedback systems. In this general framework, conic sectors are used to analyze closed loop stability, robustness properties, and steady state response to commands. The conic sector analysis techniques are not useful unless a specific conic sector can be found for the feedback system of interest. In Section 2.5 specific conic sectors are determined (due to Safonov [7,9]) for analog (CTLTI) feedback systems and then used to analyze closed loop stability and robustness properties.

Theorem 3.2 gives sufficient conditions for the existence of a new conic sector which is specifically for use in analyzing hybrid feedback systems. Part of Chapter 3 is used to prove this basic result. The most important part of this proof is Lemma 3.A, which is a frequency domain inequality that applies to all possible input-output pairs of signals of the hybrid operator.

The remainder of Chapter 3 (there are a total of 8 theorems) is used to modify Theorem 3.2. The entire loop transfer operator (not just

the hybrid operator) can be placed inside of a conic sector, but whatever is inside of a conic sector must be open loop stable. Theorem 3.2 is modified to remove this open loop stability restriction, so that the inverse of any hybrid operator (stable or unstable) can be placed outside of a conic sector (Theorem 3.6). The conic sectors of Theorems 3.2 and 3.6 are used for analysis techniques for hybrid feedback systems (just as for the general feedback system of Section 2.4) to analyze closed loop stability, robustness with respect to modelling uncertainties, and steady state response to command inputs.

The algorithms and numerical results presented in Chapter 4 are used to construct the new conic sectors. The center is arbitrary, though some are better than others, and there is not any difficulty in computing it. The radius, however, can be difficult to compute, and various ways to do so are presented and discussed.

The examples in Chapter 5 demonstrate the usefulness of the new conic sector analysis techniques. In addition to the analysis techniques mentioned above, the conic sectors are used to select the sample rate and compare discretization techniques. In the one multivariable example, the robustness results are shown to be conservative.

The material in Chapter 6 extends the conic sector results of Chapter 3 to single loop multirate hybrid (SLMRH) feedback systems. This is done by combining the two hybrid operators with different sample rates into a multirate hybrid operator which has an input-output transformation with a structure similar to a single rate hybrid operator with the slower of the two sample rates. Once this similar structure is established then Theorems 3.1 to 3.7 are extended and then demonstrated by an example.

The mathematical development leading up to and proving the major
result (Theorem 3.2) is highlighted as being of interest to control
thereoticians. The rigorous justification for treating hybrid feedback
systems as analog feedback systems, and the specific analysis techniques
based on Theorem 3.2 and its modifications are highlighted as being of
interest to control practitioners.

♣.2 Suggestions for Further Research

The idea of using conic sectors to analyze hybrid feedback systems originated with Gunter Stein and is now about 3 years old. This thesis has developed this idea to the point where it can now be said that conic sector analysis techniques are constructive and useful for hybrid control systems. Time and further developments are needed, however, if these conic sector analysis techniques are to become generally accepted.

Removal of Open Loop Stability Restriction   The major restriction to the use of conic sectors that contain hybrid operators is that the hybrid operator must be open loop stable. This restriction prevents the use of some of the conic sector analysis techniques for important control systems such as those with integral control action. While it is possible to eliminate this open loop stability restriction by placing the inverse of the hybrid operator outside of a conic sector,[1] it is still desirable to be able to place both open loop stable and unstable hybrid operators inside of conic sectors. The advantages of having the hybrid operator inside of a conic sector are (1) the center of the conic sector can be used as an analog (CTLTI) approximation of the hybrid operator, and (2) the nominal feedback system is analog (and therefore one of the sufficient conditions for hybrid closed loop stability is that the nominal analog system is closed loop stable).

It is not clear how (or even if) this open loop stability restriction

---

[1] This alternative is significant and leads to the important robustness analysis technique of Theorem 3.7. The assumption of open loop stability of the hybrid operator is replaced by an assumption that the nominal hybrid feedback system (with the nominal plant) is closed loop stable.

can be removed, This restriction can be traced back to the Small Gain
Theorem (see Subsection 2.4.4), which gives sufficient conditions for
closed loop stability, but requires that the relations that define the
feedback system be open loop stable.

One suggestion for removing the open loop stability restriction is
to define the conic sector using the gap metric [36, Section 4.2, and 37].
The basic idea behind the use of the gap metric is that there is some
exact information which must be known about an unstable system before it
can be stabilized. For analog (CTLTI) systems this exact information is
the number of open loop unstable s-plane poles. For hybrid systems this
exact information may be (it still remains to be shown) the number of
unstable s-plane poles (of the analog components) plus the number of
unstable z-plane poles (of the digital components).

Generalization of Conic Sector Techniques to Sector Techniques. A
conic sector is a special case of a sector (see Safonov [7]). It should
be possible to develop analysis techniques for hybrid systems based on
the use of sectors. If an operator (of any type) is placed inside of a
conic sector then the radius of the conic sector is analogous to an
additive perturbation. Sectors, on the other hand, can be set up so
that parts of the sector are analogous to addition, multiplication,
subtraction, and division perturbations (see Lehtomaki [38, p. 86]).

Sectors can be used to analyze combination operators. If G_1 and G_2
are inside of sectors then it is possible to find sectors that contain[1]
$G_1 + G_2$, $G_1 - G_2$, $G_1 G_2$, and $G_1 G_2^{-1}$. These types of operations are needed to

---

[1]Conic sectors can be used for addition, subtraction, and multiplication,
but the results are conservative.

analyze complicated feedback systems with multiple loops (such as multi-rate multiloop hybrid feedback systems). References for combining sectors are by Safonov [7, 10].

Less Conservative Multivariable Robustness Results. The conic sector analysis techniques developed in Chapter 3 are valid for both SISO and multivariable hybrid feedback systems, but have been shown by example to be conservative for multivariable systems.[1] This problem with conservatism must be corrected. It may be just a matter of breaking the feedback loop at a different point in order to analyze robustness, but the details remain to be worked out.

Even for SISO systems the conic sector analysis techniques are sensitive to where the feedback loop is broken (see Section 5.2). This property is counter-intuitive (at least it is counter to our intuition!) and needs to be better understood.

Synthesis Techniques The emphasis of this thesis has been on the development of analysis techniques. What the community of control system designers really need, however, are synthesis techniques. Therefore, the development of conic sector synthesis techniques is an ill-defined but necessary extension of this thesis.

In some sense the conic sector analysis techniques developed in this thesis can be considered synthesis techniques. They can be used to compare alternative designs for hybrid compensators, and they can be used as part of an iterative design process (at each step of the iteration "engineering judgement" must be used to make changes in the

---

[1] In particular, the multivariable robustness technique of Theorem 3.7 is conservative if the singular values of the nominal plant are far apart (see Subsection 5.4.4).

design). In the examples it was shown how the gain of the hybrid

operator can be used to help select the prefilter, and it was shown how

the magnitude of the multiplicative radius as a function of frequency

can be used to select the sample rate.

Ultimately, what conic sectors have to offer is a rigorous justifi-

cation for keeping the design of hybrid compensator in the analog domain.

The point of view is that the hybrid compensator is supposed to mimic an

analog compensator, and the extent to which it does not is a source of

error (i.e. a perturbation of the nominal analog comepnsator) which is

treated just as a perturbation of the nominal analog plant. Specific

algorithms for transforming an analog compensator into a prefilter,

sampler, digital computer, and hold should have the goal of keeping

the perturbation of the nominal analog compensator small relative to

the perturbations of the nominal analog plant.

Multirate Sampling Issues Chapter 6 is a preliminary extension

of conic sector analysis techniques to multirate hybrid feedback systems.

More work needs to be done in this area, specifically (1) extend the

results of Chapter 6 to multiloop and multirate hybrid feedback systems

and (2) relax the assumption that the sample rates form an integer ratio.

In Chapter 6 two single rate hybrid operators K_1 and K_2 were

combined to form a multirate hybrid operator $K_1 K_2$, and then a conic

sector was constructed that contains $K_1 K_2$. A different approach that

should be tried is to place the single rate hybrid operators K_1 and K_2

into their own respective conic sectors, and then to combine the centers

and radii to form a conic sector of the multirate hybrid operator. To

do so in a nonconservative way may require the use of sectors as opposed to conic sectors.

Asynchronous Sampling Issues   One of the assumptions made throughout this thesis is that the single rate hybrid compensator contains a synchronous sampler.   This assumption is not valid if the sample periods are variable, random, or dependent on the dynamics of the plant. These types of asynchronous samplers are rarely used, so there is little need to develop conic sector analysis techniques to handle them. It is just as well, because we do not have any suggestions for how to do so. The input-output transformation must be defined, and then the conic sector inequality (2.81) must be shown to be valid for all possible input-output pairs of signals. Unfortunately, there are no systematic ways to determine conic sectors.

More common then asynchronous sampling is synchronous that skewed sampling, which occurs when the computational delay is a fraction of a sample period. This thesis has not explicitly addressed the issue of skewed sampling, but the conic sectors of Chapters 3 and 6 can be modified to account for skew by changing the hold transfer function from $h(s)$ to $h(s)e^{-T_d s}$. This is easier, for instance, then using modified z-transforms for digital control systems.

Asynchronous sampling may occur in multirate hybrid feedback systems, especially if the clocks that control the sample intervals are not synchronized. Typical behavior is that the sample times slowly drift with respect to each other. The z-transform techniques developed for multirate systems are difficult to apply to this problem. Conic sectors (or sectors) offer the following approach: each hybrid compensator is

placed in its own conic sector, and then the conic sectors are combined
to form a conic sector of the composite operator. By treating each
hybrid compensator separately it should not matter whether or not they
are synchronized.

Finite Wordlength Issues If the effects of finite word length of
the digital computer are included in the model of the hybrid compensator
then the model is a nonlinear time varying operator. In this thesis
the effects of finite word length are assumed to be neglicable, thereby
allowing the model to be a linear time varying operator. With the 16
and 32 bit microprocessors currently available it is indeed very safe
to assume that the effects of finite word length are neglicable.
Nevertheless, this is a problem that has received a lot of attention
in the digital control literature (see [4, Chapter 7] and [39]). The
practical effects of finite word length are (1) truncation errors in
computing, (2) truncation errors in stored parameter values, and (3)
limit cycles in the feedback loop.

A motivation for further reserach is to determine if conic sectors
are useful for the analysis of hybrid feedback systems when the finite
word length of the digital computer is taken into account. As mentioned
for asynchronous sampling there are not any systematic ways to determine
conic sectors, so we cannot offer any specific guidance. If such a conic
sector is found, however, then its center can be used as an analog
(CTLTI) approximation of the hybrid compensator; and then the errors
due to the finite word length can be bounded by the radius and treated
as a perturbation of the nominal compensator.

Conic sector analysis techniques were developed for nonlinear

systems, so the fact that the effects of finite word length are nonlinear does not exclude the use of conic sectors. Difficulties will probably be encountered when the conic sector inequality (2.81) is checked for all possible input-output pairs. Also, difficulties may be encountered because the definition of stability must be changed so that limit cycles are not considered unstable.

Even it a conic is found it may not be useful due to conservativeness (as was the case for the first two conic sectors developed for linear time varying hybrid operators). The particular problem with the assumption of finite word length is that input signals of very small amplitude may fall below the first truncation level and produce zero output. Linear operators used for cone centers and radii cannot distinguish between small and large amplitudes, and therefore the radius will treat large amplitude signals at any frequency as though their output was zero.

REFERENCES

1. J.C. Doyle and G. Stein, "Multivariable Feedback Design: Concepts for a Classical/Modern Synthesis," IEEE Trans. Auto. Control, Vol. AC-26, pp. 4-16, Feb. 1981.

2. M.G. Safonov, A.J. Laub, and G.L. Hartmann, "Feedback Properties of Multivariable Systems: The Role and Use of the Return Difference Matrix," IEEE Trans. Auto. Control, Vol. AC-26, pp. 47-65, Feb. 1981.

3. N.A. Lehtomaki, N.R. Sandell, Jr., and M. Athans, "Robustness Results in Linear-Quadratic Guassian Based Multivariable Control Designs," IEEE Trans. Auto. Control, Vol. AC-26, pp. 75-92, Feb. 1981.

4. G.F. Franklin and J.D. Powell, Digital Control of Dynamic Systems, Addison-Wesley Publishing Co., Reading, Massachusetts, 1980.

5. G. Zames, "On the Input-Output Stability of Time-Varying Nonlinear Feedback Systems, Part I," IEEE Trans, Auto. Control, Vol. AC-11, pp. 228-238, April 1966.

6. G. Zames, "On the Input-Output Stability of Time-Varying Nonlinear Feedback Systems, Part II," IEEE Trans. Auto. :trol, Vol. AC-11, pp. 465-476, July 1966.

7. M.G. Safonov, Stability and Robustness of Mu: .variable Feedback Systems, The MIT Press, Cambridge, Massachusetts, 1980.

8. C.A. Desoer and M. Vidyasagar, Feedback Systems: Input-Output Properties, Academic Press, New York, 1975.

9. M.G. Safonov and M. Athans, "A Multiloop Generalization of the Circle Criterion for Stability Margin Analysis," IEEE Trans. Auto. Control, Vol. AC-26, pp. 415-422, April 1981.

10. M.G. Safonov, "Tight Bounds on the Response of Multivariable Systems with Component Uncertainty," Proc. Allerton Conf. on Communication and Computing, Monticello, Illinois, Oct. 4-6, 1978.

11. J.C. Doyle, "Advanced Topics in Robustness for Multivariable Control," Honeywell Systems and Research Center, Final report in preparation for Office of Naval Research, 1982.

12. V.C. Klema and A.J. Laub, "The Singular Value Decomposition: Its Computation and Some Applications," IEEE Trans. Auto. Control, Vol. AC-25, pp. 164-176, April 1980.

13. B.T. Smith et. al., Matrix Eigensystem Routines - EISPACK Guide, 2nd ed. (Lect. Notes in Computer Sci.), Vol. 6, New York, Springer-Verlag, 1976.

14 M. Athans, "The Role and Use of the Stochastic Linear-Quadratic-Guassian Problem in Control System Design," IEEE Trans. Auto. Control, Vol. AC-16, pp. 529-552, Dec. 1971.

15. H.H. Rosenbrock, Computer-Aided Control System Design, Academic Press, London, 1974.

16. V. Mukhopadhyay and J.R. Newson, "Application of Matrix Singular Value Properties for Evaluating Gain and Phase Margins of Multiloop Systems," AIAA Guidance and Control Conference, San Diego, California, August 9-11, 1982.

17. A. Kostovetsky, Some Investigations of Hybrid Systems, S.M. Thesis, Dept. of Mechanical Engineering, MIT, May 1970, Appendix to Lab. for Info. and Decision Systems Report LIDS-FR-960.

18. G. Stein, M. Athans, and P.M. Thompson, Hybrid Operator Models for Digitally-Implemented Control Systems, Final Report for NASA Langley Research Center, NASA Grant No. NAG1-2, MIT Lab. for Info. and Decision Systems Report LIDS-FR-1206, April 1982.

19. S.K. Berberian, Introduction to Hilbert Space, Chelsea Publishing Co., New York, 1976.

20. Jan C. Willems, The Analysis of Feedback Systems, The MIT Press, Cambridge, Massachusetts, 1971.

21. R.G. Bartle, The Elements of Integration, John Wiley and Sons, Inc., New York, 1966.

22. C.F. Van Loan, "Computing Integrals Involving the Matrix Exponential," IEEE Trans. Auto Control, Vol. AC-23, pp. 395-404, June 1978.

23. G.L. Hartmann, et al., "LQG Controls for Highly Maneuverable Aircraft," Proc. of the 19th Conf. on Decision and Control, Albuquerque, N.M., Dec. 1980.

24. G.L. Hartmann, M.F. Barrett, and C.S. Greene, "Control Design for an Unstable Vehicle," Contract Report NAS4-2578, NASA Dryden Flight Research Center, Dec. 1979.

25. D.A. Deets and C.A. Crother, " ighly Maneuverable Aircraft Technology," Active Controls in Aircraft Design, AGARDograph No. 234, November 1978.

26. G. Stein and S. Pratt, "LQG Multivariable design Tools," AGARD Lecture Series No. 117, September 1981.

27. J.C. Doyle and G. Stein, "Robustness with Observers," IEEE Trans. Auto. Control, Vol. AC-24, August 1979.

28. C.A. Harvey and G. Stein, "Quadratic Weights for Asymptotic Regulator Properties," IEEE Trans. Auto. Control, Vol. AC-23, June 1978.

29. J.L. Willems, _Stability of Dynamical Systems_, John Wiley and Sons, Inc., New York, 1970

30. P.M. Thompson and J.E. Wall, Jr., "A New Approach to Digital Control," Interoffice Correspondence, Systems and Control Tech. Section, Honeywell Systems and Research Center, Feb. 1982.

31. V.M. Walton, "State Space Stability Analysis of Multirate-Multiloop Sampled Data Systems," _AAS/AIAA Astrodynamics Specialist Conference_, Lake Tahoe, Nevada, August 3-5, 1981.

32. A.F. Konar and J.K. Mahesh, "Analysis Methods for Multirate Digital Control Systems," Honeywell Report No. F0636-TR1, Honeywell Systems and Research Center, August 1978.

33. J. Sklansky, "Network Compensation of Error-Sampled Feedback Systems," Doctoral Dissertation, Columbia University, New York, 1955.

34. J.T. Tou, _Digital and Sampled-data Control Systems_, McGraw-Hill Book Co., Inc., New York, 1959.

35. J.C. Doyle, "Multivariable Design Techniques Based on Singular Value Generalizations of Classical Control," _AGARD Lecture Series No. 117_, September 1981.

36. T. Kato, _Perturbation Theory for Linear Operators_, Springer-Verlag, New York, 1966.

37. A.K. El-Sakkary, "The Gap Metric for Unstable Systems," Ph.D Thesis, Department of Electrical Engineering, McGill University, Montreal, Canada, March 1981.

38. N.A. Lehtomaki, "Practical Robustness Measures in Multivariable Control System Analysis," PhD Thesis, Laboratory for Information and Decision Systems, MIT, May 1981, Report LIDS-TH-1093.

39. R. Moroney, "Issues in the Digital Implementation of Control Compensators," PhD Thesis, Laboratory for Information and Decision Systems, MIT, October 1979, Report LIDS-TH-951.

40. K. Fan, "Maximum Properties and Inequalities for the Eigenvalues of Completely Continuous Operators," _Proceedings of the National Academy of Science_, pp. 760-766, 1951.

BIOGRAPHICAL NOTE

    Peter Murray Thompson was born on ███████████ in ████████████ He
attended public school in Arlington, Virginia, showed an aptitude and in-
terest in mathematics and science, and graduated from Washington-Lee High
School in !ay 1972. He received his undergraduatr education at the
University of Virginia, developed an interest in system and control theory,
was elected to Tau Beta Pi and Eta Kappa Nu honor societies, and obtained
a double B.S. degree with high distinction in Electrical Engineering
and Applied Math in May 1977.

    He entered the Department of Electrical Engineering and Computer
Science at MIT in September 1977, and during his time there was a research
assistant in the Laboratory for Information and Decision Systems and a
teaching assistant for a graduate course in multivariable control theory.
He received a S.M. degree in June 1979 and an E.E. degree in June 1980.
His S.M. thesis is "Linear State Feedback, Quadratic Weights, and Closed-
Loop Eigenstructures."

    His professional experience includes three summers at Bolt Beranek and
Newman, Inc. in Cambridge, Massachusetts (working on sonar, pattern
recognition, and local area computer network problems), and one summer
at the Honeywell Systems and Research Center in Minneapolis, Minnesota
(working on a digital control problem).

    In October 1982 he will join the faculty of the Division of Engineering
and Applied Science at the California Institute of Technology in Pasadena,
California. His research interests are in digital control theory, nonlinear
stability theory, and robotics.